eman ta zabal zazu

Universidad del País Vasco
Euskal Herriko Unibertsitatea

# SYNTHESIS AND APPLICATIONS IN IMMUNOASSAYS OF ANTIBODY-PROTECTED NANOCLUSTERS

**Verónica Mora Sanz**

2022

## Thesis Supervisors:

**Dr. Valery Pavlov**

Biosensing Lab., CIC biomaGUNE, Basque Research and Technology Alliance (BRTA), Donostia-San Sebastián (Spain)

**Dra. Nerea Briz**

Biomaterials Group, Tecnalia, Basque Research and Technology Alliance (BRTA), Donostia-San Sebastián (Spain)

## University Tutor:

**Prof. Dra. Isabel Goñi**

Department of Polymer Science and Technology, Faculty of Chemistry, University of the Basque Country (UPV/EHU), Donostia-San Sebastián (Spain)

# Table of contents

## Abstract

Nanoclusters (NCs) have attained great attention in the last few years due to their size dependent optical and chemical properties. Nowadays a large number of methods using proteins as scaffold have been developed for NCs synthesis. Up to now any synthetic method has been described using an antibody as scaffold. Its structure is composed of four aminoacids chains connected by disulfide bonds between cysteine residues of different chains. This structure makes antibodies suitable biomolecules to act as templates for the incorporation of NCs. Usually the synthetic conditions for the synthesis of NCs stabilized with proteins require extreme conditions of pH or temperature. These conditions cause the denaturalization of the proteins and end up in the loss of their biological functions.

In this work we present the first method for the synthesis of NCs using antibodies as scaffold and the first immunoassays carried out using antibodies modified with NCs. The synthesis of NCs embedded in antibodies is carried out under physiological conditions, which do not affect the antibody structure. The resulting antibodies still maintain the affinity for target analyte. These NCs have measurable properties that can be related with the quantity of antigen that binds the modified antibody.

CdS was chosen as a suitable material because nanomaterials with this composition exhibit photocatalytic activity and fluorescent properties. Bimetallic NCs composed by Ag/Pt and Au/Pt are also adequate candidates for the modification of antibodies due to its reported peroxidase-like activity. It was probed that after the introduction of the NCs into the antibodies, they retain their affinity for target analyte, therefore the antibody carrying NCs can be employed in immunoassays.

The bimetallic NCs-IgG can be used as detection antibody in a sandwich immunoassay and the concentration of the target analyte can be related with the reaction rate of a chromogenic substrate oxidation. In comparison with a conventional method using an IgG labelled with HRP the LOD is improved up to 5 times using Ag/Pt NCs-IgG and 56 times greater with Au/Pt NCs-IgG. The CdS NCs-IgG were tested as energy donor in a FRET-based homogeneous competitive immunoassay using their fluorescent properties.

## Resumen

Todos los sectores de la sociedad en la que vivimos se encuentran influenciados por el constante avance de la tecnología. La gran velocidad con la que estos cambios suceden hace que la investigación desarrolle técnicas que satisfagan las nuevas necesidades. Una de las principales demandas actuales, es la detección de biomoléculas en diferentes sectores. Los biosensores son los instrumentos más eficaces para cubrir esta necesidad emergente y las futuras.

Un biosensor es un dispositivo que integra un elemento biológico que actúa como bioreceptor, como una enzima o un anticuerpo, con un transductor, que convierte un cambio biológico en una señal que es proporcional a la cantidad de analito que hay en el medio. Esta transformación se lleva a cabo generalmente, siguiendo los siguientes pasos. Primero en la etapa de reconocimiento, el analito reacciona selectivamente con el bioreceptor generando una señal primaria. Más tarde en la etapa de transducción se genera una señal que puede ser óptica, eléctrica o magnética, entre otras. Finalmente, durante el procesado de señal se genera una señal eléctrica, fácilmente interpretable por el usuario final. Es importante señalar que existen otro tipo de biosensores donde la señal óptica no se procesa y la lectura es visual (ej. ensayos de flujo lateral).

El concepto de biosensor continúa evolucionando desde su primera acepción, que consideraba un biosensor como un dispositivo capaz de medir la concentración de un compuesto químico en una muestra biológica. Esta definición no incluía ningún bioelemento y, por tanto, un sensor químico o físico trabajando en una muestra biológica era considerado un biosensor. Actualmente está aceptado que un biosensor debe integrar un elemento de detección de naturaleza biológica y un transductor en el mismo dispositivo. Incluso ahora, el concepto continúa evolucionando y el auge de la nanotecnología ha creado materiales de escala nanométrica que pueden mejorar las propiedades de los biosensores tradicionales. De la combinación de la nanotecnología con los biosensores ha surgido el concepto de los nanobiosensores. Se pueden definir a los nanobiosensores como un sensor que emplea nanomateriales para la detección de un analito a través de interacciones biológicas.

El sector de la salud y la biomedicina son actualmente el principal sector del mercado interesado en el desarrollo de biosensores. De entre todos los biomarcadores existentes, los más empleados son las proteínas porque suelen estar relacionadas con las enfermedades más comunes. Actualmente la tecnología más utilizada para la detección de proteínas son los inmunoensayos. El uso de anticuerpos presenta las ventajas de una alta selectividad hacía su antígeno y la amplia variedad de anticuerpos disponibles comercialmente. En laboratorios de rutina la técnica más empleada para la detección de proteínas empleando anticuerpos es el ensayo por inmunoabsorción ligado a enzimas (ELISA). A pesar de la alta sensibilidad de esta metodología el uso de enzimas naturales como marcadores tiene desventajas, como, por ejemplo, alta susceptibilidad a variaciones medioambientales, tendencia a la desnaturalización y además la preparación y purificación es poco económica y requiere de mucho tiempo. El bioconjugado se consigue incubando enzimas y anticuerpos con agentes de entrecruzamiento y su posterior purificación. La reactividad de las enzimas y los anticuerpos con los entrecruzantes son diferentes y como resultado se forman no solo heteropolímeros (anticuerpo-enzima) sino también de homopolímeros (anticuerpo-anticuerpo y enzima-enzima) por entrecruzamiento aleatorio. En los heteropolímeros en los que el anticuerpo no se encuentre completamente reactivo es probable que no se puedan eliminar por procesos de purificación convencionales y durante el inmunoensayo pueden causar ruido de fondo y baja precisión debido a la absorción no específica. Mientras que los homopolímeros no son útiles para la detección de analitos. Otro método para unir enzimas y anticuerpos utiliza la fuerte unión no-covalente entre avidina y biotina. Una característica de este método es la amplificación de la señal que se logra mediante la introducción de muchos residuos de biotina en los anticuerpos y la posterior unión de avidina unida a enzimas. La desventaja del método es que también se amplifican las uniones no específicas.

En esta tesis se propone el uso de la nanotecnología para superar las dificultades vinculadas al uso de enzimas como marcadores en inmunoensayos y establecer una metodología universal para el marcaje de anticuerpos eliminando el paso de la reacción de entrecruzamiento. En concreto se plantea la síntesis de nanoclusters (NCs) con propiedades ópticas y/o catalíticas usando anticuerpos como andamios estructurales

para su posterior uso en inmunoensayos. Los anticuerpos con NCs actúan como una sonda que incorpora tanto el componente de reconocimiento (anticuerpo) y el componente de transducción (NCs). La introducción de NCs en el elemento de bioreconocimiento puede resolver las desventajas del uso de los complejos anticuerpo-enzima y proporciona nuevas estrategias eficientes para el sistema de detección de inmunoensayos. El avance más allá del estado del arte es que durante la introducción de los NCs en la estructura del anticuerpo este no se desnaturaliza. La estructura de la proteína permanece sin cambios y la afinidad por el analito no se ve afectada. En la bibliografía se pueden encontrar muchos ejemplos de la síntesis de NCs empleando proteínas como andamios estructurales, sin embargo, estos métodos se suelen realizar en condiciones desnaturalizantes de pH, temperatura, entre otros, que causan la pérdida de la estructura secundaria de las proteínas, así como sus funciones biológicas.

De entre todos los nanomateriales más empleados en el campo de los biosensores se eligieron los NCs por sus dimensiones extremadamente pequeñas, menos de 2 nm, que hacen que tengan el tamaño perfecto para introducirse dentro de la estructura de un anticuerpo que tiene un tamaño de entre 12-15 nm. Sus propiedades los hacen excelentes transductores para biosensores. Por un lado, los NCs pueden tener propiedades fluorescentes y por otro pueden tener propiedades catalíticas e imitar el comportamiento de las enzimas. Los nanomateriales que poseen este tipo de comportamiento se conocen como nanoenzimas.

Para abordar estas cuestiones, la presente tesis se encuentra estructurada en un primer capítulo de introducción a los biosensores haciendo hincapié en los inmunosensores enzimáticos. También se discuten diferentes aplicaciones de la nanotecnología en el campo de los biosensores centrándose en el uso de NCs y de nanoenzimas (capítulo 1). A continuación, se exponen los objetivos e hipótesis de trabajo realizado (capítulo 2). En la parte experimental, se distinguen dos bloques. En el primero se describe la síntesis y caracterización de NCs empleando un anticuerpo como andamio (capítulo 3). Para finalizar, en el segundo bloque se estudian dos aplicaciones diferente en inmunoensayos (capítulo 4). Para finalizar se presentan las conclusiones generales (capítulo 5).

En el capítulo 3 se describen tres estrategias para la síntesis de NCs. En todas ellas se usó como anticuerpo modelo una inmunoglobulina G policlonal para la detección de albumina de suero bovino (Anti-BSA IgG). En la primera síntesis se introducen NCs compuestos de sulfuro de cadmio (CdS NCs) en la estructura del anticuerpo. Se trata de un proceso, en el que primero se pone en contacto la disolución del anticuerpo con una sal de cadmio y tras un corto tiempo de incubación se añade gota a gota un precursor de iones sulfuro e inmediatamente se forman los CdS NCs embebidos en la estructura del anticuerpo (CdS NCs-IgG). En las siguientes dos síntesis se sintetizan NCs bimetálicos. En un caso de plata y platino (Ag/Pt NCs) y en el otro de oro y platino (Au/Pt NCs). Para la síntesis se añaden precursores de ambos metales a una disolución que contiene el anticuerpo y tras un tiempo de incubación se añade $NaBH_4$ que reduce los iones metálicos. La disolución va cambiando de incolora a marrón claro por la formación de los NCs (Ag/Pt NCs-IgG y Au/Pt NCs-IgG). Después del tiempo de reacción las disoluciones se filtran para purificar los NCs-IgG y eliminar los iones que no han reaccionado.

Los NCs resultantes se caracterizaron empleando diferentes técnicas. Primero se evaluaron sus propiedades ópticas. Los CdS NCs presentan propiedades fluorescentes con un máximo de emisión ancho entre 600 y 650 nm excitando a 315 nm. Los NCs bimetálicos no son fluorescentes. Después se emplearon técnicas de microscopía electrónica para evaluar el tamaño y morfología de los NCs. En los tres casos presentaron una morfología esférica con un diámetro menor a 2 nm. El estado de oxidación de los NCs se estudió empleando espectroscopía fotoelectrónica de rayos X (XPS). Para demostrar que los NCs están unidos al anticuerpo se empleó la técnica de desorción/ionización láser asistida por matriz con detección de masas por tiempo de vuelo (MALDI-TOF). Se comparo el pico que apareció en el espectro MALDI-TOF de los NCs-IgG con los del anticuerpo sin modificar y se observó que el pico de los primeros aparecía a masas mayores. Este resultado indica que efectivamente los NCs están unidos al anticuerpo.

Los tres NCs tienen propiedades catalíticas. En concreto los CdS NCs-IgG poseen actividad fotocatalítica y son capaces de oxidar el sustrato fluorogénico Amplex Red, que cambia sus propiedades fluorescentes y cromogénicas, desencadenado por la

exposición a luz UV. El sistema mostró una cinética de Michaelis-Menten, la velocidad de reacción aumentó con la concentración de sustrato. Los NCs bimetálicos poseen actividad peroxidasa y son capaces de oxidar el sustrato TMB, que cambia sus propiedades cromogénicas, en la presencia de peróxido de hidrógeno ($H_2O_2$). En ambos casos el sistema también siguió una cinética de Michaelis-Menten. Empleando la ecuación de Lineweaver-Burk se calculó la constante de Michaelis-Menten ($K_m$), que es un indicador de la afinidad de las enzimas hacia sus sustratos y se comparó con los de la HRP. Menores valores de $K_m$ indican mayor afinidad de la enzima hacia su sustrato. Ambos NCs tienen valores de $K_m$ hacia $H_2O_2$ mayores que los de la HRP, indicando una menor afinidad hacia este substrato. En el caso de los valores de $K_m$ hacia TMB, los Ag/Pt NCs-IgG presentaron valores muy similares a los de la HRP. Los Au/Pt NCs-IgG mostraron un valor 8,5 veces menor que el de la HRP, indicando una mayor afinidad hacia el TMB. Se ha observado un comportamiento similar en otras nanoenzimas.

La estabilidad de la estructura del anticuerpo después de la síntesis se evaluó empleando diferentes estrategias. Primero se estudió la estructura secundaria empleando la técnica de dicroísmo circular (CD). No se observaron diferencias apreciables en los espectros de CD del anticuerpo sin modificar en comparación con los NCs-IgG, por tanto, la estructura secundaria del anticuerpo no se ve afectada durante la síntesis. También se emplearon micropartículas funcionalizadas con Proteína G para estudiar si la región $F_c$ del anticuerpo se veía afectada por la síntesis. Los NCs-IgG se unieron de manera eficiente a las micropartículas, lo cual indica que no existe ningún daño en esta zona del anticuerpo. Finalmente se evaluó si los anticuerpos con NCs seguían teniendo afinidad por su antígeno, BSA. Para ello se llevó a cabo un inmunoensayo directo en el que se inmovilizó BSA en la superficie de un pocillo de una microplaca y se emplearon las propiedades fotocatalíticas y catalíticas de los NCs-IgG para du detección. En todos casos se observó que el anticuerpo seguía teniendo afinidad por su antígeno, aunque en el caso de los CdS NCs es menor que en la de los NCs bimetálicos.

Se llevó a cabo un estudió más profundo sobre la posición del NC metálico en la estructura del anticuerpo y su composición en los Au/Pt NCs-IgG. Para elucidar la región del anticuerpo que está implicada en la estabilización de los NCs, se produjeron

diferentes fragmentos del anticuerpo usando las enzimas papaína y pepsina. Posteriormente se sintetizaron los Au/Pt NCs empleando estos fragmentos y se emplearon en un ELISA directo. Los resultados indican que los NCs muy probablemente se encuentren en la región bisagra, lejos de la zona de reconocimiento. Para evaluar la verdadera naturaleza bimetálica de los Au/Pt NCs se realizó un mapeo de un solo NC empleando espectroscopía de Rayos X dispersiva en energía (EDX). El espectro de EDX indica que efectivamente los NCs son bimetálicos y que poseen un porcentaje atómico de un 91 % de Pt y un 9 % de Au.

La universalidad del método sintético de Au/Pt NCs-IgG se evaluó empleando otros dos anticuerpos policlonales obteniéndose resultados positivos. Sin embargo, no se obtuvieron buenos resultados con anticuerpos monoclonales. Pese a que se observó por TEM que se habían formado NCs y que además presentaban actividad catalítica, estos no eran capaces de reconocer a su antígeno. Después de evaluar el estado de la estructura secundaria del anticuerpo tras la síntesis, se comprobó que se había desnaturalizado, perdiendo así sus funciones biológicas. Los anticuerpos policlonales son más robustos y estables a cambios en el pH y concentraciones de sales en el medio. Los anticuerpos monoclonales son más sensibles a los cambios en el medio y sus propiedades de reconocimiento se ven fácilmente afectadas. Sin embargo, hacen falta más experimentos para comprender este fenómeno y el uso de más tipos de anticuerpos diferentes.

Tras finalizar con la caracterización de los NCs-IgG resultantes. Se evaluó su desempeño en diferentes inmunoensayos que explican en el capítulo 4. En la primera parte de este capítulo se emplearon los Ag/Pt NCs-IgG y los Au/Pt NCs-IgG como anticuerpos de detección en un inmunoensayo tipo sándwich. El rendimiento de los NCs-IgG se comparó en términos de sensibilidad con un inmunoensayo tipo sándwich tradicional que emplea un anticuerpo marcado con HRP como anticuerpo de detección. En todos casos se usó el mismo anticuerpo para que los resultados fueran comparables. Primero se optimizó la concentración de anticuerpo de detección en los inmunoensayos y posteriormente se obtuvo una curva de calibración para BSA. Empleando los Ag/Pt NCs-IgG se mejoró el límite de detección (LD) 5 veces en comparación con el inmunoensayo que emplea el anticuerpo marcado con HRP. Con los Au/Pt NCs-IgG se obtuvo una

mejora aún mayor en el LD y este disminuyó más de 56 veces. Eliminando la reacción de entrecruzamiento entre el anticuerpo y la enzima y empleando NCs embebidos en la estructura del anticuerpo se consigue bajar el ruido de fondo, al haber menos absorción inespecífica. Al mejorar la ratio señal/ruido también mejora la sensibilidad del método.

Los CdS NCs-IgG y sus propiedades fotocatalíticas no se emplearon en este inmunoensayo tipo sándwich porque sería necesario usar una fuente de luz UV que hace el ensayo técnicamente más complicado. La misma cantidad de luz debe de alcanzar todos los pocillos, por tanto, la posición de la microplaca respecto a la fuente de luz es crítica para la reproducibilidad del método. Debido a esto se obtendrían desviaciones estándar muy elevadas que hacen que el método no sea adecuado. Las propiedades fluorescentes de los CdS NCs se utilizaron para llevar cabo las primeras etapas de la puesta a punto de un inmunoensayo competitivo basado en transferencia de energía de resonancia de Förster (FRET) desde un donante de energía a un aceptor. El espectro de fluorescencia del donante debe de superponerse con el espectro de absorción del aceptor. La FRET es un fenómeno de proximidad que tiene lugar cuando dos compuestos fluorescentes, donante y aceptor, se encuentran muy cerca. Por tanto, la transferencia de energía solo tiene lugar cuando el anticuerpo se une a sus correspondientes antígenos marcados con el elemento fluorescente. Cuando se introduce en el sistema el antígeno sin marcar, este desplaza al antígeno marcado y la emisión FRET disminuye.

Como conclusión, durante los estudios realizados durante esta tesis se ha podido comprobar que es posible la introducción de NCs en un anticuerpo sin dañar su estructura y sus funciones biológicas. Además, se han demostrado las ventajas del uso de NCs como elemento de transducción en inmunoensayos, mejorando la sensibilidad del sistema. La investigación continua actualmente en esta línea para su optimización y su aplicación para la detección de analitos de interés clínico.

Como resultado de esta tesis se publicaron dos artículos y una patente cuyo título es Conjugados de nanoclusters-anticuerpos y usos asociados.

# CHAPTER 1: GENERAL INTRODUCTION

# 1. BIOSENSORS

## 1.1. Biosensors: historical overview, definition and applications

Known as the "Father of Biosensors", Leland C. Clark developed the first sensor in 1954 for measuring dissolved oxygen. Clark used its experience as physiologist to adjust the oxygen level in circulating blood in a visual manner and he was required in every surgery. To achieve that his presence was not necessary in each operation, he developed an oxygen sensor that could be inserted into the blood flow by reducing oxygen at a platinum electrode. It was called the Clark electrode, which remains the standard nowadays for measuring dissolved oxygen. To calibrate the Clark electrode, he deoxygenated the solutions by adding the enzyme glucose oxidase (GOx) and glucose. This enzymatic reaction consumes oxygen and generates hydrogen peroxide ($H_2O_2$). Clark realized that this method could be also used for glucose sensing and he developed the first biosensor by immobilizing GOx in the Clark electrode in 1956[1]. Since this invention, the field of biosensing has been developing and growing until now. In Figure 1. is showed the historical overview of biosensors from 1954 to actually.

The International Union of Pure and Applied Chemistry (IUPAC) defines sensor as a device that transforms chemical information, ranging from the concentration of a specific sample component to total composition analysis, into an analytically useful signal[2]. Particularly, a biosensor uses specific biochemical reactions mediated by a biological element (isolated enzymes, immunosystems, tissues, organelles or whole cells) to generate a signal, proportional to the concentration of analyte. The concept of biosensor continues evolving since its first approximation that consider a biosensor as a device able to respond to the concentration of a chemical compound in a biological sample. This definition did not include any biological element in the device and therefore, a chemical or physical sensor operating in a biological sample was considered a biosensor. Currently it is accepted that a biosensor should integrate a biological sensing element and a transducer in a unique system. Even now, the concept continues evolving and the emerging of nanotechnology has created some materials at the nanoscale that could improve the performance of traditional biosensors. In this thesis nanotechnology is used to improve the sensitivity of some biosensors. In particular, nanoclusters (NCs) embedded in the structure of immunoglobulins G (IgG) are used as

detection antibody in immunoassays. The current state-of-the-art of the employment of nanotechnology with biosensing purposes will be discussed later in this chapter.

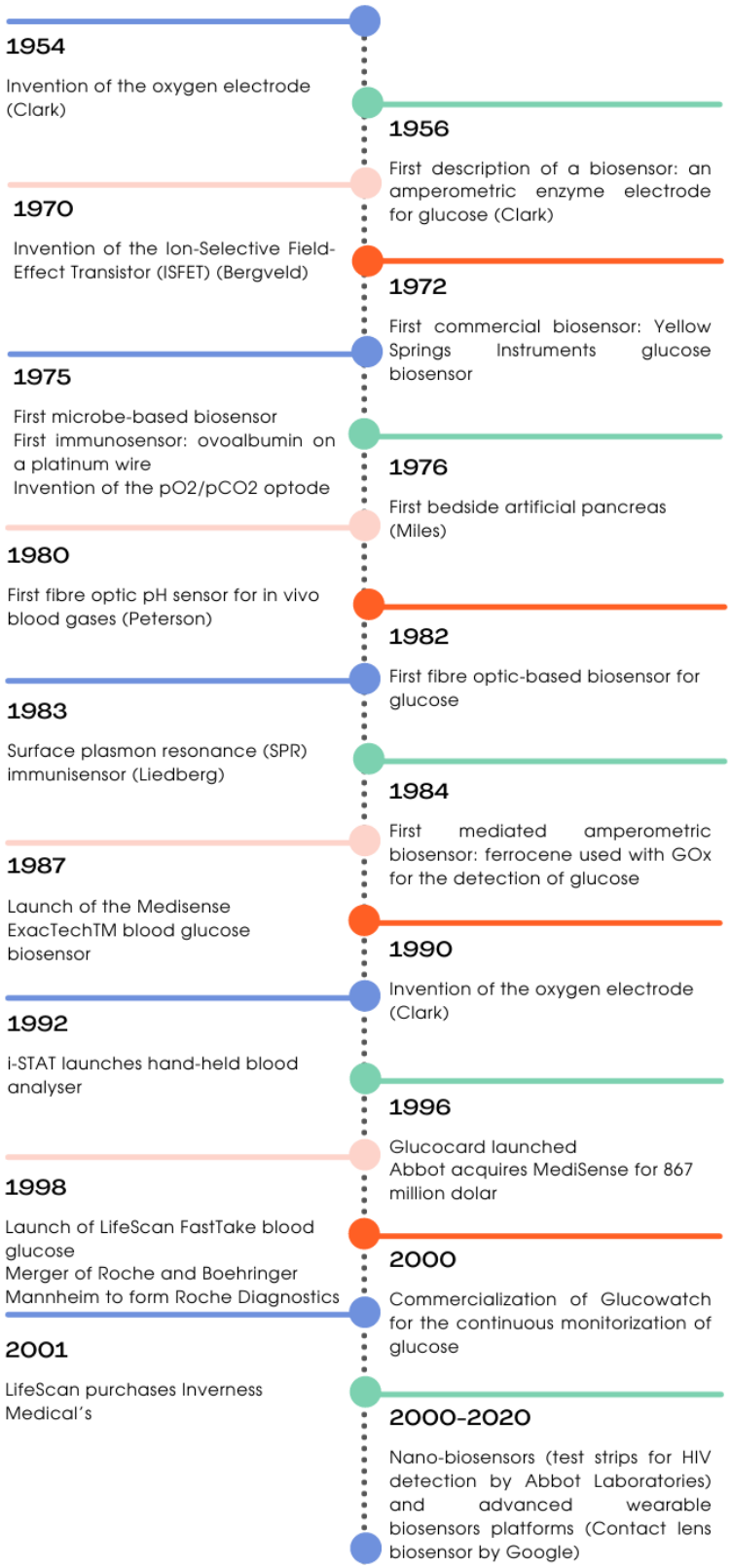


Figure 1. Timeline of most important cornerstone in the development of biosensors.

The key applications of biosensors are in industry, healthcare, monitoring of food toxicity, water quality, air pollution, environment, agriculture and chemical warfare, among others. The European Biosensor Market is expected to register a CAGR of 5.9 % during the forecast period 2021-2026 according by Mordor Intelligence. The application with more importance nowadays is diagnosis. A great number of biosensors are now commercially available for example, for glucose and cholesterol levels monitoring, malaria, HIV, uric acid… In addition to these analytes, cancer and cardiac disease markers also found great attention.

## 1.2. Components of a biosensor

Biosensors use the measurable properties generated by a biorecognition event on a transducing device. The interaction of the analyte with the bioreceptor is converted in an optical or electrical signal easily readable by the end user (Figure 2.).

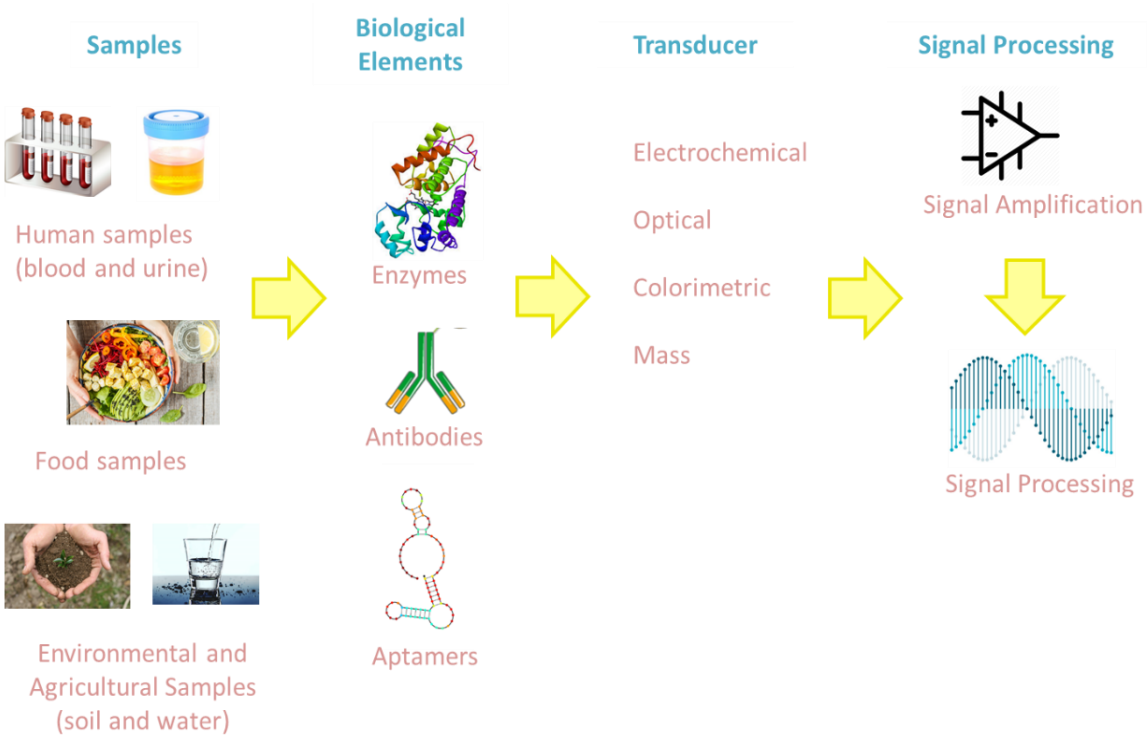


Figure 2. Components of a biosensor.

The components of a biosensor are the following ones[4]:

- Analyte: it is the substance of interest and it is located in the sample.
- Bioreceptor: it is a biological element, that specifically recognizes the analyte. There are different kinds of bioreceptors such as enzymes, antibodies or aptamers. When the biorecognition event takes place a signal in the form of light, pH, electricity or heat is generated.
- Transducer: in the transduction step the biorecognition event is convert into a measurable signal. This process of energy conversion is called signalization and it is carried out by a transducer.
- Signal processing: the transduced signal is prepared for display by a complex electronic system that amplificates and converts the signal from analogue to digital. The information that appears in display can be for example a number a graphic or an image depending of the requirements of the end user.

It must be highlighted that there are other kind of biosensors which do not follow the conventional composition. These biosensors give qualitative information (the absence or the presence of target analyte) and the result can be followed by the naked eye. A known example is the pregnancy test which is a lateral flow immunoassay.

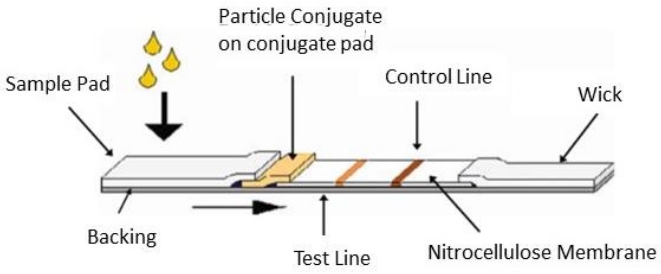


Figure 3. Typical configuration of a lateral flow immunoassay test strip.

In a typical composition of these biosensors (Figure 3.), the sample pad is composed of a material which allows the flow through it, for example cellulose. When the sample start to run through the strip it arrives to the conjugate pad where a visual marker, typically gold NPs, are conjugate to a specific biological component of the assay, either an antibody or an antigen depending of the assay format. The analyte

interacts with the conjugate and arrives to the test line where another specific biological component of the assay has been immobilized. If the analyte was present in the sample, it specifically interacts with the conjugate generating a colored line easily seen by the naked eye. The test strip has also a control line which always interacts with biological component conjugate to the colored compound in order to guarantee the proper performance of the test. Therefore, one line means that the result is negative, the analyte was not present in the sample. Two lines mean a positive result and the analyte is in the sample.

## 1.3. Classification of biosensors based on biorecognition elements

Based in the classification of biosensors based on recognition elements it is possible to find 2 classes, catalytic biosensors and affinity biosensors (Figure 4.) [5].

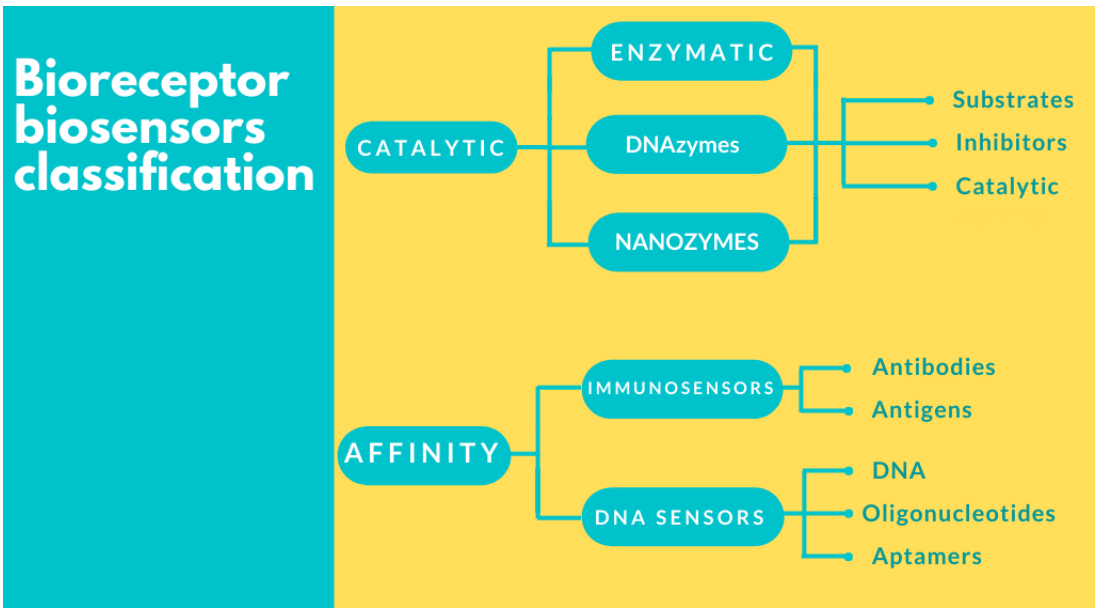


Figure 4. Classification of biosensors based on bioreceptor elements.

- Catalytic biosensors: they use components able to specifically recognize biomolecules and convert them by a chemical reaction. The most known catalytic biosensors are enzymatic ones. These biosensors use natural enzymes and combinations of them. Also, it was discovered that some DNA polynucleotides, known as DNAzymes can mimic the behavior of enzymes. More

recently the same effect was observed in nanozymes, which are nanomaterials with catalytic properties. Catalytic biosensors besides of measuring the concentration of substrates are also able to measure the inhibition rate of a catalytic reaction and the catalytic activity. Catalytic bioreceptors catalyze reactions in a very specific manner. The products generated by the reaction or the reactants consumed can be directly detected if they have any measurable optical or electrical property. In other cases, it is necessary to add a coenzyme or a substrate which changes its optical properties or gives electrons during the reaction.

- Affinity biosensors: they use the capability of a bioreceptor to recognize an analyte. Depending on the nature of these bioreceptor it is possible to distinguish between immunosensors and DNA sensors. The former uses the specific interaction between an antibody and an antigen. The latter uses DNA or aptamers specific interactions with DNA, proteins or other biomolecules.

Among the different types of biosensors based on biorecognition elements, the immunoasays are described below with special emphasis due to its further use in the experimental part of this thesis.

### 1.3.1. Immunoassays

The health and biomedicine sector are currently the main market sector interested in the development of biosensors. Among all the existing biomarkers, the most employed are proteins because they are usually related to the most common diseases. Nowadays, the most used technique for protein detection are immunoassays. Immunoassays are a type of analytical technique that uses the reaction between an antigen and its antibody to determine the amount of antigen present in a sample. The use of antibodies has the advantage of high selectivity towards its antigen. In immunoassays, a large number of samples can be evaluated at once and extensive sample preparation is rarely required due to the great specificity of immunoassay methods.

### 1.3.1.1. Classification of immunoassays

Immunoassays use the capability of an antibody to specifically recognize an antigen. The most used immunosensors are shown in Figure 5.

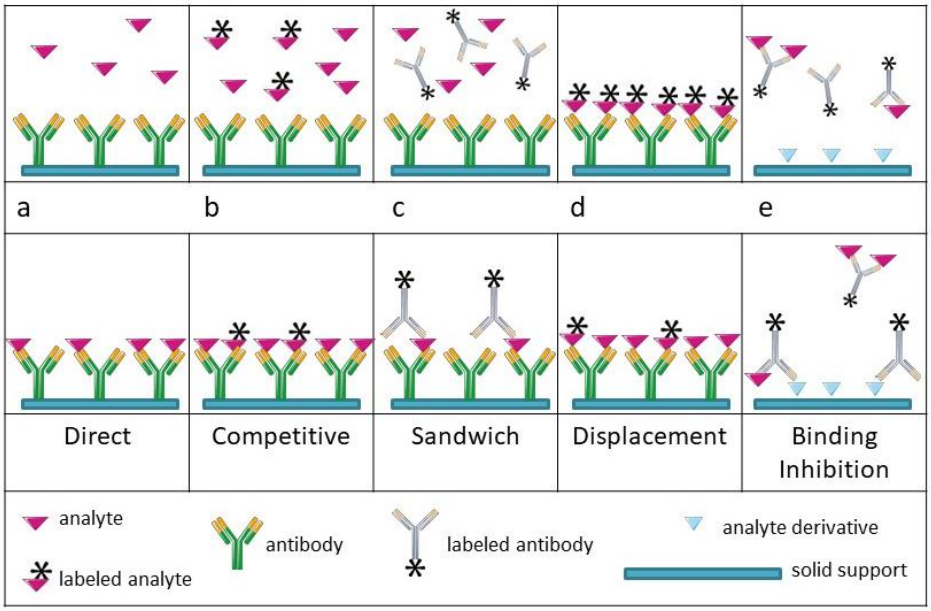


Figure 5. Types of immunosensors: direct (a), competitive (b), sandwich (c), displacement (d) and binding inhibition (e).

- Direct Immunosensors: an unlabelled antigen binds to an unlabelled antibody. The change in refractive index is measured. However, the change is small due to the low mass of antigens and these kinds of immunosensors are not used often.
- Competitive Immunosensors: the unlabelled antigen and its labelled form compete for a binding site of the antibody. This method can be also employed for the detection of antibody concentration by immobilizing the antigen and making a competition between the naked antibody and the labelled antibody.
- Sandwich Immunosensors: the antigen is trapped by the capture antibody. After, a labelled antibody acting as the detection antibody is added and it bound to the antigen. The signal given by the optical property of the detection antibody is proportional to the concentration of antigen.
- Displacement Immunosensors: the capture antibody binding sites are saturated with labelled antigen. The introduction in the media of the unlabelled antigen causes the displacement of the labelled antigen.

- Binding inhibition Immunosensors: an unlabeled analyte derivative is immobilized on a surface. Then a labeled antibody is mixed with the sample containing the antigen. In the absence of antigen in the sample, the labeled antibody can bind the surface. The presence of the antigen blocks the paratopes and the binding is inhibited.

Various immunoassays were evaluated in this thesis with different aim based on the characteristics of antibodies containing NCs. The first immunoassay that has been tested is a simple direct immunoassay to test if the antibody still has affinity for its antigen. The analyte has been immobilized in the surface of a microplate and the catalytic properties of the antibody carrying NCs were used to detect the analyte adsorb in the surface. The second is a sandwich immunoassay to probe than the antibody carrying NCs are potential candidates to be used as detection antibodies in commercial ELISA due to its competitive performance. In this immunoassay a naked antibody is immobilized in the surface of a well, this antibody specifically interacts with the analyte and finally the detection is carried out using the catalytic properties of the modified antibody. Finally, a competitive immunoassay based on FRET has been developed taking advantage of the fluorescent properties of the antibody carrying NCs. FRET is a phenomenon which takes place when two fluorescent compounds, donor and acceptor are very close. The excitation of the donor leads to transfer energy to the acceptor which emits at a specific wavelength. In this case the donors are the NCs and the acceptor a fluorophore bound to the analyte. FRET emission depends on the distance between the two fluorophores. Therefore, the energy transfer will only take place when the antibodies are bound to their corresponding antigens. If the unlabelled antigen is introduced into the system, it will displace their labeled analogues and the FRET emission will decrease.

#### 1.3.1.2. Classical labelling strategies for immunoassays

To label a molecule means to carry out a chemical reaction between an analyte and a reagent. As a result of the reaction a product, which makes possible the detection of a biorecognition event, is produced. The classical labeling strategies for antibodies to be used in immunoassays distinguish between the direct labeling strategies and the enzyme labeling. In the former, we found radioimmunoassays and fluoroimmunoassays.

Both labeling strategies have in common that the detection of the analyte is directly possible after the binding. In the case of enzyme labeling a chemical amplification reaction with a formation of a substance, with some measurable property, is needed for the detection.

- Radioimmunoassay

The working principle of radioimmunoassays is based in the competition between labeled and unlabeled antigen for corresponding antibody and the formation of antigen-antibody complexes. The antigens are labeled with radioisotopes such as $^{125}I$ or $^{3}H$. When the equilibrium is reached the radioactive complexes are separated from the radioactive antigens free in solution. The ratio between the antibody-antigen radioactive complexes and the free radioactive antigen (C/F) depends in the concentration of nonradioactive antigen. The determination of the unknown unlabeled antigen concentration is determined by comparing the ratio of (C/F) obtained by the incubation with different known concentrations of nonradioactive antigen with same quantity of antibody and then in the sample with unknown concentration of unlabeled antigen[13].

The first radioimmunoassay was develop by Rosalyn Yallow and Solomon Berson in 1960[14] for the quantification of insulin in plasma using insulin labeled with the radioisotope $^{131}I$. After, other radioimmunoassays were developed, for example for the protein hormone leptin in human plasma. In this method the radioisotope $^{125}I$ was used for the labeling of leptin. This method achieves accurate and sensitive measurements of leptin with a limit of detection (LOD) of 0.5 µg/mL. The leptin concentration increased in a linear manner with the body mass index in both men and women, however the increasing was greater in women[15].

Radioimmunoassays found different applications because they were one of the most sensitive and accurate methods and were used for a long period. Currently they are in lack in use because its application has lot of problems. The major drawback is the radioactivity, the duration of the antigens labeled with isotopes is short and during the development of the immunoassy it is needed safety precautions and special laboratory

equipment which results in high cost. Due to these problems other kinds of immunoassays with competitive LOD have gain popularity[16].

- Fluoroimmunoassay

In this direct labelling strategy, an antibody or an antigen is labelled with a fluorescent dye. Labelling antibodies with fluorophores combines the selectivity of antibody-binding interaction with simple, sensitive, inexpensive and hazard-free fluorescent detection. Two different kinds of fluoroimmunoassays can be distinguished the heterogeneous one and the homogeneous one. In the former it is necessary to separate the bound from free fluorescent dye. In the latter the separation is not required.

The first fluorophore used as dye in homogeneous assays and coupled to an antibody without changing their specificity was a rhodamine[17]. Another fluorophores thoroughly used are or Lucifer yellow VS[18] or fluorescein[19]. With this kind of labels detection limits tends to be high due to background fluorescence and quenching problems.

In order to overcome the drawback of background signal, fluorophores excited in the red or the IR-near region were employed[20]. The other strategy was to use homogeneous immunoassays such as FRET that improve the LOD of immunoassays, avoid washing steps and also quenching problems. Although this last approach has reduced the LOD of fluoroimmunoassays they are not as good as in the radioimmunoassys. In the case of need an immunoassays in which moderate LOD need to be obtain, these immunoassays would be a good choice due to the easy handling[16]. Antibody carrying NCs with fluorescent properties will be tested as candidates to act as donor in FRET immunoasays.

- Enzyme immunoassay

A big number of enzymes are currently used in bioassays with a variety of detection systems such as fluorescence, UV-vis absorbance, electrochemical detection, bioluminescence or chemiluminiscence. Enzymes in bioassays required high selectivity, no contamination, pH optimum should fit with the conditions of the assay and a competitive cost[21]. In Table 1. is showed a selection of most used enzymes in bioassays with the detection system employed and substrate.

Table 1. Enzymes used in bioassays.

| Enzyme | Origin | Molecular mass (kDa) | pH optimum | Detection | Substrate |
|---|---|---|---|---|---|
| **Alkaline phosphatase** | Calf intestine | 140 | 9.8 | Fluorescence | 2-(5'-chloro-2'-phosphoryloxyphenyl)-6-chloro-4-(3H)-quinazolinone (ELF-97)[22] |
| | | | | UV-vis | p-nitrophenyl phosphate (pNPP) [23] |
| | | | | Electrochemistry | Hydroquinone diphosphate (HQDP) [24] |
| **β-D-Galactosidase** | *Escherichia coli* | 465 | 8 | Fluorescence | 9H-(1,3-dichloro-9,9-dimethylacridin-2-one-7-yl) beta-d-galactopyranoside (DDAOG) [25] |
| | | | | UV-vis | 7-β-D-Galactopyranosyloxy-9,9-dimetyl-9H-acrindin-2-one[26] |
| **β-D-Glucose oxidase** | *Aspergillus niger* | 160 | 5.5-6.5 | Fluorescence | Homovanillic Acid [27] |
| | | | | UV-vis | 3-methyl-2-benzothiazolinone hydrazone (MBTH) and 3-(dimethylamino)benzoic acid (DMAB)[28] |
| **Luciferase** | *Photinus pyralis* | 100 | 7.5-7.8 | Bioluminiscence | ATP [29] |
| **Peroxidase** | Horseradish | 44 | 6.0-7.0 | Fluorescence | Polisulfane (HSnH) [30] |
| | | | | Fluorescence | Amplex Red[31] |
| | | | | UV-vis | 2,2'-Azino-bis(3-ethylbenzthiazoline-6-sulfonic acid) (ABTS)[32] |
| | | | | UV-vis | *o*-Phenylenediamine (OPD)[33] |
| | | | | UV-vis | 3,3',5,5'-tetramethylbenzidine (TMB)[34] |
| | | | | Amperometric | TMB [35] |
| **Xanthine oxidase** | Bovine milk | 283 | 8.5-9 | Chemiluminiscence | Luminol[36] |

Enzymes are currently the most employed method for labelling antibodies or antigens for its further use in immunoassays. The great acceptance of the method yields in the competitive LOD achieved, similar to those obtained with radioimmunoassays and because no radioactive substances are necessary anymore. The requirements for the use of enzymes as labels in immunoassays are that the coupling of the enzyme to the antibody or the antigen should not change the affinity properties of the antibodies and the enzyme activity should not decrease. In the last step of the immunoassay the enzyme catalyzes a reaction that yields in a measurable chromogenic or fluorescent change in a substrate. The most used enzymes with this purpose are ALP and HRP.

Although the LOD improve and the problem of radioactivity is solved with the use of natural enzymes as markers, the method has several disadvantages, for example high susceptibility to environmental variations, easy denaturation and digestion, costly and time-consuming preparation and purification [37]. The enzymes and antibodies are incubated with crosslinking reagents and then the conjugate is purified. Some of the most used crosslinkers reagents are glutaraldehyde [38], periodate [39] or maleimide [40]. The reactivities of enzymes and antibodies with the crosslinkers are different, resulting in the formation of not only heteropolymers but also homopolymers by random coupling. Polymers in which antibodies are not full reactive may not be eliminated by conventional purification processes and cause high background signals and low precision due to nonspecific absorption of heteropolymers, while homopolymers (IgG-IgG and HRP-HRP) are of no use at all for detection of analytes. These methods are not suitable for ultrasensitive enzyme immunoassays [41]. Antibodies and enzymes can be indirectly and non-covalently crosslinked based on the strong affinity between biotin and avidin [42]. A feature of this method is amplification signals achieved by introduction of many biotin residues into antibody molecules and subsequent binding of avidin linked to enzyme molecules. However, nonspecific binding is also amplified. Therefore, a new kind of label for biomolecules is needed, that gives better signals and retains enough biological activity for use in immunoassays. The introduction of NCs with enzyme-like properties in the structure of antibodies avoid the labelling drawbacks linked to the use of enzymes as labels.

## 1.4. Classification of biosensor based on transduction elements

Based on the transduction element used by a biosensor, it is possible to distinguish between electrochemical, optical, mass-based, thermal and energy-based biosensor (Figure 6.)

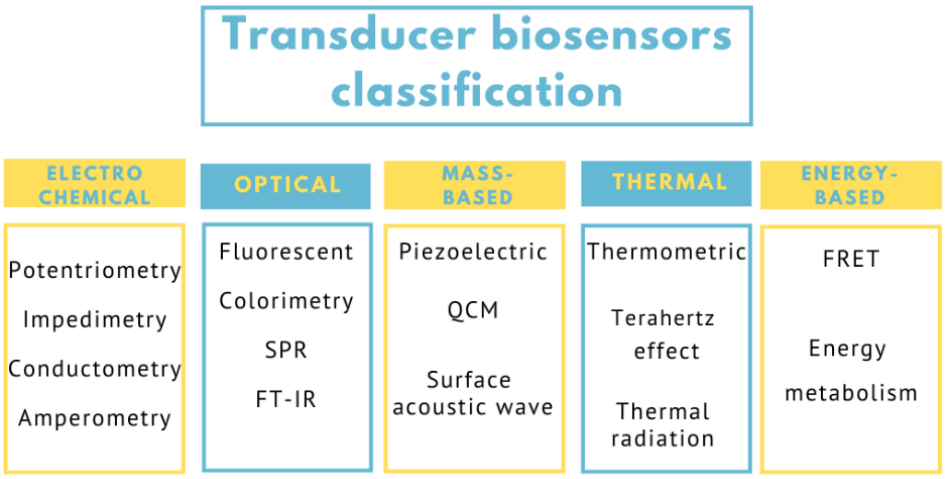


Figure 6. Classification of biosensors based on transduction elements.

- Electrochemical biosensors: These kinds of biosensors are able to provide analytical information by converting a biorecognition event to an electrochemical transduced signal. These biosensors present the advantages of high sensitivity, portability, low cost and simplicity of construction. It is possible to distinguish between different electrochemical techniques. For example, potentiometry, impedimetry or conductrimetry, among others.
- Optical biosensors: they are well-established and have high sensitivity. Usually, these biosensors measure an optical property or its change after the binding of the analyte to the bioreceptors. They are immune to electromagnetic interferences, capable of performing remote sensing and can provide multiplexed detection within a single device[7].

  It is possible to distinguish between different optical biosensors depending of the optical property that is measured. For example, surface Plasmon resonance (SPR), Raman and Fourier transform (FT-IR) spectroscopy, fluorescence effects or colorimetric effects[6]. The colorimetric biosensors relate the absorbance intensity with the analyte concentration. The colored product can be noted by

the naked eye or using a spectrophotometer. Due to the simplicity of the technique and the inexpensive measurement setup it is widely used in the fabrication of cost-effective biosensors, such as paper-based or chip-based microfluidic devices[9].

- Mass-based biosensors: these biosensors measure mass change during the biorecognition event. There are 3 main classes mass-based biosensors, the piezoelectric, the quartz crystal microbalance (QCM) and the surface acoustic wave[6].
- Thermal biosensors: the working principle of these biosensors is the measurement of heat evolved or absorbed during a biochemical reaction. The heat exchanged is proportional to the molar enthalpy and to the amount of products generated during the reaction[10].
- Energy biosensors: they can be classified in biosensors based on energy metabolism and Fluorescence Resonance Energy (FRET). In the former the biosensors detect perturbations in the physiological state of living cells by monitoring perturbations in metabolic activity. The molecule Adenosine Triphosphate (ATP) is one of the most monitored in these systems[11]. In FRET a stimulated state donor transfer energy to a proximal ground-state acceptor by resonance process. Energy transfer takes place at the emission wavelength of the donor where the acceptor absorbs energy[12]. Biosensors based on FRET phenomenon could also be classified into optical ones because at the end, a fluorescence signal is measured.

Here in this work a colorimetric biosensor and a FRET biosensor were developed, based on the properties of the probe formed by the antibody and the NCs. In the case of the bimetallic NCs, they exhibit peroxidase-like activity and are able to transform uncolored compounds into colored ones, thus the transduction step is due through colorimetric measurements. On the other hand, CdS NCs have fluorescent properties and the transduction step of the FRET-based biosensor is due to an energy transfer and measured by fluorescence spectroscopy.

# 2. NANOTECHNOLOGY APPLIED TO BIOSENSORS

## 2.1. Nanotechnology of yesterday and today

*Why cannot we write the entire 24 volumes of the Encyclopaedia Brittanica on the head of a pin?* [43] With that question, Richard Feynman introduced his famous talk *There's Plenty of Room at the Bottom*, which he gave at Caltech in 1959. Feynman is considered the father of nanotechnology and suggested the use of small machines to make even tinier machines, and so on down to the atomic level itself. But it was necessary to wait until 1974 to hear for the first time a description of Nanotechnology. The definition of Norio Taniguchi, of Tokyo science University still stands as the basic statement: *Nanotechnology mainly consists of the processing of separation, consolidation and deformation of materials by one atom or one molecule*[44]. However, the idea of nanotechnology as it is currently understood is the brainchild of a Feynman's student, K. Eric Drexler who proposed in 1986 the conception of a nanoscale assembler which would be able to build a copy of itself and of other items of arbitrary complexity[45].

Before giving a definition of nanotechnology it is interesting to pay attention to the etymology of the prefix *nano*. It comes from the Greek word *νᾶνος* and means extremely small, exactly, $10^{-9}$ m, one thousand times smaller than a micron. Although the simplest manner to define nanotechnology is as the technology on the nanoscale[46], since the beginning of its appearance different definitions have been attributed to it. Nanotechnology can be defined like an engineering discipline that will make possible to build devices and structures in which every atom is in a known, selected position[47]. Also as the term used for the description of the creation and exploitation of materials with structural features in between those of atoms and bulk materials, with at least one dimension in the nanometer range[48]. As well the branch of knowledge, within a subclassification of technology in colloidal science, chemistry, physics, biology, and other scientific fields, encompassing the study of phenomena at the nanoscale[49].

From the study of the objects at the nanoscale a new science arose, it is the nanoscience. The emerging science of objects that are intermediate in size between the largest molecules and the smallest structures, the science of objects with the smallest dimensions [50]. To summarize nanoscience studies are considered those that deal with

matter that have at least one dimension less than 100 nm, have building block properties and employ methodologies that illustrate the fundamental control of the physical and chemical characteristics of molecular-scale structures[46].

Currently, materials at the nanoscale have important applications in electronics[51, 52], water treatment[53, 54], photovoltaic[55, 56], batteries[57, 58], sensing[59, 60], biosensing[61, 62, 63], theranostic[64, 65] , photothermal therapy[66, 67], bactericides[68, 69] or drug delivery[70, 71], among others. This is due to its unique physicochemical properties in comparison with bulk materials such as optical[72, 73, 74], electrical[75, 76, 77], thermal[78, 79, 80], magnetic[81, 82, 83] or catalytic properties[84, 85, 86] because of the nanoscale effect. This effect consists in dramatic changes in properties due to the increase of the ratio surface/volume[87]. It is easy to understand if we consider a cube of a side length of 10. The volume of the cube is 1000 (10x10x10) and the surface area of the cube is 600 (6x10x10), then the ratio surface/volume is 0.6. Next, we repeat but using a cube with a side length of 1. The volume is 1 (1x1x1) and the surface area is 6 (6x1x1). The ratio surface/volume is 6, greater than for the previous cube. Thus, smaller the size, greater the surface/volume ratio.

A good example of this phenomenon is gold. This yellow metal is so appreciated in bulk for the fabrication of jewels and prostheses because it is an extremely inert metal[88]. However, when the dimensions of gold are reduced to the nanoscale its properties drastically change. The yellow color disappears and it is possible to find gold at the nanoscale in a wide variety of colors, depending of the size of the nanoparticles (NPs)[89] and it also lose its inert properties and became catalytic[90, 91]. Carbon in its allotropic form graphite is composed by layers of hexagonal arrangement of atoms. One carbon atom is forming a sigma bond with three other carbon atoms and there is a non hybridized p orbital that forms a $\pi$ valence band and a $\pi^*$ conduction band with the p orbitals of neighboring carbon atoms. Each layer is connected by weaker intermolecular bonds, making graphite soft and malleable. It is also a heat and electric conductor due to delocalized $\pi$ electrons, which have a great mobility in directions parallel to the layers. When graphite is exfoliated and a unique layer is achieved it is called graphene and it has a dimension at the nanoscale. The planar structure of graphene makes its properties

highly anisotropic. Graphene has unique properties of electrical and heating conduction greater than those of graphite, due to the enhanced phonons mobility[92].

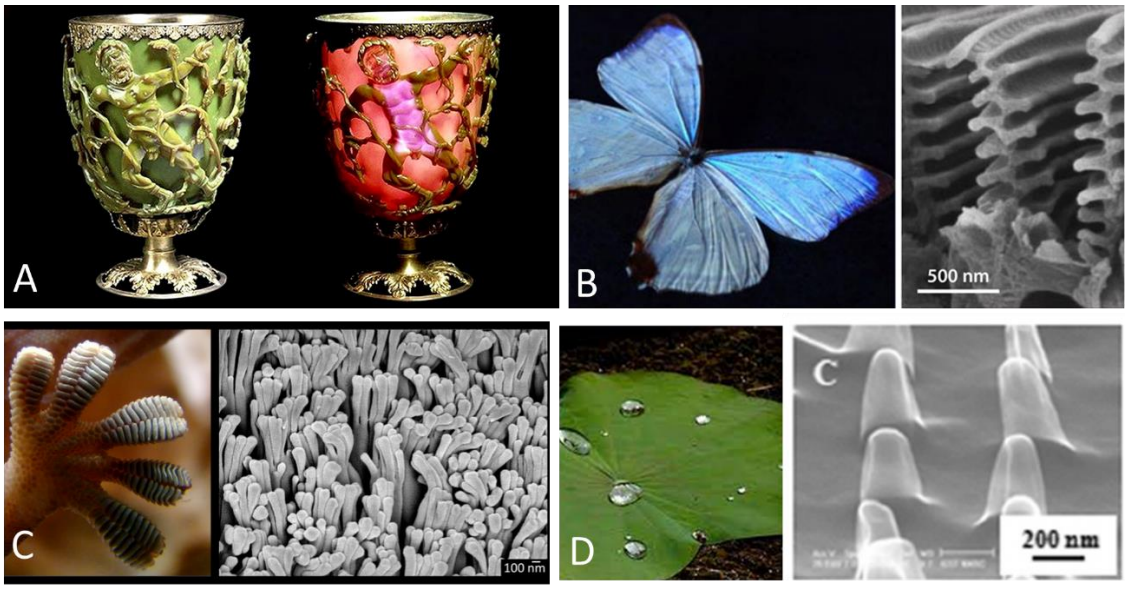


Figure 7. Licurgus cup with reflected light (left) and transmitted light (right) (A), wings of the butterfly *T. opisena* (B), toe of a gecko (C) and leaves of a Lotus plant (D) at the macroscale (left) and the nanoscale (right).

Nanotechnology and nanoscience could look like such a very new field, however we can find an ornamental example of the use of nanomaterials in the 4$^{th}$ century in the Roman age, the famous Lycurgus cup (Figure 7A.). This glass exhibit dichroism, it has a green color when the light is reflected and a red one when white light is transmitted across it[93]. This particular effect has shocked scientist during centuries, until the presence of NPs in the glass was discovered[94]. The red color is due to the presence of gold NPs and the green one due to silver NPs[95]. Although, almost sure that Romans did not know anything about nanomaterials they were able to use nanotechnology with a decorative purpose a lot of years ago before nanoscience boom.

Neither butterflies, geckos nor leaves know anything about nanotechnology, but they take advantage of it. The green color of the wings of the butterfly *T. opisena* is caused by a nanostructured biophotonic gyroid material, presumably formed by the chitin polymerization[96] (Figure 7B.). Geckos are able to climb vertical walls due to hair-like nanostructures of 200 nm placed on their toes(Figure 7C.). These nanostructures are

formed by hydrophobic keratin and act as a bed of springs[97]. The leaves of *Nelumbo nucifera*, colloquially known as Lotus plant, stay always in a perfect state of cleanliness even though are surrounded by muddy water. This effect of self-cleaning or Lotus-effect is due to the presence of nanometric wax crystals that form 3D structures similar to nipples (Figure 7D.). The presence of these nanostructures and the water repellent properties of waxes gives the surface of leaves superhydrophobic properties with a contact angle of a water droplet greater than 150°[98]. The observation of nature inspire scientist and copy these natural nanostructures. The nanostructures of the wings of butterflies have been used as templates for the synthesis of 3D rutile nanostructures for further use as coatings of high refractive index for particular optical devices applications such as efficient waveguides or mirrors[99]. Other example is a new kind of dry adhesives inspire in Gecko's feet. This technology uses macroscopic arrays of vertically-aligned multi-walled carbon nanotubes that showed adhesion forces 200 times higher than those of geckos[100]. Also the superhydrophobicity of Lotus leaves has been mimic for the production of synthetic superhydrophobic materials such as surface modified ZnO NPs for the production of superhydrophobic textiles[101].

As we can see nanomaterials have been around for longer than we think and much more before than the words nanotechnology or nanoscience were coined. However, it was necessary a lot of time to be able of see that there's *Plenty of Room at the Bottom.*

## 2.2. Nanobiosensors: general overview

By the merging of nanotechnology with biosensors a new concept has emerged, nanobiosensors. A nanobiosensor can be described as a sensor system that includes the use of nanomaterials for the detection of an analyte via biological interactions.

There is a growing demand in medicine for rapid, reliable, and low-cost systems for detecting, monitoring and the diagnosis of biological molecules and diseases. The ability to detect related proteins, nucleic acid sequences, organelles, cell receptors, enzymes, and other indicators linked with diseases and pathogens can give biological researchers and physicians a complete understanding of disease processes and patient situation.

However, many of the existing traditional tests are slow, require a considerable amount of sample material, and might result in false positive or negative results. This demand extends to other fields such as environmental pollutant monitoring, food pathogen detection and so on. To address the needs in a range of fields, the next generation of biosensors will require significant improvements in sensitivity and specificity. The current state-of-the-art diagnostic biosensors are based on several technologies, often including immunoassays. Nanobiosensor research intends to integrate nanomaterials into low-cost, user-friendly, and efficient biosensors with applications in a variety of sectors, including diagnosis and food analysis.

Although few sensors based on nanomaterials work at all in commercial applications, they have fascinating prospects. The nanobiosensor market is expected to register a CAGR of 10 %, during the forecast period 2021-2026 according by Mordor Intelligence.

There is no competition between significant companies and therefore the market is neither fragmented nor consolidated. As a result, there will be a moderate level of market concentration. To maintain their market dominance and form strategic relationships, the top companies continue to innovate. ACON laboratories, Abbot Point of Care, Agilent Technologies, Nanowear and AerBetic are the leading contenders.

## 2.3. Nanomaterials for biosensing purposes

The size constraints of nanomaterials provide them very special properties since they have most of their atoms located at the surface. These properties highly differ from the properties of the same material in bulk. Nanomaterials can play very efficient roles in the sensing mechanism of biosensor technology[103]. Nanomaterials can contribute to either the biorecognition element or the transducer or both, of the biosensor[102]. The most employed ones and their key benefits are:

- Carbon nanotubes: they can serve as scaffolds for immobilization of biomolecules at their surface. Also, combine several exceptional physical, chemical, electrical, and optical characteristics properties which make them one

of the best suited materials for the transduction of signals associated with the recognition of analytes[104].

- Metallic nanoparticles: they show unique physicochemical properties, such as ease of functionalization via simple chemistry and high surface-to-volume ratios, that allied with their unique spectral and optical properties have prompted the development of numerous biosensing platforms. They also provide an additional or enhanced layer of application for commonly used techniques, such as fluorescence, infrared and Raman spectroscopy. Additionally, catalytic behavior and enzyme-like activity has been also found in this nanomaterial[105].
- Magnetic nanoparticles: these NPs are inexpensive to produce, physically and chemically stable, biocompatible and environmentally safe. In addition, biological samples exhibit no magnetic background, and thus highly sensitive measurements can be performed[106].
- Quantum dots: they exhibit unique properties due to quantum confinement effects. Their most remarkable properties are broad excitation and narrow size-tunable emission spectra, negligible photobleaching and high photochemical stability. Fluorescence is a powerful tool in biological research, therefore the optical and spectroscopic features of QDs make them attractive alternatives to traditional fluorophores[107].
- Nanorods: their advantages include spectral tunability, strong enhancement of the local electric field and the localized plasmons provide them improved sensitivity in biosensing applications[108].
- Nanoclusters: they exhibit molecule-like properties, such as fluorescence emission or catalytic activity, acting as nanozymes. NCs have higher surface/volume ratio than bigger NPs, brighter emission and higher catalytic activity in comparison with other nanomaterials of the same mass.

Here in this thesis NCs are going to be used to the development of various immunoassays. Due to their extremely small dimensions, lower than 2 nm, they have the perfect size to be introduced in an antibody structure which is around 12-15 nm. Their properties make them excellent transducers for biosensing applications. On the one hand, the NCs can have nanozyme properties and can mimic the behaviour

of enzymes. On the other hand, NCs can also exhibit fluorescent properties and act as QDs in biosensing applications. Below, there are extensively discussed the properties and applications in biosensing of nanozymes, QDs and NCs.

## 2.4. Nanozymes: definition, classification and applications

### 2.4.1. Definition and historical overview

Natural enzymes are used to catalyze the transformation of molecules, regularly these reactions are performed under mild conditions due to its fragile nature. Enzymes are used in different fields like industry, medical or biological due to its substrate specificity and catalytic activities[109]. In industry enzymes are used in food manufacturing, animal nutrition, cosmetics, medication and as a tool for research and development. However, enzymes are considered too delicate to survive the extreme conditions in real reaction vessels[110]. Industrial catalysts should deal with harsh conditions such as high temperature and pressure, organic solvents or extreme pH conditions[111].

The intrinsic limitations of natural enzymes such as high cost for preparation and purification, low stability, difficulty in storage, sensitivity of catalytic activity to environmental conditions and difficulties in recycling and storage have stimulated the emergence and development of enzyme mimics also called artificial enzymes [112]. The term artificial enzymes was coined by Ronald Breslow[113] in 1970.

Different materials can act as artificial enzymes such as cyclodextrins, cyclophanes, palladium-artificial enzyme, hemin based organic phase artificial enzymes, Vitamin B12 or Ethyleneimine Polyethyleneimine[114]. In Figure 8. a short timeline for the development of artificial enzymes is showed.

Among them the most promising materials are nanozymes, since the discovery of peroxidase-like activity of $Fe_3O_4$ in 2007[115]. Nanozymes are materials in the nanoscale that can mimic the behaviour of an enzyme. In comparison with natural enzymes, nanozymes have stable structure, adjustable activity and diverse functions, making them potential substitutes for natural enzymes in many applications[116].

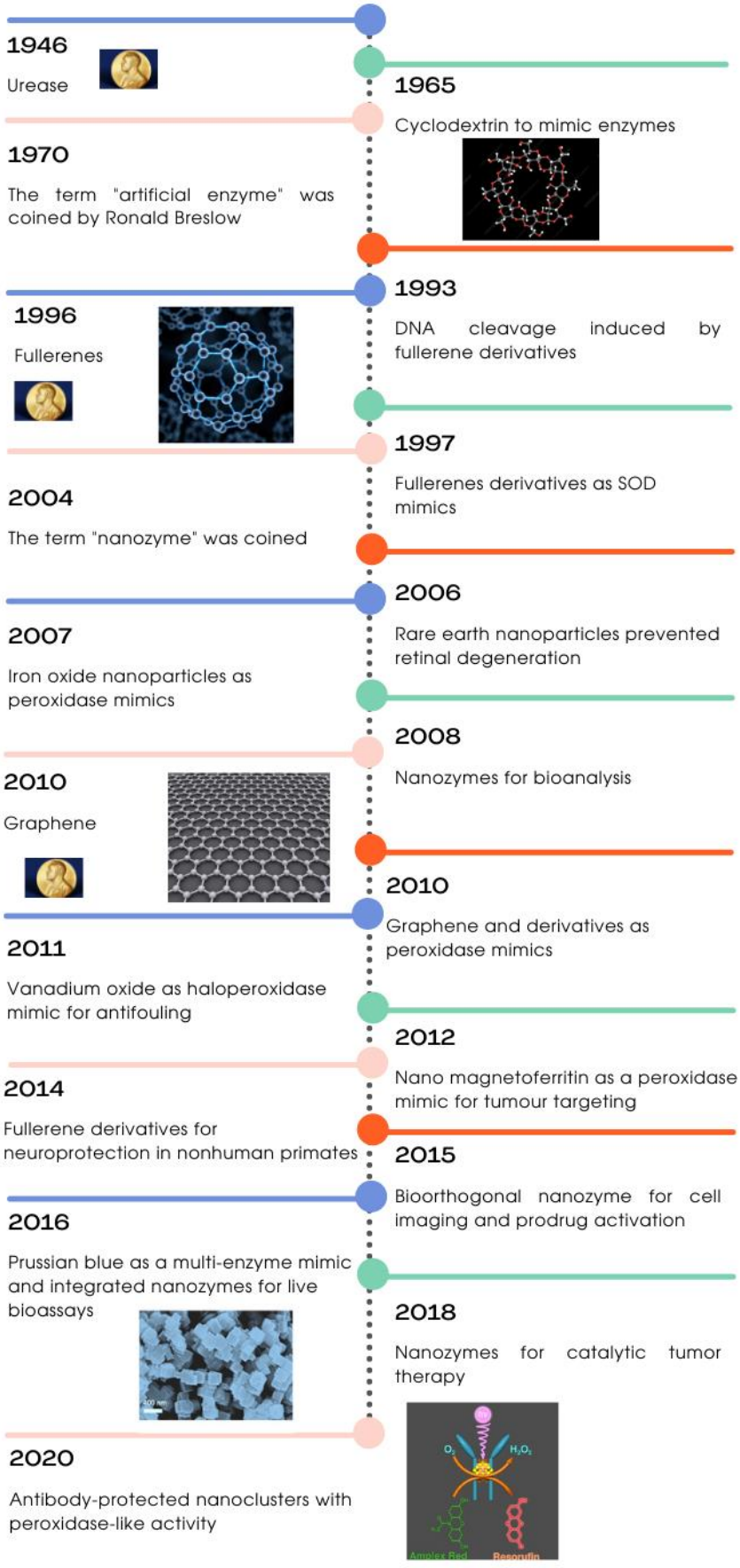


Figure 8. Time line for the development of artificial enzymes[117].

### 2.4.2. Classification of nanozymes based on its enzymatic behaviour

Throughout the last years, different nanomaterials have been found to have unexpected enzyme-like catalytic properties. The increasing interest in the field of nanozymes arise from improve characteristics in comparison with natural enzymes and even with conventional artificial enzymes. In Table 2. a nanozyme classification is exposed based on the enzyme-like behaviour of nanomaterials. It is possible to find nanozymes with glucose oxidase, laccase, sulfite oxidase, nitric oxide synthase, HRP, glutathione peroxidase, haloperoxidase and catalase behaviour.

In this work three different types of nanozymes with peroxidase-like properties have been developed.

### 2.4.3. Nanozymes in sensing and other applications

Due to its unique properties nanozymes have found a place in the field of sensing. Also, it is possible to find examples of nanozymes in other applications such as environmental treatment, antibacterial and antioxidation agents, imaging, cancer treatment or biorthogonal catalysis (Figure 9.).

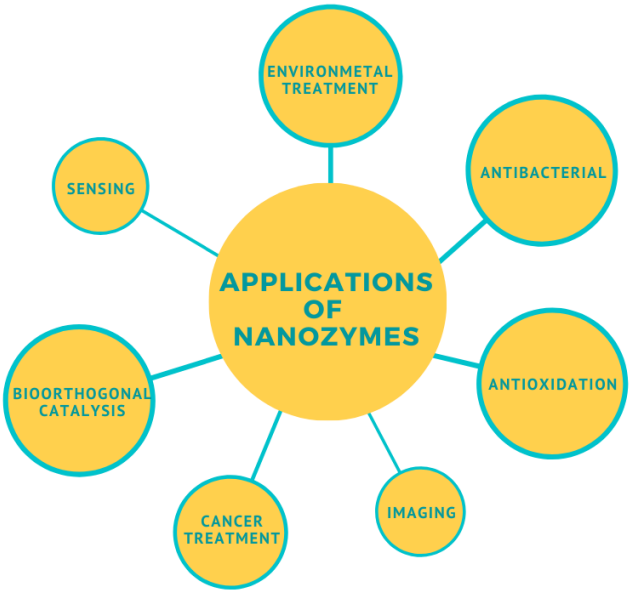


Figure 9. Current applications of nanozymes

Table 2. Nanomaterials with enzyme-like behaviour and their application.

| Enzyme-like activity | Nanomaterial | Application | Ref |
|---|---|---|---|
| **Glucose oxidase** | AuNPs | Sensing | 118 |
| | AuNPs@AuNCs | Sensing | 119 |
| | $CeO_2$ | Sensing | 120 |
| | Graphitic carbon nitride | Sensing | 121 |
| **Laccase** | CuNPs | Degradation pollutants | 122 |
| **Sulfite Oxidase** | $MoO_3$ | Cytoprotection | 123 |
| **Nitric Oxide Synthase** | Graphene-hemin | Antithrombosis | 124 |
| **HRP** | $Fe_3O_4$ NPs | Immunoassay | 125 |
| | AuNPs | Immunoassay | 126 |
| | Au/Pt/Co NPs | Waterwaste decontamination | 127 |
| | Co/Fe-hemin | Detection SARS-CoV-2 | 128 |
| | $Fe_3O_4$ NPs | Gelation | 129 |
| | Au Nanowires | Glucose sensing | 130 |
| | Au@Co-Fe NPs | Antibacterial | 131 |
| | Co@ $Fe_3O_4$ NPs | Cancer therapy | 132 |
| **Glutathione peroxidase** | Au NPs | Sensing | 133 |
| | Se@Carbon QDs | Antioxidant, imaging | 134 |
| **Haloperoxidase** | $CeO_{2-X}$ Nanorods | Antibacterial | 135 |
| **Catalase** | Au NPs | Antioxidant | 136 |
| | $Co_3O_4$ | Sensing | 137 |
| | Pt-C6 NPs | Cancer therapy | 138 |
| **Superoxide dismutase** | Au/Ag NPs | Antioxidant | 139 |
| | $Mn_3O_4$ | Cytoprotection | 140 |
| | Pt@Mn-MOF | Anti-inflammatory therapy | 141 |
| **Nuclease** | Graphene oxide | DNA cleavage | 142 |
| **Phosphatase** | $CeO_2$ | Sensing | 143 |
| | $CeO_2$ | Degradation of nerve agents | 144 |
| | AuNPs@POMD-8pe | Alzheimer's disease therapy | 145 |

- **Sensing**

The peroxidase-like activity of some nanozymes has led the successfully design of nanozyme-based biosensors for the detection of ions, small molecules, nucleic acids or proteins.

○ Detection of ions: Heavy metal ions are not well metabolized by humans and their accumulation in some organs can lead in serious health injuries. These metal ions can achieve human organism by water or food; therefore, it is important to measure their concentration. A colorimetric sensor was developed for the detection of $As^{3+}$ based on the peroxidase-like activity of Pd NPs capped with dithiothreitol[146]. These NPs are able to oxidise the chromogenic substrate TMB from colourless to blue. The $As^{3+}$ ions chelate the sulfhydryl groups present in dithiothreitol generating a decrease in the peroxidase-like behaviour of the Pd NPs. The concentration of $As^{3+}$ ions can be related with a decrease in the absorbance signal due to TMB oxidation. For $Hg^{2+}$ ions detection a portable smartphone sensor based on chitosan-functionalized $MoSe_2$ nanosheets has been developed[147]. This nanozyme exhibit also peroxidase-like activity, however in this case the presence of the heavy metal ion active the surface of the nanosheet enhancing the oxidation of TMB. Moreover, nanozymes can be also used for the detection of dangerous non-metal ions such as cyanide ion ($CN^-$). This ion has strong affinity to cytochrome C and it damage central nervous system. A visual detection method was developed for CN- ions in water and laboratory wastes employing amorphous cobalt hydroxide/oxide modified graphene oxide probe[148]. This nanozyme can mimic horseradish peroxidase (HRP) and is able to oxidise non-fluorescent Amplex Red to fluorescent Resorufin. $CN^-$ ions inhibit the catalytic activity of the nanohybrid.

○ Detection of molecules: $H_2O_2$ is a significant target for some diagnosis test because it is a typical product formed by enzymatic reactions and a useful molecule for cell signalling. $H_2O_2$ detection is traditionally made using colorimetric methods based in HRP. However, it shows the typical drawbacks associated to the use of enzymes. A method that used bimetallic Au/Pt NPs with graphene oxide has been developed for its detection[149]. The synergistic effect of both metals gives the nanozyme a strong peroxidase-like activity toward the oxidation of TMB in the presence of $H_2O_2$. The

detection was performed by the immobilization of the nanozyme on agarose microbeads and packed in the surface of an electrode. TMB in the presence of $H_2O_2$ can be electrochemically reduced by the nanozyme.

*Diabetes mellitus* is one of the most spread disease in the world. It causes increasing disability and reduced life expectancy. Glucose is a marker for the diagnosis of diabetes, therefore is one of the most sensed analytes. Nanozymes can achieve the detection of glucose by combining the enzyme GOx and a nanozyme with peroxidase-like properties. For example, a colorimetric method for the analysis of glucose in fruit juice has been developed using reusable $VS_2$ nanosheets[150]. This nanozyme exhibit peroxidase-like activity and its able to oxidise TMB in the presence of $H_2O_2$. Enzyme-free systems for glucose sensing have been also developed with the aid of nanozymes. An hybrid nanosheet composed by AuNPs and a metallorganic framework (MOF) has been developed for this purpose[151]. AuNPs exhibit GOx-like activity and oxidise glucose into gluconic acid, the MOF have peroxidase behaviour and produces as final product $H_2O_2$. Then $H_2O_2$ oxidizes the no Raman-active leucomalachite green into the Raman-active malachite green. In the presence of AuNPs selective surface-enhanced Raman scattering (SERS) the determination of glucose is achieved.

Glutathione (GSH) is the most abundant intracellular thiols containing molecule. It has an important role in many life processes. Especially GSH is a powerful antioxidant, it participates in the detoxification of electrophilic compounds and peroxides via catalysis by glutathione S-transferase and glutathione peroxidase. Moreover, GSH participates also in the glyoxalase system, reduction of ribonucleotides to deoxyribonucleotides, regulation of protein and gene expression[152]. Abnormal concentrations of GSH could cause inflammation, cancer or cardiovascular diseases, therefore is important to control GHS levels. $MnO_2$ nanosheets exhibit peroxidase-like activity and it have been used for GSH sensing[153]. The nanosheets could be decomposed by trace amounts of GSH and therefore the peroxidase-like activity of the nanozyme decreases, leading to the decrease of absorbance at 650 nm.

- Detection of Nucleic Acids: The different affinity of nanomaterials for single-stranded DNA and double-stranded DNA has been used to detect DNA hybridization. For

example, AuNPs which exhibit GOx-like activity, have stronger affinity for single-stranded DNA than for double-stranded DNA. The enzymatic activity of AuNPs is extremely sensitive to surface properties, therefore the non-covalent coupling of the AuNPs with the single stranded DNA reduce the GOx-like activity of the nanozyme. When the GOx-like activity of AuNPs is coupled with HRP and the addition of the chromogenic substrate ABTS it is possible to relate the DNA hybridization with the colour change[154]. Another method for distinguish the DNA hybridization use hemin-graphene nanosheets, stabilised through π-π interactions. This nanozyme have peroxidase-like activity due to the presence of hemin on the graphene surface and it is also able to differentiate between single-stranded DNA and double-stranded DNA. Single-stranded DNA can be adsorbed by graphene due to π-π stacking interactions, in contrast double-stranded DNA cannot stably adsorb on the nanozyme surface. Hemine-graphene nanosheets precipitate in the presence of double-stranded DNA by adding the correct amount of electrolyte, while single-stranded DNA inhibit the precipitation. After centrifugation, by adding the colorimetric substrate TMB and $H_2O_2$ to the supernatant it is possible to distinguish by the naked eye the change in absorbance. Besides this DNA sensor it is also able to differentiate single-nucleotides polymorphisms which are related with tumour development[155].

- Detection of proteins: ELISA is one of the most important applications of HRP. Due to the intrinsic shortcomings of natural enzymes, nanozymes with peroxidase-like activity are attractive substitutes for HRP in this application. In Table 3. some nanozymes used in ELISA are showed.

Many noble metals NPs, including AuNPs or PtNPs are used in biosensors. Both are able to oxidise the chromogenic substrate TMB from colourless to blue in the presence of $H_2O_2$. For example, AuNPs have been used to improve the LOD in a sandwich aptasensor for C-reactive protein detection[156]. The presence of high levels of this protein is related with the risk of developing cardiovascular events. The AuNPs were synthesised by chemical reduction using sodium citrate as reducing and capping agent. The AuNPs were coupled to the sulfydryl modified C-reactive protein aptamer by activating the sulfhydryl group with tris(2-carboxyethyl)phosphine).

Besides ELISA applications, nanozymes with peroxidase-like properties can also be used for sensing proteins using other strategies, for example, for the detection of acetylcholinesterase. This enzyme regulates the level of acetylcholine by its hydrolyzation generating thiocholine. Acetylcholine is a neurotransmitter which participates in synapsis. An incorrect working of acetylcholinesterase is related with neurodegenerative diseases such as Parkinson's disease, Alzheimer's disease or Huntington's disease. $MnO_2$ nanosheets have peroxidase-like properties and are able to oxidise TMB in the presence of $H_2O_2$. The presence of thiocholine trigger the decomposition of the nanozyme causing a decrease in the catalytic performance of the nanosheets and can be related with acetylcholinesterase activity[157].

- Detection of cancer cells: Besides the previously mentioned sensing applications, nanozymes can be used for the detection of cancer cells. The folate receptor is overexpressed on the majority of cancer cells, this fact has been used in various works for the detection of this kind of cells. For example, folate conjugated $CeO_2$ NPs which exhibit oxidase properties can selectively be attached to the overexpressed folate receptor and the colorimetric detection of cancer cells is achieved[172]. Similar approaches have been followed by using other nanozymes. For example, by using folic acid graphene oxide-AuNCs[173]. In this system lysozyme stabilized AuNCs are adsorb on the surface of graphene oxide via electrostatic interaction. The composite exhibit peroxidase-like properties and is able to detect cancer cells. In another example, AuNPs growth on the surface of periodic mesoporous silica-modified reduced graphene oxide is conjugated to folate acid and used for the colorimetric detection of cancer cells[174].

Table 3. Nanozymes used in ELISA assays as substitutes for HRP.

| Type of nanozyme | Type of ELISA | Substrate | Analyte | Detection range | LOD | LOD improvement * |
|---|---|---|---|---|---|---|
| **Mesoporous $SiO_2$/Au-Pt**[158] | sandwich | TMB/$H_2O_2$ | Aflatoxin B1 | 0.01 – 1000 ng $mL^{-1}$ | 5 pg $mL^{-1}$ | 600 |
| **Fe-MOF**[159] | Indirect competitive | TMB/$H_2O_2$ | Aflatoxin B1 | 0.01 – 20 ng $mL^{-1}$ | 0.009 ng $mL^{-1}$ | 20 |
| **AuNPs**[156] | sandwich | TMB/$H_2O_2$ | C-reactive protein | 0.1 – 200 ng $mL^{-1}$ | 8 pg $mL^{-1}$ | 51250 |
| **Prussian blue NPs**[160] | sandwich | TMB/$H_2O_2$ | HSA | 1.2 ng – 1000 ng $mL^{-1}$ | 1.2 ng $mL^{-1}$ | 3 |
| **AuNPs**[161] | sandwich | TMB/$H_2O_2$ | Influenza virus | $5x10^{-15}$ - $5x10^{-6}$ g $mL^{-1}$ | $5x10^{-12}$ g $mL^{-1}$ | 2000 |
| **Graphene-AuNPs**[162] | direct | TMB/$H_2O_2$ | Norovirus | 100 pg $mL^{-1}$– 10 µg $mL^{-1}$ | 92.7 pg $mL^{-1}$ | 112 |
| **$ZnFe_2O_4$@WNT**[163] | sandwich | TMB/$H_2O_2$ | carcinoembryonic antigen | 0.005–30 ng $mL^{-1}$ | 2.6 pg $mL^{-1}$ | 77 |
| **Ceria**[164] | sandwich | TMB/$H_2O_2$ | CA15-3 | 0.01 ng $mL^{-1}$-100 µg $mL^{-1}$ | 0.01 ng $mL^{-1}$ | 10 |
| **Ceria**[165] | direct | Ampliflu/$H_2O_2$ | EpCAM | 300–6000 cells | 300 cells | - |
| **Pt nanocubes**[166] | sandwich | TMB/$H_2O_2$ | PSA | 20–2000 pg $mL^{-1}$ | 0.8 pg $mL^{-1}$ | 10 |
| **PtNPs**[167] | sandwich | TMB/$H_2O_2$ | HIV p24 | 1–10000 pg $mL^{-1}$ | 0.8 pg $mL^{-1}$ | 1.3 |
| **Hemin-Au@MOF**[168] | sandwich | TMB/$H_2O_2$ | α-fetoprotein | 0.080–43 ng $mL^{-1}$ | 0.020 ng $mL^{-1}$ | 5 |
| **Cu-MOF**[169] | sandwich | TMB/$H_2O_2$ | mouse IgG | 1–100 ng $mL^{-1}$ | 0.34 ng $mL^{-1}$ | 3 |
| **PdNPs**[170] | sandwich | CN/DAB/ $H_2O_2$ | PSA | 2–1200 pg $mL^{-1}$ | 0.67 pg $mL^{-1}$ | 110 |
| **$MnO_2$**[171] | sandwich | TMB/$H_2O_2$ | α-fetoprotein | 6.25–400 ng $mL^{-1}$ | 21.6 pg $mL^{-1}$ | 5 |

*LOD improvement in comparison with traditional ELISA.

- **Nanozymes in environmental treatment**

In some occasions industry causes problems to the surrounding environment causing the destruction of the ecological system. One example is the contamination of natural water by organic pollutants such as lindane. Lindane is the gamma isomer of 1,2,3,4,5,6-hexachlorocyclohexane (HCH) and it has been one of the most used pesticides. Only the gamma isomer exhibit pesticide properties, the other isomers must be separate and became waste. To produce 1 tonne of lindane, 8-12 tonnes of waste HCH isomers are generated. Special attention was given to the huge contamination caused by the lindane producer Inquinosa, which produced 140000 tonnes of HCH waster between 1947 and 1992 that were buried in several uncontrolled dumps in Sabiñánigo (Spain). The lindane filtrate and contaminate the soil and the Gállego river. More than 20 years after the Inquinosa company stopped its activity the population living at the border of Gállego was warned of too high lindane concentration in their drinking water[175]. Natural enzymes for water treatment and the decomposition of organic pollutant have been used, the most used enzyme is HRP. It catalyse $H_2O_2$ to generate OH radicals, which can oxidise the pollutant organic compounds to insoluble precipitated products[109]. In order to overcome the drawbacks associated to the use of natural enzymes, nanozymes as enzyme mimics are used in environmental treatment. For example, N-doped $TiO_2$ NPs exhibit photocatalytic activity triggered by the exposure to visible light and have been used to degrade lindane in water[176]. Also, reduced graphene oxide-silver nanocomposites are able to convert lindane in to AgCl and different isomers of trichlorobenzene, which are adsorbed on the graphene substrate by π-π interactions. The high conversion capacity of this nanocomposite and its recycling ability makes this nanozyme a promising material for applications in sustainable water treatment[177].

- **Nazozymes as antibacterial**

Infections caused by bacteria affect to millions of people and it still being a health problem in all the world. The most used antimicrobial agents are antibiotic. The overuse of antibiotics causes the increasing appearance of multi-drug-resistant bacteria; therefore, it is necessary the development of new materials with antibacterial properties. Nanozymes as antibacterial have become a promising alternative due to its

broad band antimicrobial ability and a lack of resistance[178]. Nanozymes with oxidase and peroxidase activity can convert molecules from the environment into toxic components for bacteria, such as reactive oxygen species (ROS), causing the bacteria death. Interestingly, Pd nanocrystals exhibit antibacterial properties generated by ROS, which change with its crystalline structure. {100}-faceted Pd cubes have higher enzyme-like activity than {111}-faceted Pd octahedrons. In Gram-positive bacteria, Pd nanocrystals tend to accumulate on the surface of membrane, therefore {100}-faceted Pd cubes have higher kill activity in this case. Nevertheless, in the case of Gram-negative bacteria {111}-faceted Pd octahedrons exhibit higher penetration into bacterial membranes causing higher damage to bacteria than Pd cubes[179].

- **Antioxidant**

ROS, as $O_2^{\cdot-}$, ·OH and $H_2O_2$, are products of cell metabolism. They do not involve a risk at low levels since they act as second messengers and participate in signalling processes. However, when ROS are overexpressed, they induce oxidative damages to biomolecules and can cause cell apoptosis by activating the enzyme caspase[180]. Also, ROS are related with neurodegeneration, cancer, diabetes, atherosclerosis, arthritis and kidney diseases. In the cell system there are enzymes with antioxidant properties, such as, catalase, superoxide dismutase or glutathione peroxidase[181]. When ROS are overexpressed, these natural enzymes are not enough to eliminate it. Nanozymes seem promising materials to remove the overexpressed ROS.

Pt nanomaterials have been widely used as antioxidant agents since it is well known their ability to reduce ROS levels. For example, citrate-capped Pt NPs exhibit dismutase, catalase and peroxidase-like behaviour, with equal or even better performance than natural enzymes and they have superior adaptability to environmental changes. Their antioxidant properties were tested towards the Cerebral Cavernous Malformation (CCM), which is associated to an increase in ROS levels. As expected, Pt NPs were able to reduce ROS levels and restoring physiological homeostasis[182]. Another nanomaterial that has been used for the scavenging of ROS are ultrasmall CuO NPs which can also mimic the activity of the enzymes catalase, superoxide dismutase and glutathione peroxidase[183]. Besides, this nanomaterial has rapid renal clearance and high

biocompatibility. The cytoprotective effects appear at very low dosage of NPs and improve the treatment in acute kidney injury, acute liver injury and wound healing.

The abnormal expression of ROS is a possible cause of Alzheimer's disease. The accumulation of amyloid protein in brain is an indicator of this disease and the presence of amyloids causes mitochondrial dysfunction and the abnormal expression of ROS. Therefore, protecting the mitochondria of oxidative damage could be adequate for Alzheimer's disease prevention and early treatment. Magnetite/ceria NPs decorated with anti-amyloids antibodies have been used for the remove of amyloids in the blood of transgenic mice[184]. The antibodies capture the amyloids and the magnetite NPs in the core isolate it by using an external magnetic field. The ceria NPs placed in the shell, since they have superoxide dismutase and catalase activity, are able of scavenging ROS produced by the presence of amyloids. The transgenic mice undergo a decrease in amyloids protein in the blood and the brain and also prevents spatial working memory deficits.

- **Imaging**

Nanozymes can be used for targeting and visualising tumor tissues. A strategy is the use of nanozymes with peroxidase-like activity, since cancer cells secrete a large amount of endogenous $H_2O_2$. FeWOx nanosheets with this enzymatic behaviour have been used for tumor visualisation[185]. The nanozyme is loaded with TMB and it enables the photoacoustic imaging of endogeneous $H_2O_2$. Also, ferritin-based cobalt nanozymes specifically target and visualize hepatocellular carcinoma tissues, due to the modification of the surface of ferritin with the SP94 peptide which specifically recognises this tumoral tissue. This nanozyme has also peroxidase-like activity and it is loaded with the substrate 3,3'-diaminebencidine (DAB) which gave a deep-brown colour if $H_2O_2$ is also present[186].

- **Biorthogonal catalysis**

Biorthogonal catalysis is a strategy for the in-situ generation of molecules unattainable through natural biological processes. Transition metals are able to perform reactions that cannot be accomplished by natural enzymes; however, its use is complicated due

to poor biocompatibility, water solubility and stability. These problems can be solved by loading the transition metals into nanomaterials. Biorthogonal catalysis has been used for imaging bacterial biofilms. With conventional imaging agents the visualization of biofilms is difficult due to the dense matrix and false positive/negative responses are usual. Transition metal catalysts composed by Ru have been encapsulated in pH-responsive sulphonamide-functionalized AuNPs. Since biofilms have an acidic environment, the nanozyme is able to target the bacterial accumulation and to activate a pro-fluophore and finally imaging the biofilm[187].

## 2.5. Quantum Dots in fluorescence-based biosensing

Biosensing methodologies based on fluorescence are one of the most employed due to high sensitivity and simplicity. Fluorescent nanomaterials such as QDs have started to replace classic organic fluorophores because they exhibit brighter fluorescence, wider selection of excitation and emission wavelengths and higher photostability.

QDs are semiconductor nanocrystals composed by atoms of groups II to VI (e.g., Cd, Zn, Se, Te) or III-V (e.g., In, P, As) in the periodic table. Due to their very small size (<10 nm) the quantum confinement effect causes wide UV-visible absorption spectra, narrow emission bands and tunable optical properties by size, composition and shape[188]. Compared to organic dyes, QDs have similar quantum yields but extinction coefficients are 10-50 times larger and reduced photobleaching rates. The overall effect is that QDs have 10-20 brighter fluorescence and 100-200 times better photostability[189].

Although QDs are a promising strategy to replace classical fluorophores, their surface properties need to be improved for better solubility and stability. Also, toxicity of these materials is a drawback for biomedical studies performed *in vivo*, although it is not a problem in *in vitro* assays[190].

QDs have been widely used in FRET assays. FRET is a through-space dipolar coupling interaction that allows electronic energy to be transferred from a donor to an acceptor. The rate of energy transfer depends on the distance between the donor and the acceptor, their relative orientations and the spectral overlap[191]. This technique is very sensitive to nanoscale changes in distance between molecules. Traditional FRET pairs are organic dyes, currently QDs are used as energy donors. They exhibit narrow emission

spectra and broad absorption which allow single-wavelength excitation of multiple donors and avoid crosstalk with acceptor fluorophores[190]. However, they are not adequate to be used as energy acceptors due to broad absorption spectra. QDs have been employed as donors in FRET for DNA point mutations analysis, detection of pathogenic DNA, construction of molecular beacons and immunoassays.

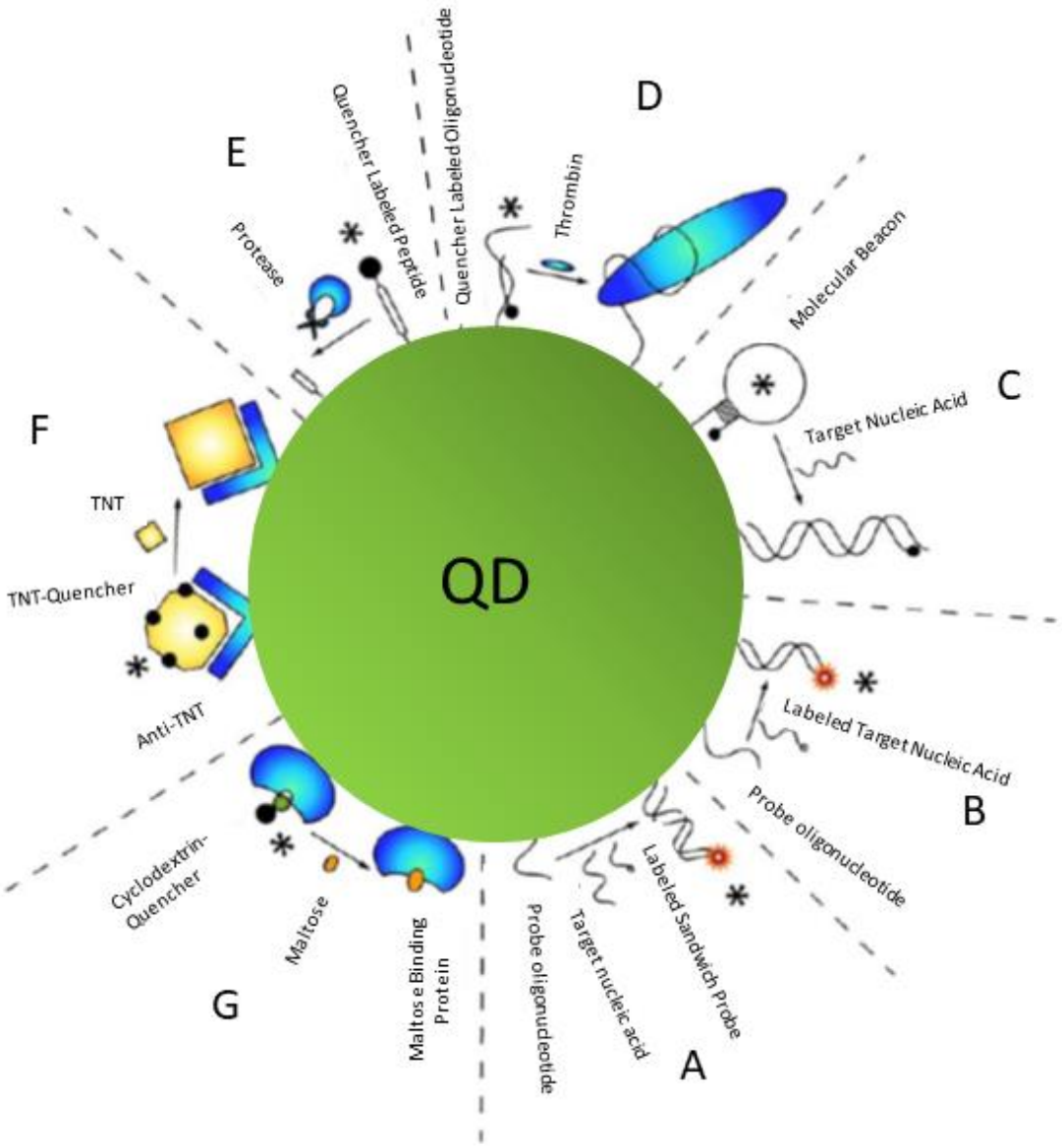


Figure 10. FRET-based bioanalysis using QDs as donors. A sandwich assay for oligonucleotides (A). Hybridization assay for oligonucleotides (B). A QD-based molecular beacon (C). An aptamer-based binding assay for thrombin (D). An assay for proteases (E). An immunoassay for TNT (F). A binding assay for maltose (G). The *asterisks* indicate the state in which efficient FRET occurs.

In Figure 10A. a sandwich assay for nucleic acids is represented. A QD coated with streptavidin emitting at 605 nm was paired with Cy5 as acceptor. A probe oligonucleotide labelled with biotin complementary to one half of the target sequence and a Cy5-labeled probe complementary to the other half of the target built the sandwich. The interaction biotin-streptavidin binds the sandwich to the surface of the QD. FRET between the QD and the Cy5 acceptor takes place. The assay has a detection limit of 4.8 fM[192].

In Figure 10B. is showed a system for the multidetection of two target nucleic acid sequences diagnostic of spinal muscular atrophy and pathogenic *Escherichia coli.* The sequences were labelled with Cy3 and Alexa Fluor 647, respectively. Complementary sequences to these ones were coupled to a green QD and red one. The conjugation of the probe oligonucleotides increased the QD fluorescence approximately twofold[193].

Molecular beacons can be constructed using a QD and a quencher (Figure 10C.). In the presence of a complementary target an increase on the fluorescence of the QD is observed. The conformational change increases the distance between the QD and the quencher that causes a decrease in the quenching efficiency. A molecular beacon using DABCYL as a quencher was prepared. The presence of complementary target increases sixfold the fluorescence of the QD[194].

Thrombin has been analysed using FRET and employing its well-known aptamer (Figure 10D.). The FRET-based probe was constructed using a QD as a donor, the aptamer was bound to a complementary sequence labelled with a quencher. When thrombin was added, the sequence containing the quencher is displaced because thrombin is bound to the aptamer and the fluorescence increases 19 times[195].

The recovery of QD fluorescence due to the displacement of quenching substances has been used for the analysis of proteases (Figure 10E.). Quenching moieties can be bound to the surface of a QD helped by a peptide sequence. The proximity of the quencher causes a decrease of the QD fluorescence. In the presence of the correct protease the peptide sequence is cleaved and the fluorescence increases. This strategy has been used with AuNPs as quenchers bound to the surface of a QD by a peptide that is degrade by collagenase[196].

FRET has also been used in immunoassays, for example for the detection of trinitrotoluene (TNT) (Figure 10F.). An anti-TNT antibody was assembled on the surface

of a QD. The antibody binding site was occupied by TNT labelled with a quencher that causes a decrease in the fluorescence of the QD. When the unlabelled antigen is was added it displaces the labelled TNT and the fluorescence of the QD is recovered[197]. Maltose has also been detected using FRET technology (Figure 10G.) using a QD bound to the maltose binding protein (MBP). MBP can bind both maltose and cyclodextrin but binds the former with much more affinity. Cyclodextrin labelled with a quencher was able to quench the fluorescence of the QD through FRET. When maltose was added the cyclodextrin labelled with a quencher was displaced and a recovery in the QD fluorescence was observed[198].

## 2.6. Nanoclusters (NCs) as emerging tool in biosensing

### 2.6.1. Properties of NCs

Nanoclusters fill the gap between NPs and single atoms and are composed of few to roughly several hundred of atoms, with sizes between 0.2 to 3 nm [199,200]. NCs are characterized by sizes comparable to the Fermi wavelength of electrons and exhibit molecule-like properties, such as fluorescence emission or catalytic activity[201]. Due to their unique properties, NCs find important applications in biodetection, bioimaging, electronics and photovoltaic[202]

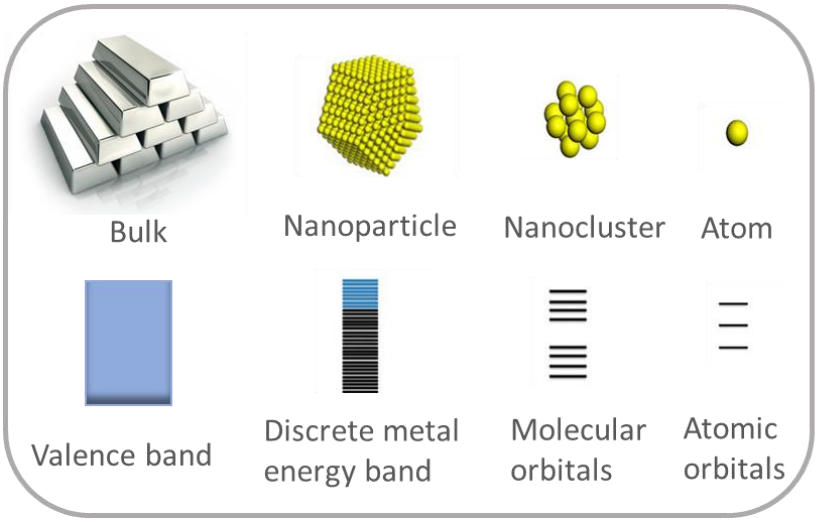


Figure 11. Representation of the electronic structure of bulk silver, a silver nanoparticle, a cluster of silver atoms and a single silver atom.

NCs have higher surface/volume ratio than bigger NPs, brighter emission and higher catalytic activity in comparison with other nanomaterials of the same mass. As the diameter of the particle decreases the fraction of exposed surface sites increases, resulting in an improvement of the catalytic activity. Also, the continuous valence band of bulk metal starts to separate in a discrete states, similar to that of semiconducting oxides[203] (Figure 11.).

The band gap (δ) can be expressed by:

$$\delta = 4/3\ \varepsilon_f / N$$

where $\varepsilon_f$ is the Fermi level energy and N is the number of atoms in the particle. When δ is greater than the thermal energy, Kt, (k, Boltzmann constant; T, temperature), the particle loses its metallic properties. For example, an icosahedral Au particle composed by 309 atoms with a diameter of 2.2 nm possess a $\varepsilon_f$ of 5.51 eV, and each Au atom has one free electron. Therefore, δ achieve a value of 2.38 x $10^{-2}$ eV which is higher than the thermal energy, 2.35 x $10^{-2}$ eV at 0 °C[203].

NCs can be synthesized using different methods, for example, the gas-phase method, the template method, the photoreduction method, the sonochemical method, the microemulsion method, the radiolytic method, the electrochemical method or the microwave-assisted synthesis. The template method uses organic molecules, dendrimers, DNA, gels or proteins as scaffolds for the synthesis of NCs, metallic salts as precursors and usually it is necessary a reducing step. Here we are going to focus in methods that use biopolymers as scaffold and its further application in biosensing.

### 2.6.2. Synthesis of NCs using biopolymers as scaffolds

Several types of biomolecules such as proteins, peptides or DNA have been used as scaffold for the synthesis of NCs. Instead of using organic molecules as stabilizers and reducing agents, such as sodium borohydride ($NaBH_4$), these biomolecules have in their composition natural stabilizing groups, like sulfhydryl groups, hydroxyl groups, carboxyl groups, amines or nucleotides and reductant functional groups, for example, thiol, tryptophan and tyrosine. The coordination chemistry between the metal surface that composed the NCs and the biomolecules, the large steric hindrance and the reducing

properties makes possible the controllable synthesis of NCs. Several techniques are employed for the characterisation of the NCs capped by biomolecules: UV-Vis absorption spectrometry, fluorescence spectrometry, matrix-assisted laser desorption/ionization time-of-flight mass spectrometry (MALDI-TOF), transmission electron microscopy (TEM), X-ray crystallography (XPS), circular dichroism (CD) spectroscopy or FTIR spectroscopy.

- **Proteins**

The first reported AuNCs synthesized using a protein as capping agent, employed BSA as scaffold[204]. The "green" synthesis procedure was inspired by the natural biomineralization process, using an alkaline solution of pH 12 at 37 °C and $HAuCl_4$ as gold precursor. At this basic pH the reducing properties of the phenolic groups of the 21 tyrosine residues are improved. The 35 cysteine residues of BSA serve to stabilize Au ions through Au-S bonds. The AuNCs exhibit red fluorescence with a quantum yield (QD) of 6 %. Since, this first green synthesis of AuNCs using a protein as scaffold, it is possible to find in the literature lot of other examples using different proteins and metals precursors (Table 4.).

As we can see in Table 4. by changing the temperature, the pH, the reducing methodology and the reaction time it is possible to tune the AuNCs size and the fluorescence emission[205, 206, 207]. Also, the protein size and aminoacid content affect the AuNCs formation. Four model proteins, BSA, pepsin, trypsin and lysozyme were studied[208]. The size of the proteins decreases in the order of BSA> pepsin> trypsin> lysozyme. Except for BSA, the other proteins have similar cysteine content (between 7-8 residues). However, there is a considerable difference on the amine-containing residues wit 60, 14, 6 and 1 for BSA, trypsin, lysozyme and pepsin, respectively. In comparison with BSA-capped AuNCs, the fluorescence emission of the other NCs exhibit a shift towards shorter wavelengths, at least 60 nm. Also, a decrease in the intensity was observed, in particular for pepsin. Pepsin with less amines residues but higher amount of tyrosine/tryptophan produce larger AuNPs, with non-fluorescent properties. The few amine residues are not able to complex Au ions. Furthermore, due to the high tyrosine/tryptophan content, it strongly reduces the Au ions and produce larger NPs.

Table 4. Protein-capped metal NCs: metal core composition, metal precursor, protein acting as scaffold, reducing agent, Tª, pH, incubation time, fluorescence emission and diameter.

| Metal core composition | Metal precursor | Protein acting as scaffold | Reducing agent | Tª/pH/Incubation time | Fluorescence emission | Diameter |
|---|---|---|---|---|---|---|
| **$Au_{25}$**[205] | $HAuCl_4$ | BSA | Tyr residues | 37 °C/12/24 h | 620 nm | 2.5 nm |
| **$Au_8$**[205] | | | Ascorbic acid | 37 °C/8/24 h | 425 nm | 1.9 nm |
| **$Au_{16}$**[206] | $HAuCl_4$ | BSA | Tyr residues | 37 °C/12/12 h | 604 nm | 0.233 nm |
| **$Au_{25}$**[207] | $HAuCl_4$ | Pepsin | Tyr residues | 37 °C/12/2 h | 670 nm | ≈ 1-2 nm |
| **$Au_{13}$**[207] | | | | 37 °C/1/100 h | 510 nm | ≈ 1 nm |
| **$Au_5$/ $Au_8$**[207] | | | | 25 °C/9/ 24 h | 402 nm/480 nm | ≈ 1 nm |
| **Au**[208] | $HAuCl_4$ | BSA | Tyr residues | RT/ 12/1 h | 705 nm | 2 nm |
| | | Pepsin | | | 620 nm | ≈ 6 nm |
| | | Trypsin | | | 643 nm | ≈ 2 nm |
| | | Lysozyme | | | 640 nm | ≈ 4 nm |
| **$Ag_{13}$**[209] | $AgNO_3$ | BSA | Tyr and $NaBH_4$ | -/12/1 h | 625 nm | < 2 nm |
| **Pt**[210] | $H_2PtCl_6$ | Yeast extract | Tyr residues | 100 °C/-/12 h | 448 nm | 3 ± 0.3nm |
| **Cu**[211] | CuSO4 | BSA | Tyr residues | 55 °C/12/6-8 h | 410 nm | 2.8 ± 0.5nm |
| **Cu**[212] | CuSO4 | Papain | $N_2H_4$ | 37 °C/12/2 h | 620 nm | 2.3 ± 0.7nm |
| **Cd**[213] | $CdCl_2$ | HSA | Tyr residues | 55 °C/12/3 h | 485 nm | 2 nm |
| **Au/Pt**[214] | $HAuCl_4/H_2PtCl_6$ | BSA | Tyr residues | 70 °C/12/20 min | 640 nm | 2.25 ± 0.18 nm |

Lower cysteine content and the smaller size of the proteins caused blue shifts of the fluorescence emission in the case of trypsin and lysozyme due to ineffective protection.

Moreover AuNCs, other metals have been employed for the synthesis of fluorescent protein capped NCs. Such as Ag[209], Pt[210], Cu[211,212], Cd[213] and even bimetallic NCs composed by Au and Pt[214].

And in addition to metal NCs, although there are few examples in literature, semiconductor NCs have been also synthesised using proteins as scaffold. For example, CdS NCs[215] and CdSe NCs[216] have been synthesized using BSA as capping agent. In both cases, first the Cd precursor is mixed with the protein to sequester the ions. After the incubation time the S precursor and the Se precursor were added, respectively, to form the colloidal solution. As a result, fluorescent NCs appeared with emission at 509 for CdS NCs and 433 nm for CdSe.

- **Peptides and aminoacids**

Peptides, composed from several to dozen of aminoacids residues, have been widely used as capping agents for the synthesis of metal NCs, due to simple composition and spatial structures. In Table 5. there are some examples of peptide protected NCs. Glutathione (GSH) composed by three aminoacids, glutamate, cysteine and glycine (Glu-Cys-Gly) is a classical thiolate peptide that has been used for the synthesis of metal NCs. In the literature it is possible to find AuNCs[217], AgNCs[218] or CuNCs[219] synthesized using this peptide, which act as scaffold. Other short peptides have been used for the synthesis of metallic NCs, for example L-Cysteine (L-Cys) has been employed for the synthesis of fluorescent CuNCs[220]. This aminoacid serve to encapsulate Cu ions from the salt $CuSO_4$ which act as precursor. Another example is the use of the dipeptide L-Cys-L-Cys for the synthesis of high fluorescence emitting Au NCs[221]. Besides thiol groups, peptides containing carboxyl groups exhibit high affinity towards Ag ions. For example, by using a dipeptide composed by Valine and Asparagine (Val-Asp) protected by Fmoc forming an hydrogel[222]. Also, polypeptides have been used as etchants for the synthesis of NCs. L-Cys can act as an etchant of larger AuNPs for the synthesis of AuNCs[223].

- **DNA**

DNA templates have been used for the synthesis of metal NCs, it is possible to find some examples in Table 6. DNA exhibit a high affinity towards Ag due to the presence of cytosine (C) and guanine (G) nucleotides in its structure. Ag NCs using an oligonucleotide as scaffold were synthesized for the first time by Dickson et al[224]. The fluorescence emission of Ag NCs can be tuned by changing the DNA nucleotide sequence. Microarray technology has been used for this issue and NCs emitting in the blue, green, yellow and red region of the spectrum have been synthesized[225]. Also, Ag NCs emitting in the near infrared have been produced[226]. Furthermore, DNA sequence templates containing aptamers and fragments to act as scaffold for the synthesis of AgNCs have been employed. For example, a sequence containing an aptamer for 8-hydroxydeoxyguanosine (OHdG)[227]. In addition, DNA templates can be used for the synthesis of NCs composed by other metallic cores such as Au[228] or Cu[229] and even bimetallic NCs composed by Ag and Pt[230].

Table 5. Peptide-capped metal NCs: metal core composition, metal precursor, peptide acting as scaffold, reducing agent, Tª, pH, incubation time, fluorescence emission and diameter.

| Metal core composition | Metal precursor | Peptide acting as scaffold | Reducing agent/ Other method | Tª/pH/Incubation time | Fluorescence emission | Diameter |
|---|---|---|---|---|---|---|
| **Au**[217] | $HAuCl_4$ | GSH | Reducing properties of aminoacids | 70 °C/-/24 h | 614 nm | 0.235 nm |
| **Ag**[25] | AgNPs | GSH | GSH acting as etchant | 65 °C /-/1 day | 450 nm | <2 nm |
| | | | | 65 °C /-/3 day | 570 nm | |
| | | | | 65 °C /-/8 day | 720 nm | |
| **Cu**[219] | $CuSO_4$ | GSH | Ascorbic acid | 85 °C/12/ 7 h | 440 nm | 2-3 nm |
| **Cu**[220] | $CuSO_4$ | L-Cys | Reducing properties of aminoacids | 55 °C/12/ 4.5 h | 480 nm | 2-3 nm |
| **Au**[221] | $HAuCl_4$ | L-Cys- L-Cys | $NaBH_4$ | RT/-/ 48 h | 410 nm | <1.5 nm |
| **Ag**[222] | $AgNO_3$ | (Val-Asp) | Sun light | RT/7.4/ 3 min | 634 nm | 2-3 nm |
| **Au**[223] | AuNPs | L-Cys | L-Cys acting as etchant | 100 °C/12/ 24 h | 495 nm | 1.35 nm |

Table 6. DNA-capped metal NCs: metal core composition, metal precursor, DNA sequence acting as scaffold, reducing agent and fluorescence emission.

| Metal core composition | Metal precursor | DNA sequence | Reducing agent/ Other method | Fluorescence emission |
|---|---|---|---|---|
| **Ag**[224] | $AgNO_3$ | 5'-AGGTCGCCGCCC-3' | $NaBH_4$ | 400-600 nm |
| **Ag**[225] | $AgNO_3$ | 5'- CCCTTTAACCCC-3' | $NaBH_4$ | 485 nm |
| | | 5'-CCCTCTTAACCC-3' | | 520 nm |
| | | 5'-CCCTTAATCCCC-3' | | 572 nm |
| | | 5'-CCTCCTTCCTCC-3' | | 620 nm |
| **Ag**[226] | $AgNO_3$ | 5'-CCCGGAGAAG-3' | $NaBH_4$ | 721 nm |
| **Ag**[227] | $AgNO_3$ | 5'GCGGGCGATCGGCG GGGGGTGCGTGCGCT CTGTGCCAGGGGGTG GGACAGATCATATGG GGGTGCTCCCCCCCCC CCC3′ (Aptamer for OHdG) | $NaBH_4$ | 630 nm |
| **Au** [228] | $HAuCl_4$ | 5'HS(CH2)6GCACTGGT CGGCCATGGGTAGCG ACGGTCCCTAACGTTT 3'(Aptamer for MUC1) | Dimethylamine borane (DMAB) | 650 nm |
| **Cu**[229] | $CuSO_4$ | 5'TTTTTTTTTTTTTTTT TTTTTTTTTTTTTTTT TTTT-3' | Sodium ascorbate | 550nm-650nm |
| **Ag/Pt**[230] | $AgNO_3$ and $K_2PtCl_4$ | 5'-CCCCCTAACTCCCCC-3' | $NaBH_4$ | - |

## 2.6.3. Biosensing strategies based on NCs

NCs synthesized using biomolecules as scaffold find important applications in biosensing due to their desirable selectivity and sensitivity, ease of fabrication, ultrafine subnanometer size and high biocompatibility. It is possible to find sensing strategies which take advantage of the fluorescent properties of NCs and there are others which uses their catalytic activity.

- **Fluorescence sensing approach**

NCs exhibit strong photoluminescence, combined with tunable fluorescence emission, high photostability, large Stokes shift and good quantum yields[231], making them excellent probes for biosensing applications. Among the strategies which uses the fluorescent emission of NCs, it worth highlight the "turn-on" and the "turn-off" methods. It has been used for the sensing of ions, DNA, MicroRNA (MiRNA), proteins, cells or small biomolecules[232]. For example, the great affinity of $Au^{+}$ towards $Hg^{2+}$ ions have been employed for the sensing of the latter, using fluorescent AuNCs capped with BSA. This NCs exhibit strong fluorescence that is quenched by the presence of $Hg^{2+}$ ions in solution. The LOD of detection is 0.1 ppb which is lower than the maximum level (2.0 ppb) allowed by the Environmental Protection Agency (EPA) in drinking water[233]. AgNCs synthesized using DNA as scaffold have been employed as DNA detection probe. The red fluorescence of this NCs is enhanced 500-fold when are near to DNA sequences rich in guanine nucleotides, acting as a beacon. Using this methodology is possible to detect an influenza target with an improvement of 5-fold than using a conventional molecular beacon[234]. Using the methodology of the florescence quenching a DNA sequence has been synthesized for the detection of thrombin. This DNA sequence is composed by a C-rich region and a thrombin aptamer in the opposite side. The C-rich region is used for the synthesis of highly fluorescent Ag NCs, when thrombin binds to its aptamer a structural change quenches the fluorescence[235]. Proteases can be detected taking advantage of their ability to hydrolize peptides bonds. The fluorescence of AuNCs capped with BSA is quenched by the presence of proteases, because the protein shell is degraded. The $O_2$ molecules can penetrate through the shell and quench the fluorescence of the Au core[236].

- **Catalytic sensing approach**

Many NCs synthesized using proteins as scaffolds have demonstrated to have enzyme-like properties, principally peroxidase, oxidase and catalase, and are suitable candidates to be used in biosensing applications. Due to their ultrasmall size, they exhibit greater catalytic activity and better biocompatibility in comparison with larger nanozymes. In

Table 7. it is possible to find some examples of NCs synthesized using proteins as scaffolds and their application in sensing.

Table 7. Examples of protein-protected NCs with enzyme-like activity and their applications.

| NCs | Protective biomolecule | Catalytic type | Catalytic activity | Application |
|---|---|---|---|---|
| **AuNCs**[237] | BSA | Peroxidase | $H_2O_2$ $K_M$: 25.3 mM<br>TMB $K_M$: 0.00253 mM (125 times lower than that of HRP) | Colorimetric detection of $H_2O_2$ (LOD: $2.10^{-8}$ M) and xanthine (LOD: $5.10^{-7}$ M) |
| **AuNCs**[238] | BSA | Peroxidase | $H_2O_2$ $K_M$: 2.46 mM<br>TMB $K_M$: 0.00664 (lower than that of HRP) | Tumor molecular location and diagnosis |
| **AuNCs**[239] | Apoferritin | Peroxidase | $H_2O_2$ $K_M$: 199.4 mM<br>TMB $K_M$: 0.097 mM (4 times lower than that of HRP) | Colorimetric detection of glucose |
| **AuNCs**[240] | Protamine | Peroxidase | $H_2O_2$ $K_M$: 1.49 Mm (2.5 times lower than that of HRP)<br>TMB $K_M$: 0.169 (much lower than that of HRP) | Colorimetric detection of $Hg^{2+}$ (LOD: 1.16 nM) |
| **PtNCs**[241] | BSA | Peroxidase | $H_2O_2$ $K_M$: 41.8 mM<br>TMB $K_M$: 0.119 mM (3 times lower than that of HRP) | Colorimetric detection of $Hg^{2+}$ (LOD: 7.2 nM) |
| **CuNCs**[242] | BSA | Peroxidase | $H_2O_2$ $K_M$: 0.0089 mM<br>TMB $K_M$: 0.00138 (17 times lower than that of HRP) | Colorimetric detection of xanthine (LOD: $3.8.10^{-7}$ M) |
| **AgNCs**[243] | BSA | Oxidase | - | Colorimetric immunoassay for Listeria Monocytogenes (LOD: 10 cfu/mL) |
| **PtNCs**[244] | Lysozyme | Oxidase | TMB $K_M$: 0.63 mM | Degradation of methylene blue in absence of $H_2O_2$ |
| **PtNCs**[245] | Ferritin | Catalase | $H_2O_2$ $K_M$: 420.6 mM (pH=12, 85 °C) | - |

This sensing approach was studied in this thesis by incorporating NCs with peroxidase-like activity in the structure of an antibody. The conjugate will be used as detection antibody in an immunoassay acting as the recognition element and the transduce component.

## References


1. Heineman, W. R. & Jensen, W. B. Leland C. Clark Jr. (1918–2005). *Biosens. Bioelectron.* **21**, 1403–1404 (2006).
2. IUPAC. Glossary for chemist for terms used in biotechnology. *Pure Appl. Chem.* **64**, 143–168 (1992).
3. Mahato, K., Maurya, P. K. & Chandra, P. Fundamentals and commercial aspects of nanobiosensors in point-of-care clinical diagnostics. *3 Biotech* **8:149**, (2018).
4. Bhalla, N., Jolly, P., Formisano, N. & Estrela, P. Introduction to biosensors. *Essays Biochem.* **60**, 1–8 (2016).
5. Borisov, S. M. & Wolfbeis, O. S. Optical Biosensors. *Chem. Rev.* **108**, 423–461 (2008).
6. Yang, F., Ma, Y., Stanciu, S. G. & Wu, A. Transduction Process-Based Classification of Biosensors. *Nanobiosensors* 23–44 (2020) doi:10.1002/9783527345137.ch2.
7. Fan, X. *et al.* Sensitive optical biosensors for unlabeled targets: A review. *Anal. Chim. Acta* **620**, 8–26 (2008).
8. Ibraheem, A. & Campbell, R. E. Designs and applications of fluorescent protein-based biosensors. *Curr. Opin. Chem. Biol.* **14**, 30–36 (2010).
9. Su, L., Jia, W., Hou, C. & Lei, Y. Microbial biosensors: A review. *Biosens. Bioelectron.* **26**, 1788–1799 (2011).
10. Ramanathan, K. & Danielsson, B. Principles and applications of thermal biosensors. *Biosens. Bioelectron.* **16**, 417–423 (2001).
11. Owicki, J. C. & Wallace Parce, J. Biosensors based on the energy metabolism of living cells: The physical chemistry and cell biology of extracellular acidification. *Biosens. Bioelectron.* **7**, 255–272 (1992).
12. Sapsford, K. E., Berti, L. & Medintz, I. L. Materials for fluorescence resonance energy transfer analysis: Beyond traditional donor-acceptor combinations. *Angew. Chem. Int. Ed.* **45**, 4562–4589 (2006).
13. Goldsmith, S. J. Radioimmunoassay: Review of basic principles. *Semin. Nucl. Med.* **5**, 125–152 (1975).
14. Yalow, R. S. & Berson, S. A. Immunoassay of endogenous plasma insulin in man. *J. Clin. Invest.* **39**, 1157–1175 (1960).
15. Ma, Z. *et al.* Radioimmunoassay of leptin in human plasma. *Clin. Chem.* **42**, 942–946 (1996).
16. Ie, E. V, Hempen, C. & Karst, U. Labeling strategies for bioassays. *Anal. Bioanal. Chem.* **384**, 572–583 (2006).
17. Coons, A. H., Creech, H. J. & Jones, R. N. Immunological Properties of an Antibody Containing a Fluorescent Group. *Exp. Biol. Med.* **47**, 200 (1941).

18. Bailey, M. P., Rocks, B. F. & Riley, C. Use of Lucifer yellow VS as a label in fluorescent immunoassays illustrated by the determination of albumin in serum. *Ann. Clin. Biochem.* **20**, 213–216 (1983).
19. Chen, F. A. Characterization of charge-modified and fluorescein-labeled antibody by capillary electrophoresis using laser-induced fluorescence Application to immunoassay of low level immunoglobulin A. *J. Chromatogr.* **680**, 419–423 (1994).
20. Daneshvar, M. I. *et al.* Design and development of a fiber-optic immunosensor utilizing near-infrared fluorophores. *J. Fluoresc.* **6**, 69–75 (1996).
21. Hempen, C. & Karst, U. Labeling strategies for bioassays. *Anal. Bioanal. Chem.* **384**, 572–583 (2006).
22. Telford, W. G., Cox, W. G., Stiner, D., Singer, V. L. & Doty, S. B. Detection of endogenous alkaline phosphatase activity in intact cells by flow cytometry using the fluorogenic ELF-97 phosphatase substrate. *Cytometry* **37**, 314–319 (1999).
23. Fernley, H. N. & Walker, P. G. Kinetic behaviour of calf-intestinal alkaline phosphatase with 4-methylumbelliferyl phosphate. *Biochem. J.* **97**, 95 (1965).
24. Wilson, M. S. & Rauh, R. D. Hydroquinone diphosphate: An alkaline phosphatase substrate that does not produce electrode fouling in electrochemical immunoassays. *Biosens. Bioelectron.* **20**, 276–283 (2004).
25. Tung, C. H. *et al.* In Vivo Imaging of β-Galactosidase Activity Using Far Red Fluorescent Switch. *Cancer Res.* **64**, 1579–1583 (2004).
26. Corey, P. F., Trimmer, R. W. & Biddlecom, W. G. A New Chromogenic B-Galactosidase Substrate: 7-B-D-Galactopyranosyloxy-9,9-dimetyl-9H-acrindin-2-one. *Angew. Chem. Int. Ed.* **30**, 1646–1648 (1991).
27. Guilbault, G. G., Brignac, P. & Zimmer, M. Homovanillic Acid as a Fluorometric Substrate for Oxidative Enzymes. Analytical Applications of the Peroxidase, Glucose Oxidase, and Xanthine Oxidase Systems. *Anal. Chem.* **38**, 190–196 (1966).
28. Ngo, T. T. & Lenhoff, H. M. A Sensitive and Versatile Chromogenic and Peroxidase-Coupled. *Anal. Biochem.* **105**, 389–397 (1980).
29. Kimmich, G. A., Randles, J. & Brand, J. S. Assay of picomole amounts of ATP, ADP, and AMP using the luciferase enzyme system. *Anal. Biochem.* **69**, 187–206 (1975).
30. Tang, B., Wang, Y., Sun, Y. & Xi Shen, H. Spectrofluorimetric determination of hydrogen peroxide with 2-hydroxy-1-naphthaldehyde salicyloylhydrazone (HNSH) as the substrate for horseradish peroxidase (HRP). *Spectrochim. Acta A* **58**, 141–148 (2002).
31. Mishin, V., Gray, J. P., Heck, D. E., Laskin, D. L. & Laskin, J. D. Application of the Amplex red/horseradish peroxidase assay to measure hydrogen peroxide generation by recombinant microsomal enzymes. *Free Radic. Biol. Med.* **48**, 1485–1491 (2010).
32. Rodriguez-Lopez, J. N., Gilabert, M. A., Tudela, J., Thorneley, R. N. F. & Garcia-Canovas, F. Reactivity of horseradish peroxidase compound II toward substrates: Kinetic evidence for a two-step mechanism. *Biochemistry* **39**, 13201–13209 (2000).
33. Fornera, S. & Walde, P. Spectrophotometric quantification of horseradish peroxidase with o-phenylenediamine. *Anal. Biochem.* **407**, 293–295 (2010).
34. Cao, X. *et al.* Catalytic activity and stability of glucose oxidase/horseradish peroxidase co-confined in macroporous silica foam. *Analyst* **137**, 5785–5791

(2012).
35. Fanjul-Bolado, P., González-García, M. B. & Costa-García, A. Amperometric detection in TMB/HRP-based assays. *Anal. Bioanal. Chem.* **382**, 297–302 (2005).
36. Radi, R., Rubbo, H., Thomson, L. & Prodanov, E. Luminol chemiluminescence using xanthine and hypoxanthine as xanthine oxidase substrates. *Free Radic. Biol. Med.* **8**, 121–126 (1990).
37. Feng, J., Huang, P. & Wu, F. Gold–platinum bimetallic nanoclusters with enhanced peroxidase-like activity and their integrated agarose hydrogel-based sensing platform for the colorimetric analysis of glucose levels in serum. **142**, 4106–4115 (2017).
38. Avrameas, S. Coupling of enzymes to proteins with glutaraldehyde. Use of the conjugates for the detection of antigens and antibodies. *Immunochemistry* **6**, 43–52 (1969).
39. Nakane, P. K. & Kawaoi, A. Peroxidase-labeled antibody a new method of conjugation. *J. Histochem. Cytochem.* **22**, 1084–1091 (1974).
40. Kato, K., Hamaguchi, Y., Fukui, H. and Ishikawa, E. Enzyme-liked Immunoassay. A simple method for the synthesis of the Rabbit Antibody-B-D-Galactosidase Complex and Its General Applicability. *J. Biochem.* **78**, 423–425 (1975).
41. Ishikawa, E. Enzyme-labeling of antibodies. in *Laboratory Techniques in Biochemistry and Molecular Biology* 223–248 (1999).
42. Guesdon, J. L., Ternynck, T. & Avrameas, S. The Use of Avidin-Biotin Interaction in Immunoenzymatic Techniques. *J. Histochem. Cytochem.* **27**, 1131–1139 (1979).
43. Feynman, R. P. There's Plenty of Room at the Bottom. *Caltech Eng. Sci.* **23:5**, 22–36 (1960).
44. Taniguchi, N. On the Basic Concept of Nano-Technology. *Proc. Intl. Conf. Prod. Eng. Tokyo, Part II, Japan Soc. Precis. Eng.* (1974).
45. Drexler, K. E. *Engines of creation. The coming era of nanotechnology.* (Doubleday, 1986).
46. Nasrollahzadeh, M., Sajadi, S. M., Sajjadi, M. & Issaabadi, Z. *An Introduction to Nanotechnology*. *Interface Science and Technology* vol. 28 (Elsevier Ltd., 2019).
47. Kaehler, T. Nanotechnology : Basic Concepts and Definitions. *Clin. Chem.* **40**, 1797–1799 (1994).
48. Rao, C. N. R. & Cheetham, A. K. Science and technology of nanomaterials: Current status and future prospects. *J. Mater. Chem.* **11**, 2887–2894 (2001).
49. Mansoori, G. A. & Soelaiman, T. A. F. Nanotechnology - An introduction for the standards community. *J. ASTM Int.* **2**, 17–38 (2005).
50. Whitesides, G. M. Nanoscience, nanotechnology, and chemistry. *Small* **1**, 172–179 (2005).
51. Wu, Z. *et al.* Carbon-Nanomaterial-Based Flexible Batteries for Wearable Electronics. *Adv. Mater.* **31**, 1–25 (2019).
52. Wu, W. Inorganic nanomaterials for printed electronics: A review. *Nanoscale* **9**, 7342 (2017).
53. Santhosh, C. *et al.* Role of nanomaterials in water treatment applications: A review. *Chem. Eng. J.* **306**, 1116–1137 (2016).
54. Gautam, P. K., Singh, A., Misra, K., Sahoo, A. K. & Samanta, S. K. Synthesis and applications of biogenic nanomaterials in drinking and wastewater treatment. *J. Environ. Manage.* **231**, 734–748 (2019).

55. Rajapaksha, R. D., Fuierer, P. A. & Ranasinghe, M. I. Colloidal CuZnInS3 nanocrystals as the sensitizer in photovoltaic solar cells. *Sol. Energy* **189**, 503–509 (2019).
56. Jia, G. *et al.* CuInTe 2 nanocrystals: Shape and size control, formation mechanism and application, and use as photovoltaics. *Nanomaterials* **9**, 409 (2019).
57. Zoller, F., Böhm, D., Bein, T. & Fattakhova-Rohlfing, D. Tin Oxide Based Nanomaterials and Their Application as Anodes in Lithium-Ion Batteries and Beyond. *ChemSusChem* **12**, 4140–4159 (2019).
58. Xu, X., Xiong, F., Meng, J., An, Q. & Mai, L. Multi-electron reactions of vanadium-based nanomaterials for high-capacity lithium batteries: challenges and opportunities. *Mater. Today Nano* **10**, 100073 (2020).
59. Ahmad, R., Majhi, S. M., Zhang, X., Swager, T. M. & Salama, K. N. Recent progress and perspectives of gas sensors based on vertically oriented ZnO nanomaterials. *Adv. Colloid Interface Sci.* **270**, 1–27 (2019).
60. Liu, X., Yao, Y., Ying, Y. & Ping, J. Recent advances in nanomaterial-enabled screen-printed electrochemical sensors for heavy metal detection. *Trends Anal. Chem.* **115**, 187–202 (2019).
61. Uzak, D., Atiroğlu, A., Atiroğlu, V., Çakıroğlu, B. & Özacar, M. Reduced Graphene Oxide/Pt Nanoparticles/Zn-MOF-74 Nanomaterial for a Glucose Biosensor Construction. *Electroanalysis* **32**, 1–11 (2019).
62. Yang, Y. *et al.* A Highly Sensitive Electrochemiluminescence Choline Biosensor Based on Poly(aniline-luminol-hemin) Nanocomposites. *Electroanalysis* **31**, 624–631 (2019).
63. Saa, L., Díez-Buitrago, B., Briz, N. & Pavlov, V. CdS quantum dots generated in-situ for fluorometric determination of thrombin activity. *Microchim. Acta* **186**, 657 (2019).
64. Bakshi, S., Zakharchenko, A., Minko, S., Kolpashchikov, D. & Katz, E. Towards Nanomaterials for Cancer Theranostics: A System of DNA-Modified Magnetic Nanoparticles for Detection and Suppression of RNA Marker in Cancer Cells. *Magnetochemistry* **5**, 24 (2019).
65. Lai, W. F., Wong, W. T. & Rogach, A. L. Development of Copper Nanoclusters for In Vitro and In Vivo Theranostic Applications. *Adv. Mater.* **1906872**, (2020).
66. Sharma, N., Sharma, A. K., Pandey, S. & Wu, H. F. Electrocatalytic synthesis of black tin oxide nanomaterial as photothermal agent for cancer therapy. *Mater. Sci. Eng. C* **108**, 110350 (2019).
67. Tao, K. *et al.* Targeted multifunctional nanomaterials with MRI, chemotherapy and photothermal therapy for the diagnosis and treatment of bladder cancer. *Biomater. Sci.* **8**, 342 (2020).
68. Gama-Lara, S. A., Pérez Mendoza, M. S., Vilchis-Nestor, A. R. & Natividad, R. Bionanotechnology: Silver Nanoparticles Supported on Bovine Bone Powder Used as Bactericide. *Materials (Basel).* **13**, 462 (2020).
69. Wang, J., Wang, Y. & Zhang, D. Exploring the bactericidal performance and application of novel mimic enzyme Co4S3. *J. Colloid Interf. Sci.* **561**, 327–337 (2020).
70. Jiang, Q., Liu, S., Liu, J., Wang, Z. G. & Ding, B. Rationally Designed DNA-Origami Nanomaterials for Drug Delivery In Vivo. *Adv. Mater.* 1804785 (2018) doi:10.1002/adma.201804785.

71. Ju, J., Regmi, S., Fu, A., Lim, S. & Liu, Q. Graphene quantum dot based charge-reversal nanomaterial for nucleus-targeted drug delivery and efficiency controllable photodynamic therapy. *J. Biophotonics* **12**, :e201800367 (2019).
72. Debnath, S. & Das, R. Study of the optical properties of Zn doped Mn spinel ferrite nanocrystals shows multiple emission peaks in the visible range –a promising soft ferrite nanomaterial for deep blue LED. *J. Mol.* **1199**, 127044 (2020).
73. Sang, D. K. *et al.* Two dimensional β-InSe with layer-dependent properties: Band alignment, work function and optical properties. *Nanomaterials* **9**, 82 (2019).
74. Sergii Golovynskyi, Oleksandr I. Datsenko, Luca Seravalli, Giovanna Trevisi, PaolaFrigeri, Ivan S. Babichuk, Iuliia Golovynska, Baikui Li, J. Q. Structural, Dielectric, and Magneto-optical Properties of Cu2+-Er3+ Substituted Nanocrystalline Strontium Hexaferrite. *Mater. Res. Express* **6**, 5 (2019).
75. Lee, H. K., Nam, I. W., Tafesse, M. & Kim, H. K. Fluctuation of electrical properties of carbon-based nanomaterials/cement composites: Case studies and parametric modeling. *Cem. Concr. Compos.* **102**, 55–70 (2019).
76. Migliorini, F. L. *et al.* Tuning the Electrical Properties of Electrospun Nanofibers with Hybrid Nanomaterials for Detecting Isoborneol in Water Using an Electronic Tongue. *Surfaces* **2**, 432–443 (2019).
77. Min, S. H. *et al.* Simulation of electrical conductivity for nanoparticles and nanotubes composite sensor according to geometrical properties of nanomaterials. *Compos. B. Eng.* **174**, 107003 (2019).
78. Dubyk, K. *et al.* Thermal conductivity of silicon nanomaterials measured using the photoacoustic technique in a piezoelectric configuration. *J. Phys. Chem. Solids* **126**, 267–273 (2019).
79. Rafiee, M. *et al.* Thermal properties of doubly reinforced fiberglass/epoxy composites with graphene nanoplatelets, graphene oxide and reduced-graphene oxide. *Compos. Part B Eng.* **164**, 1–9 (2019).
80. Sharma, B. B. & Parashar, A. A review on thermo-mechanical properties of bi-crystalline and polycrystalline 2D nanomaterials. *Crit. Rev. Solid State* **45**, 134–170 (2019).
81. Iqbal, M. J. & Siddiquah, M. R. Electrical and magnetic properties of chromium-substituted cobalt ferrite nanomaterials. *J. Alloy. Compd.* **453**, 513–518 (2008).
82. Fuentes, S., Barraza, N., Veloso, E., Villarroel, R. & Llanos, J. Effects of Eu substitution on luminescent and magnetic properties of BaTiO3 nanomaterials. *J. Alloys Compd.* **569**, 52–57 (2013).
83. Purushotham, S. & Ramanujan, R. V. Thermoresponsive magnetic composite nanomaterials for multimodal cancer therapy. *Acta Biomater* **6**, 502–510 (2010).
84. Mu, J., Zhang, L., Zhao, G. & Wang, Y. The crystal plane effect on the peroxidase-like catalytic properties of Co3O4 nanomaterials. *Physi. Chem. Chem. Phys.* **16**, 15709–15716 (2014).
85. Zhu, C., Wang, P., Wang, L., Han, L. & Dong, S. Facile synthesis of two-dimensional graphene/SnO2/Pt ternary hybrid nanomaterials and their catalytic properties. *Nanoscale* **3**, 4376–4382 (2011).
86. Li, L. *et al.* A novel two-dimensional MgO-h-BN nanomaterial supported Pd catalyst for CO oxidation reaction. *Catal. Today* **332**, 214–221 (2019).
87. Tian, J. *et al.* Application of nanomaterials in sample preparation. *J. Chromatogr. A* **1300**, 2–16 (2013).

88. Thakor, A. S., Jokerst, J., Zaveleta, C., Massoud, T. F. & Gambhir, S. S. Gold nanoparticles: a revivial in precious metal administration to patients. *Nano Lett.* **25**, 4029–4036 (2015).
89. McFarland, A. D., Haynes, C. L., Mirkin, C. A., Van Duyne, R. P. & Godwin, H. A. Color My Nanoworld. *J. Chem. Educ.* **81**, 544A (2004).
90. Ma, M. *et al.* Gold nanoparticles supported by amino groups on the surface of magnetite microspheres for the catalytic reduction of 4-nitrophenol. *J. Mater, Sci.* **54**, 323–334 (2019).
91. Nadaf, N. Y. & Kanase, S. S. Biosynthesis of gold nanoparticles by Bacillus marisflavi and its potential in catalytic dye degradation. *Arab. J. Chem.* **12**, 4806–4814 (2016).
92. Solis Fernández, P. Modificación superficial de materiales de carbono: grafito y grafeno. in *Universidad de Oviedo. Departamento de Ciencia de los Materiales e Ingeniería Metalúrgica.* (2011).
93. Freestone, I., Meeks, N., Sax, M. & Higgit, C. The Lycurgus Cup- A Roman Nanotechnology. *Gold Bull.* **40**, 270–277 (2007).
94. Kool, L. *et al.* Gold and silver dichroic nanocomposite in the quest for 3D printing the Lycurgus cup. *Beilstein J. Nanotechnol.* **11**, 16–23 (2020).
95. BARBER, D. J. & FREESTONE, I. C. An Investigation of the Origin of the Colour of the Lycurgus Cup By Analytical Transmission Electron Microscopy. *Archaeometry* **32**, 33–45 (1990).
96. Wilts, B. D. *et al.* Butterfly gyroid nanostructures as a time-frozen glimpse of intracellular membrane development. *Sci. Adv.* **3**, e1603119 (2017).
97. Autumn, K. & Gravish, N. Gecko adhesion: Evolutionary nanotechnology. *Phil. Trans. R. Soc.* **366**, 1575–1590 (2008).
98. Yan, Y. Y., Gao, N. & Barthlott, W. Mimicking natural superhydrophobic surfaces and grasping the wetting process: A review on recent progress in preparing superhydrophobic surfaces. *Adv. Colloid Interface Sci.* **169**, 80–105 (2011).
99. Weatherspoon, M. R., Cai, Y., Crne, M., Srinivasarao, M. & Sandhage, K. H. 3D rutile titania-based structures with Morpho butterfly wing scale morphologies. *Angew. Chem. Int. Ed.* **47**, 7921–7923 (2008).
100. Qu, L. & Dai, L. Gecko-foot-mimetic aligned single-walled carbon nanotube dry adhesives with unique electrical and thermal properties. *Adv. Mater.* **19**, 3844–3849 (2007).
101. Patil, G. D., Patil, A. H., Jadhav, S. A., Patil, C. R. & Patil, P. S. A new method to prepare superhydrophobic cotton fabrics by post-coating surface modification of ZnO nanoparticles. *Mater. Lett.* **255**, 126562 (2019).
102. Mohith, S., Karanth, P. N. & Kulkarni, S. M. Recent trends in nanobiosensor and their applications - a review. *Rev. Adv. Mater. Sci.* **36**, 62–69 (2014).
103. Malik, P. *et al.* Nanobiosensors: Concepts and Variations. *ISRN Nanomater.* **2013**, 1–9 (2013).
104. Tîlmaciu, C. M. & Morris, M. C. Carbon nanotube biosensors. *Front. Chem.* **3:59**, (2015).
105. Doria, G. *et al.* Noble metal nanoparticles for biosensing applications. *Sensors* **12**, 1657–1687 (2012).
106. Haun, J. B., Yoon, T. J., Lee, H. & Weissleder, R. Magnetic nanoparticle biosensors. *Wiley Interdiscip. Rev. Nanomed. Nanobiotechnology* **2**, 291–304 (2010).

107. Frasco, M. F. & Chaniotakis, N. Semiconductor quantum dots in chemical sensors and biosensors. *Sensors* **9**, 7266–7286 (2009).
108. Kabashin, A. V. *et al.* Plasmonic nanorod metamaterials for biosensing. *Nat. Mater.* **8**, 867–871 (2009).
109. Huang, Y., Ren, J. & Qu, X. Nanozymes: Classification, Catalytic Mechanisms, Activity Regulation, and Applications. *Chem. Rev.* **119**, 4357–4412 (2019).
110. Li, S., Yang, X., Yang, S., Zhu, M. & Wang, X. Technology prospecting on enzymes: Application, marketing and engineering. *Comput. Struct. Biotechnol. J.* **2**, e201209017 (2012).
111. Behrens, M. *et al.* The Active Site of Methanol Synthesis over Cu/ZnO/Al2O3 Industrial Catalysts. *Science (80-. ).* **759**, 893–898 (2012).
112. Wu, J. *et al.* Nanomaterials with enzyme-like characteristics (nanozymes): Next-generation artificial enzymes (II). *Chem. Soc. Rev.* **48**, 1004 (2019).
113. Breslow, R. & Overman, L. E. A Molecular Palladium (II) Complex Containing Both Sulfur- and Nitrogen-Bonded Thiocyanate Groups. *J. Am. Chem. Soc.* **92**, 1075–1077 (1970).
114. Sharma, V. & Bachwani, M. Artificial Enzymes: A Review. *Curr. Enzym. Inhib.* **7**, 178–189 (2011).
115. Gao, L. *et al.* Intrinsic peroxidase-like activity of ferromagnetic nanoparticles. *Nat. Nanotechnol.* **2**, 577–583 (2007).
116. Zhang, R., Fan, K. & Yan, X. Nanozymes: created by learning from nature. *Sci. China Life Sci.* **63**, 1183–1200 (2020).
117. Wei, H. & Wang, E. Nanomaterials with enzyme-like characteristics (nanozymes): Next-generation artificial enzymes. *Chem. Soc. Rev.* **42**, 6060–6093 (2013).
118. Cao, L., Wang, P., Chen, L., Wu, Y. & Di, J. A photoelectrochemical glucose sensor based on gold nanoparticles as a mimic enzyme of glucose oxidase. *RSC Adv.* **9**, 15307 (2019).
119. Chen, J., Wu, W., Huang, L., Ma, Q. & Dong, S. Self-Indicative Gold Nanozyme for H2O2 and Glucose Sensing. *Chem. - A Eur. J.* **25**, 11940–11944 (2019).
120. Liu, M., Li, Z., Li, Y., Chen, J. & Yuan, Q. Self-assembled nanozyme complexes with enhanced cascade activity and high stability for colorimetric detection of glucose. *Chin. Chem. Lett.* **30**, 1009–1012 (2019).
121. Zhang, P. *et al.* Modified carbon nitride nanozyme as bifunctional glucose oxidase-peroxidase for metal-free bioinspired cascade photocatalysis. *Nat. Commun.* **10**, 1–14 (2019).
122. Wang, J. *et al.* Construction of a bioinspired laccase-mimicking nanozyme for the degradation and detection of phenolic pollutants. *Appl. Catal. B Environ.* **254**, 452–462 (2019).
123. Ragg, R. *et al.* Molybdenum trioxide nanoparticles with intrinsic sulfite oxidase activity. *ACS Nano* **8**, 5182–5189 (2014).
124. Xue, T. *et al.* Integration of molecular and enzymatic catalysts on graphene for biomimetic generation of antithrombotic species. *Nat. Commun.* **5**, 1–6 (2014).
125. Li, W. *et al.* High-activity Fe3O4 nanozyme as signal amplifier: A simple, low-cost but efficient strategy for ultrasensitive photoelectrochemical immunoassay. *Biosens. Bioelectron.* **127**, 64–71 (2019).
126. Wu, L. *et al.* Nanozyme-linked immunosorbent assay for porcine circovirus type 2 antibody using HAuCl4/H2O2 coloring system. *Microchem. J.* **157**, 105079 (2020).

127. Wang, F., Zhang, Y., Liu, Z., Ren, J. & Qu, X. Mesoporous encapsulated nanozyme for decontaminating two kinds of wastewater and avoiding secondary pollution. *Nanoscale* **12**, 14465–14471 (2020).
128. Liu, D. *et al.* Nanozyme chemiluminescence paper test for rapid and sensitive detection of SARS-CoV-2 antigen. *Biosens. Bioelectron.* **173**, 112817 (2021).
129. Šálek, P. *et al.* Iron oxide nanozyme as catalyst of nanogelation. *Mater. Lett.* **269**, 1–4 (2020).
130. Jiao, L. *et al.* Dopamine-induced Au hydrogel nanozyme for enhanced biomimetic catalysis. *Chem. Commun.* **55**, 9865–9868 (2019).
131. Mirhosseini, M. *et al.* Core-shell Au@Co-Fe hybrid nanoparticles as peroxidase mimetic nanozyme for antibacterial application. *Process Biochem.* **95**, 131–138 (2020).
132. Wang, Y., Li, H., Guo, L., Jiang, Q. & Liu, F. A cobalt-doped iron oxide nanozyme as a highly active peroxidase for renal tumor catalytic therapy. *RSC Adv.* **9**, 18815 (2019).
133. Zhang, D. *et al.* A novel nanozyme based on selenopeptide-modified gold nanoparticles with a tunable glutathione peroxidase activity. *RSC Adv.* **10**, 8685–8691 (2020).
134. Li, F. *et al.* Selenium-Doped Carbon Quantum Dots for Free-Radical Scavenging. *Angew. Chem. Int. Ed.* **56**, 9910–9914 (2017).
135. He, X. *et al.* Haloperoxidase Mimicry by CeO2-x Nanorods of Different Aspect Ratios for Antibacterial Performance. *ACS Sustain. Chem. Eng.* **8**, 6744–6752 (2020).
136. Wang, F., Ju, E., Guan, Y., Ren, J. & Qu, X. Light-Mediated Reversible Modulation of ROS Level in Living Cells by Using an Activity-Controllable Nanozyme. *Small* **13**, 1–6 (2017).
137. Mu, J., Zhang, L., Zhao, M. & Wang, Y. Catalase mimic property of Co3O4 nanomaterials with different morphology and its application as a calcium sensor. *ACS Appl. Mater. Interfaces* **6**, 7090–7098 (2014).
138. Chen, Q. *et al.* A versatile Pt-Ce6 nanoplatform as catalase nanozyme and NIR-II photothermal agent for enhanced PDT/PTT tumor therapy. *Sci. China Mater.* 1–21 (2020) doi:10.1007/s40843-020-1431-5.
139. Dashtestani, F., Ghourchian, H. & Najafi, A. Silver-gold-apoferritin nanozyme for suppressing oxidative stress during cryopreservation. *Mater. Sci. Eng. C* **94**, 831–840 (2019).
140. Singh, N., Savanur, M. A., Srivastava, S., D'Silva, P. & Mugesh, G. A Redox Modulatory Mn3O Nanozyme with Multi-Enzyme Activity Provides Efficient Cytoprotection to Human Cells in a Parkinson's Disease Model. *Angew. Chem.* **129**, 14455–14459 (2017).
141. Liu, Y. *et al.* Integrated cascade nanozyme catalyzes in vivo ROS scavenging for anti-inflammatory therapy. *Sci. Adv.* **6**, (2020).
142. Zhang, J., Wu, S., Ma, L., Wu, P. & Liu, J. Graphene oxide as a photocatalytic nuclease mimicking nanozyme for DNA cleavage. *Nano Res.* **13**, 455–460 (2020).
143. Tian, X. *et al.* Highly sensitive chemiluminescent sensing of intracellular Al3+ based on the phosphatase mimetic activity of cerium oxide nanoparticles. *Biosens. Bioelectron.* **152**, 112027 (2020).
144. Vernekar, A. A., Das, T. & Mugesh, G. Vacancy-Engineered Nanoceria: Enzyme

Mimetic Hotspots for the Degradation of Nerve Agents. *Angew. Chem. Int. Ed. Engl.* **55**, 1412–1416 (2016).
145. Gao, N. *et al.* Polyoxometalate-based nanozyme: Design of a multifunctional enzyme for multi-faceted treatment of Alzheimer's disease. *Nano Res.* **9**, 1079–1090 (2016).
146. Xu, X. *et al.* Highly sensitive colorimetric detection of arsenite based on reassembly-induced oxidase-mimicking activity inhibition of dithiothreitol-capped Pd nanozyme. *Sens. Actuat B-Chem* **298**, 126876 (2019).
147. Huang, L. *et al.* Portable Colorimetric Detection of Mercury(II) Based on a Non-Noble Metal Nanozyme with Tunable Activity. *Inorg.Chem.* **58**, 1638–1646 (2019).
148. Lien, C. W. *et al.* Visual detection of cyanide ions by membrane-based nanozyme assay. *Biosens. Bioelectron.* **102**, (2018).
149. Ko, E. *et al.* Characterization of Au@PtNP/GO nanozyme and its application to electrochemical microfluidic devices for quantification of hydrogen peroxide. *Sens. Actuat B-Chem* **294**, 166–176 (2019).
150. Huang, L. *et al.* Layered vanadium(IV) disulfide nanosheets as a peroxidase-like nanozyme for colorimetric detection of glucose. *Microchim. Acta* **185**, 1–8 (2018).
151. Hu, S. *et al.* Enzyme-Free Tandem Reaction Strategy for Surface-Enhanced Raman Scattering Detection of Glucose by Using the Composite of Au Nanoparticles and Porphyrin-Based Metal–Organic Framework. *ACS Appl. Mater. Interfaces* **12**, 55324–55330 (2020).
152. Townsend, D. M., Tew, K. D. & Tapiero, H. The importance of glutathione in human disease. *Biomed. Pharmacother.* **57**, 145–155 (2003).
153. Yang, Q. *et al.* Generation of MnO2 nanozyme in spherical polyelectrolyte brush for colorimetric detection of glutathione. *Mater. Lett.* **248**, 89–92 (2019).
154. Zheng, X. *et al.* Catalytic Gold Nanoparticles for Nanoplasmonic Detection of DNA Hybridization. *Angew. Chem. Int. Ed.* **50**, 11994–11998 (2011).
155. Detection, L. C. & Polymorphism, S. Hemin - Graphene Hybrid Nanosheets with Intrinsic Peroxidase-like Activity. *ACS Nano* **5**, 1282–1290 (2011).
156. Xie, J. *et al.* A sandwich ELISA-like detection of C-reactive protein in blood by citicoline-bovine serum albumin conjugate and aptamer-functionalized gold nanoparticles nanozyme. *Talanta* **217**, 121070 (2020).
157. Yan, X. *et al.* Oxidase-mimicking activity of ultrathin MnO2 nanosheets in colorimetric assay of acetylcholinesterase activity. *Nanoscale* **9**, 2317–2323 (2017).
158. Wu, L., Zhou, M., Wang, Y. & Liu, J. Nanozyme and aptamer- based immunosorbent assay for aflatoxin B1. *J. Hazard. Mater.* **399**, 123154 (2020).
159. Xu, Z., Long, L., Chen, Y., Chen, M. & Cheng, Y. A nanozyme-linked immunosorbent assay based on metal – organic frameworks ( MOFs ) for sensitive detection of aflatoxin B 1. *Food Chem.* **338**, 128039 (2021).
160. Farka, Z. *et al.* Prussian Blue Nanoparticles as a Catalytic Label in a Sandwich Nanozyme-Linked Immunosorbent Assay. *Anal. Chem.* **90**, (2018).
161. Oh, S. *et al.* Magnetic Nanozyme-Linked Immunosorbent Assay for Ultrasensitive Influenza A Virus Detection. *ACS Appl. Mater. Interfaces* **10**, 12534–12543 (2018).
162. Rahin, S. *et al.* Size-controlled preparation of peroxidase-like graphene-gold nanoparticle hybrids for the visible detection of norovirus-like particles NoV-LPs Adsorbed. *Biosens. Bioelectron* **87**, 558–565 (2017).

163. Liu, W. *et al.* Paper-based colorimetric immunosensor for visual detection of carcinoembryonic antigen based on the high peroxidase-like catalytic performance of ZnFe2O4–multiwalled carbon nanotubes. *Analyst* **139**, 251–258 (2014).
164. Tian, Z. *et al.* Biomaterials Highly sensitive and robust peroxidase-like activity of porous nanorods of ceria and their application for breast cancer detection. *Biomaterials* **59**, 116–124 (2015).
165. Asati, A., Kaittanis, C., Santra, S. & Perez, J. M. pH-Tunable Oxidase-Like Activity of Cerium Oxide Nanoparticles Achieving Sensitive Fluorigenic Detection of Cancer Biomarkers at. *Anal. Chem.* **83**, 2547–2553 (2011).
166. Gao, Z., Lv, S., Xu, M. & Tang, D. High-index {hk0} faceted platinum concave nanocubes with enhanced peroxidase-like activity for an ultrasensitive colorimetric immunoassay of the human prostate-specific antigen. *Analyst* **142**, 911–917 (2017).
167. Loynachan, C. N. *et al.* Platinum Nanocatalyst Amplification: Redefining the Gold Standard for Lateral Flow Immunoassays with Ultrabroad Dynamic Range. *ACS Nano* **12**, 279–288 (2018).
168. Zhang, L. *et al.* Biominerized gold-Hemin@MOF composites with peroxidase-like and gold catalysis activities: A high-throughput colorimetric immunoassay for alpha-fetoprotein in blood by ELISA and gold-catalytic silver staining. *Sens. Actuat B-Chem* **266**, 543–552 (2018).
169. Wang, C., Gao, J. & Tan, H. Integrated Antibody with Catalytic Metal-Organic Framework for Colorimetric Immunoassay. *ACS Appl. Mater. Interfaces* **10**, 25113–25120 (2018).
170. Xia, X. *et al.* Pd-Ir Core-Shell Nanocubes: A Type of Highly Efficient and Versatile Peroxidase Mimic. *ACS Nano* **9**, 9994–10004 (2015).
171. Li, Y. *et al.* Manganese dioxide nanoparticle-based colorimetric immunoassay for the detection of alpha-fetoprotein. *Microchim. Acta* **184**, 2767–2774 (2017).
172. Asati, A., Santra, S., Kaittanis, C., Nath, S. & Perez, J. M. Oxidase-like activity of polymer-coated cerium oxide nanopartieles. *Angew. Chem. Int. Ed.* **48**, 2308–2312 (2009).
173. Tao, Y., Lin, Y., Huang, Z., Ren, J. & Qu, X. Incorporating graphene oxide and gold nanoclusters: A synergistic catalyst with surprisingly high peroxidase-like activity over a broad pH range and its application for cancer cell detection. *Adv. Mater.* **25**, 2594–2599 (2013).
174. Maji, S. K., Mandal, A. K., Nguyen, K. T., Borah, P. & Zhao, Y. Cancer cell detection and therapeutics using peroxidase-active nanohybrid of gold nanoparticle-loaded mesoporous silica-coated graphene. *ACS Appl. Mater. Interfaces* **7**, 9807–9816 (2015).
175. Vijgen, J., de Borst, B., Weber, R., Stobiecki, T. & Forter, M. HCH and lindane contaminated sites: European and global need for a permanent solution for a long-time neglected issue. *Environ. Pollut.* **248**, 696–705 (2019).
176. Senthilnathan, J. & Philip, L. Photocatalytic degradation of lindane under UV and visible light using N-doped TiO2. *Chem. Eng. J.* **161**, 83–92 (2010).
177. Sen Gupta, S. *et al.* Simultaneous dehalogenation and removal of persistent halocarbon pesticides from water using graphene nanocomposites: A case study of lindane. *ACS Sustain. Chem. Eng.* **3**, 1155–1163 (2015).

178. Wang, Y., Yang, Y., Shi, Y., Song, H. & Yu, C. Antibiotic-Free Antibacterial Strategies Enabled by Nanomaterials: Progress and Perspectives. *Adv. Mater.* 1904106 (2019) doi:10.1002/adma.201904106.
179. Fang, G. *et al.* Differential Pd-nanocrystal facets demonstrate distinct antibacterial activity against Gram-positive and Gram-negative bacteria. *Nat. Commun.* **9**, 129 (2018).
180. Berlett, B. S. & Stadtman, E. R. Protein oxidation in aging, disease, and oxidative stress. *JBC* **272**, 20313–20316 (1997).
181. Cai, H. & Harrison, D. G. Endothelial dysfunction in cardiovascular diseases: The role of oxidant stress. *Circ. Res.* **87**, 840–844 (2000).
182. Moglianetti, M. *et al.* Platinum nanozymes recover cellular ROS homeostasis in an oxidative stress-mediated disease model. *Nanoscale* **8**, 3739–3752 (2016).
183. Liu, T. *et al.* Ultrasmall copper-based nanoparticles for reactive oxygen species scavenging and alleviation of inflammation related diseases. *Nat. Commun.* **11**, 1–16 (2020).
184. Kim, D., Kwon, H. J. & Hyeon, T. Magnetite/Ceria Nanoparticle Assemblies Assemblies for Extracorporeal Cleansing of Amyloid-β in Alzheimer's Disease. *Adv.* **31**, 1–6 (2019).
185. Gong, F. *et al.* Oxygen-Deficient Bimetallic Oxide FeWOX Nanosheets as Peroxidase-Like Nanozyme for Sensing Cancer via Photoacoustic Imaging. *Small* **16**, 1–12 (2020).
186. Jiang, B. *et al.* Biomineralization Synthesis of the Cobalt Nanozyme in SP94-Ferritin Nanocages for Prognostic Diagnosis of Hepatocellular Carcinoma. *ACS Appl. Mater. Interfaces* **11**, 9747–9755 (2019).
187. Gupta, A., Das, R., Yesilbag Tonga, G., Mizuhara, T. & Rotello, V. M. Charge-Switchable Nanozymes for Bioorthogonal Imaging of Biofilm-Associated Infections. *ACS Nano* **12**, 89–94 (2018).
188. Biju, V., Itoh, T., Anas, A., Sujith, A. & Ishikawa, M. Semiconductor quantum dots and metal nanoparticles: Syntheses, optical properties, and biological applications. *Anal. Bioanal. Chem.* **391**, 2469–2495 (2008).
189. Gao, X. *et al.* In vivo molecular and cellular imaging with quantum dots. *Curr. Opin. Biotechnol.* **16**, 63–72 (2005).
190. Zhong, W. Nanomaterials in fluorescence-based biosensing. *Anal. Bioanal. Chem.* **394**, 47–59 (2009).
191. Algar, W. R. & Krull, U. J. Quantum dots as donors in fluorescence resonance energy transfer for the bioanalysis of nucleic acids, proteins, and other biological molecules. *Anal. Bioanal. Chem.* **391**, 1609–1618 (2008).
192. Zhang, C. Y., Yeh, H. C., Kuroki, M. T. & Wang, T. H. Single-quantum-dot-based DNA nanosensor. *Nat. Mater.* **4**, 826–831 (2005).
193. Algar, W. R. & Krull, U. J. Towards multi-colour strategies for the detection of oligonucleotide hybridization using quantum dots as energy donors in fluorescence resonance energy transfer (FRET). *Anal. Chim. Acta* **581**, 193–201 (2007).
194. Kim, J. H., Chaudhary, S. & Ozkan, M. Multicolour hybrid nanoprobes of molecular beacon conjugated quantum dots: FRET and gel electrophoresis assisted target DNA detection. *Nanotechnology* **18**, (2007).
195. Nutiu, R. & Li, Y. Structure-Switching Signaling Aptamers. *JACS* **18**, 4771–4778

(2003).
196. Chang, E. *et al.* Protease-activated quantum dot probes. *Biochem. Biophys. Res. Commun.* **334**, 1317–1321 (2005).
197. Goldman, E. R. *et al.* A hybrid quantum dot - Antibody fragment fluorescence resonance energy transfer-based TNT sensor. *JACS* **127**, 6744–6751 (2005).
198. Medintz, I. L. *et al.* Self-assembled nanoscale biosensors based on quantum dot FRET donors. *Nat. Mater.* **2**, 630–638 (2003).
199. Chen, L.-Y., Wang, C.-W., Yuan, Z. & Chang, H.-T. Fluorescent Gold Nanoclusters: Recent advances in Sensing and Imaging. *Anal. Chem.* **87**, 216–229 (2015).
200. Le Guével, X. Recent Advances on the Synthesis of Metal Quantum Nanoclusters and Their Application for Bioimaging. *IEEE J. Sel. Top. Quantum Electron.* **20**, (2014).
201. Guo, S. & Wang, E. Noble metal nanomaterials : Controllable synthesis and application in fuel cells and analytical sensors. *Nano Today* 240–264 (2011) doi:10.1016/j.nantod.2011.04.007.
202. Jariwala, D., Sangwan, V. K., Lauhon, L. J., Marks, T. J. & Hersam, M. C. Carbon nanomaterials for electronics, optoelectronics, photovoltaics, and sensing. *Chem. Soc. Rev.* **42**, 2824 (2013).
203. Ishida, T., Murayama, T., Taketoshi, A. & Haruta, M. Importance of Size and Contact Structure of Gold Nanoparticles for the Genesis of Unique Catalytic Processes. *Chem. Rev.* **120**, 464–525 (2020).
204. Xie, J., Zheng, Y. & Ying, J. Y. Protein-Directed Synthesis of Highly Fluorescent Gold Nanoclusters. *J. Am. Chem. Soc.* **131**, 888–889 (2009).
205. Wang, G. L., Jin, L. Y., Dong, Y. M., Wu, X. M. & Li, Z. J. Intrinsic enzyme mimicking activity of gold nanoclusters upon visible light triggering and its application for colorimetric trypsin detection. *Biosens. Bioelectron.* **64**, 523–529 (2015).
206. Li, H. W., Yue, Y., Liu, T. Y., Li, D. & Wu, Y. Fluorescence-enhanced sensing mechanism of BSA-protected small gold-nanoclusters to silver(I) ions in aqueous solutions. *J. Phys. Chem. C* **117**, 16159–16165 (2013).
207. Kawasaki, H., Hamaguchi, K., Osaka, I. & Arakawa, R. Ph-dependent synthesis of pepsin-mediated gold nanoclusters with blue green and red fluorescent emission. *Adv. Funct. Mater.* **21**, 3508–3515 (2011).
208. Xu, Y. *et al.* The role of protein characteristics in the formation and fluorescence of Au nanoclusters. *Nanoscale* **6**, 1515–1524 (2014).
209. Yu, Y., Geng, J., Ong, E. Y. X., Chellappan, V. & Tan, Y. N. Bovine Serum Albulmin Protein-Templated Silver Nanocluster (BSA-Ag13): An Effective Singlet Oxygen Generator for Photodynamic Cancer Therapy. *Adv. Healthc. Mater.* **5**, 2528–2535 (2016).
210. Jin, L. *et al.* Ultrasmall Pt Nanoclusters as Robust Peroxidase Mimics for Colorimetric Detection of Glucose in Human Serum. *ACS Appl. Mater. Interfaces* **9**, 10027–10033 (2017).
211. Goswami, N. *et al.* Copper quantum clusters in protein matrix: Potential sensor of Pb 2+ ion. *Anal. Chem.* **83**, 9676–9680 (2011).
212. Miao, H., Zhong, D., Zhou, Z. & Yang, X. Papain-templated Cu nanoclusters: Assaying and exhibiting dramatic antibacterial activity cooperating with H2O2. *Nanoscale* **7**, 19066–19072 (2015).
213. Noh, Y., Jo, E. J., Mun, H., Ahn, Y. deok & Kim, M. G. Homogeneous and selective

detection of cadmium ions by forming fluorescent cadmium-protein nanoclusters. *Chemosphere* **174**, 524–530 (2017).
214. Pajooheshpour, N. *et al.* Protein templated Au-Pt nanoclusters-graphene nanoribbons as a high performance sensing layer for the electrochemical determination of diazinon. *Sens. Actuat B-Chem* **275**, 180–189 (2018).
215. Han, S. Q., Liu, J. L., Gan, Z. G., Liang, J. G. & Zhao, S. M. Application of luminescent BSA-capped CdS quantum dots as a fluorescence probe for the detection of Cu2+. *J. Chinese Chem. Soc.* **55**, 1069–1073 (2008).
216. Wang, Q. *et al.* Bovine serum albumin-directed synthesis of biocompatible CdSe quantum dots and bacteria labeling. *J. Colloid Interface Sci.* **355**, 9–14 (2011).
217. You, J. G. & Tseng, W. L. Peptide-induced aggregation of glutathione-capped gold nanoclusters: A new strategy for designing aggregation-induced enhanced emission probes. *Anal. Chem.* **1078**, 101–111 (2019).
218. Le Guével, X., Spies, C., Daum, N., Jung, G. & Schneider, M. Highly fluorescent silver nanoclusters stabilized by glutathione: A promising fluorescent label for bioimaging. *Nano Res.* **5**, 379–387 (2012).
219. Luo, T., Wang, Y., Wang, M. & Liao, M. Glutathione - stabilized Cu nanocluster - based fluorescent probe for sensitive and selective detection of Hg 2 + in water. *Luminiscence* 1–8 (2017) doi:10.1002/bio.3296.
220. Yang, X. *et al.* One-step synthesis and applications of fluorescent Cu nanoclusters stabilized by l-cysteine in aqueous solution. *Anal. Chim. Acta* **847**, 49–54 (2014).
221. Roy, S., Palui, G. & Banerjee, A. The as-prepared gold cluster-based fluorescent sensor for the selective detection of As III ions in aqueous solution. *Nanoscale* **4**, 2734–2740 (2012).
222. Adhikari, B. & Banerjee, A. Short-peptide-based hydrogel: A template for the in situ synthesis of fluorescent silver nanoclusters by using sunlight. *Chem. Eur. J.* **16**, 13698–13705 (2010).
223. Chen, Y. *et al.* Cysteine-directed fluorescent gold nanoclusters for the sensing of pyrophosphate and alkaline phosphatase. *J. Mater. Chem. C* **2**, 4080–4085 (2014).
224. Petty, J. T., Zheng, J., Hud, N. V. & Dickson, R. M. DNA-Templated Ag Nanocluster Formation. *JACS* **126**, 5207–5212 (2004).
225. Richards, C. I. *et al.* Oligonucleotide-stabilized Ag nanocluster fluorophores. *JACS* **130**, 5038–5039 (2008).
226. Neacşu, V. A. *et al.* Unusually large fluorescence quantum yield for a near-infrared emitting DNA-stabilized silver nanocluster. *Chem. Comm.* **56**, 6384–6387 (2020).
227. Lan, J. *et al.* Aptamer-Modified Silver Nanoclusters for Fluorescence Detection of Intracellular 8-Hydroxydeoxyguanosine. *ACS Appl. Nano Mater.* **3**, 1332–1338 (2020).
228. Feng, B., Xing, Y., Lan, J., Su, Z. & Wang, F. Synthesis of MUC1 aptamer-stabilized gold nanoclusters for cell-specific imaging. *Talanta* **212**, 120796 (2020).
229. Chai, Y. lin *et al.* A novel fluorescent nanoprobe that based on poly(thymine) single strand DNA-templated copper nanocluster for the detection of hydrogen peroxide. *Spectrochim. Acta A* **239**, 118546 (2020).
230. Xian-ming, Q., Liu, Z., Cai, S., Zhao, Y. & Wu, D. Electrochemical aptasensor for the detection of vascular endothelial growth factor ( VEGF ) based on DNA-templated Ag / Pt bimetallic nanoclusters. *Chin. Chem. Lett.* 1–7 (2016) doi:10.1016/j.cclet.2016.04.014.

231. Tao, Y., Li, M., Ren, J. & Qu, X. Metal nanoclusters: Novel probes for diagnostic and therapeutic applications. *Chem. Soc. Rev.* **44**, 8636–8663 (2015).
232. Wang, B., Zhao, M., Mehdi, M. & Wang, G. Biomolecule-assisted synthesis and functionality of metal nanoclusters for biological sensing : a review. *Mater. Chem. Front.* **3**, 1722–1735 (2019).
233. Xie, J., Zheng, Y. & Ying, J. Y. Highly selective and ultrasensitive detection of Hg2+ based on fluorescence quenching of Au nanoclusters by Hg2+-Au+ interactions. *Chem. Comm.* **46**, 961–963 (2010).
234. Yeh, H. C., Sharma, J., Han, J. J., Martinez, J. S. & Werner, J. H. A DNA-silver nanocluster probe that fluoresces upon hybridization. *Nano Lett.* **10**, 3106–3110 (2010).
235. Sharma, J., Yeh, H. C., Yoo, H., Werner, J. H. & Martinez, J. S. Silver nanocluster aptamers: In situ generation of intrinsically fluorescent recognition ligands for protein detection. *Chem. Comm.* **47**, 2294–2296 (2011).
236. Wang, Y., Wang, Y., Zhou, F., Kim, P. & Xia, Y. Protein-protected Au clusters as a new class of nanoscale biosensor for label-free fluorescence detection of proteases. *Small* **8**, 3769–3773 (2012).
237. Wang, X., Wu, Q., Shan, Z. & Huang, Q. BSA-stabilized Au clusters as peroxidase mimetics for use in xanthine detection. *Biosens. Bioelectron.* **26**, 3614–3619 (2011).
238. Hu, D. *et al.* Folate receptor-targeting gold nanoclusters as fluorescence enzyme mimetic nanoprobes for tumor molecular colocalization diagnosis. *Theranostics* **4**, 142–153 (2014).
239. Jiang, X., Sun, C., Guo, Y., Nie, G. & Xu, L. Peroxidase-like activity of apoferritin paired gold clusters for glucose detection. *Biosens. Bioelectron.* **64**, 165–170 (2015).
240. Huang, Y. Q. *et al.* Protamine-gold nanoclusters as peroxidase mimics and the selective enhancement of their activity by mercury ions for highly sensitive colorimetric assay of Hg(II). *Anal. Bioanal. Chem.* **410**, 7385–7394 (2018).
241. Li, W. *et al.* BSA-stabilized Pt nanozyme for peroxidase mimetics and its application on colorimetric detection of mercury(II) ions. *Biosens. Bioelectron.* **66**, 251–258 (2015).
242. Yan, Z. *et al.* A novel colorimetric method based on copper nanoclusters with intrinsic peroxidase-like for detecting xanthine in serum samples. *J. Nanopart. Res.* **19**, 235 (2017).
243. Liu, Y. *et al.* Colorimetric immunoassay for Listeria monocytogenes by using core gold nanoparticles, silver nanoclusters as oxidase mimetics, and aptamer-conjugated magnetic nanoparticles. *Microchim. Acta* **185**, 2–8 (2018).
244. Yu, C. J., Chen, T. H., Jiang, J. Y. & Tseng, W. L. Lysozyme-directed synthesis of platinum nanoclusters as a mimic oxidase. *Nanoscale* **6**, 9618–9624 (2014).
245. Fan, J. *et al.* Direct evidence for catalase and peroxidase activities of ferritin e platinum nanoparticles. *Biomat.* **32**, 1611–1618 (2011).

# CHAPTER 2: MOTIVATION AND OBJECTIVES

## Motivation and objectives

Biosensors are nowadays all-over in biomedical diagnosis as well as a wide range of other areas such as POC monitoring of treatment and disease progression, environmental monitoring, food control, drug discovery, forensics, biomedical research and healthcare. These last two are the main market sections interested in the development of biosensors. At the present time, analytical methodologies based on immunoassays are considered as one of the most powerful tools for these sectors, because proteins are related with the most common diseases. Despite this, there is a need of improving the sensitivity and stability of immunological assays. Traditional methodologies for labelling antibodies for its further use in immunoassays involve a chemical reaction between the antibody and an enzyme. As a result of the linking process, some species are formed by random coupling. These species cause background signal and nonspecific binding, which reduces the sensitivity of immunoassays. In this thesis, we propose the use of nanotechnology to overcome these drawbacks and to set up a universal methodology for labelling antibodies, eliminating the step of the chemical reaction.

The hypothesis of this work is: **the synthesis of atomic nanoclusters with optical and/or catalytic properties using antibodies as scaffold without changing its affinity for target analyte and their further use in immunoassays. The use of antibody carrying NCs decreases the detection limit and improves the signal-to-noise ratio of the immunoassay.** Thereby, the antibody carrying nanoclusters incorporate both a recognition component (to sense selective the interaction with the bioanalyte) and a transduction component (to deliver the corresponding interaction). The incorporation of the nanoclusters inside the biorecognition element may address the drawbacks related with enzymes-label complex, and results in the development of new efficient strategies for the detection system of immunoassays. The advance beyond the state of the art is the non-denaturation of the antibody during the introduction of the NCs into its structure. The protein structure remains unchanged and the affinity for target analyte do not change. In the literature there are multiple examples of the synthesis of NCs using proteins as scaffolds, however, these methods are performed under denaturing

conditions and in most of the cases the proteins structure is altered, and it lose its biological properties.

This research was made based on the wide knowledge from the laboratories of Biosensing Lab group (CIC biomaGUNE) and Biomaterials group (Tecnalia Research & Innovation) in the field of sensing. The Biosensing Lab group pioneered enzymatic synthesis of nanomaterials and has applied it to the development of simple, sensitive, and inexpensive bioanalytical assays. This enzymatic manipulation of nanomaterials has been applied to detect different analytes in ELISA through the biocatalytic formation of CdS QDs *in situ*. In addition, the Biosensing lab has also experience in selection and synthesis of DNA aptamers for a number of target proteins and has successfully developed aptasensors for MnSOD and for a human herpes virus. On the other hand, Biomaterials group in Tecnalia has expertise in the oriented immobilization of antibodies for immunoassays based on polystyrene surface modification with different functional groups such as amines, carboxylic acids, alquenes or epoxys. Also, there is a research line focused on the design and development of miniaturized chips for biosensing and they have developed the first miniaturized portable chip used as a photoelectrochemical immunosensor.

Since I was interested on biosensor technology and passionate about nanoscience, I decided to perform this PhD thesis under the supervision of Dr. Valery Pavlov (CIC biomaGUNE) and Dra. Nerea Briz (Tecnalia Research & Innovation). The main goal of this work was to develop an immunoassay based on the technology of antibody carrying nanoclusters with an improved performance in terms of sensitivity and step processes of that of a commercial kit. In order to achieve this, some specific objectives were proposed:

1. **Synthesis of nanoclusters with some measurable property (fluorescence, photocatalytic or catalytic activity) using antibodies as scaffold without changing their biological properties.**
2. **Development of immunoassays for the detection of biomolecules using the optical, photocatalytic or catalytic properties of the antibodies carrying nanoclusters; that improve conventional ELISA assays.**

The first task of the work was to set up the methodology for the introduction of NCs inside the antibody structure without changing its secondary structure and neither its affinity for target analyte. As a model antibody a polyclonal Anti-BSA IgG from rabbit was selected. Three different types of materials were tested for this issue: CdS, Ag/Pt and Au/Pt (Chapter 3). On the one hand, CdS was chosen for its fluorescent and photocatalytic properties. On the other hand, the bimetallic materials were selected for their peroxidase-like activity and ability to oxidise chromogenic substrates. The three types of nanoclusters were successfully introduced in the polyclonal model antibody without changing its affinity for BSA. The performance of the synthetic procedure was tested in other polyclonal antibodies and in a monoclonal antibody.

Then, the model antibody carrying NCs was used as a probe, acting as the recognition element and the transduce component, in different kinds of immunoassays (Chapter 4). The bimetallic NCs were used as detection antibody in a sandwich immunoassay and its performance was compared with the same antibody labelled with HRP. The semiconductor NCs were tested as fluorescent donor in a FRET-based homogeneous immunoassay.

# CHAPTER 3: SYNTHESIS AND CHARACTERIZATION OF ANTIBODY-PROTECTED NANOCLUSTERS

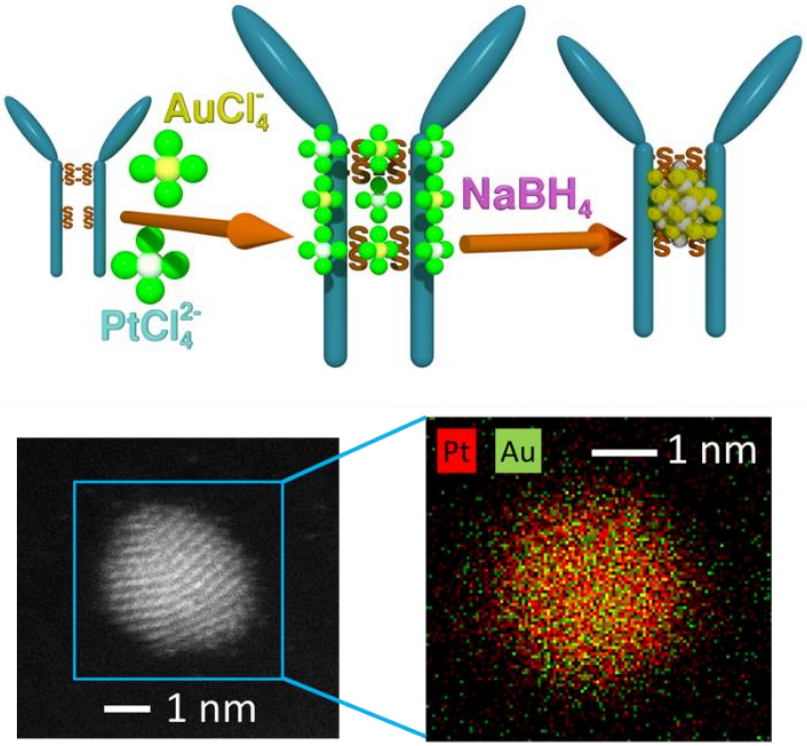


## Synthesis and Characterization of Antibody-protected Nanoclusters

There is a large number of examples of the synthesis of NCs using proteins as scaffold. Usually the synthetic conditions for the synthesis of NCs stabilized with proteins require extreme conditions in terms of pHs or temperature. These conditions cause the denaturalization of the biomolecules and end up in the loss of their biological functions. Until now there are no examples of the use of antibodies as NCs stabilisers. In this chapter we present the first method for the synthesis of bimetallic and semiconductor NCs that employes antibodies as scaffold. A polyclonal IgG from rabbit was used as a model antibody. The synthesis is carried out under non denaturing conditions, which do not affect the antibody structure. The resulting antibodies-NCs conjugates still maintain the affinity for target antigens and protein G.

## 1. Introduction

Metallic and semiconductor NCs are composed of several atoms with a size smaller than 2-3 nm[1] and demonstrate very peculiar optical, electronic and catalytic features. Due to their unique properties, NCs find important applications in biodetection, bioimaging, electronics and photovoltaic[2]. Their specific properties arise from their subnanometric dimensions, comparable to the Fermi wavelength of electrons. The spatial isolation of free electrons in NCs provide electronic transitions tunable with size[3]. Several biopolymers like bovine serum albumin (BSA)[4,5,6], lysozyme[7,8], GOx[9] , HRP[10], glutathione[11] or DNA[12] have been used as stabilizer for semiconductor and metallic clusters of atoms. The harsh conditions employed during the synthesis of NCs, such high temperature or extremely basic pH, with these biopolymers as scaffolds cause partial or complete loss of their initial biological properties due to denaturalization. To the best of our knowledge, antibodies, which play the important part in immune response of living organisms, have never been employed as scaffolds for the synthesis of catalytic semiconductor or metallic NCs.

In the present work a polyclonal IgG was used as scaffold for the synthesis of NCs composed of different materials without changing its conformation and maintaining the binding for its antigen by using mild conditions during the synthesis. As a model antibody-antigen system BSA and corresponding antibody, anti-BSA IgG, were selected. This system is commonly used as a model in research [13,14,15]. Albumin functions as a carrier protein for steroids, fatty acids, and thyroid hormones in the blood and plays a major role in stabilizing extracellular fluid volume by contributing to colloid osmotic pressure of plasma. BSA is the most abundant protein in plasma and has very important applications in cell culture, clinical diagnosis, electrophoresis chromatography and immune biochemistry [16] and it is usually used as a standard protein. It is composed by a single peptide chain protein composed of 582 amino acids and its sequence is similar to that of human serum albumin (HSA)[17]. Three different materials were chosen for the synthesis of NCs, semiconductor NCs composed by cadmium sulphide (CdS) and bimetallic NCs composed by silver/platinum (Ag/Pt) and gold/platinum (Au/Pt). These

materials have been selected due to their optical and catalytic properties for the further use of the NCs-IgG conjugate in inmmunosensing applications.

Most of the known nanozymes can play the catalytic role without special lighting requirements. However, there are some that need to be stimulated by light to exhibit enzyme-like properties. CdS was chosen for the synthesis of CdS NCs-IgG due to their photocatalytic properties towards oxidation of *N*-acetyl-3,7-dihydroxyphenoxazine (Amplex Red). CdS nanomaterials, as quantum dots (QDs) are photosensitive nanozymes capable of generating reactive oxygen species (ROS), as hydrogen peroxide ($H_2O_2$) triggered by the exposure to ultraviolet light (UV-light)[18]. When nanomaterials composed by semiconductor materials such as CdS, CdSe, ZnS or $TiO_2$ are excited with light energy greater than their band gap, electrons are promoted from the valence band to the conduction band and the generated electron-hole pair can emit a photon or undergo electron transfer with the environment. Due to the latter these materials exhibit photocatalytic activity[19] Photocatalytic activity of proteins conjugated with CdS nanoparticles (NPs) has been demonstrated with the enzyme cytochrome P450 monooxygenase[20,21], cytochrome c peroxidase and HRP[22]. Moreover Amplex Red, CdS nanomaterials can oxidize other typical peroxidase substrates, such as guaiacol, or 2,2'-azinobis (3-ethylbenzthiazolin-6-sulfonate) (ABTS)[23].

CdS NCs also exhibit fluorescent properties and can be employed for sensing applications. For example CdS QDs synthesized using D-penicillamine as capping agent have been employed for the detection of cysteamine[24]. Another example is the synthesis of fluorescent CdS QDs using thioglycolic acid as scaffold, the presence of dopamine[25] quenches the QDs fluorescence and serve for its quantification. CdS QDs capped by cysteine use the same quenching strategy for the sensing of trinitrophenol[26]. CdS QDs have been also employed for the multiplexed detection of three heavy metal ions($Cr^{3+}$, $Fe^{3+}$ and $Sn^{2+}$)[27].

NCs composed by Ag and Pt have been chosen for the synthesis of Ag/Pt NCs-IgG due to their capacity to catalyze the oxidation of TMB in the presence of $H_2O_2$. Previously, Ag/Pt bimetallic NCs, synthesized using a single stranded DNA as a template, demonstrated

catalytic activity. This feature was used for the sensing of different analytes, for example mercury ions[28], L-cysteine[29] or thrombin[30].

Au/Pt NCs exhibit the same peroxidase behavior than Ag/Pt NCs and they have been synthesized previously using GSH as scaffold and used for the sensing of glucose[31]. Other nanomaterials composed by gold and platinum also have peroxidase-like activity and have been used in sensing applications. For example, Au/Pt NPs decorated on molybdenum disulfide surface have been employed for the selectively colorimetric analysis of cysteine[32]. Nanohybrids with a core composed by gold and a shell by platinum also present catalytic properties and can be used in a immunoassay for the determination of the prostate specific antigen (PSA)[33].

## 2. Experimental section

### 2.1. Chemicals and materials

Cadmium nitrate ($CdNO_3$), sodium sulfide ($Na_2S$), silver nitrate ($AgNO_3$), chloroauric acid ($HAuCl_4$), potassium tetracholoroplatinate ($K_2PtCl_4$), BSA, polyclonal anti-BSA IgG (developed in rabbit), monoclonal anti-vinculin IgG (developed in mouse), polyclonal anti-mouse IgG (developed in rabbit), casein, TMB, Amplex Red, sodium borohydride ($NaBH_4$), phosphate buffer saline (pH 7.4) (PBS), sodium phosphate monobasic ($NaH_2PO_4$), TWEEN and other chemicals were supplied by Sigma-Aldrich. One µm diameter polyvinyl chloride microbeads decorated with Protein G (beadBALL-Protein G) were obtained from Chemicell. Hydrogen peroxide ($H_2O_2$) was supplied by Panreac. Polyclonal rabbit anti-human prostate-specific antigen (PSA) IgG was supplied by Dako. PSA was commercially available from Lee BioSolutions. Human Interleukin-6 (IL-6) Antibody Pair- BSA and Azide free and IL-6 were purchased from Abcam.

## 2.2. Characterization of materials

Fluorescence and UV-visible

The spectra were performed on a Varioskan Flash microplate reader (Thermo Scientific) at room temperature. The system was controlled by SkanIt Software 2.4.3. for Varioskan Flash. The measurements were carried out using 96-wells black microtiter plates.

Transmission electron microscope (TEM) and scanning transmission electron microscopy (STEM)

TEM and STEM images were recorded with a JEOL JEM 2100F microscope equipped with a high-angle annular dark field (HAADF) detector and with a digital camera of type F-216 operating at 200 kV. The samples have immediately been prepared from the solution of the freshly prepared assay by desiccating a tiny droplet of the solution on the hydrophilized surface of a freshly glow-discharged treated ultrathin carbon film coated Cu-grid.

Cryo-Transmission electron microscope (cryo-TEM)

Cryo-TEM images were taken after sample vitrification with a Vitrobot Mark III (FEI Company, USA). In the sample preparation chamber of the Vitrobot a temperature of 8 ˚C and saturated relative humidity have been maintained during the droplet deposition and blotting phase. 4 microliters of sample solution have initially been deposited for 30 seconds onto freshly glow-discharge treated holey carbon film, and in order to end up with a thin liquid film of typically bellow 100 nanometer film thickness, blotting with absorbent standard filter paper was processed afterwards. The obtained thin liquid film containing the sample was plunged into liquid ethane for receiving the vitrified TEM sample. Sample holders of model 626 (Gatan, USA) have then been used for the cryo transfer to and imaging at a cryo-TEM of type JEOL JEM-2200FS/CR (JEOL, Japan) equipped with a UltraScan 4000 SP camera (Gatan, UK). Zero-loss energy filtering by the in-column Omega filter of this 200 kV FEG-TEM could be applied for the enhanced image acquisition.

Energy-dispersive X-ray (EDX)

The elemental maps were obtained using a probe-corrected ThermoFisher Titan electron microscope equipped with a Super-X detector, operated at 300 kV. Elemental maps were acquired over the course of 40 min at 150 pA electron beam current and analysed using Bruker Esprit software.

X-ray photoelectron spectroscopy (XPS)

The experiments were performed in a SPECS Sage HR 100 spectrometer with a non-monochromatic X-ray source (Magnesium Kα line of 1253.6 eV energy and 252 W), placed perpendicular to the analyzer axis and calibrated using the $3d_{5/2}$ line of Ag with a full width at half maximum (FWHM) of 1.1 eV. The selected resolution for the spectra was 15 eV of Pass Energy and 0.15 eV/step. All measurements were made in an ultra-high vacuum (UHV) chamber at a pressure around $8.10^{-8}$ mbar. An electron flood gun was used to neutralize for charging. Samples were deposited on carbon adhesive tabs and dried in a Desiccator Cabinet (Scienceware®) for 48 hours.

Circular dichroism (CD)

The spectra were measured using a JASCO J-815CD Spectrometer using a 1 mm path length quartz cuvette. All CD spectra were recorded with a band-with of 1 nm at 1 nm increments and 10 s average time.

Matrix Assisted Laser Desorption/Ionization time-of-flight (MALDI-TOF)

The measurements were performed in a MALDI/TOF-TOF MS UltrafleXtreme III (Bruker) with Flex Control 3.3. software. For the MALDI-TOF characterization the thin layer method as approach for sample deposition and a mixture of two matrixes were used[34]. For the thin layer, a saturated solution of α-cyano-4-hydroxycinnamic acid (α-CHCA) in acetone was prepared. A 10 µL pipette tip was dipped in the solution, then the MALDI target was touched by the pipette tip and deposit the α-CHCA solution. The matrix was composed by a mixture 1:1 ratio (vol/vol) of 20 mg/mL of α-CHCA in acetonitrile (ACN) and 5% formic acid (70:30, vol/vol) and a 20 mg/mL of 2,5-dihydroxybenzoic acid (DHB) in ACN and 0.1% trifluoroacetic acid (TFA) (70:30, vol/vol). Finally, 0.5 µL of the sample

was mixed with 0.5 µL of the mixture of matrix solution and deposited on the thin layer previously deposited in the MALDI target.

## 2.3. Methods

Photocatalytic and Catalytic Activity Evaluation of NCs-IgG

The assays were carried out at room temperature in a 96-well NUNC Microwell plate. The photocatalytic activity of the CdS NCs-IgG was quantified by photooxidation of the commercially available fluorogenic substrate Amplex Red. The system was composed of TRIS buffer (5 mM, pH=8.0) containing CdS NCs-IgG and Amplex Red (0.4 mM). The fluorescence spectra were recorded after incubation under a 365 nm wavelength UV lamp, using an excitation and emission wavelength of 530 nm and 590 nm respectively.

The peroxidase-like activity of Ag/Pt NCs-IgG and Au/Pt NCs-IgG was analysed by calculating steady-state kinetic parameters. The assays were carried out at room temperature in a 96-well NUNC Microwell plate. The catalytic activity of both NCs-IgG conjugates was evaluated using the chromogenic substrate TMB. The system was composed 100 µL of citrate buffer (10 mM, pH=4.0) containing Ag/Pt NCs-IgG or Au/Pt NCs-IgG and varying concentrations of TMB at a fixed concentration of $H_2O_2$ or *vice versa*. The colour change of the substrate from colourless to blue was monitored along the time at an absorption wavelength of 655 nm. The Michaelis-Menten constant (Km), which is an indicator of enzyme affinity for its substrate was obtained by using Lineweaver-Burk plot: $\frac{1}{v} = \frac{K_m}{V_{max}} . \frac{1}{[S]} + \frac{1}{V_{max}}$

Where $v$ is the initial velocity, [S] is the concentration of the substrate, and $V_{max}$ is the maximal reaction velocity.

Preparation of Polyvinyl Chloride Microbeads decorated with Protein G/ NCs-IgG composites

Microbeads decorated with protein G (600 µL, 10 mg/mL) were added into a 1.5 mL microcentrifuge tube and centrifuged (500 g, 1 min). The supernatant was discarded, and the beads were washed with PBS (600 µL, pH 7.4) three times and resuspended in PBS (600 µL). 100 µL of the beads were added to six different tubes. CdS NCs-IgG (100

µL, 5 mg/mL) (referred to Anti-BSA IgG concentration), Ag/Pt NCs-IgG (100 µL, 0.33 mg/mL) (referred to Anti-BSA IgG concentration), Au/Pt NCs-IgG (100 µL, 0.33 mg/mL) (referred to Anti-BSA IgG concentration), CdS NCs-BSA (100 µL, 5 mg/mL) (referred to BSA concentration), Ag/Pt NCs-BSA (100 µL of 0.33 mg/mL) (referred to BSA concentration) and Au/Pt NCs-BSA (100 µL of 0.33 mg/mL) (referred to BSA concentration) were added to each tube respectively. After 15 minutes incubation at room temperature (RT) under stirring the beads were washed three times with PBS/0.05 % (v/v) Tween (PBST) and resuspended in 100 µL of PBS.

Procedure for a direct ELISA based on the photocatalytic and catalytic activity of NCs-IgG

The immunoassays were carried out in a 96-well plate Nunc MaxiSorpt. First, different BSA concentrations (100 µL) in PBS were added into the wells and incubated (overnight (ON), 4 °C). Then, a solution of casein (100 µL, 20.5 mg/mL) was added as a blocking agent and incubated (1 h, room temperature (RT)). CdS NCs-IgG (100 µL, 500 µg/mL), Ag/Pt NCs-IgG (100 µL, 33 µg/mL) or Au/Pt NCs-IgG (100 µL, 33 µg/mL) were added and incubated (1h, RT). Finally, the antigen concentration was related with the photocatalytic activity of CdS NCs-IgG with Amplex Red (100 µL, 0.4 mM), the catalytic activity of Ag/Pt NCs-IgG with 100 µL of TMB (200 µM) and $H_2O_2$ (125 mM) or the catalytic activity of Au/Pt NCs-IgG with 100 µL of TMB (200 µM) and $H_2O_2$ (250 mM) After each step the wells were washed three times with PBST (100 µL).

Fab and F(ab')2 fragments generation

Fab and F(ab')2 fragments were prepared using Pierce™ Fab Micro Preparation Kit and Pierce™ F(ab')2 Micro Preparation Kit (ThermoFisher Scientific), respectively, from intact rabbit anti BSA IgG antibodies. For generation of Fab fragments, immobilized papain digests IgG antibodies, and Fab fragments are purified using Protein A agarose. For production of F(ab')2, immobilized pepsin protease is employed. Fab and F(ab´)2 fragments were used for the synthesis of Au/Pt NCs, following the same protocol described in Experimental Section for the intact Anti-BSA IgG antibody. Afterwards, the resulting solutions were employed for detection of BSA in a direct ELISA assay, as described in Experimental section.

# 3. Results and discusión

## 3.1. Synthesis and characterization

Three different methods have been developed for the modification of polyclonal Anti-BSA IgG (developed in rabbit) with NCs.

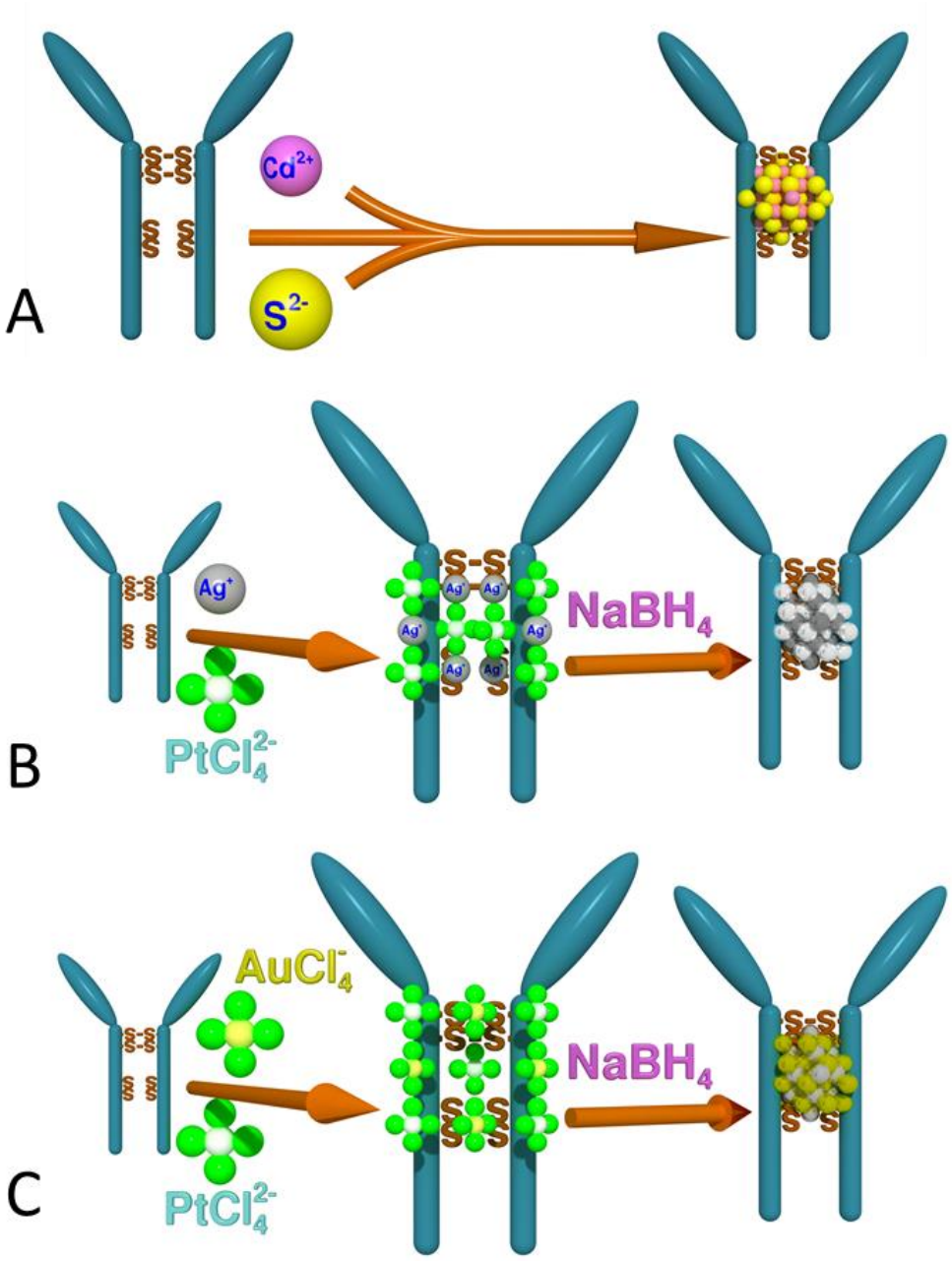


Figure 1. Scheme of the synthesis of semiconductor NCs composed by CdS (A), bimetallic NCs composed by Ag and Pt (B) and bimetallic NCs composed by Au and Pt (C).

For the synthesis of CdS NCs-IgG (Figure 1A), a solution of $CdNO_3$ (5 µL, 0.1 M) was added to an Anti-BSA antibody solution (200 µL, 5 mg/mL). The mixture was gently stirred for 15 min at RT. Then, $Na_2S$ (5 µL, 0.05 M) was added dropwise, immediately fluorescent NCs appeared. In Chapter 4 this synthesis was optimised by changing some parameters.

For the synthesis of Ag/Pt NCs-IgG (Figure 1B.), first $AgNO_3$ (50 µL, 150 µM) and $K_2PtCl_4$ (120 µL, 125 µM) were added to an anti-BSA antibody solution (100 µL of 1 mg/mL) in phosphate buffer (10 mM, pH 7.0). The mixture was incubated for 30 minutes in the dark. Then, a freshly prepared solution of $NaBH_4$ (30 µL, 5 mM) was added under gently stirring for initiating the reduction of the metal ions, until the colour of the mixture changed from colourless to pale brown. The mixture was allowed to react for three hours at room temperature.

Au/Pt NCs-IgG (Figure 1C.) were synthesized by mixing a gold precursor ($HAuCl_4$) and a platinum precursor ($K_2PtCl_4$) with a polyclonal anti-BSA antibody from rabbit in phosphate buffer (10 mM, pH 7.0). The mixture was incubated for 30 min in the dark. Then, a freshly prepared solution of $NaBH_4$ was added under gently stirring for initiating the reduction of the metal ions, until the colour of the mixture changed from colourless to pale brown. The mixture was allowed to react for three hours at RT. Different concentrations of the reagents were tested before choosing the optimal conditions for Au/Pt NCs IgG (Table 1.) The optimisation was carried out based on the performance of the catalytic Au/Pt NCs-IgG in a direct ELISA. In Figure 2. the reaction rate of TMB oxidation is represented for each synthesis. The best reaction rate of TMB oxidation was obtained with Synthesis 5. Further experiments were carried out using these conditions.

After the reaction time the reaction mixtures were filtrated (15 minutes, 10000 x g) using a 0.5 mL Amicon with a molecular weight cut-off of 30 kDa. The filtration was performed to separate the free ions from the atoms forming NCs. Control synthesis of the three methods were carried out using BSA as scaffold instead anti-BSA antibody. CdS NCs-BSA, Ag/Pt NCs-BSA and Au/Pt NCs-BSA were produced.

Table 1. Different concentrations of metal precursors and reducing agent used for the synthesis of Au/Pt NCs-IgG.

| | [Anti-BSA IgG] | [$HAuCl_4$] | [$K_2PtCl_4$] | [$NaBH_4$] |
|---|---|---|---|---|
| Synthesis 1 | 100 µL, 1 mg/mL | 50 µL, 150 µM | 120 µL, 125 µM | 30 µL, 5 mM |
| Synthesis 2 | 100 µL, 1 mg/mL | 50 µL, 150 µM | 120 µL, 250 µM | 30 µL, 5 mM |
| Synthesis 3 | 100 µL, 1 mg/mL | 50 µL, 150 µM | 120 µL, 500 µM | 30 µL, 5 mM |
| Synthesis 4 | 100 µL, 1 mg/mL | 50 µL, 250 µM | 120 µL, 500 µM | 30 µL, 5 mM |
| Synthesis 5 | 100 µL, 1 mg/mL | 50 µL, 250 µM | 120 µL, 500 µM | 30 µL, 10 mM |
| Synthesis 6 | 100 µL, 1 mg/mL | 50 µL, 500 µM | 120 µL, 1000 µM | 30 µL, 10 mM |
| Synthesis 7 | 100 µL, 1 mg/mL | 50 µL, 1000 µM | 120 µL, 1000 µM | 30 µL, 10 mM |
| Synthesis 8 | 100 µL, 1 mg/mL | 50 µL, 1000 µM | 120 µL, 2000 µM | 30 µL, 10 mM |

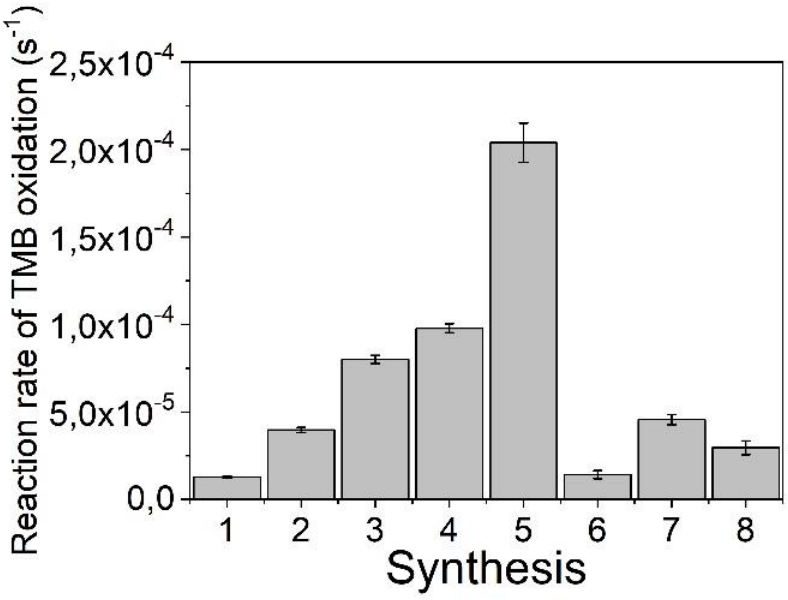


Figure 2. Reaction rate of TMB oxidation for each synthesis of Table 1.

Fluorescent properties of CdS NCs-IgG were evaluated after filtration. The fluorescence emission could be easily seen by the naked eye under UV light and recorded by digital camera (Figure 3A.). In Figure 3B. the fluorescence emission spectrum of CdS NCs-IgG is shown. The maximum emission peak was observed at 610 nm using an excitation wavelength of 315 nm. No fluorescence emission was observed for Ag/Pt NCs-IgG. The absorption spectra of both NCs are shown in Figure 3C. Characteristic absorption band for proteins appeared at 280 nm in all the NCs, also an absorption band appeared at 425 nm for CdS NCs-IgG.

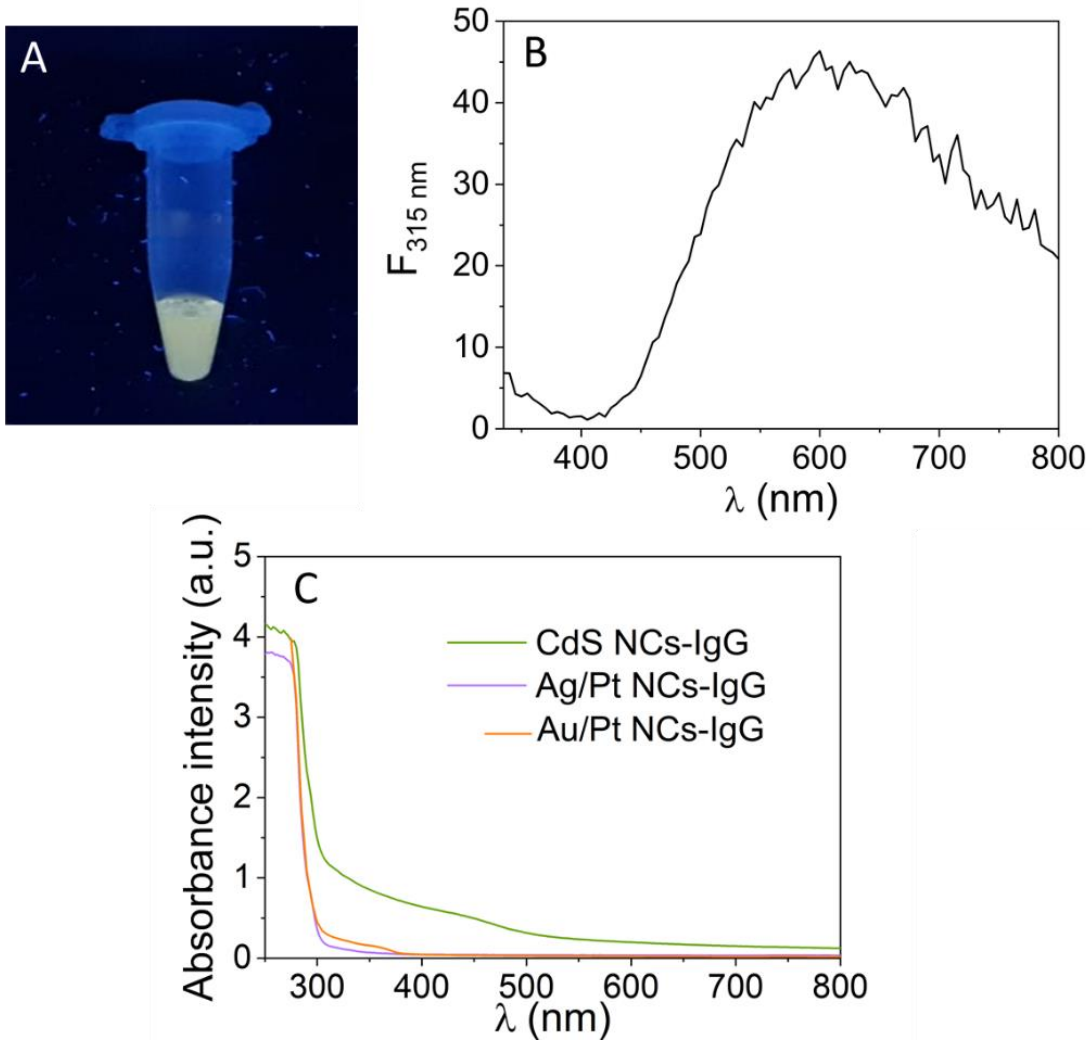


Figure 3. Image of CdS NCs-IgG under UV-light (365 nm) recorded by digital camera (A). Fluorescence emission spectrum of CdS NCs-IgG ($\lambda_{ex}$ = 315 nm) (B). Absorption spectra of CdS NCs-IgG, Ag/Pt NCs-IgG and Au/Pt NCs-IgG (C).

The NCs composed by CdS and Ag/Pt were characterized by cryo-TEM, where the size and the morphology of the cores were shown clearly. STEM was used to determine the morphology and the size of the metallic cores of Au/Pt NCs. The images revealed that the three types of NCs have a spherical morphology (Figure 4A, 4C, 4E). Based on the statistics over 100 individual particles, the diameter of the CdS NCs-IgG was 1.74 ± 0.30 nm (Figure 4B.). They have similar diameter as Ag/Pt NCs-IgG (Figure 4D.) and Au/Pt NCs-IgG (Figure 4F.) with 1.83 ± 0.30 nm and 1.97 ± 0.71 nm, respectively.

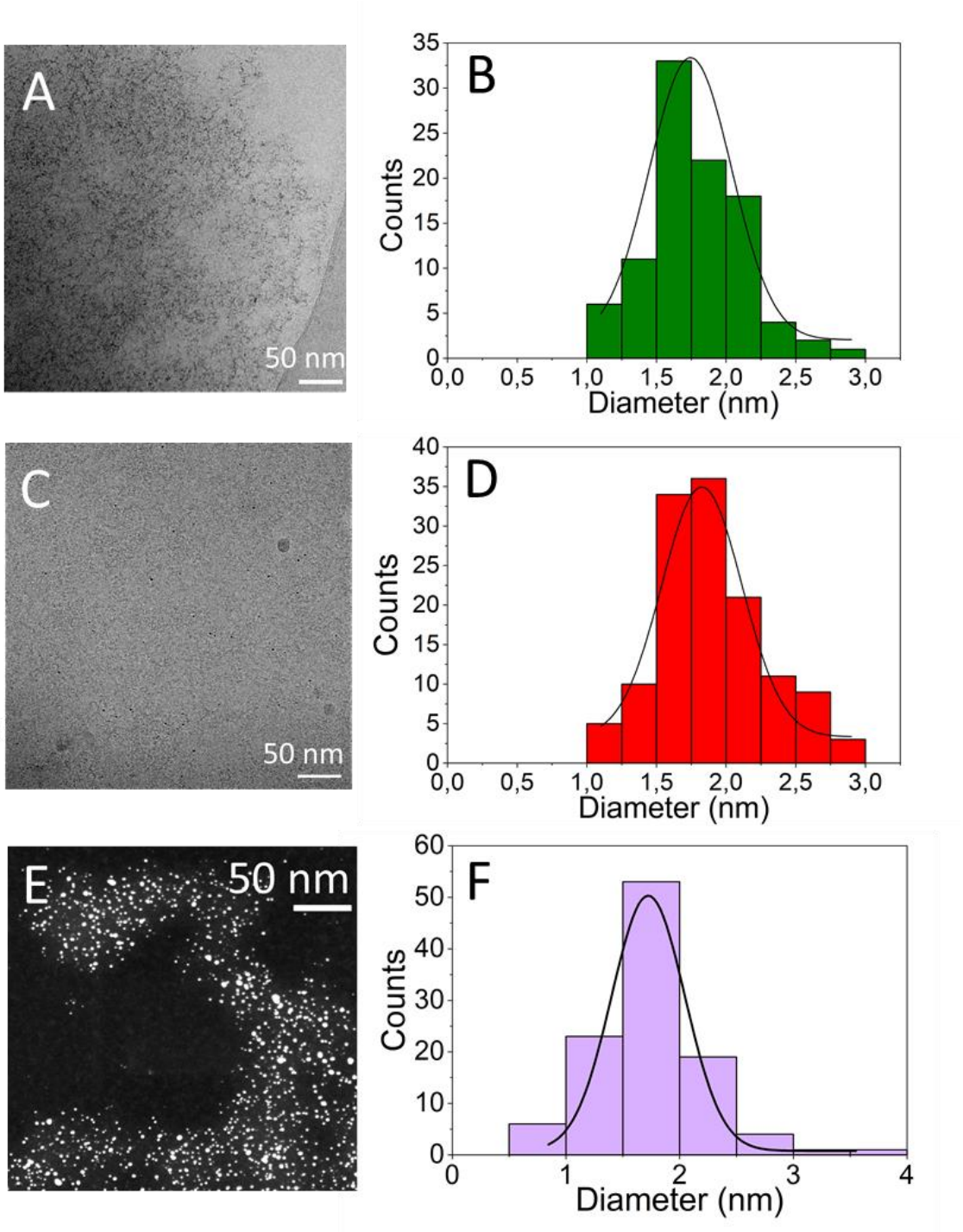


Figure 4. Representative TEM image of CdS NCs-IgG (A), Ag/Pt NCs-IgG (C) and STEM image of Au/Pt NCs-IgG (E). Size distribution of CdS NCs-IgG (B), Ag/Pt NCs-IgG (D) and Au/Pt NCs-IgG (F) based on the statistics over 100 individual particles.

XPS measurements were performed to study the valence state of the cores of NCs-IgG. Cd 3d peaks were fitted by two components (Figure 5.). One associated to CdS bond and another one associated to Cd oxide or carbonate. The Cd $3d_{3/2}$ energy band related to

the presence of CdS bond usually appears at 411.8 eV[35] and for CdO bond at 411 eV[36] which agree with the experimental results.

The Pt 4f spectra (Figure 5.) exhibit a doublet containing the Pt $4f_{7/2}$ energy band at 71.1 eV and the Pt $4f_{5/2}$ at 74.3 eV which indicates the presence of metallic state Pt[37]. In the Pt $4f_{7/2}$ spectrum, a broad peak was found. It was fitted by an asymmetric Lorentzian curves in the case of Pt(0) (70.1eV) and Pt(II) with a symmetric Gaussian-Lorentzian curve (71.7). This suggest that both Pt(0) and Pt(II) coexist as has been previously reported in bimetallic NCs[38]. The ratio between Pt (0)/Pt (II) was 1.1. The peaks of Pt $4f_{7/2}$ are usually found at 71 eV and 72.4 eV respectively. In this case they are slightly shifted to lower binding energies. These results suggests electron transfer from Ag to Pt, which is related to the perturbed electronic interaction between Pt and Ag atomic orbits and forms an alloy[39]. The XPS spectrum of Ag (Figure 5.) showed a binding energy value at 368.3 eV for Ag $3d_{5/2}$ and 374.4 for Ag $3d_{3/2}$ confirming the presence of elemental Ag(0), which agree with the results obtained with Ag NCs[40]. The Ag $3d_{5/2}$ centered at 368.3 eV is between the value for Ag(0) (368 eV) and Ag(I) (368.4 eV)[41] which indicates the presence of Ag(I) as has been previously reported[42].

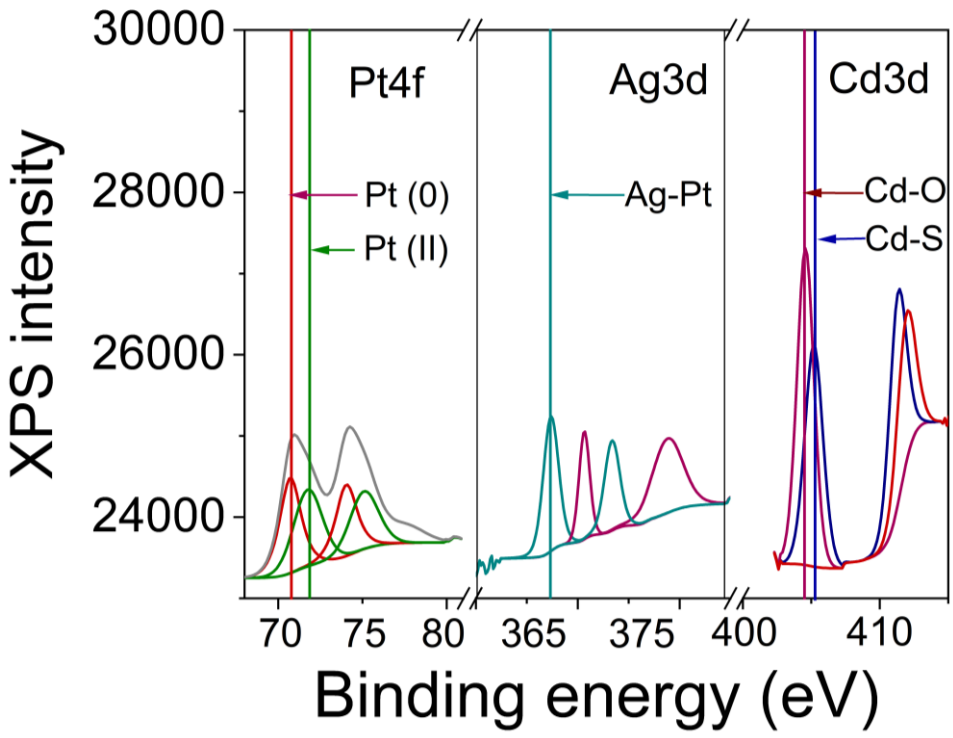


Figure 5. XPS spectra of CdS NCs-IgG and Ag/Pt NCs-IgG.

Figure 6. shows the Pt 4f spectra of Au/Pt NCs-IgG. This spectrum is composed of two energy bands. On the one hand the Pt $4f_{7/2}$ energy band is evident and on the other hand Pt $4f_{5/2}$ energy band at 71.1 eV and 74.2 eV respectively can be seen. Such distribution of bands is characteristic of Pt in metallic state [37]. The Pt $4f_{7/2}$ spectrum was fitted to two curves, one asymmetric Lorentzian curve in the case of Pt(0) (71 eV) and a symmetric Gaussian-Lorentzian curve for Pt(II) (72,4 eV). These peaks are usually found at 71 eV and 72.4 eV[39]. In the Au 4f region the spectra present characteristic doublet with the $4f_{7/2}$ and $4f_{5/2}$ energy bands separated by 3.67 eV. The Au $4f_{7/2}$ can be deconvoluted to two curves, one for Au(0) (83.1 eV) and another for Au(I) (84.8 eV). These peaks usually appear at binding energies of 84 eV and 85 eV respectively [43]. The difference between the widespread values and the NCs values suggest a strong interaction between Au and Pt atoms with the consequent formation of Au-Pt alloys as will be demonstrated below. This effect has been observed in other bimetallic NCs [31].

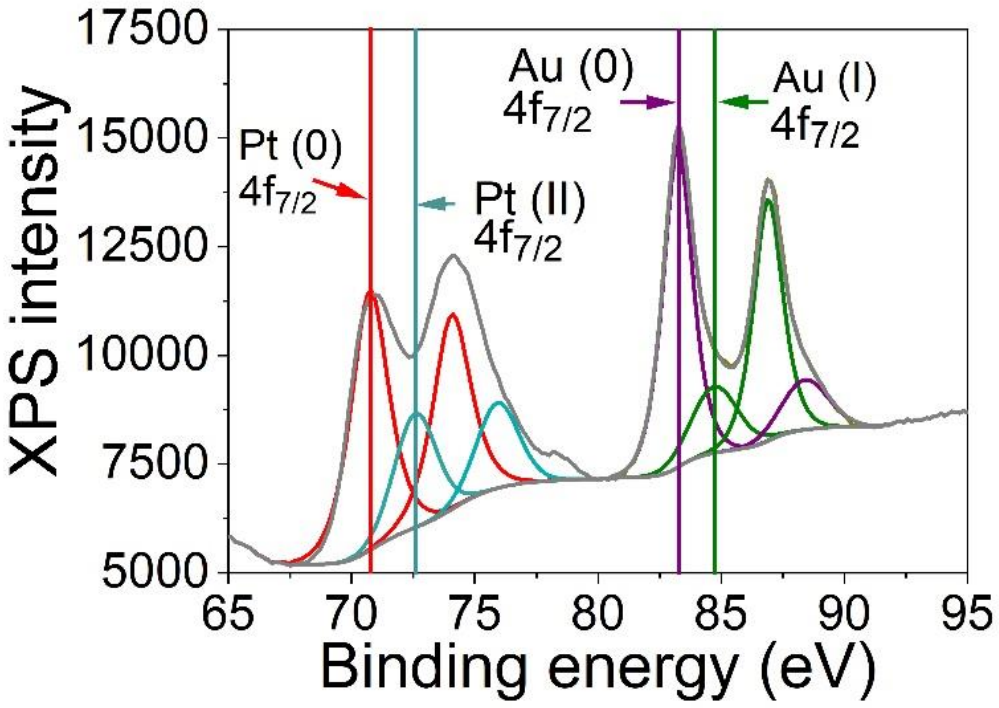


Figure 6. XPS spectra of Au/Pt NCs-IgG.

MALDI-TOF measurements were carried out in order to make sure that the metallic nanoclusters are bound to the IgG. In Figure 7. mass spectra ($m/z^+$, z=2) for pristine Anti-BSA IgG, CdS NCs-IgG, Ag/Pt NCs-IgG and Au/Pt NCs-IgG are shown. A shift of the peak corresponding to the NC-containing samples towards greater masses can be observed.

From the analysis of the spectrum one can conclude that the NCs are bound to Anti-BSA IgG macromolecules. Despite the appearance of the mass peak shift in the spectrum, it is not possible to give an accurate mass evaluation of the metallic core due to several issues such as, broad spectral peaks and contradictions between TEM and MALDI-TOF results. The mass peaks of pristine IgG and modified IgG are broad due to the use of a polyclonal antibody that has a polydispersed mass and the polydispersity of metallic cores observed in TEM images (Figures 4A, 4C and 4E). TEM images show larger size of NCs compared to that obtained in MALDI-TOF because during TEM measurements the NCs can aggregate on the grids [7,44]. The larger are NCs, the lower is the ionization propensity. Hence larger NCs are not detected by MALDI-TOF [45,46].

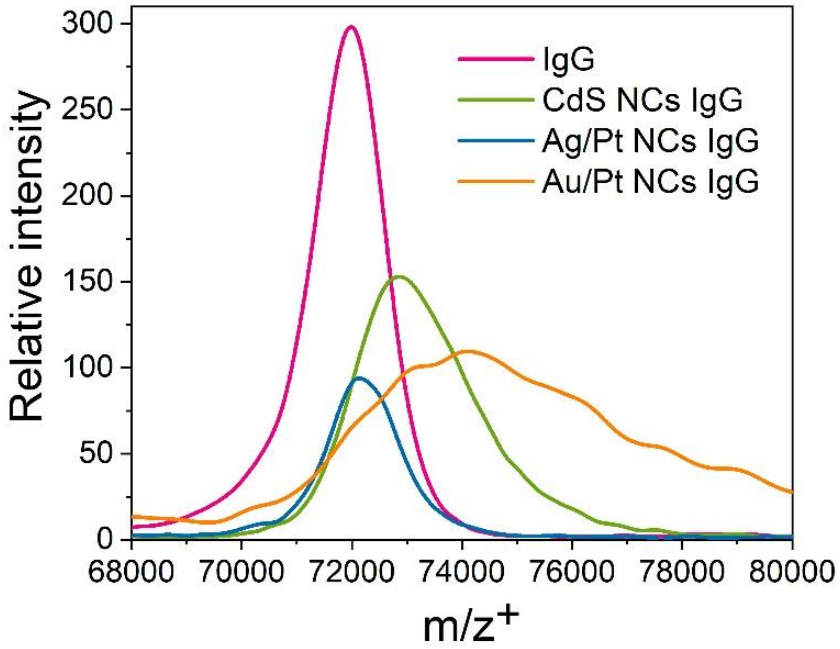


Figure 7. MALDI-TOF spectra of Anti-BSA IgG, CdS NCs IgG, Ag/Pt NCs IgG and Au/Pt NCs IgG.

## 3.2. Photocatalytic activity of CdS NCs-IgG and catalytic activity of Ag/Pt NCs-IgG and Au/Pt NCs-IgG

CdS NCs-IgG were able to oxidise Amplex Red to resorufin under UV-light (Figure 8B). The substrate changes from colorless and non-fluorescent to pink and fluorescent ($\lambda_{ex}$ = 530 nm, $\lambda_{em}$ = 590 nm). The colour change could be easily seen by the naked eye and recorded by digital camera (Figure 8A). The photocatalytic activity of CdS NCs-IgG is dependent of Amplex Red concentration. This dependence was measured while varying

the Amplex Red concentration from 0 to 0.8 mM. The CdS NCs-IgG concentration was kept constant to 500 µg/mL (referred to Anti-BSA IgG concentration). The solution containing CdS NCs-IgG and Amplex Red was irradiated with UV-light ($\lambda_{ex}$=365nm) for 20 minutes and the fluorescent spectra were recorded (Figure 8C.). The system follows a Michaelis-Menten kinetics, the reaction rate (fluorescence of Amplex Red) increases with increasing substrate concentration (Figure 8D.).

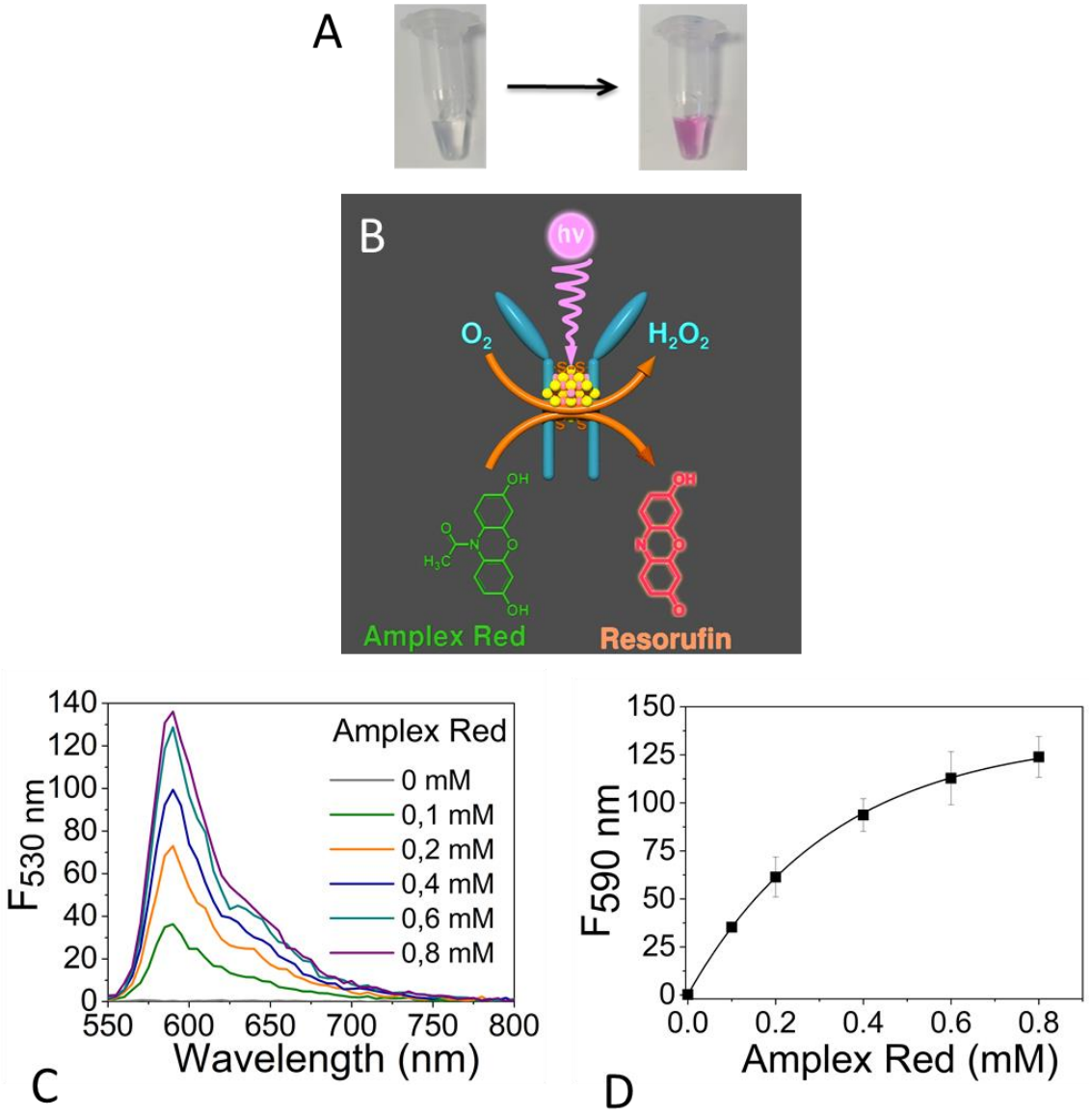


Figure 8. Colour change of Amplex Red due to the photocatalytic activity of CdS NCs IgG (A). Scheme of Amplex Red oxidation to Resorufin by the photocatalytic activity of CdS NCs-IgG under UV-light (B). Fluorescence emission spectra of the system containing the same concentration of CdS NCs-IgG and different concentrations of Amplex Red ($\lambda_{ex}$ =530 nm) (C). Position of emission peak at different Amplex Red concentration ($\lambda_{ex}$ =530nm, $\lambda_{em}$ =590 nm) (D).

The stability of CdS NCs-IgG under UV light was studied, by measuring both the fluorescence and the photocatalytic activity of CdS NCs-IgG after incubation of the samples under UV light for different times. It was observed that while fluorescence is decreasing with irradiation time, the photocatalytic activity of NCs remains stable and is not affected by a previous UV light irradiation (Figure 9.).

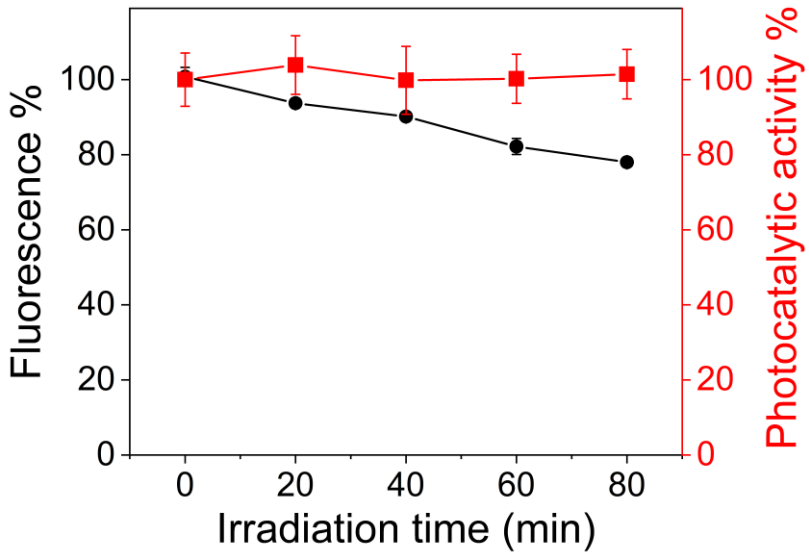


Figure 9. Effect of UV light irradiation time on emission and photocatalytic activity of CdS NCs-IgG. The values of those parameters measured at initial time prior to irradiation were considered to be 100%.

It was found that Ag/Pt NCs IgG and Au/Pt NCs IgG had enzymatic peroxidase activity, like the commonly used enzyme HRP. These NCs catalysed the oxidation of the chromogenic substrate TMB with $H_2O_2$ which changes its colour from colourless to blue ($\lambda_{abs}$=655 nm) (Figure 10B. and Figure 11A.). The colour change could be easily seen by the naked eye and recorded by digital camera (Figure 10A.). The peroxidase-like activity of both NCs is dependent on TMB and $H_2O_2$ concentration. To measure the dependence of the initial reaction rate on concentration of both substrates, the concentration of one of the substrates was fixed while the concentration of other one was changed. On the one hand, the TMB concentration dependence was measured by maintaining the $H_2O_2$ amount fixed at 125 mM for Ag/Pt NCs-IgG and 250 mM for Au/Pt NCs-IgG and by changing the TMB concentration. On the other hand, the $H_2O_2$ concentration dependence was measured by maintaining the TMB concentration fixed at 200 mM and by varying the $H_2O_2$ concentration. In all cases the Ag/Pt NCs IgG and Au/Pt NCs IgG

concentration was kept constant to 33 µg/mL (referred to Anti-BSA IgG concentration). In Figure 10C., 10D., 11B. and 11C. it is shown how the reaction rate of TMB oxidation increases with the rise of substrate concentration following a Michaelis-Menten like kinetics. With the Lineweaver-Burk equation the Michaelis-Menten constant ($K_m$) was obtained (Figure 10E., 10F., 11D. and 11E.). $K_m$ is an indicator of enzyme affinity to substrates. Lower the $K_m$ stronger affinity and *vice versa*[47, 48]. In Table 2. the $K_m$ values for Ag/Pt NCs-IgG, Au/Pt NCs-IgG and HRP[49] are shown. The $K_m$ value of Ag/Pt NCs IgG was almost the same as that of HRP towards TMB, which indicates that Ag/Pt NCs-IgG had similar affinity as HRP to TMB as a substrate, while the $K_m$ for Ag/Pt NCs IgG was significantly higher than that for HRP towards $H_2O_2$, indicating that Ag/Pt NCs IgG had a lower affinity for $H_2O_2$ than HRP. In the case of Au/Pt NCs-IgG, the $K_m$value is more than 8.5 times lower than that of HRP towards TMB, which indicates that Au/Pt NCs-IgG has a higher affinity than HRP to TMB as a substrate. While the value of $K_m$ for Au/Pt NCs IgG is significantly higher than that for HRP to $H_2O_2$, indicating Au/Pt NCs IgG has a lower affinity for $H_2O_2$ than HRP, which is the same effect that was observed with Ag/Pt NCs-IgG. This phenomena has been also observed in others nanozymes[50, 51].

Table 2. Comparison of the apparent Michaelis-Menten constant ($K_m$) between Ag/Pt NCs-IgG, Au/Pt NCs IgG and HRP.

| Catalyst | Substrate | $\boldsymbol{K_m}$ (mM) |
|---|---|---|
| Au/Pt NCs IgG | TMB | 0.0418 |
| | $H_2O_2$ | 102.35 |
| Ag/Pt NCs IgG | TMB | 0.345 |
| | $H_2O_2$ | 90.363 |
| HRP | TMB | 0.362 |
| | $H_2O_2$ | 0.522 |

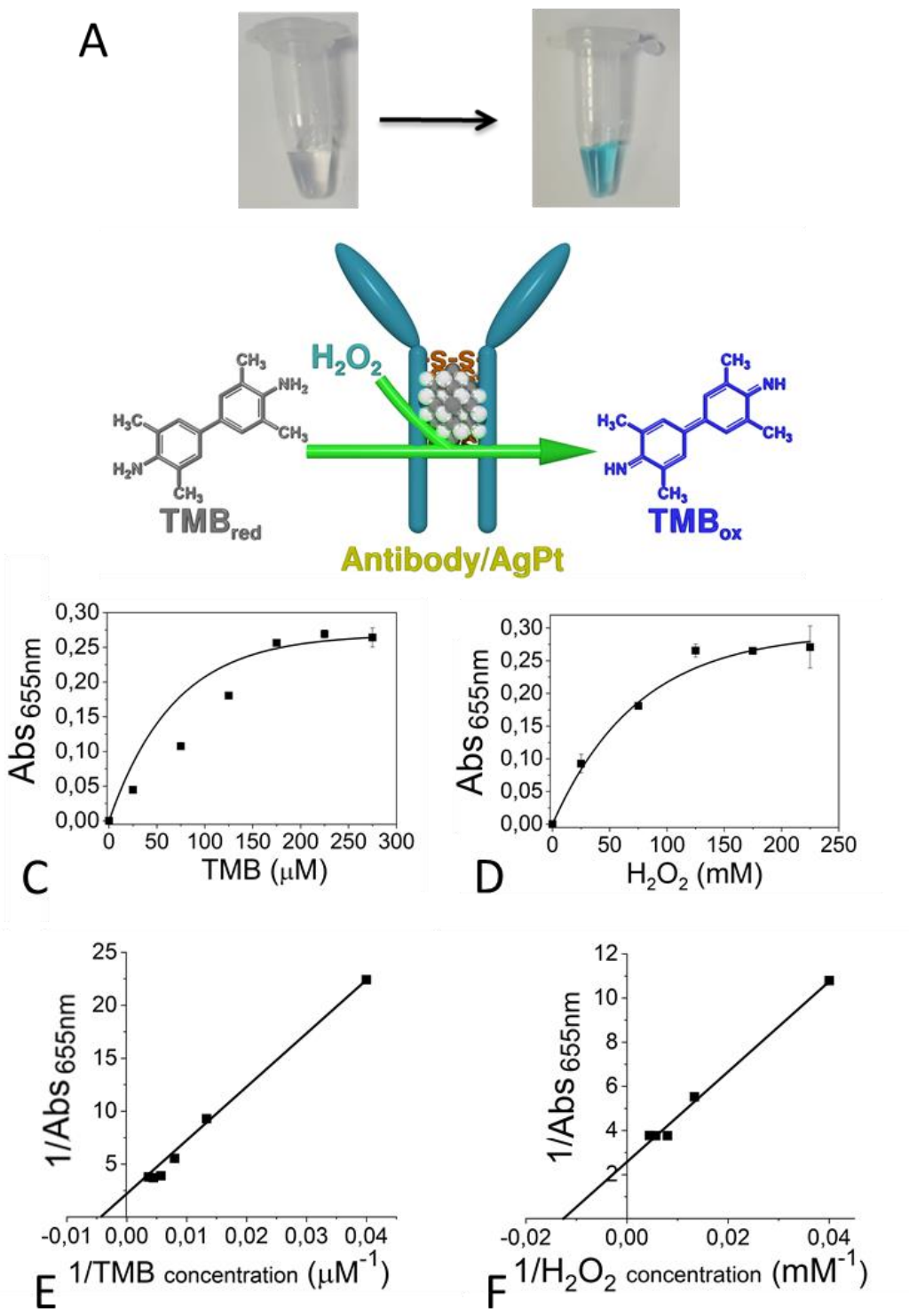


Figure 10. Colour change of the substrate TMB due to the catalytic activity of Ag/Pt NCs IgG (A). Scheme of TMB oxidation by the catalytic activity of Ag/Pt NCs-IgG in presence of $H_2O_2$ (B). Intensity of absorbance peak (655 nm) at different TMB concentrations (C) and $H_2O_2$ concentrations (D). Double reciprocal plots of catalytic activity of Ag/Pt NCs IgG with TMB (E) and $H_2O_2$ (F)

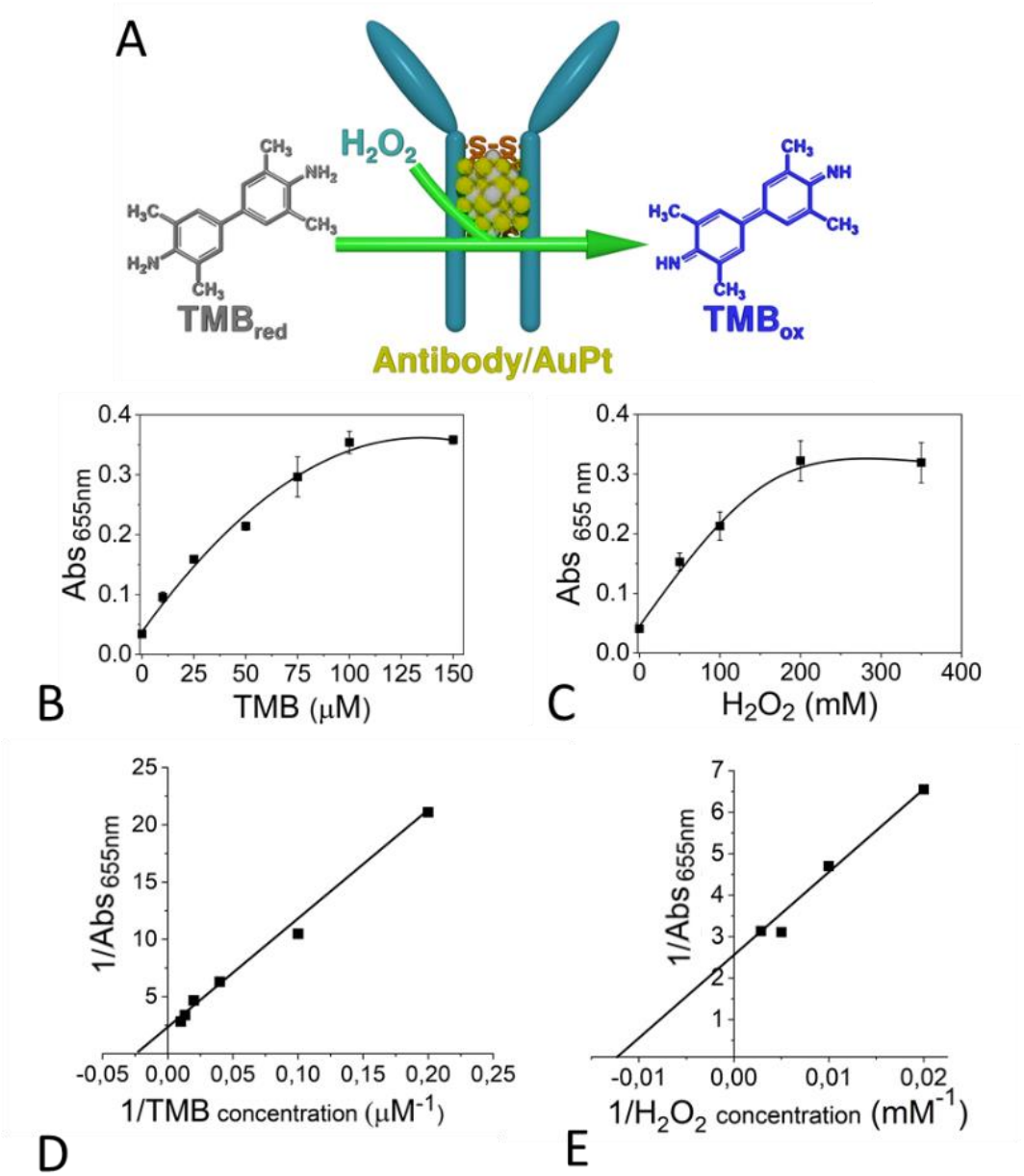


Figure 11. Scheme of TMB oxidation by the catalytic activity of Au/Pt NCs-IgG in presence of $H_2O_2$ (A). Intensity of absorbance peak (655 nm) at different TMB concentrations (B) and $H_2O_2$ concentrations (C). Double reciprocal plots of catalytic activity of Au/Pt NCs IgG with TMB (D) and $H_2O_2$ (E).

In order to evaluate the stability of the NCs, a fresh solution of the Au/Pt NCs-IgG was prepared using the optimized synthesis procedure. Then, the peroxidase-like activity of the resulting modified antibody was measured under the same experimental conditions during several days after the synthesis. During this period of time, the solution of Au/Pt NCs-IgG was kept at 4 °C in a fridge. According to this stability study (Figure 12.), the half-life of the active bimetallic clusters was around 10 days. Such stability of Au/Pt NCs-

IgG was sufficient to validate this nanomaterial in immunoassays because the employment of modified antibodies in bioassays is usually limited to several hours. The shelf-life of the produced Au/Pt NCs-IgG was studied in the absence of any stabilizers because the optimization of storage conditions was not among the priorities of this work. Potentially, the shelf-life can be extended by using more appropriate storage conditions such as the addition of preservatives, lyophilization of Au/Pt NCs- IgG, and oxygen elimination. Extension of the shelf-life of Au/ Pt NCs-IgG under optimized storage conditions can become the main goal of a future investigation.

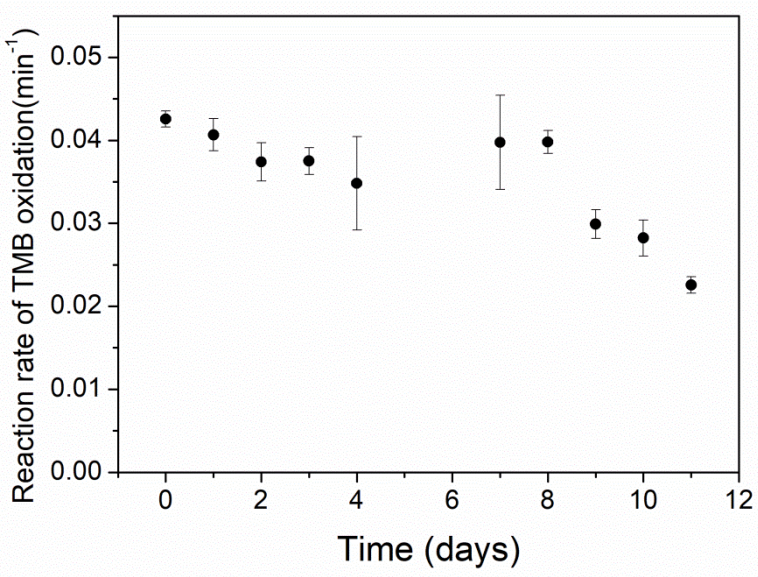


Figure 12. Catalytic Activity of Au/Pt NCs-IgG as a function of time after synthesis.

## 3.3. Antibody Structure stability after the synthesis of NCs

Most of the methods described in literature about the synthesis of metallic NCs using proteins as scaffold uses harsh conditions that causes the denaturation of the proteins and the loss of biological functions [4]. The maintenance of the conformation of the antibody is the key factor for future applications in immunoassays of the antibodies carrying NCs. Different experiments were performed to test if the antibody structure is changed in the course of NC synthesis.

CD spectroscopy was used to characterize the secondary structure and conformation of proteins[52]. In the far-UV CD spectra (180-250 nm) we found the predominant

secondary structure for IgG, antiparallel β-sheet and random coil conformations[53]. The presence of β-sheets can be detected by the presence of a broad minimum at 218 nm in the far-UV CD spectra [52]. After the synthesis of NCs using an antibody as a scaffold its secondary structure could be damaged or completely disappear. However, in the CD spectra of the pristine antibody and the antibody carrying NCs shown in Figure 13., no significant differences between plots are evident, so it can be concluded that the introduction of Au/Pt NCs into the IgG structure does not cause any significant alteration in the IgG conformation.

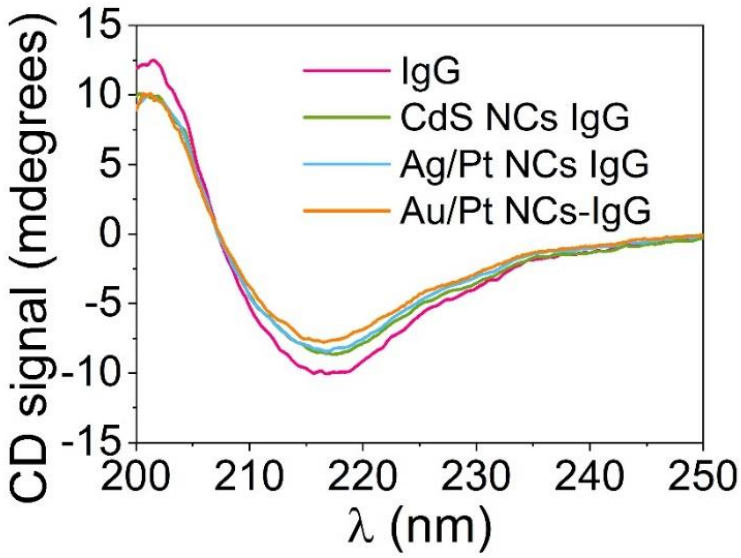


Figure 13. Far-UV CD spectra of IgG, CdS NCs-IgG, Ag/Pt NCs-IgG and Au/Pt NCs-IgG.

Protein G was used to check if the introduction of NCs inside of the antibody causes any damage to the structure of the Fc region. The Fc region of an IgG binds specifically to protein G. Polyvinyl chloride microbeads decorated with Protein G were incubated with the antibodies carrying semiconductor and bimetallic NCs as described in the experimental section. NCs of CdS, Ag/Pt and Au/Pt produced using BSA as scaffold were synthesized in order to be used as controls. These BSA-stabilized NCs were characterized by TEM and XPS, to ensure that they have similar properties to those stabilized in IgG. (Figure 14. and Figure 15.). TEM images reveal than the both NCs have a spherical morphology and a mean diameter between 1 and 3 nm. XPS measurements showed that Ag/Pt NCs are composed by Pt in oxidation state 0 and 2 and demonstrate Ag-Pt interactions. In the case of CdS NCs-BSA there were Cd-O and Cd-S interactions. This

results indicates that the BSA capped NCs have similar size and chemical composition to those synthesized using an IgG as scaffold.

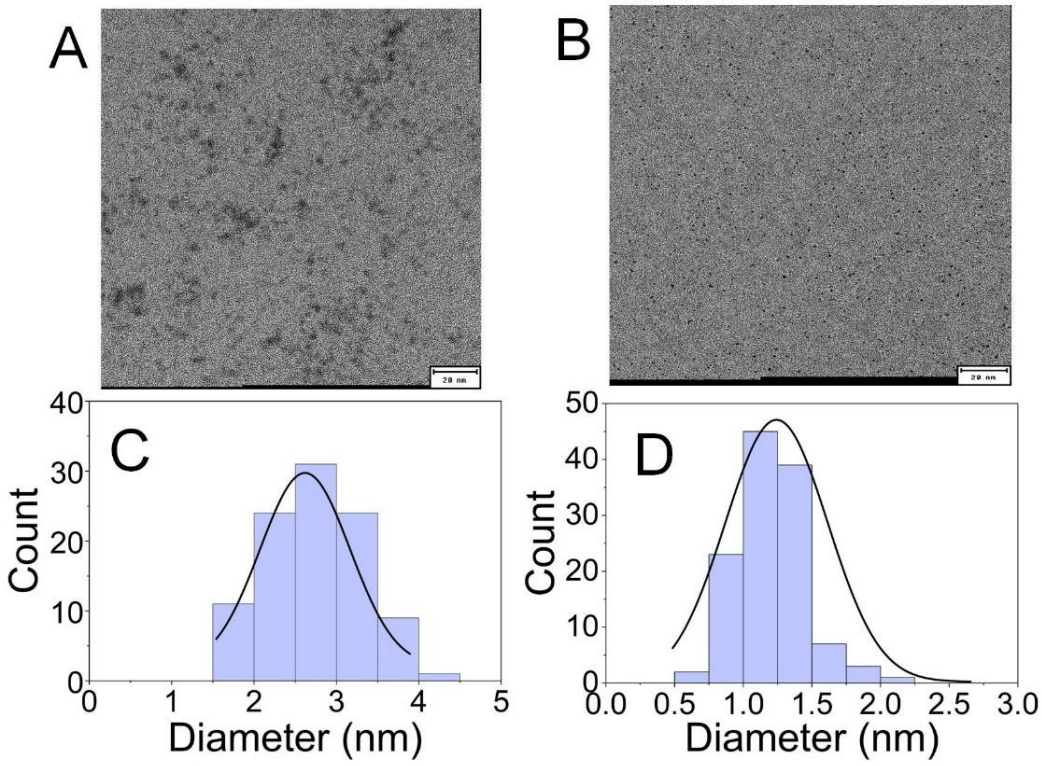


Figure 14. Representative TEM image of CdS NCs-BSA (A). Representative TEM image of Ag/Pt NCs-BSA (B). Size distribution of CdS NCs-BSA (C) and Ag/Pt NCs-BSA (D) based on the statistics over 100 individual particles.

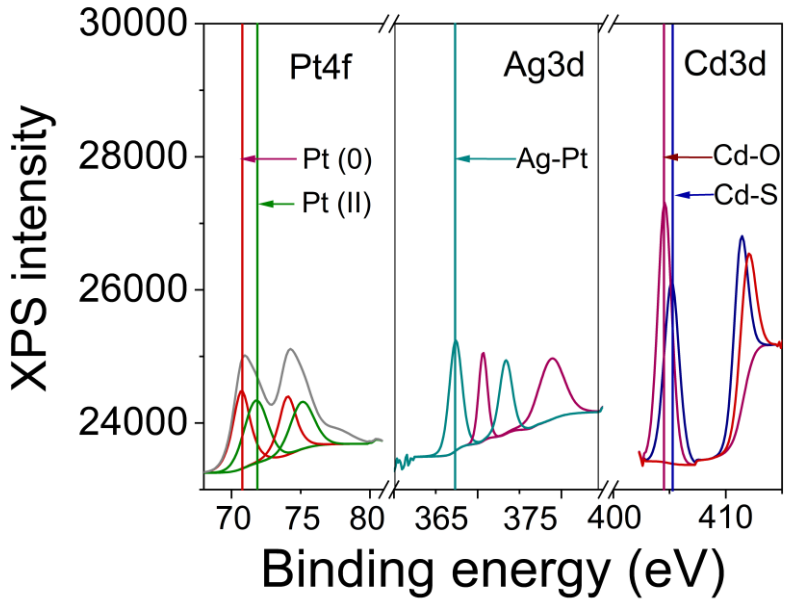


Figure 15. XPS spectra of Ag/Pt NCs-BSA (left and central panel) and CdS NCs-BSA (right panel).

BSA does not have any affinity for Protein G, therefore any binding to the protein G should be detected. The CdS NCs stabilized using BSA are fluorescent[6] and have catalytic activity towards the oxidation of Amplex Red triggered by the exposure to UV-light (Figure 16.). BSA carrying Ag/Pt NCs and Au/Pt NCS showed catalytic properties with respect to oxidation of TMB in presence of $H_2O_2$. (Figure 17. and Figure 18.). In all cases the system follows a Michaelis Menten Kinetics, the reaction rate increases with substrate concentration. Similar results where obtained with the IgG capped NCs revealing similar enzyme-like properties.

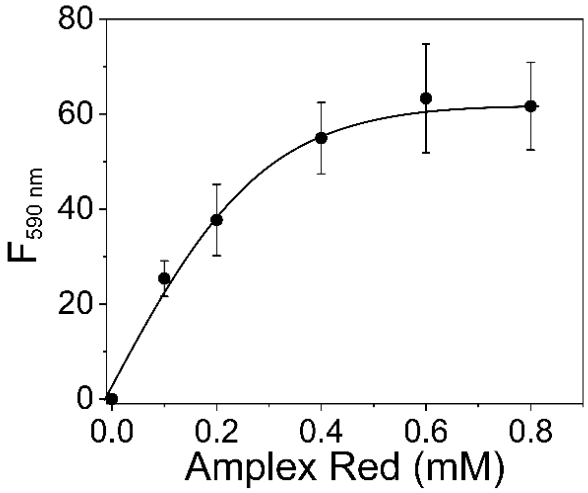


Figure 16. Effect of Amplex Red concentration on photocatalytic activity of CdS NCs-BSA.

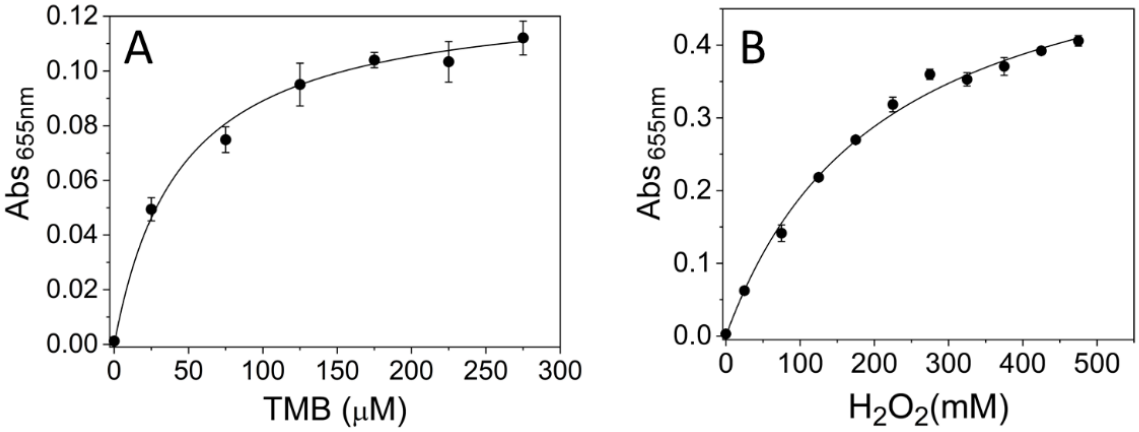


Figure 17. Effect of TMB (A) and $H_2O_2$ (B) concentrations on catalytic activity of AgPt NCs-BSA.

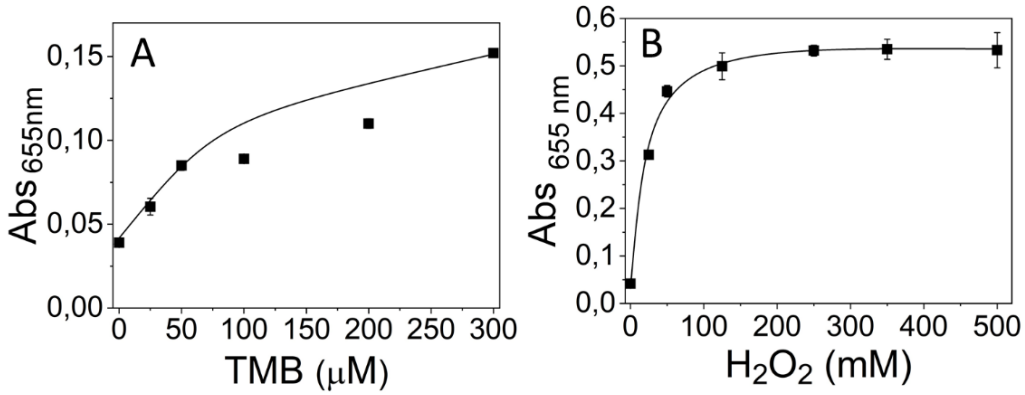


Figure 18. Effect of TMB (A) and $H_2O_2$ (B) concentrations on catalytic activity of AuPt NCs-BSA.

The fluorescent properties of CdS NCs-IgG and the catalytic properties of Ag/Pt NCs-IgG and Au/Pt NCs-IgG were used to verify that the IgG modified with NCs bind specifically to Protein G microbeads while BSA carrying CdS, Ag/Pt and Au/Pt do not adsorb non-specifically on protein G microbeads.

The fluorescence spectra of the CdS NCs-IgG and CdS NCs-BSA incubated with the microbeads were measured using an excitation wavelength of 315 nm. Also, the fluorescence of CdS NCs-IgG and CdS NCs-BSA in solution without microbeads was measured. The fluorescent spectra are showed in Figure 19A. The spectrum of CdS NCs-IgG in solution is practically the same as the spectrum of Protein G microbeads after washing which were pre-incubated with CdS NCs-IgG. When BSA carrying CdS NCs was incubated with Protein G microbeads, practically no fluorescence was observed after washing. Taking into consideration that BSA carrying CdS NCs show good fluorescence in solution we conclude that fluorescence shown by Protein G microbeads modified with CdS NCs-IgG is attributed to specific binding of CdS NCs-IgG to protein G and Fc region of Anti-BSA IgG modified with CdS NCs was not altered.

The catalytic activity with TMB in the presence of $H_2O_2$ was used to probe the binding of Ag/Pt NCs-IgG to Protein G microbeads. The microbeads were incubated with Ag/Pt NCs-IgG and Ag/Pt NCs-BSA. The supernatant was discarded and microbeads were washed by centrifuging three times. Next, 100 µL of a solution of TMB (200 µM) and $H_2O_2$ (125 mM) in acetate buffer (10 mM, pH=4.0) was added to pellets. The activity of free Ag/Pt NCs-IgG and Ag/Pt NCs-BSA in solution was determined by the addition of the same solution of TMB and $H_2O_2$. In Figure 19B. the absorbance spectra are showed. The

catalytic activity of Ag/Pt NCs-IgG in solution is practically the same as that of the Ag/Pt NCs-IgG incubated with Protein G microbeads. However, with Ag/Pt NCs-BSA incubated with Protein G microbeads no catalytic activity was detected. Free Ag/Pt NCs-BSA in solution demonstrates catalytic activity.

The same procedure was followed for Au/Pt NCs. Free Au/Pt NCs-IgG exhibit catalytic activity in a bulk solution. Microbeads tethered to Au/ Pt NCs-IgG via Protein G also demonstrated catalytic activity. Catalytic oxidation of TMB was observed in the presence of free Au/Pt NCs-BSA. However, microbeads decorated with Protein G do not show catalytic activity after incubation with Au/Pt NCs-BSA (Figure 19C.).

These results indicate that the Fc structure of the IgG was not changed during the synthesis of CdS NCs-IgG, Ag/Pt NCs-IgG and Au/Pt NCs-IgG because the IgG still has affinity for Protein G, moreover this binding is specific for IgG because no binding of CdS NCs-BSA, Ag/Pt NCs-BSA and Au/Pt NCs-BSA to Protein G microbeads was observed.

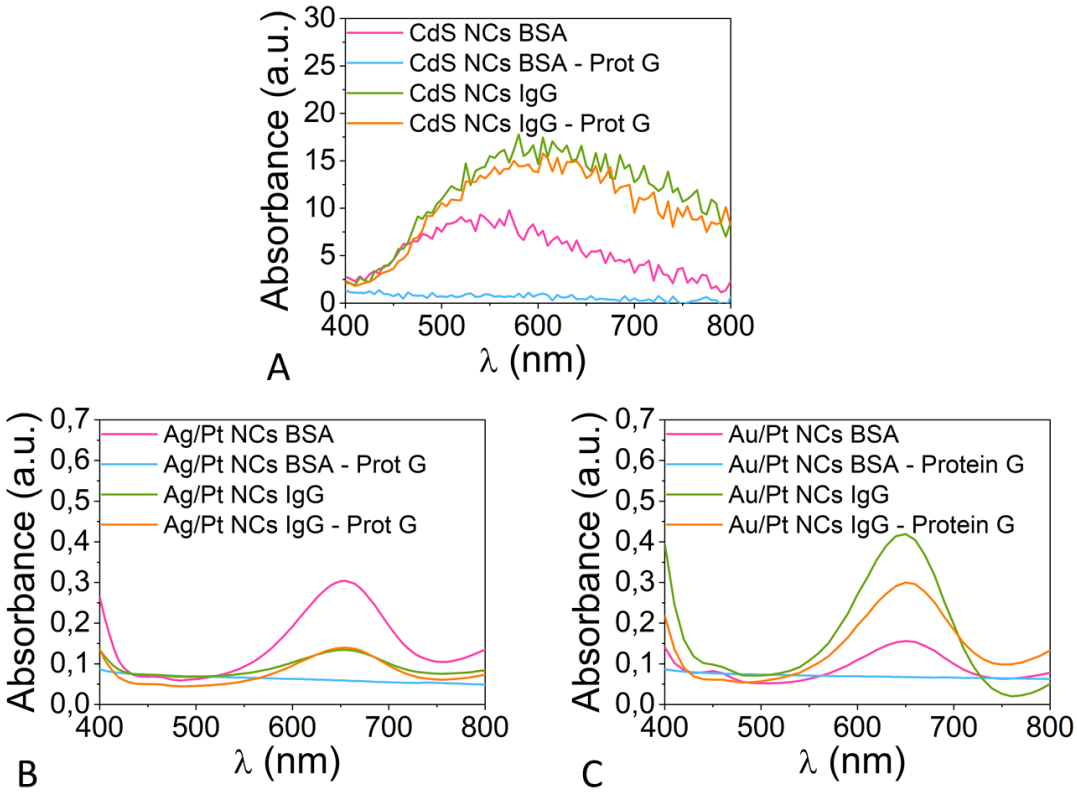


Figure 19. Fluorescence spectra ($\lambda_{ex}$=315 nm) of CdS NCs-IgG and CdS-BSA incubated with microbeads decorated with Protein G and free in solution (A). Catalytic properties of Ag/Pt NCs-IgG and Ag/Pt NCs-BSA with TMB in presence of $H_2O_2$ incubated with microbeads decorated with Protein G and free in solution (B). Catalytic properties of Au/Pt NCs-IgG and Au/Pt NCs-BSA with TMB in presence of $H_2O_2$ incubated with microbeads decorated with Protein G and free in solution (C).

## 3.4. Evaluation of Anti-BSA IgG affinity for its antigen after the introduction of NCs in its structure

In order to know if the antibody maintains its affinity for target analyte after the introduction of NCs in its structure three direct immunoassays were performed, using the antibody carrying NCs as detection antibody.

Figure 20A. represents the method used to evaluate the binding of CdS NCs-IgG with different amounts of BSA immobilized on the surface of microplates obtained by incubation with varying concentrations of BSA (from 0 to 10 µg/mL) in PBS. The higher was the amount of BSA adsorbed the greater photooxidation rate of Amplex Red to Resorufin was observed. The calibration curve shows (Figure 20B.) that the fluorescence emission at $\lambda_{em}$=590 nm ($\lambda_{ex}$=530 nm) increases with BSA concentration. The fluorescence values were recorded after 30 minutes of incubation of Amplex Red solutions, placed in microplates wells, under UV-light (365 nm).

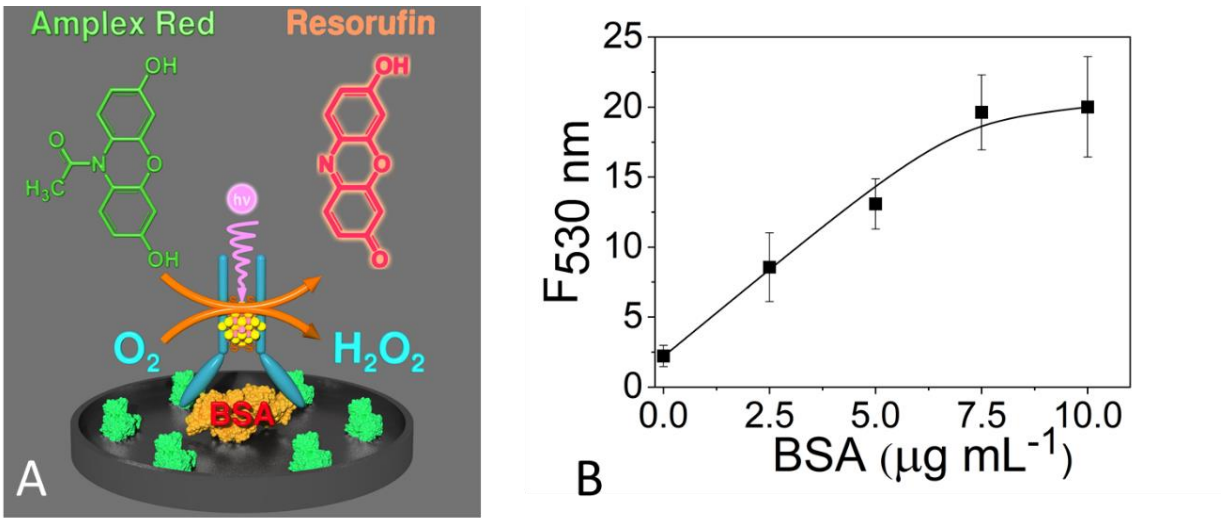


Figure 20. Schematic representation of a direct immunoassay for BSA using CdS NCs-IgG as a detection antibody (A). Calibration curve of BSA obtained in a direct ELISA assay based on CdS NCs-IgG using $\lambda_{ex}$=530 nm and $\lambda_{em}$=590 nm (B).

In Figure 21A. the direct immunoassay based on the catalytic properties of Ag/Pt NCs-IgG is showed. The amount of BSA adsorbed was controlled by incubation with solutions containing varying concentrations of BSA (0 to 1400 ng/mL). When the surface coverage of BSA immobilized on the microplate increased, the oxidation rate of TMB increased proportionally measured by UV-Vis spectroscopy ($\lambda_{abs}$=655 nm). The calibration curve

shows (Figure 21B.) how the initial TMB oxidation rate (measured for 4 minutes) increased with increasing BSA concentration.

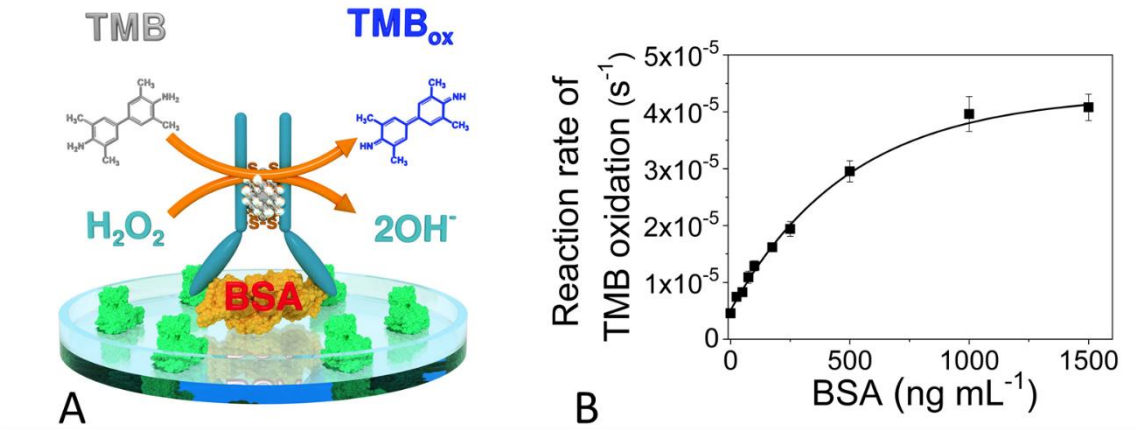


Figure 21. Schematic representation of a direct immunoassay for BSA using Ag/Pt NCs-IgG as a detection Antibody (A). Calibration curve of BSA obtained in a direct ELISA assay based on Ag/Pt NCs-IgG using $\lambda_{abs}$ = 655 nm (B).

In Figure 22A., the scheme of the direct immunoassay based on the catalytic properties of Au/Pt NCs-IgG is shown. Different BSA concentrations (0–500 ng/mL) were adsorbed on a microplate. The calibration curve (Figure 22B.) demonstrates the dependence of the initial oxidation rate of TMB, which was registered during the first 4 min, in the increasing concentrations of TMB. According to the observed experimental data, IgG carrying bimetallic nanoclusters still retains its affinity to its target analyte and can be used as a detection antibody in a direct sandwich ELISA.

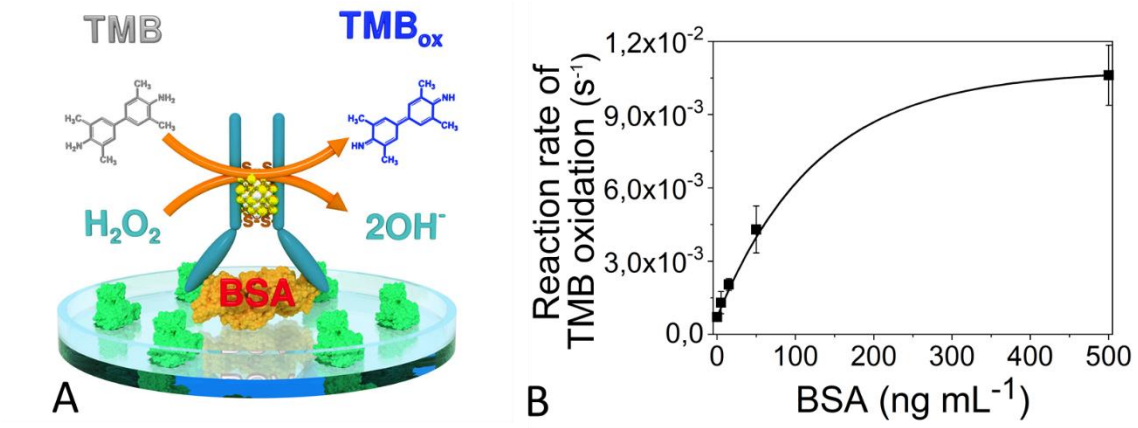


Figure 22. Schematic representation of a direct immunoassay for BSA using Au/Pt NCs-IgG as a detection Antibody (A). Calibration curve of BSA obtained in a direct ELISA assay based on Au/Pt NCs-IgG using $\lambda_{abs}$ = 655 nm (B).

Comparing the three immunoassays, the methods using metallic NCs showed several advantages. First, they are faster, because only 4 minutes of catalytic oxidation of TMB with $H_2O_2$ were needed to calculate the initial oxidation rate. In case of assay based on CdS NCs-IgG the photooxidation with Amplex Red required 30 minutes to produce calibration plot. The use of the UV-light made the photocatalytic method technically more complicated. The same intensity of light must reach all wells, so the position of the microplate with respect to the UV-light source is critical for the reproducibility of the method. Due to its use greater relative standard deviations were achieved with CdS NCs-IgG.

## 3.5. Evaluation of the bimetallic Composition of the Au/Pt NC Cores and their position in the antibody structure

In order to elucidate the region of the antibodies involved in the stabilization of Au/Pt NCs, different antibody fragments were produced and used as scaffolds for the synthesis of NCs. For generation of Fab fragments (50 kDa), immobilized papain digests IgG antibodies, and Fab fragments are purified using Protein A agarose. For production of F(ab')2 (110 kDa), immobilized pepsin protease is employed (Figure 23.). A representative SDS-PAGE gel of the obtained fragments is shown in Figure 24. Afterward, the performance of the resulting antibody fragments modified with Au/Pt NCs in a direct ELISA assay for the detection of BSA was evaluated. Antigen binding fragment (Fab) is a region on an antibody that binds to the antigens, and F(ab)2 fragments have two antigen-binding Fab parts bound by disulfide bonds. In the ELISA assay, in the case of using Au/Pt NCs Fab fragments for stabilization of NCs, no peroxidase activity was detected (Figure 25.), whereas this activity was detected in the sample corresponding to the incubation with Au/Pt F(ab')2 and the intact antibody. These results suggest that the hinge region of the antibodies, rich in disulfide bonds, could play an important role in the Au/Pt NCs stabilization. Only F(ab')2 fragments form composites with peroxidase-like activity show affinity to BSA, and Fab fragments cannot yield such composites. This means that bimetallic NCs are not metalized within Fab fragments in close vicinity to antigen-binding sites. Given the medium diameter of bimetallic clusters of 1.8 nm and overall dimensions of IgG (14.5 nm × 8.5 nm × 4.0 nm),

with antigen binding sites separated by 13.7 nm[54, 55] it can be concluded that, most probably, bimetallic clusters are located exactly at the hinge region of the antibodies, sufficiently far away from binding sites. Therefore, in the majority of produced Au/Pt NCs-IgG, metallization does not sequester active sites on antibodies due to the small size of NCs and their well-defined position at the center of IgG macromolecules.

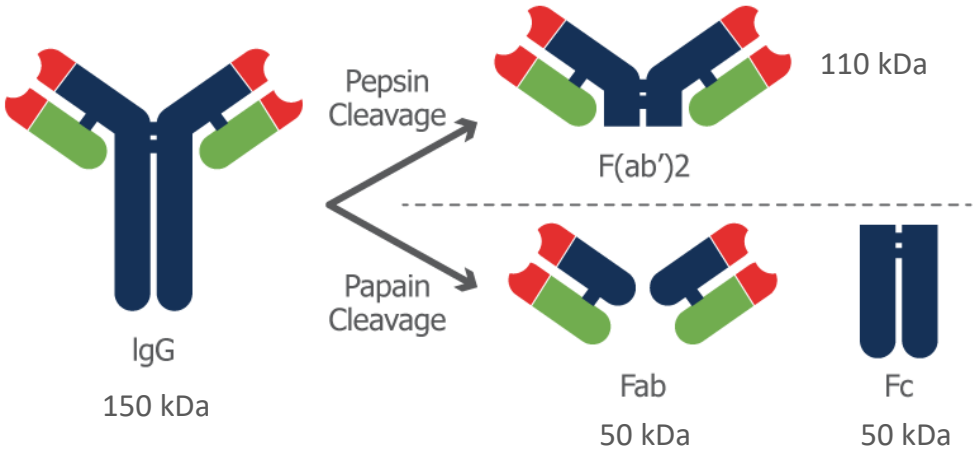


Figure 23. Antibody cleavage into F(ab')2 fragment using pepsin or into Fab and Fc fragments using papain.

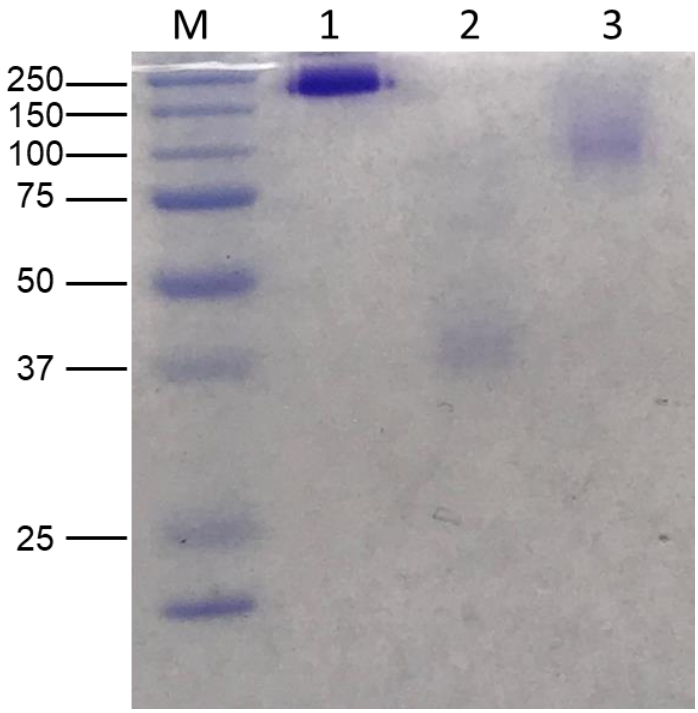


Figure 24. Electrophoretic analysis (SDS-PAGE 4-12%) of the generated fragments of antibodies under non-reducing conditions. (M): molecular weigth standards. (1): Anti-BSA IgG antibody. (2): Fab fragments. (3): F(ab')2 fragments.

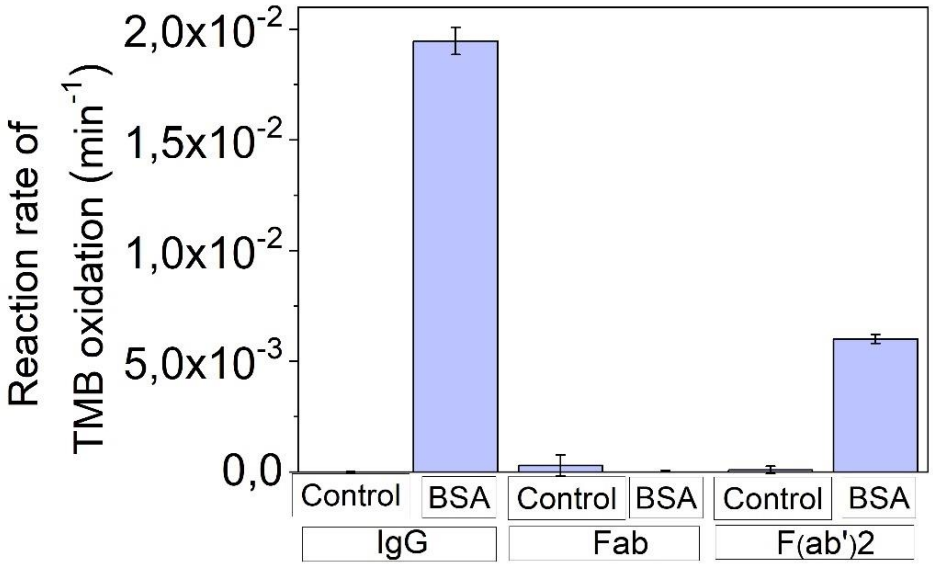


Figure 25. Reaction rate of TMB oxidation in the direct ELISA performed with Au/Pt NCs-IgG, Au/Pt NCs Fab, and Au/Pt NCs F(ab)2 fragments in the absence (control) or presence of 200 ng/mL BSA.

In order to confirm that the catalytic activity of the Au/Pt NCs-IgG is related to the presence of both metals, the synthesis of the NCs was carried out three times. One of the synthesis was carried out without the addition of $K_2PtCl_4$; therefore, monometallic NCs composed of gold were synthesized (Au NCs-IgG). The second synthesis was performed without the addition of $HAuCl_4$ in order to prepare monometallic NCs composed of platinum (Pt NCs-IgG). The third synthesis of Au/Pt NCs-IgG was carried out as usual (with both metal precursors). A direct sandwich ELISA was used to compare the applicability to immunoassays of the next three modified IgGs: Au NCs-IgG, Pt NCs-IgG, and Au/Pt NCs-IgG. The reaction rate for each NC is shown in Figure 26. The maximum reaction rate of TMB oxidation was found for Au/Pt NCs-IgG. Very low catalytic activity was achieved with Pt NCs-IgG in comparison with that shown by Au/Pt NCs-IgG, and no catalytic activity was observed with Au NCs-IgG. These results suggest that the presence of both metal precursors is necessary during the synthesis to achieve the formation of catalytic NCs. The synergistic effect between Au and Pt atom was observed in other Au/Pt bimetallic NCs [31]

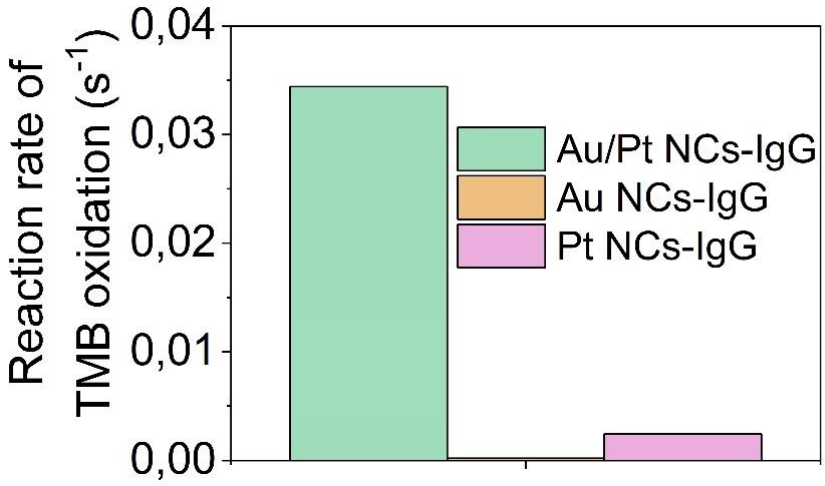


Figure 26. Reaction rate of TMB oxidation of Au/Pt NCs-IgG, Au NCs-IgG, and Pt NCs-IgG.

EDX mapping of a single Au/Pt NC-IgG (Figure 27A.) was used to further confirm the bimetallic composition of NCs. The red dots belong to Pt atoms and the green ones belong to Au atoms (Figure 27B.) with an atomic percentage of 91 and 9%, respectively. In Figure 28. the EDX spectrum of Au/Pt NCs-IgG is showed. The results of this experiment effectively confirm that Au/Pt NCs-IgG have a bimetallic composition.

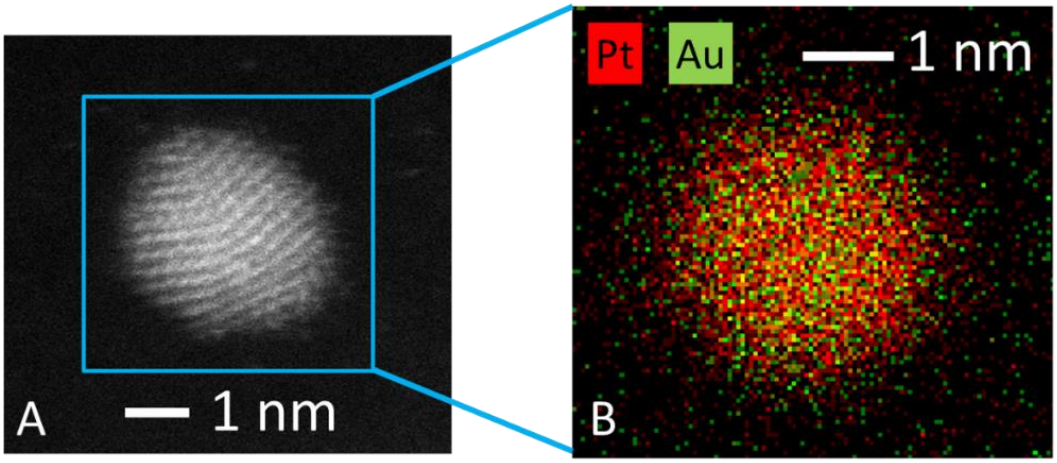


Figure 27. TEM image (A) and EDX mapping (B) of a single Au/Pt NCs-IgG.

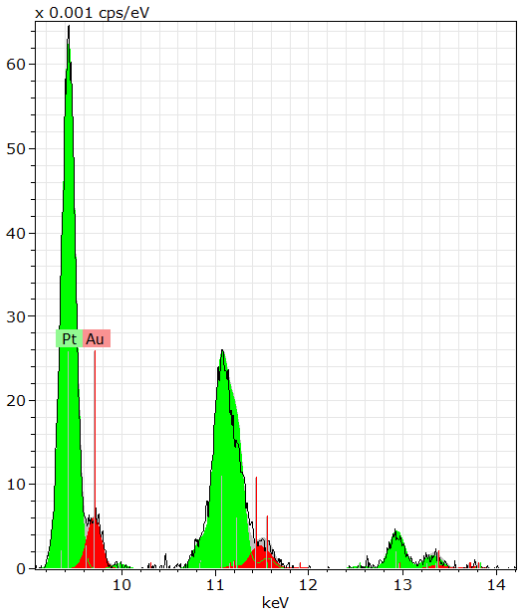


Figure 28. EDX spectrum of Au/Pt NCs IgG.

### 3.6. Evaluation of the universality of the synthetic method for catalytic Au/Pt NCs-IgG using polyclonal antibodies and their application for various immunoassays

In order to evaluate the universality and robustness of the new route to antibodies with peroxidase activity, the synthesis of bimetallic Au/Pt NCs was carried out with two additional polyclonal IgGs acting as scaffolds for the synthesis of NCs: a polyclonal anti-PSA IgG and a polyclonal anti-mouse IgG. The synthesis of the Au/Pt NCs anti-PSA IgG and Au/Pt NCs anti-mouse IgG was performed as described in the Experimental Section with little changes. In Figure 29. a typical TEM image of Au/Pt NCs anti-PSA IgG and size distribution is showed. The concentration of IgG was changed to 0.5 mg/mL.

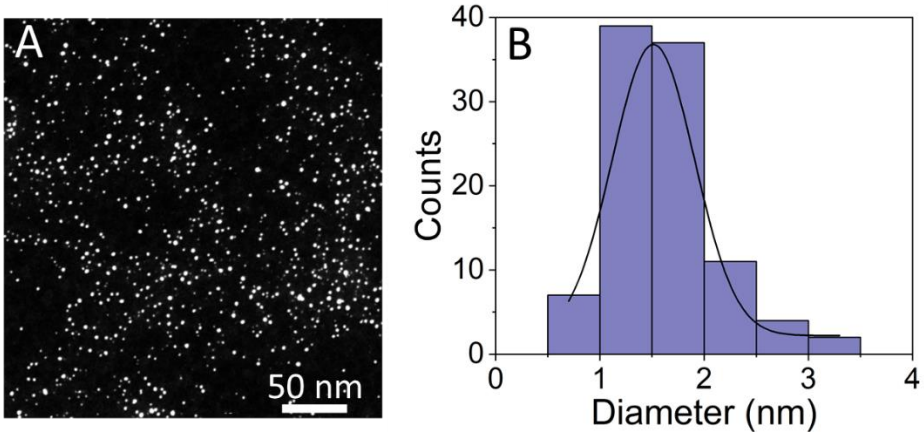


Figure 29. Typical STEM image (A) and size distribution (B) of Au/Pt NCs Anti-PSA IgG.

The prepared Au/Pt NCs anti-PSA IgG and Au/Pt NCs anti-mouse IgG exhibited peroxidase-like activity with the chromogenic substrate TMB in the presence of $H_2O_2$. Their catalytic properties were used in a direct ELISA to relate concentrations of PSA and anti-vinculin IgG from mouse, respectively, with the reaction rate of TMB oxidation. To perform these immunoassays, first, the surface of a MaxiSorp microplate was covered with different concentrations of PSA or anti-vinculin IgG from mouse and incubated (overnight, 4 °C). Then, casein (100 µL, 20.5 mg/mL) was added as a blocking agent and incubated (1 h, RT). Afterward, Au/Pt NCs anti-PSA IgG (100 µL, 16 µg/mL) or Au/Pt NCs anti-mouse IgG (100 µL, 8 µg/mL) were added and incubated (1 h, RT). Finally, the antigen concentration was related to the catalytic activity of the modified antibodies with 100 µL of TMB (200 µM) and $H_2O_2$ (250 mM). After each step, the wells were washed three times with PBST (100 µL). In Figure 30A. and 31A. a schematic representation for a direct ELISA for PSA and anti-vinculin IgG from mouse respectively, are showed. In Figure 30B. and 31B., the calibration curves for the direct ELISA for PSA and anti-vinculin IgG from mouse are shown. The reaction rate of TMB oxidation increases with enhancing PSA and anti-vinculin IgG from mouse concentrations. Thus, Au/Pt NCs anti-PSA IgG and Au/Pt NCs anti-mouse IgG synthesized according to the present method retain their affinity to target analytes. Therefore, immunoassays for the quantification of PSA and anti-vinculin IgG can be built using the catalytic activity of Au/Pt clusters.

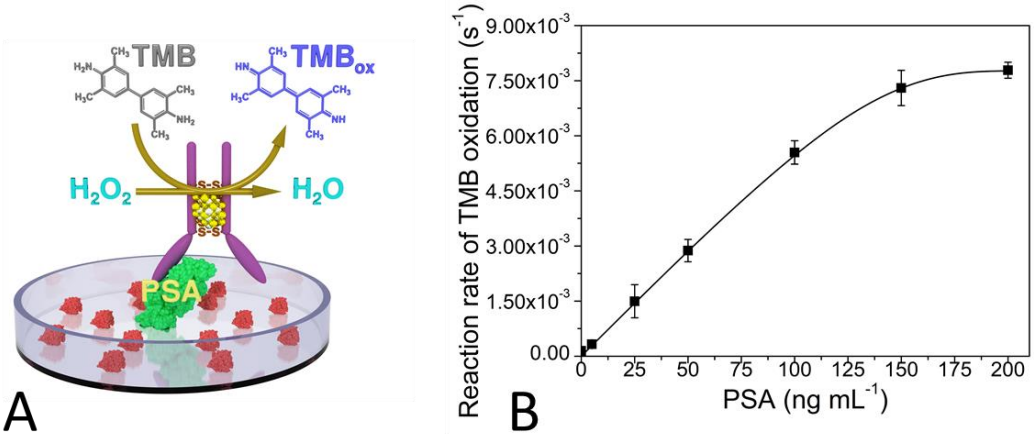


Figure 30. Schematic representation of a direct immunoassay for PSA using Au/Pt NCs-IgG as a detection Antibody (A). Calibration curve of PSA obtained in a direct ELISA assay based on Au/Pt NCs-IgG using (λ = 655 nm) (B).

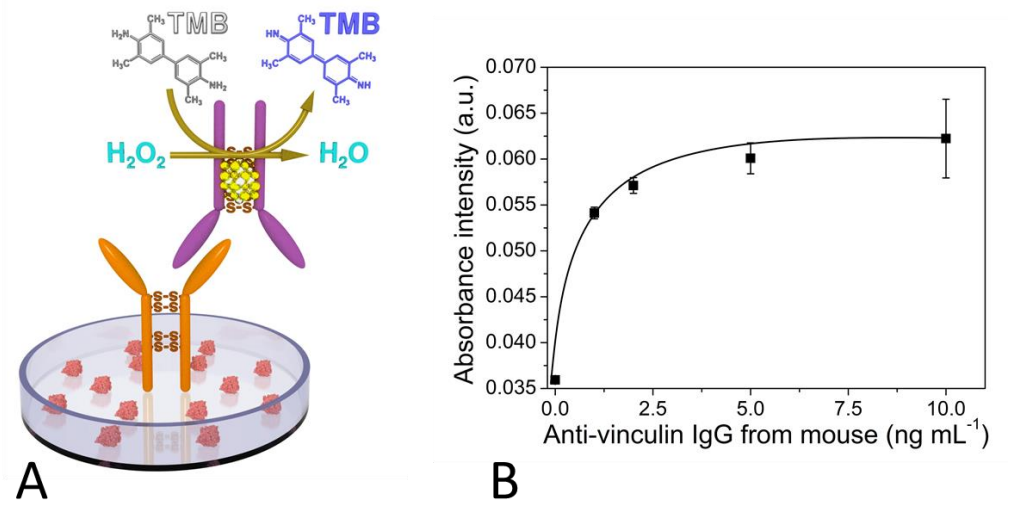


Figure 31. Schematic representation of a direct immunoassay for Anti-vinculin IgG from mouse using Au/Pt NCs-IgG as a detection antibody (A). Calibration curve of Anti-vinculin IgG from mouse obtained in a direct ELISA assay based on Au/Pt NCs-IgG using (λ = 655 nm) (B).

## 3.7. Evaluation of the performance of the synthetic method for catalytic Au/Pt NCs-IgG using monoclonal antibodies and their application in immunoassays

The synthesis of Au/Pt NCs was demonstrated using polyclonal antibodies. Then the same synthetic method was employed with a monoclonal antibody. An antibody against interleukin-6 (IL-6) was chosen as a model analyte because IL-6 is an analyte with high research relevance. It is a protein that belongs to the glycoprotein-130 cytokine family and it is composed by 184 aminoacids. In 1986 it was originally recognized as a regulator of B-cell differentiation[56]. Different cells are able to synthesize this protein, such as monocytes, macrophages, lymphocytes, fibroblasts, keratinocytes, endothelial cells and some tumor cells[57]. IL-6 participates in different biological processes like immune regulation, hematopoiesis, inflammation and oncogenesis[58]. The concentration of IL-6 in the plasma of healthy human adults is less than 10 pg/mL. However, newborns have IL-6 concentrations between 18-26 pg/mL[59]. Typically, IL-6 sensing is performed by ELISA, chemiluminescent immunoassay among others (Table 3.)

Table 3. Different assays for IL-6 sensing.

| Type of assay | Sensitivity | Linear range | Reference |
|---|---|---|---|
| ELISA | 1 pg/mL | 1 pg/mL-1 µg/mL | 60 |
| Chemiluminescence immunoassay | 0.5 pg/mL | 4.0-625.0 pg/mL | 61 |
| Electrochemical sensor | 1 pg/mL | 0.002-20 ng/mL | 62 |
| Surface plasmon resonance (SPR) biosensors | 0.78 ng/mL | 0.78–12.5 ng/mL | 63 |
| SERS-based lateral flow assay biosensor | 1 pg/mL | 0.01-400 ng/mL | 64 |
| Electrochemical impedance sensor | 0.01 fg/mL | 0.01-100 fg/mL | 65 |
| Liquid-gated field-effect transistor (FET) sensors | 1.37 pg/mL | - | 66 |
| Graphene Oxide-based amperometric sensor | 4.7 pg/mL | 4.7-300 pg/mL | 67 |
| Electrochemical immunosensor | 0.059 pg mL | 0.1-100000 pg/ mL | 68 |
| Electrochemical magnetoimmunosensor | 0.39 pg/mL | 1.75-500 pg/mL | 69 |
| Photoelectrochemical immunoassay | 0.38 pg/mL | 1.0 pg/mL-100 ng/mL | 70 |
| Label-free electrochemical aptasensor | 0.33 pg mL | 1 pg/mL-15 µg/mL | 71 |
| Magnetic colorimetric immunoassay | 0.04 pg mL | 0.0001-10 ng/mL | 72 |

The majority have a good sensitivity and a wide linear range; therefore, the objective is not to develop a more sensitive assay but to test the performance of Au/Pt NCs synthesized using a monoclonal IgG as scaffold in an immunoassay.

The requirements for the detection of IL-6 using this strategy are:

1. To select a matched pair antibodies.
2. The detection antibody should be free of BSA or any protein as preservative. Since the metallic NCs are formed due to the presence of some functional groups present in aminoacid residues, the presence of other proteins would cause the

indiscriminate formation of the NCs in the antibodies and the proteins used as preservative.

All these requirements were accomplished by the Human IL-6 Antibody Pair- BSA and Azide free from abcam (ab243973). Both capture and detection antibodies are rabbit monoclonal antibodies.

The synthesis was performed as described in the Experimental Section with changes in the antibody concentration. The concentration of IgG was reduced 10 times, from 1 mg/mL to 0.1 mg/mL. It was necessary this drastic shrinking of the antibody concentration because of the little amount of antibody that was provided and the high cost. If the concentration proposed in the Experimental Section was employed, the synthetic method would not be economically viable. As a control, the synthesis using the reduced antibody concentration was performed also with the polyclonal Anti-BSA IgG from rabbit. This control was performed to be sure that if there are changes in the performance of the synthetic method is due to the monoclonal nature of the antibody and not to the decrease of antibody concentration during the synthesis.

In Figure 32. a typical TEM image of Au/Pt NCs anti-IL-6 IgG and size distribution is showed. The metallic cores showed a spherical shape and a mean diameter of 1.76 ± 0.24 nm. In Figure 33. a TEM image and size distribution of the control synthesis are showed. The NCs have a mean diameter of 2.10 ± 0.40 nm.

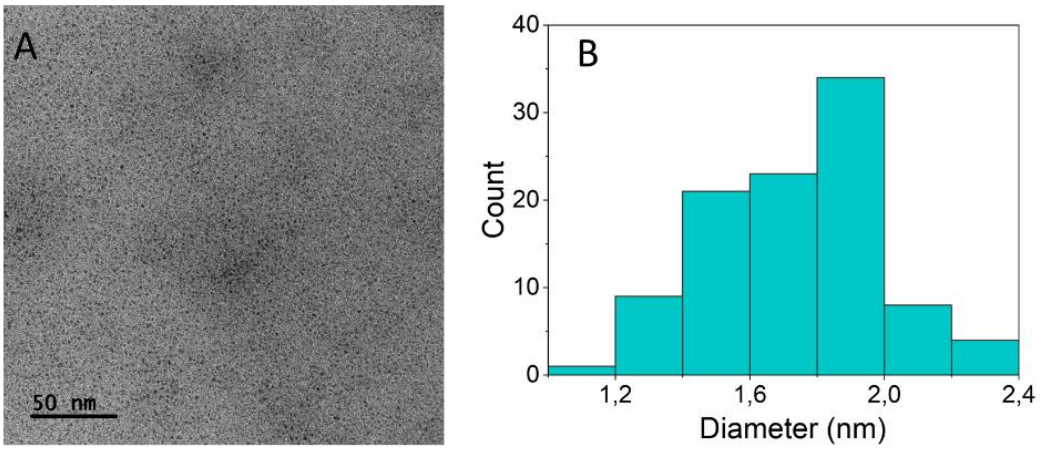


Figure 32. Representative TEM image (A) of Au/Pt NCs-Anti-IL-6 IgG and size distribution (B) based on the statistics over 100 individual particles.

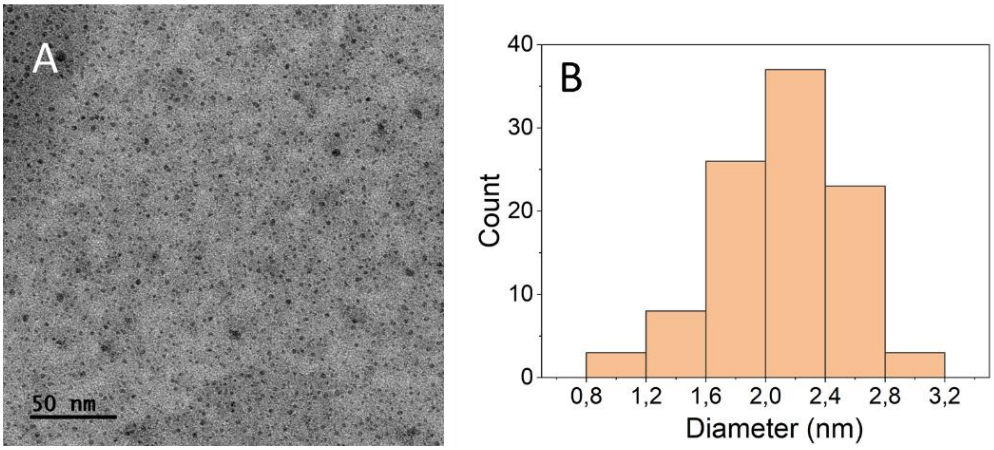


Figure 33. (A) Typical TEM image and (B) size distribution of Au/Pt NCs Anti-BSA IgG (control synthesis with reduced volume of Anti-BSA IgG employed during the synthesis).

XPS measurements were performed to study the valence state of the cores of Au/Pt NCs-Anti-IL-6 IgG (Figure 34.). This spectrum is composed of two energy bands for Pt, the Pt $4f_{7/2}$ and the Pt $4f_{5/2}$ at 71.1 eV and 74.2 eV respectively. Such distribution of bands is characteristic of Pt in metallic state [37]. In the Au 4f region the spectra present characteristic doublet with the $4f_{7/2}$ (83.1 eV) and $4f_{5/2}$ (85 eV) energy bands usually found for Au in oxidation state 0.

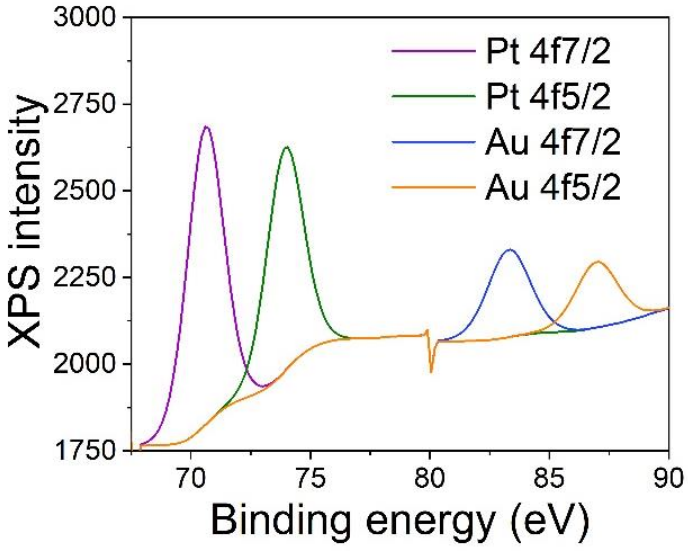


Figure 34. XPS spectra of Au/Pt NCs-Anti-IL-6 IgG.

It was found that Au/Pt NCs-Anti-IL-6 IgG had peroxidase-like activity as expected. This activity is dependent on TMB and $H_2O_2$ concentration. To measure the dependence of the initial reaction rate on concentration of both substrates, the concentration of one of the substrates was fixed while the concentration of the other one was changed. In

Figure 35A. and 35B. it is shown how the reaction rate of TMB oxidation increases with the rise of substrate concentration following a Michaelis-Menten like kinetics. With the Lineweaver-Burk equation the $K_m$ was obtained (Figure 35C. and 35D).

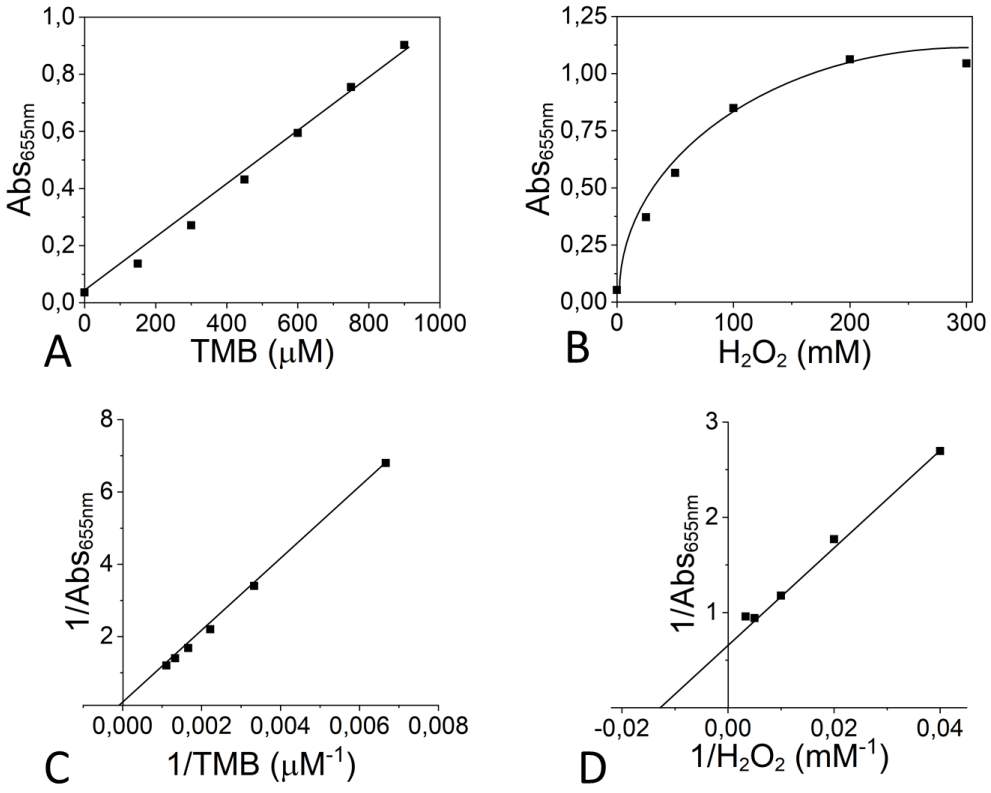


Figure 35. Intensity of absorbance peak (655 nm) at different TMB concentrations (A) and $H_2O_2$ concentrations (B). Double reciprocal plots of catalytic activity of Au/Pt NCs-Anti-IL-6 IgG with TMB (C) and $H_2O_2$ (D).

In Table 4. the $K_m$ values for Au/Pt NCs-Anti-IL-6 IgG, Au/Pt NCs-Anti-BSA IgG and HRP[49] are shown. The value of $K_m$ for both bimetallic NCs is significantly higher than that of HRP to $H_2O_2$, indicating that both nanozymes have a lower affinity for $H_2O_2$ than HRP. As it was showed previously, the $K_m$value for Au/Pt NCs-Anti-BSA IgG is more than 8.5 times lower than that of HRP towards TMB, which indicates that it has a higher affinity than HRP to TMB as a substrate. The same effect was expected to be found in the case of Au/Pt NCs-Anti-IL-6 IgG, unfortunately the achieved $K_m$ value is higher than that of HRP indicating that the affinity towards TMB was not improved.

Table 4. Comparison of the apparent $K_m$ between Au/Pt NCs IgG and HRP.

| Catalyst | Substrate | $K_m$ (mM) |
|---|---|---|
| Au/Pt NCs Anti-IL-6 IgG | TMB | 56.7 |
| | $H_2O_2$ | 107.4 |
| Au/Pt NCs-Anti-BSA | TMB | 0.0418 |
| | $H_2O_2$ | 102.35 |
| HRP[49] | TMB | 0.362 |
| | $H_2O_2$ | 0.522 |

A direct immunoassay for IL-6 was performed employing the antibodies bearing NCs as detection antibody to see if the affinity of the IgG for target analyte was maintained after the insertion of NCs into its structure (Figure 36A).

The amount of IL-6 adsorbed was regulated by incubation with solutions containing different amounts of IL-6 (0 to 500 pg/mL). After the blocking step with casein, it was added 100 µL of a solution containing Au/Pt NCs-Anti-IL-6 IgG with a concentration 3.3 µg/mL. This concentration is referred to the concentration of Anti-IL-6 IgG. It is important to highlight that the final concentration of IgG in the direct immunoassay is 10 times lower than the final IgG concentration employed in the direct immunoassay for BSA in Figure 22.

The control synthesis of Au/Pt NCs using the reduced antibody concentration with the polyclonal Anti-BSA IgG from rabbit was used also in a direct immunoassay (Figure 37A.). The BSA concentrations employed range from 0 to 500 ng/mL. The concentration of Au/Pt NCs-Anti-BSA IgG was 3.3 µg/mL, the same IgG concentration added of detection antibody for the direct immunoassay for IL-6.

Another aspect to consider is that the amount of target analyte adsorbed is different in these assays due to the performance of the matched pair antibodies selected. Thinking about a further application as detection antibody in a sandwich immunoassay, of the Au/Pt NCs-Anti-IL-6 IgG, a matched pair antibodies were selected (ab243973). The optimal range for these antibodies in sandwich immunoassay is from 7.8 pg/ml to 500 pg/ml, this is why IL-6 concentrations in this range were used in the direct immunoassay. It was expected that the oxidation rate of TMB increased proportionally with the IL-6 concentration. The calibration curve shows (Figure 36B.) that this assumption was not correct and no TMB oxidation was observed with any IL-6 concentration. In the case of

calibration curve for BSA the reaction rate of TMB oxidation increased with the analyte concentration (Figure 37B). This result indicates that the bad performance of Au/Pt NCs-Anti-IL-6 IgG in direct immunoassay it is not due to the decrease in concentration of the IgG during the synthesis and the immunoassay.

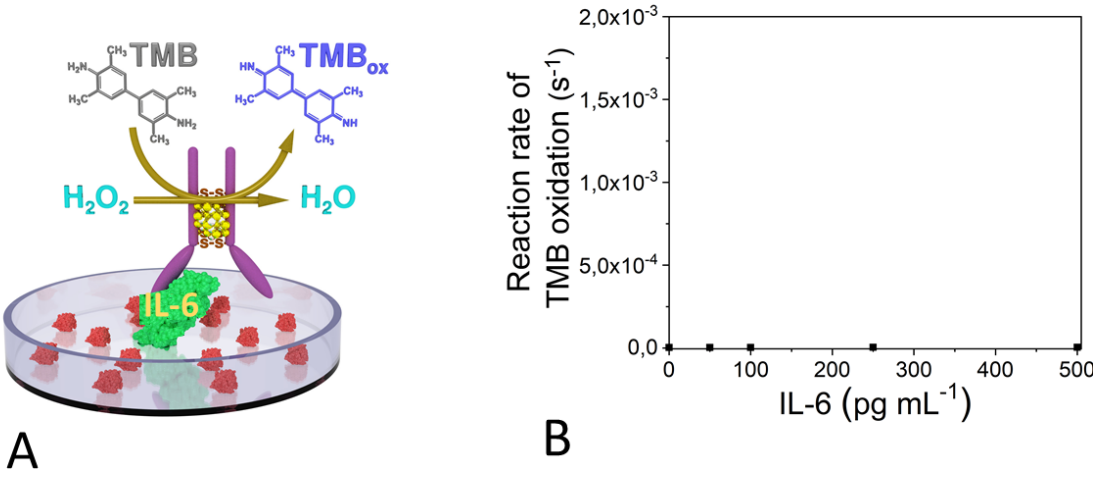


Figure 36. Schematic representation of a direct immunoassay for IL-6 using Au/Pt NCs-Anti-IL-6 IgG as a detection antibody (A). Calibration curve of IL-6 obtained in a direct ELISA assay based on Au/Pt NCs-Anti-IL-6 IgG (λ = 655 nm) (B).

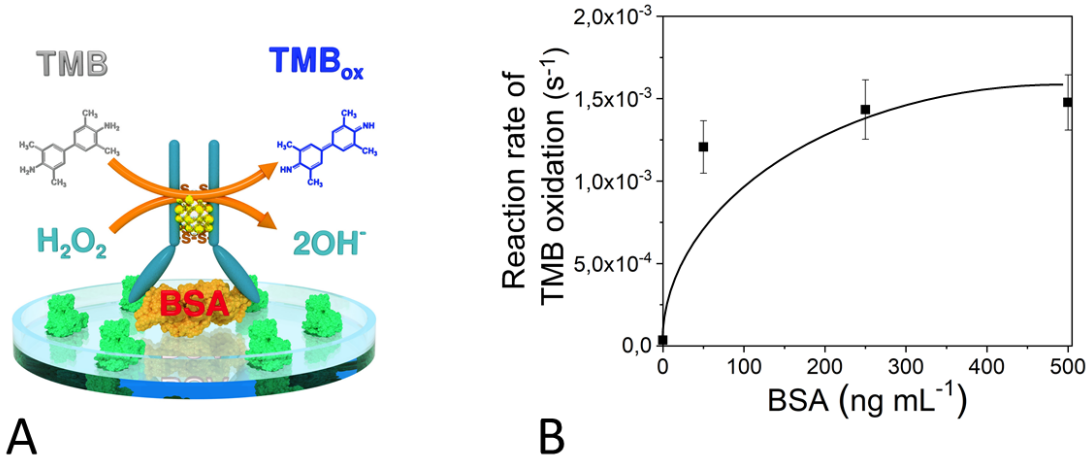


Figure 37. Schematic representation of a direct immunoassay for BSA using Au/Pt NCs-Anti-BSA IgG as a detection antibody (control synthesis) (A). Calibration curve of BSA obtained in a direct ELISA assay based on Au/Pt NCs-Anti-BSA IgG (λ = 655 nm) (B).

In order to understand this result, it was decided to study the secondary structure of the antibody carrying NCs and the naked antibody using CD spectroscopy (Figure 38.).

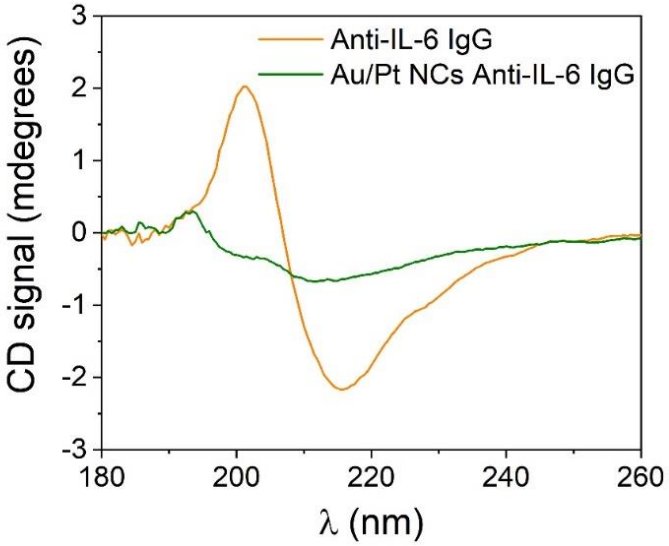


Figure 38. Far-UV CD spectra of Anti-IL-6 IgG and Au/Pt NCs- Anti-IL-6 IgG.

The maintenance of the conformation of the antibody is the key factor for applications in immunoassays. We discovered the major secondary structure for the monoclonal IgG in the far-UV CD spectra, antiparallel β-sheets and random coil conformations. The occurrence of a large minimum at 218 nm indicates the presence of β-sheets. The synthesis of NCs employing an antibody as a scaffold may degrade or destroy entirely the secondary structure of the IgG. This assumption was confirmed after measuring the CD spectrum of the antibody carrying NCs. The loss of the secondary structure of the antibody after the synthesis of the NCs explains the unexpected results of the immunoassay. In the case of the IgG for BSA the introduction of Au/Pt NCs in the antibody did not cause any significant alteration in the IgG conformation. The difference in the IgG employed for BSA and for IL-6 is that, in the former a polyclonal antibody was employed and in the later a monoclonal one.

The main differences between monoclonal and polyclonal antibodies are that polyclonal ones are mixture of heterogeneous which are produced by different B cell clones in the body. They are able to recognize different epitopes of a single antigen. On the other hand, monoclonal antibodies are generated by identical B cells which are clones from a single parent cell. Therefore, monoclonal antibodies have monovalent affinity and can only specifically bind an epitope of an antigen. The homogeneity and consistency of monoclonal antibodies are their main characteristics. Monoclonal antibodies are effective for analyzing changes in molecular conformation, protein-protein interactions, and phosphorylation states, as well as recognizing single members of protein families,

because of their monospecificity. On the other hand, the monospecidicity of monoclonal antibodies may limit their utility. Small changes in the structure of an epitope (due to genetic polymorphism, glycosylation, or denaturation) might have a significant impact on monoclonal antibodies function. As a result, monoclonal antibodies should be made in the condition of the antigen to which they will eventually bind. Because polyclonal antibodies are diverse and identify a variety of antigenic epitopes, changes to a single or limited number of epitopes are unlikely to have a major impact[73].

Polyclonal antibodies are also more stable throughout a wide range of pH and salt concentrations, whereas monoclonal can be highly sensitive to even little changes in both. Antibodies that have been covalently linked to a fluorophore or other label may have their binding properties altered. When employing polyclonal antibodies, which recognize a wide range of epitopes, this potential is less of a problem, but it can be substantial for monoclonal antibodies if the modification alters the monospecific binding site[73]. This phenomenon could be extrapolated to the introduction of NCs in the antibody structure. Even if the conditions used during the synthesis, did not cause an important change in the secondary structure of polyclonal antibodies and neither in its binding properties. It seems to be very different in the case of monoclonal antibodies. The synthesis conditions cause the denaturalization and loss of secondary structure of the antibody and the disappearance of affinity for target analyte. The synthesis of bimetallic NCs using a monoclonal antibody as scaffold have been only tried in the Anti-IL-6 IgG used in this chapter. Further experiments will be required to fully understand this phenomenon and the use of other monoclonal antibodies will be also necessary.

## 4. Conclusions

This study provides the first methods for the synthesis of semiconductor and bimetallic NCs using polyclonal antibodies as scaffolds. The nondenaturing conditions used during the synthesis cause the antibody structure to remain unalterable after the modification; thus, antibody still has affinity for its target analyte and protein G. The CdS NCs-IgG show fluorescent and photocatalytic properties, and they are able to oxidize the fluorogenic substrate Amplex Red triggered by the exposition to UV-light. The Ag/Pt NCs-IgG and

Au/Pt NCs-IgG exhibit peroxidase-like activity and oxidize the chromogenic substrate TMB in the presence of $H_2O_2$. Both reactions follow the Michaelis− Menten kinetics; the reaction rate increases with substrate concentration. The position and the composition of the metallic core in Au/Pt NCs-IgG was studied. EDX measurements showed that effectively, the metallic core is composed of Au and Pt. The synthesis of Au/Pt NCs using different antibody fragments as scaffold suggest that the presence of the hinge region of the antibody composed by disulphide moieties is mandatory for the stabilization of NCs. The synthetic route to Au/Pt NCs-IgG is robust and can be applied to the synthesis of different polyclonal antibodies with catalytic activity. The same synthesis was performed using a monoclonal IgG, resulting in the denaturalization of the antibody and the loss of affinity of target analyte. This behaviour indicates that the method cannot be extrapolated to monoclonal antibodies. The results obtained in this work suggest that polyclonal IgG carrying NCs are potential candidates for be used in biosensing applications. Their ability and performance to act as detection antibody in immunoassays, providing the recognition element and the transduce component is studied in next chapter.

## References


1. Chen, L.-Y., Wang, C.-W., Yuan, Z. & Chang, H.-T. Fluorescent Gold Nanoclusters: Recent advances in Sensing and Imaging. *Anal. Chem.* **87**, 216–229 (2015).
2. Jariwala, D., Sangwan, V. K., Lauhon, L. J., Marks, T. J. & Hersam, M. C. Carbon nanomaterials for electronics, optoelectronics, photovoltaics, and sensing. *Chem. Soc. Rev.* **42**, 2824 (2013).
3. Chib, R. *et al.* Effect of quencher, denaturants, temperature and pH on the fluorescent properties of BSA protected gold nanoclusters. *J. Lumin.* **168**, 62–68 (2015).
4. Xie, J., Zheng, Y. & Ying, J. Y. Protein-Directed Synthesis of Highly Fluorescent Gold Nanoclusters. *J. Am. Chem. Soc.* **131**, 888–889 (2009).
5. Das, T. *et al.* Protein-templated gold nanoclusters: Size dependent inversion of fluorescence emission in the presence of molecular oxygen. *Nanoscale* **4**, 6018–6024 (2012).
6. Han, S.-Q., Liu, J. L., Gan, Z.-G., Liang, J. G. & Zhao, S. M. Application of Luminescent BSA-Capped CdS Quantum Dots as a Fluorescence Probe for the Detection of Cu 2+. *J. Chin. Chem.* **55**, 1069–1073 (2015).
7. Ghosh, R., Sahoo, A. K., Ghosh, S. S., Paul, A. & Chattopadhyay, A. Blue-emitting copper nanoclusters synthesized in the presence of lysozyme as candidates for cell labeling. *ACS Appl. Mater. Interfaces* **6**, 3822–3828 (2014).

8. Zhou, T. *et al.* Facile synthesis of red-emitting lysozyme-stabilized Ag nanoclusters. *Nanoscale* **4**, 5312 (2012).
9. Xia, X., Long, Y. & Wang, J. Glucose oxidase-functionalized fluorescent gold nanoclusters as probes for glucose. *Anal. Chim. Acta* **772**, 81–86 (2013).
10. Wen, F. *et al.* Horseradish Peroxidase Functionalized Fluorescent Gold Nanoclusters for Hydrogen Peroxide Sensing Characterization. *Anal. Chem.* **83**, 1193–1196 (2011).
11. Ding, W., Guan, L., Han, J., Mangala, R. & Luo, Z. Fluorescence chemosensing of water-soluble Ag14nanoclusters for lysozyme and Hg2+ions. *Sensors Actuators B* **250**, 364–371 (2017).
12. Schultz, D. *et al.* Evidence for rod-shaped DNA-stabilized silver nanocluster emitters. *Adv. Mater.* **25**, 2797–2803 (2013).
13. Kessler, S. W. Rapid Isolation of Antigens from Cells with A Staphylococcal Protein A-Antibody Adsorbent : Parameters of the Interaction of Antibody-Antigen Complexes with Protein A. *J. Immunol.* **115**, 1617–1624 (1975).
14. Barroso, J., Saa, L., Grinyte, R. & Pavlov, V. Photoelectrochemical device based on modified by osmium polymer to detection of enzymatic activities. *Biosens. Bioelectron.* **77**, 323–329 (2016).
15. Malashikhina, N., Garai-Ibabe, G. & Pavlov, V. Unconventional application of conventional enzymatic substrate: First fluorogenic immunoassay based on enzymatic formation of quantum dots. *Anal. Chem.* **85**, 6866–6870 (2013).
16. Deschaume, O., Shafran, K. L. & Perry, C. C. Interactions of bovine serum albumin with aluminum polyoxocations and aluminum hydroxide. *Langmuir* **22**, 10078–10088 (2006).
17. Huang, D. *et al.* Biomimetic interactions of proteins with functionalized cadmium sulfide quantum dots. *Colloids Surfaces A Physicochem. Eng. Asp.* **392**, 191–197 (2011).
18. Ipe, B. I., Lehnig, M. & Niemeyer, C. M. On the generation of free radical species from quantum dots. *Small* **1**, 706–709 (2005).
19. Rajendran, V., Konig, A., Rabe, K. S. & Niemeyer, C. M. Photocatalytic activity of protein-conjugated CdS nanoparticles. *Small* **6**, 2035–2040 (2010).
20. Slocik, J. M., Govorov, A. O. & Naik, R. R. Photoactivated biotemplated nanoparticles as an enzyme mimic. *Angew. Chemie* **47**, 5335–5339 (2008).
21. Gandubert, V. J., Torres, E. & Niemeyer, C. M. Investigation of cytochrome P450-modified cadmium sulfide quantum dots as photocatalysts. *J. Mater. Chem.* **18**, 3824–3830 (2008).
22. Fruk, L., Rajendran, V., Spengler, M. and Niemeyer, C. M. Light-induced triggering of peroxidase activity using quantum dots. *ChemBioChem* **8**, 2195–2198 (2007).
23. Fruk, L., Rajendran, V., Spengler, M. & Niemeyer, C. M. Light-induced triggering of peroxidase activity using quantum dots. *ChemBioChem* **8**, 2195–2198 (2007).
24. Ngamdee, K., Kulchat, S., Tuntulani, T. & Ngeontae, W. Fluorescence sensor based on D-penicillamine capped cadmium sulfide quantum dots for the detection of cysteamine. *J. Lumin.* **187**, 260–268 (2017).
25. Kulchat, S., Boonta, W., Todee, A., Sianglam, P. & Ngeontae, W. A fluorescent sensor based on thioglycolic acid capped cadmium sulfide quantum dots for the determination of dopamine. *Spectrochim. Acta A* **196**, 7–15 (2018).
26. Wang, H. *et al.* A highly sensitive and selective chemosensor for 2,4,6-

trinitrophenol based on L-cysteine-coated cadmium sulfide quantum dots. *Talanta* **198**, 242–248 (2019).

27. Faraz, M. *et al.* Polyindole/cadmium sulphide nanocomposite based turn-on, multi-ion fluorescence sensor for detection of Cr3+, Fe3+ and Sn2+ ions. *Sens. Actuators B Chem.* **269**, 195–202 (2018).
28. Wu, L. L., Wang, L. Y., Xie, Z. J., Xue, F. & Peng, C. F. Colorimetric detection of Hg2+based on inhibiting the peroxidase-like activity of DNA-Ag/Pt nanoclusters. *RSC Adv.* **6**, 75384–75389 (2016).
29. Wu, L. L., Wang, L. Y., Xie, Z. J., Pan, N. and Peng, C. F. Colorimetric assay of l-cysteine based on peroxidase-mimicking DNA-Ag/Pt nanoclusters. *Sensors Actuators, B Chem.* **235**, 110–116 (2016).
30. Zheng, C., Zheng, A. X., Liu, B., Zhang, X. L. & He, Y., Li, J., Yang, H. H. and Chen, G. One-pot synthesized DNA-templated Ag/Pt bimetallic nanoclusters as peroxidase mimics for colorimetric detection of thrombin. *Chem. Commun.* **50**, 13103–13106 (2014).
31. Feng, J., Huang, P. & Wu, F. Gold–platinum bimetallic nanoclusters with enhanced peroxidase-like activity and their integrated agarose hydrogel-based sensing platform for the colorimetric analysis of glucose levels in serum. **142**, 4106–4115 (2017).
32. Wan, L. *et al.* High peroxidase-mimicking activity of gold@platinum bimetallic nanoparticle-supported molybdenum disulfide nanohybrids for the selective colorimetric analysis of cysteine. *Chem. Comm.* **56**, 12351–12354 (2020).
33. Gao, Z., Xu, M., Lu, M., Chen, G. & Tang, D. Urchin-like (gold core)@(platinum shell) nanohybrids: A highly efficient peroxidase-mimetic system for in situ amplified colorimetric immunoassay. *Biosens. Bioelectron.* **70**, 194–201 (2015).
34. Signor, L. & Erba, E. B. Matrix-assisted Laser Desorption / Ionization Time of Flight ( MALDI-TOF ) Mass Spectrometric Analysis of Intact Proteins Larger than 100 kDa. *J. Vis. Exp.* **79**, e50635 (2013).
35. Barreca, D., Gasparotto, A. & Tondello, E. Nanostructured Cadmium Sulfide Thin Films by XPS. *Surf. Sci. Spectra* **9**, 46–53 (2003).
36. Subramanyam, T. K., Naidu, B. S. & Uthanna, S. Studies on dc magnetron sputtered cadmium oxide films. *Appl. Surf. Sci.* **169**–**170**, 529–534 (2001).
37. Davis, D. J., Kyriakou, G. & Lambert, R. M. Uptake of n -Hexane , 1-Butene , and Toluene by Au / Pt Bimetallic Surfaces : A Tool for Selective Sensing of Hydrocarbons under High-Vacuum Conditions. *J. Phys. Chem B* **110**, 11958–11961 (2006).
38. Xu, J. B., Zhao, T. S. & Liang, Z. X. Synthesis of Active Platinum - Silver Alloy Electrocatalyst toward the Formic Acid Oxidation Reaction. *J. Phys. Chem C* **112**, 17362–17367 (2008).
39. Zeng, J., Yang, J., Lee, J. Y. & Zhou, W. Preparation of Carbon-Supported Core - Shell Au - Pt Nanoparticles for Methanol Oxidation Reaction : The Promotional Effect of the Au Core. *J. Phys. Chem B* 24606–24611 (2006).
40. Yang, X., Gan, L., Han, L., Wang, E. & Wang, J. High-Yield Synthesis of Silver Nanoclusters Protected by DNA Monomers and DFT Prediction of their Photoluminescence Properties **. *Angew. Chem. Int. Ed.* **52**, 2022–2026 (2013).
41. Volkov, I. L. *et al.* DNA with Ionic , Atomic , and Clustered Silver : An XPS Study. *J. Phys. Chem B* **121**, 2400–2406 (2017).

42. Aires, A. *et al.* A simple approach to design proteins for the sustainable synthesis of metal nanoclusters. *Angew. Chem. Int. Ed.* **58**, 6214–6219 (2019).
43. Casaletto, M. P., Longo, A., Martorana, A., Prestianni, A. & Venezia, A. M. XPS study of supported gold catalysts: the role of Au0 and Au+d species as active sites. *Surf. Interface Anal.* **38**, 215–218 (2006).
44. Lin, Y., Chen, P., Yuan, Z., Ma, J. & Chang, H. The isomeric effect of mercaptobenzoic acids on the preparation and fluorescence properties of copper nanoclusters. *Chem. Commun.* **51**, 11983–11986 (2015).
45. Wang, C., Ling, L., Yao, Y. & Song, Q. One-step synthesis of fluorescent smart thermo- responsive copper clusters : A potential nanothermometer in living cells. *Nano Res.* **8**, 1975–1986 (2015).
46. Jia, X., Li, J. & Wang, E. Cu Nanoclusters with Aggregation Induced Emission Enhancement. *Small* **9**, 3873–3879 (2013).
47. Jiang, X., Sun, C., Guo, Y., Nie, G. & Xu, L. Peroxidase-like activity of apoferritin paired gold clusters for glucose detection. *Biosens. Bioelectron.* **64**, 165–170 (2015).
48. Wang, X., Wu, Q., Shan, Z. & Huang, Q. BSA-stabilized Au clusters as peroxidase mimetics for use in xanthine detection. *Biosens. Bioelectron.* **26**, 3614–3619 (2011).
49. Feng, J., Huang, P. & Wu, F. Gold–platinum bimetallic nanoclusters with enhanced peroxidase-like activity and their integrated agarose hydrogel-based sensing platform for the colorimetric analysis of glucose levels in serum. *Analyst* **142**, 4106–4115 (2017).
50. Gao, L. *et al.* Intrinsic peroxidase-like activity of ferromagnetic nanoparticles. *Nat. Nanotechnol.* **2**, 577–583 (2007).
51. Xian-ming, Q., Liu, Z., Cai, S., Zhao, Y. & Wu, D. Electrochemical aptasensor for the detection of vascular endothelial growth factor ( VEGF ) based on DNA-templated Ag / Pt bimetallic nanoclusters. *Chin. Chem. Lett.* 1–7 (2016) doi:10.1016/j.cclet.2016.04.014.
52. Joshi, V., Shivach, T., Yadav, N. & Rathore, A. S. Circular Dichroism Spectroscopy as a Tool for Monitoring Aggregation in Monoclonal Antibody Therapeutics. *Anal. Chem.* **86**, 11606–11613 (2014).
53. Vermeer, A. W. P., Bremer, M. G. E. G. & Norde, W. Structural changes of IgG induced by heat treatment and by adsorption onto a hydrophobic Teflon surface studied by circular dichroism spectroscopy. *Biochim. Biophys. Acta* **1425**, 1–12 (1998).
54. Bagçi, H., Kohen, F., Kusçuoglu, U., Bayer, E. A. & Wilchek, M. Monoclonal anti-biotin antibodies simulate avidin m the recognition of biotin. *FEBS Lett.* **322**, 47–50 (1993).
55. Tan, Y. H. *et al.* A Nanoengineering Approach for Investigation and Regulation of Protein Immobilization. *ACS Nano* **2**, 2374–2384 (2008).
56. Yale, B. The biology of interleukin-6. *Blood* **74**, 1–8 (1989).
57. Yao, X. *et al.* Targeting interleukin-6 in inflammatory autoimmune diseases and cancers. *Pharmacol. Ther.* **141**, 125–139 (2014).
58. Kishimoto, T. IL-6: From its discovery to clinical applications. *Int. Immunol.* **22**, 347–352 (2010).
59. Song, M. & Kellum, J. A. Interleukin-6. *Crit Care Med* **33**, 10–12 (2005).

60. M. Helle, L. Boeije, E.d. Grrot, A.d. Vos, L. A. Sensitive ELISA for interleukin-6 Detection of IL-6 in biological fluids: synovial fluids and sera, Journal of immunological methods. *J. Immunol. Methods* **138**, 47–56 (1991).
61. Luo, L., Zhang, Z., Hou, L., Wang, J. & Tian, W. The study of a chemiluminescence immunoassay using the peroxyoxalate chemiluminescent reaction and its application. *Talanta* **72**, 1293–1297 (2007).
62. Li, T. & Yang, M. Electrochemical sensor utilizing ferrocene loaded porous polyelectrolyte nanoparticles as label for the detection of protein biomarker IL-6. *Sens. Actuators B Chem.* **158**, 361–365 (2011).
63. Chou, T. H., Chuang, C. Y. & Wu, C. M. Quantification of Interleukin-6 in cell culture medium using surface plasmon resonance biosensors. *Cytokine* **51**, 107–111 (2010).
64. Wang, Y. *et al.* A SERS-based lateral flow assay biosensor for quantitative and ultrasensitive detection of interleukin-6 in unprocessed whole blood. *Biosens. Bioelectron.* **141**, 111432 (2019).
65. Yang, T. *et al.* An electrochemical impedance sensor for the label-free ultrasensitive detection of interleukin-6 antigen. *Sensors Actuators B* **178**, 310–315 (2013).
66. Chen, H. *et al.* Label-free electronic detection of interleukin-6 using horizontally aligned carbon nanotubes. *Mater. Des.* **90**, 852–857 (2016).
67. Huang, J., Harvey, J., Derrick Fam, W. H., Nimmo, M. A. & Alfred Tok, I. Y. Novel biosensor for interleukin-6 detection. *Procedia Eng.* **60**, 195–200 (2013).
68. Lou, Y., He, T., Jiang, F., Shi, J. J. & Zhu, J. J. A competitive electrochemical immunosensor for the detection of human interleukin-6 based on the electrically heated carbon electrode and silver nanoparticles functionalized labels. *Talanta* **122**, 135–139 (2014).
69. Ojeda, I., Moreno-Guzmán, M., González-Cortés, A., Yáñez-Sedeño, P. & Pingarrón, J. M. Electrochemical magnetoimmunosensor for the ultrasensitive determination of interleukin-6 in saliva and urine using poly-HRP streptavidin conjugates as labels for signal amplification. *Anal Bional Chem* **406**, 6363–6371 (2014).
70. Fan, G. C., Ren, X. L., Zhu, C., Zhang, J. R. & Zhu, J. J. A new signal amplification strategy of photoelectrochemical immunoassay for highly sensitive interleukin-6 detection based on TiO2/CdS/CdSe dual co-sensitized structure. *Biosens. Bioelectron.* **59**, 45–53 (2014).
71. Tertiş, M., Ciui, B., Suciu, M., Săndulescu, R. & Cristea, C. Label-free electrochemical aptasensor based on gold and polypyrrole nanoparticles for interleukin 6 detection. *Electrochim. Acta* **258**, 1208–1218 (2017).
72. Peng, J., Guan, J., Yao, H. & Jin, X. Magnetic colorimetric immunoassay for human interleukin-6 based on the oxidase activity of ceria spheres. *Anal. Biochem.* **492**, 63–68 (2016).
73. Lipman, N. S., Jackson, L. R., Trudel, L. J. & Weis-Garcia, F. Monoclonal versus polyclonal antibodies: Distinguishing characteristics, applications, and information resources. *ILAR J.* **46**, 258–267 (2005).

# CHAPTER 4: APPLICATION IN IMMUNOASSAYS OF ANTIBODY-PROTECTED NANOCLUSTERS

- Setting of sandwich-type immunosensor using antibody-protected bimetallic NCs.
- First steps towards the development of a FRET-based homogeneous competitive immunoassay using antibody-protected CdS NCs.

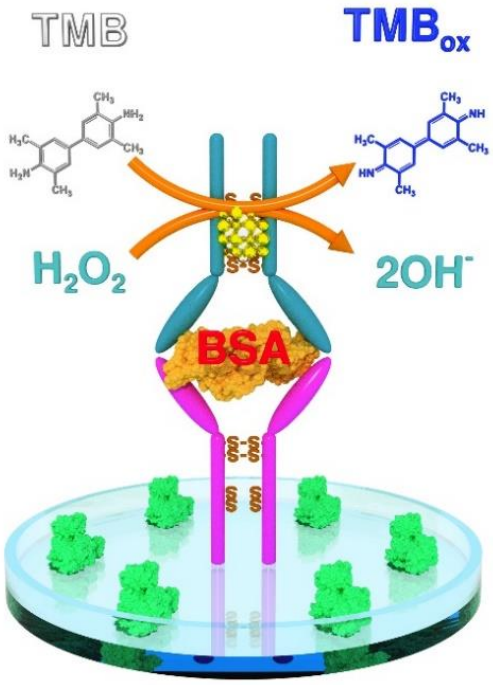


## Development of sandwich-type immunosensor using antibody-protected bimetallic NCs.

Herein, the catalytic properties of bimetallic NCs embedded in antibodies presented in the previous chapter are used in an immunoassay for the detection of target antigen. The non-denaturing conditions used during the synthesis maintains intact the structure of IgG and its affinity for BSA. Bimetallic NCs exhibit higher catalytic activity than monometallic NCs, due to the synergistic effect of two different atoms. This peroxidase-like activity and the retained affinity to its antigen make Au/Pt NCs-IgG a suitable material for its use as a detection antibody in a sandwich-type immunosensor. The mode that the signal is generated is similar to that of HRP-based ELISA endowing our method a promising approach for quantitative detection. Employment of bimetallic NCs-IgG instead of IgG labeled with horseraddish peroxidase in  as detection antibody in sandwich-type immunosensor allows to improve its LOD by 56 times.

## 1. Introduction

Immunoassays are analytical techniques in which the selectivity and sensitivity are provided by the specific interaction between an antibody and its target analyte [1]. Among all the immunosensors the colorimetric ones are the most popular. Enzyme-linked immunosorbent assay (ELISA) takes advantage of enzymes attached to the antibody, like HRP or alkaline phosphatase (ALP), and its ability to generate colour change in chromogenic substrates. Usually, a simple microplate reader is enough for measuring the signal. Furthermore, the colour change can be distinguished by the naked eye, allowing the visual detection. It is possible to use smartphones to record and to analyse the colorimetric response, making it very attractive for POC testing. For example, a POC platform for the diagnosis of Zika[2] has been developed using a sandwich ELISA. The detection was performed by measuring the saturation intensity of the developed colour generated by TMB oxidation with the camera of a smartphone. A similar assay was developed for the HIV p24 antigen detection[3]. In a typical sandwich ELISA, the target analyte is bound to the capture antibody through the specific antibody-antigen interaction and the antibody labelled with an enzyme is further attached to the recognized analyte. The enzyme catalyses some chromogenic reaction providing a colorimetric signal that can be related with the concentration of target analyte.

Natural enzymes as markers have several disadvantages, such as, high susceptibility to environmental variations, easy denaturation and digestion, costly and time-consuming preparation and purification [4]. Therefore, new labels for biomolecules that give more specific signal and facilitate retention of sufficient biological activity for use in bioassays are needed. The discovery of nanomaterials with enzyme-like properties, the nanozymes, provides a potential solution to overcome the above drawbacks. By using nanozymes instead of natural enzymes, the immunosensor would have lower cost and improved stability, extending the expiration date of the kits, along with comparable sensitivity and selectivity[5].

The bioconjugation step of nanozymes and enzymes to antibodies is a critical step for the immunoassay development[6]. To increase the biocompatibility of nanozymes and to make easier the bioconjugation, usually they are functionalized with molecules, such as

histidine[7], dextran[7], 3-aminopropyltriethoxysilane (APTES)[8] or polyethylene glycol (PEG)[9]. The most employed strategies for this bioconjugation are the glutaraldehyde, the 1-Ethyl-3-(3-dimethylaminopropyl)carbodiimide/N-hydroxysuccinimide (EDC/NHS) methodology and the biotin-streptavidin system. The crosslinking using glutaraldehyde allows the oriented coupling of carboxyl and amino groups. For example, $Fe_3O_4$ magnetic NPs have been modified with APTES and linked to antibodies using glutaraldehyde[8]. The resulting antibody has been employed for the detection of breast cancer cells. Other analytes have been sensed using biomolecules conjugate to nanozymes using this strategy, such as *Mycoplasma pneumoniae*[10] or Human chorionic gonadotropin[11]. The EDC/NHS enables amide bond between amino and carboxyl groups. For example, a MOF has been conjugated to a secondary antibody by the EDC/NHS coupling[12]. The probe generated was used for detecting PSA. Other nanozymes such as $Cu(OH)_2$[13] and $Fe_3O_4$ NPs[14] have been linked to biomolecules using the EDC/NHS coupling, for the sensing of cyanobacterial hepatotoxin microcystin and *Listeria monocytogenes*, respectively. The streptavidin-biotin non-covalent strong bonding has been also used with the purpose of bioconjugation of nanozymes to antibodies. For example, 8-hydroxy-2'-deoxyguanosine and PSA were detected using biotinylated antibody and streptavidin-coated AuNPs[15]. Also, other nanozymes such as, $Fe_3O_4$ NPs[16] and $MnO_2$ nanosheets[17] have been bioconjugate to aptamers or DNA, using this strategy for the sensing of *Streptococcus mutans* and Ochratoxin A, respectively.

The different reactivities of nanozymes and antibodies with crosslinkers result in the formation of not only bioconjugates, antibody-nanozyme but also in the formation of nanozyme-nanozyme and antibody-antibody conjugates. The former causes high background signals and low precision due to nonspecific absorption and the latter are not use at all for detection of analytes. With the biotin-streptavidin strategy the amplification of signals is achieved by introduction of many biotin residues into antibody molecules and subsequent binding of avidin linked to nanozymes. However, nonspecific binding is also amplified.

The introduction of NCs with enzyme-like properties in the structure of antibodies avoid the labelling drawbacks linked to the use of enzymes and nanozymes as labels. In the

previous chapter three different NCs were described. Two of them were bimetallic NCs and the other ones were CdS semiconductor NCs. The former exhibit peroxidase-like activity and the latter photocatalytic properties triggered by the exposure to UV-light. The use of a source of light made the photocatalytic method technically more complicate. The same intensity of light must reach all wells, so the position of the microplate with respect to the UV-light source is critical for the reproducibility of the method. The results obtained for direct immunoassay in Chapter 3 reveal that greater relative standard deviations were achieved with CdS NCs-IgG than with the bimetallic ones. Due to better sensitivity for immobilized BSA, the lower standard deviations and the possibility to perform the assay without the source of the UV-light, antibodies wearing bimetallic NCs are used in this chapter to set up the methodology of sandwich immunoassay. The possibilities of CdS NCs-IgG in immunoassay will be discussed in the final part of this chapter.

## 2. Experimental section

### 2.1. Chemicals and materials

Silver nitrate ($AgNO_3$), chloroauric acid ($HAuCl_4$), potassium tetracholoroplatinate ($K_2PtCl_4$), BSA, polyclonal anti-BSA IgG (developed in rabbit), casein, TMB, TMB liquid substrate system for ELISA, sodium borohydride ($NaBH_4$), PBS, sodium phosphate monobasic ($NaH_2PO_4$), TWEEN and other chemicals were supplied by Sigma-Aldrich. Hydrogen peroxide ($H_2O_2$) was supplied by Panreac. Polyclonal anti-BSA IgG (developed in chicken) was purchased from Abyntek. HRP conjugation kit was obtained from Abcam.

### 2.2. Methods

Labelling of Anti-BSA IgG with HRP

For the labelling of Anti-BSA IgG (from rabbit) with HRP a kit purchased from Abcam was used. Polyclonal Anti-BSA IgG from rabbit (100 µL, 4 mg/mL) was mixed with the modifier reagent (10 µL). Then, this solution was added directly onto the lyophilized HRP and resuspended. The reaction mixture is allowed to react for 3 hours. After incubating,

the quencher reagent (10 µL) was added. The conjugate does not require further purification and can be used after 30 minutes.

Procedure for a direct sandwich immunoassay for BSA based on the catalytic activity of Ag/Pt NCs Anti-BSA IgG and Au/Pt NCs Anti-BSA IgG

The immunoassay was carried out in a 96-well plate Nunc MaxiSorp. Capture antibody from chicken (100 µL, 10 µg/mL) was immobilised on the surface of a microplate (2 hours, 37 °C) next the surface was blocked with casein (100 µL, 20.5 mg/mL) and incubated (ON, 4 °C). The target analyte at different concentrations was added in different wells and incubated (1 h, RT). Upon incubation, Ag/Pt NCs-IgG or Au/Pt NCs-IgG (from rabbit) (100 µL, 33 µg/mL) was added and incubated (1 h, RT). 100 µL of TMB (200 µM) and $H_2O_2$ (125 mM) solution were added to the microplate in the case of Ag/Pt NCs-IgG and 100 µL of TMB (200 µM) and $H_2O_2$ (250 mM) in the case of Au/Pt NCs-IgG. The change absorbance of the oxidised TMB at 652 nm was measured on the standard plate reader during 4 min. The spectra were performed on a Varioskan Flash microplate reader (Thermo Scientific). The system was controlled by SkanIt Software 2.4.3. for Varioskan Flash. After each step the wells were washed three times with PBST (100 µL).

Procedure for a direct sandwich ELISA for BSA based on the catalytic activity of Anti-BSA IgG/HRP (from rabbit)

The immunoassay was carried out in a 96-well plate Nunc MaxiSorp. Capture antibody from chicken (100 µL, 10 µg/mL) was immobilised on the surface of a microplate (2 h, 37 °C) next the surface was blocked with casein (100 µL, 20.5 mg/mL) and incubated (ON, 4 °C). The target analyte was added at different concentrations in different wells and incubated (1 h, RT). 100 µL of antibody for BSA (from rabbit) labelled with HRP (using the kit of Abcam for the labelling of antibodies with HRP) at different concentrations was added and incubated (1 h, RT). Finally, 100 µL of TMB liquid substrate system for ELISA was added. Then the absorbance of the oxidised TMB was measured on the standard plate reader. After each step the wells were washed three times with PBST (100 µL).

## 3. Results and discussion

The performance of a novel direct sandwich immunoassay carried out using as detection antibody, IgG carrying bimetallic NCs was compared with a conventional direct sandwich ELISA performed using an IgG labelled with HRP as detection antibody. First, we obtained the calibration curve from the direct sandwich immunoassay carried out using Au/Pt NCs Anti-BSA IgG and Ag/Pt NCs Anti-BSA IgG. Second, we studied the performance of the conventional direct sandwich immunoassay using an antibody labelled with HRP as a detection antibody. In the three assays the concentration of detection antibody was optimised in order to get the best sensitivity. To optimise the concentration of detection antibody in both immunoassays, first capture antibody was immobilised on the surface of the well and then the surface of the well was blocked with casein. After, the target analyte was added in a concentration of 0 and 200 ng/mL and finally different concentrations of detection antibody were added. The reaction rate of TMB oxidation was represented for the assays with and without the target analyte (Figure 1.A., Figure 2.A. and Figure 3.A.) and also the ratio of the readout signals for each Au/Pt NCs-IgG (Figure 1.B.), Ag/Pt NCs-IgG (Figure 2.B.) and IgG-HRP (Figure 3.B.) concentration.

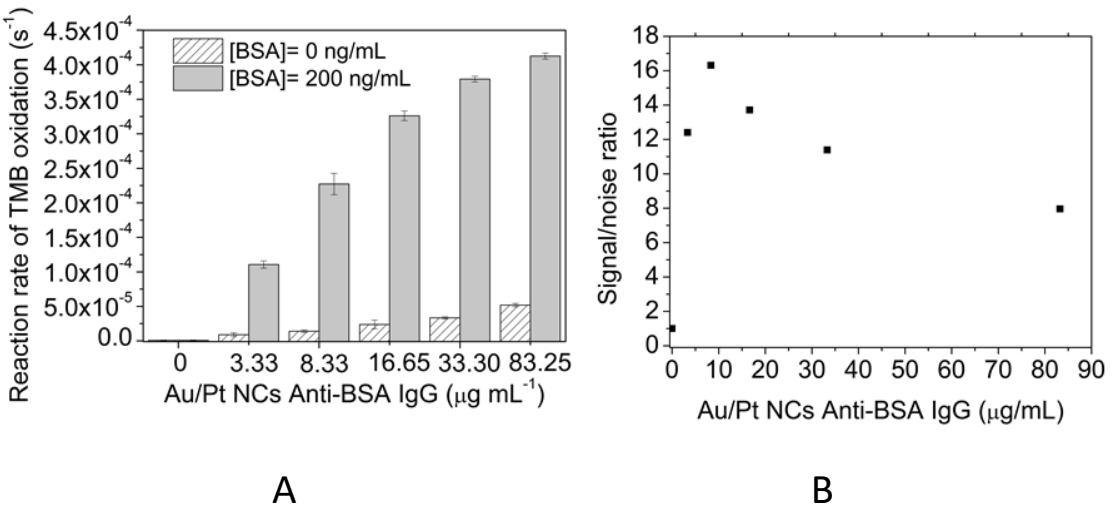


Figure 1. Reaction rate of TMB oxidation in the direct sandwich immunoassay performed with Au/Pt NCs Anti-BSA IgG as detection antibody with and without target analyte (A). The ratio of readout signals with and without the target analyte (B).

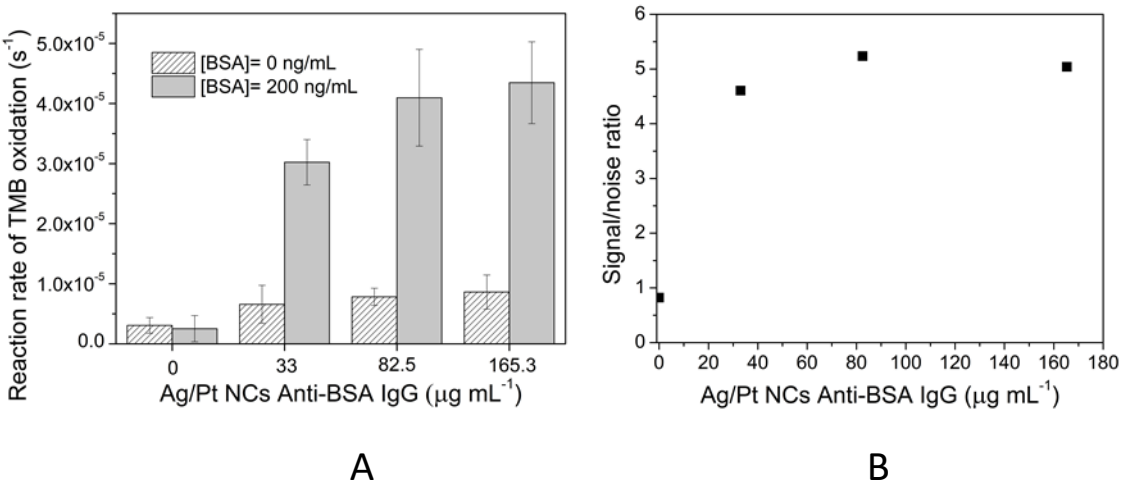


Figure 2. Reaction rate of TMB oxidation in the direct sandwich immunoassay performed with Ag/Pt NCs Anti-BSA IgG as detection antibody with and without target analyte (A). The ratio of readout signals with and without the target analyte (B).

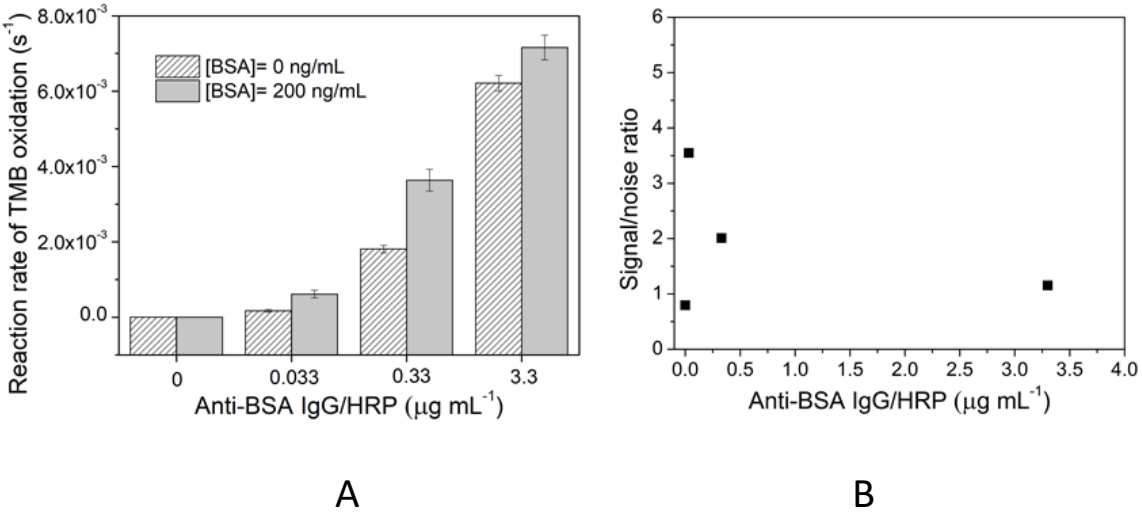


Figure 3. Reaction rate of TMB oxidation in the direct sandwich ELISA performed with IgG-HRP as detection antibody with and without target analyte (A). The ratio of readout signals measured with and without the target analyte (B).

The highest ratio between two signals observed with and without the target analyte was 16.31 for the system using Au/Pt NCs-IgG as detection antibody (Figure 1.B.) , 5.23 for the system using Ag/Pt NCs-IgG (Figure 2.B.) and 3.54 for the system using IgG-HRP as detection antibody (Figure 3.B.). After optimization of the experimental conditions in terms of detection antibody concentrations, the effect of various concentrations of the analyte on the read-out signals was studied.

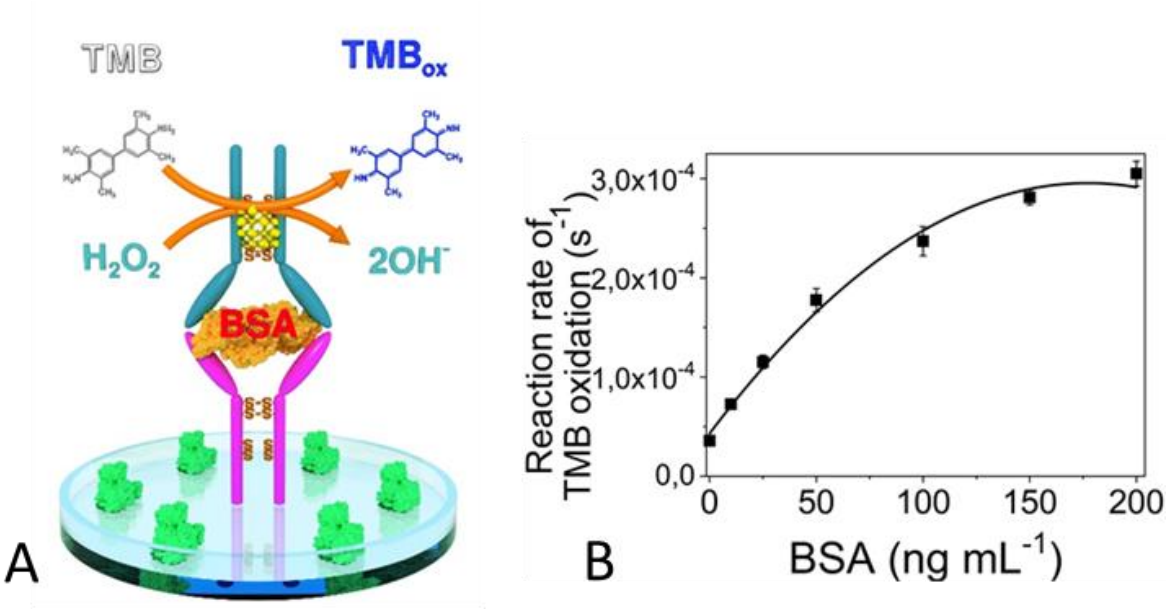


Figure 4. Direct sandwich immunoassay for BSA quantification using Au/Pt NCs Anti-BSA IgG as detection antibody (A). Calibration curve of the direct sandwich immunoassay system based on Au/Pt NCs Anti-BSA IgG using BSA as a target analyte (B).

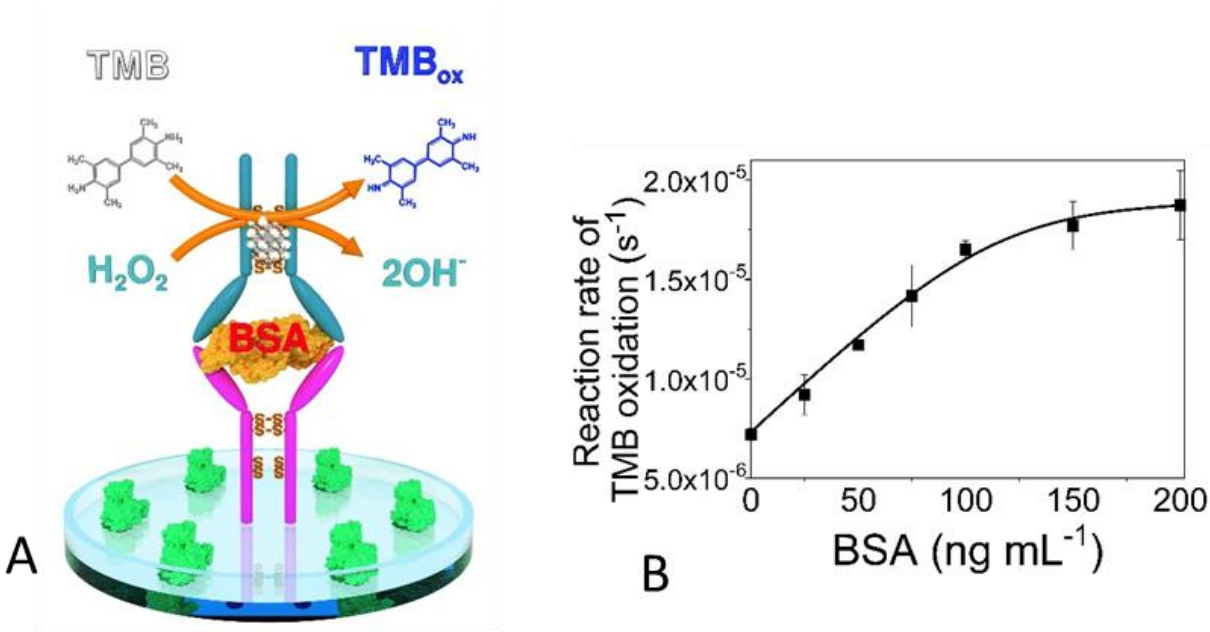


Figure 5. Direct sandwich immunoassay for BSA quantification using Ag/Pt NCs Anti-BSA IgG as detection antibody (A). Calibration curve of the direct sandwich immunoassay system based on Ag/Pt NCs Anti-BSA IgG using BSA as a target analyte (B).

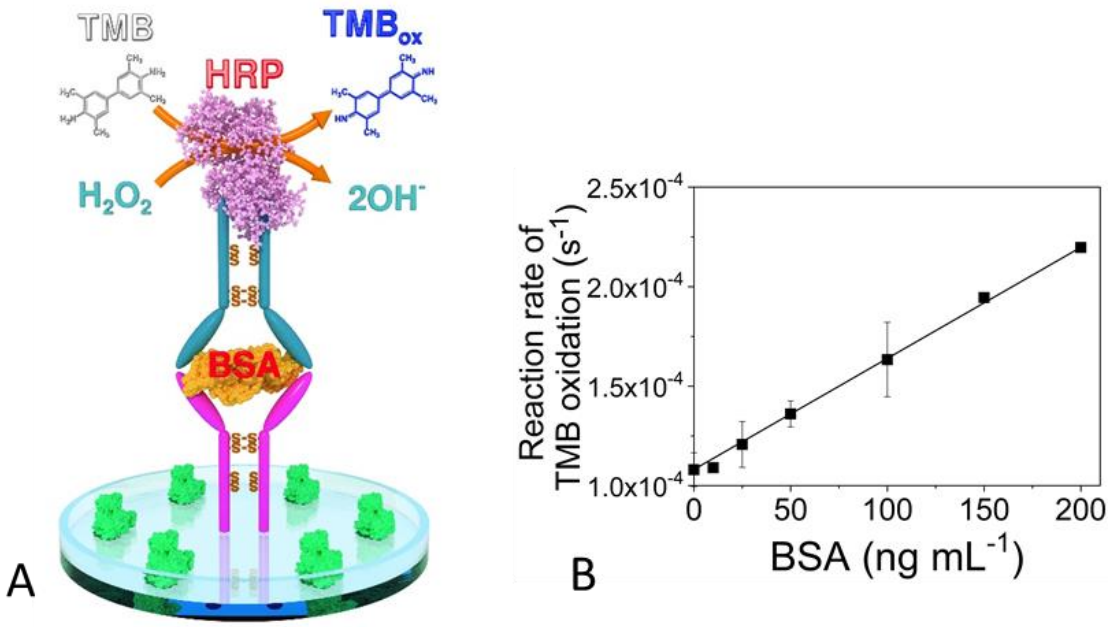


Figure 6. Direct sandwich ELISA for BSA quantification using Anti-BSA IgG-HRP as detection antibody (A). Calibration curve of the direct sandwich ELISA system based on Anti-BSA IgG-HRP using BSA as a target analyte (B).

In Figure 4.B., Figure 5.B. and Figure 6.B. the calibration curves for the three systems are shown. The limit of detection (LOD) was calculated like three times of standard deviation of negative control divided by the slope of regression line. A LOD of 0.93 ng/mL was achieved for the system using Au/Pt NCs-IgG, 10.4 ng/mL with Ag/Pt NCs-IgG and 52.03 ng/mL with IgG-HRP. The LOD was increased up to 5 times using Ag/Pt NCs and it was 56 times greater with Au/Pt NCs-IgG in comparison with IgG-HRP. In the three cases, capture and detection antibodies were the same. In case of the immunoassays using the IgG carrying bimetallic NCs, the antibody used for its preparation was the same as the antibody employed for the labelling with HRP. This means that the comparison between the three different assays was performed under the most similar conditions. To perform the direct sandwich ELISA based on IgG-HRP, the commercially available kit from Abcam, specifically designed and optimized for conjugation of antibodies with HRP was employed for the bioconjugation. Nevertheless, the assay based on "Abcam modified" antibodies showed a lower signal-to-noise ratio than that or our assays employing bimetallic NCs. Such a difference between LODs shown by three immunoassays can be explained by lower nonspecific adsorption of Au/Pt NCs-IgG and Ag/Pt NCs-IgG. The

labelling of IgG with HRP by the cross-linking reaction leads to the formations of by-products prone to nonspecific adsorption and consequently to an increase in the background signal. The best performance obtained with Au/Pt NCs-IgG than with Ag/Pt NCs-IgG is due to the higher affinity towards TMB of Au/Pt NCs-IgG discussed in Chapter 3.

## 4. Conclusions

After the metallization of bimetallic NCs inside a polyclonal anti-BSA IgG, the antibody activity remains intact and the NCs exhibit high peroxidase-like properties. Both characteristics make Au/Pt NCs-IgG and Ag/Pt NCs-IgG potential candidates to act as a detection antibody in a colorimetric sandwich-type immunosensor. The antibody carrying NCs act as a probe and incorporate the recognition component and the transduce component. The inclusion of the NCs inside the antibodies address the drawbacks related with the tethering of enzymes and NPs to antibodies and results in a new efficient strategy for immunoassays. By using antibody carrying bimetallic NCs, for the detection of BSA, the LOD was improved by 56 times in comparison with a conventional method that employs the same detection antibody but labelled with HRP. The increase in the sensitivity of the method by employing NCs-IgG as detection antibody can be explained by the formation of homopolymers during the IgG-HRP bioconjugation, which causes an increase in the background signal due to non-specific absorption. By using bimetallic NCs-IgG the conjugation step is no longer necessary, since the NCs are formed in the structure of the antibody.

## References

1. Hempen, C. & Karst, U. Labeling strategies for bioassays. *Anal. Bioanal. Chem.* **384**, 572–583 (2006).
2. Kabir, M. A., Zilouchian, H., Sher, M. & Asghar, W. Development of a flow-free automated colorimetric detection assay integrated with smartphone for Zika NS1. *Diagnostics* **10**, 1–11 (2020).
3. Li, F. *et al.* Smartphone assisted immunodetection of HIV p24 antigen using reusable, centrifugal microchannel array chip. *Talanta* **203**, 83–89 (2019).
4. Feng, J., Huang, P. & Wu, F. Gold–platinum bimetallic nanoclusters with enhanced peroxidase-like activity and their integrated agarose hydrogel-based sensing platform for the colorimetric analysis of glucose levels in serum. **142**, 4106–4115

(2017).
5. Niu, X., Cheng, N., Ruan, X., Du, D. & Lin, Y. Review—Nanozyme-Based Immunosensors and Immunoassays: Recent Developments and Future Trends. *J. Electrochem. Soc* **167**, 037508 (2020).
6. Tao, X., Wang, X., Liu, B. & Liu, J. Conjugation of antibodies and aptamers on nanozymes for developing biosensors. *Biosens. Bioelectron.* **168**, 112537 (2020).
7. Li, W. *et al.* High-activity Fe3O4 nanozyme as signal amplifier: A simple, low-cost but efficient strategy for ultrasensitive photoelectrochemical immunoassay. *Biosens. Bioelectron.* **127**, 64–71 (2019).
8. Woo, M. A. *et al.* A novel colorimetric immunoassay utilizing the peroxidase mimicking activity of magnetic nanoparticles. *Int. J. Mol. Sci.* **14**, 9999–10014 (2013).
9. Chen, G. *et al.* Colorimetric bio-barcode immunoassay for parathion based on amplification by using platinum nanoparticles acting as a nanozyme. *Microchim. Acta* **186**, (2019).
10. Yang, M. *et al.* A sensitive and rapid immunoassay for mycoplasma pneumonia based on Fe3O4 nanoparticles. *Mater. Lett.* **137**, 113–116 (2014).
11. Yang, M. *et al.* Peroxidase-like activity of amino-functionalized magnetic nanoparticles and their applications in immunoassay. *J. Colloid Interface Sci.* **405**, 291–295 (2013).
12. Khoshfetrat, S. M., Khoshsafar, H., Afkhami, A., Mehrgardi, M. A. & Bagheri, H. Enhanced Visual Wireless Electrochemiluminescence Immunosensing of Prostate-Specific Antigen Based on the Luminol Loaded into MIL-53(Fe)-NH 2 Accelerator and Hydrogen Evolution Reaction Mediation. *Anal. Chem.* **91**, 6383–6390 (2019).
13. Liu, W. *et al.* Double-integrated mimic enzymes for the visual screening of Microcystin-LR: Copper hydroxide nanozyme and G-quadruplex/hemin DNAzyme. *Anal. Chim. Acta* **1054**, 128–136 (2019).
14. Zhang, L. *et al.* Rapid and visual detection of Listeria monocytogenes based on nanoparticle cluster catalyzed signal amplification. *Biosens. Bioelectron.* **86**, 1–7 (2016).
15. Zhu, X. *et al.* Using a glucose meter to quantitatively detect disease biomarkers through a universal nanozyme integrated lateral fluidic sensing platform. *Biosens. Bioelectron.* **126**, 690–696 (2019).
16. Zhang, L. *et al.* Engineering DNA-Nanozyme Interfaces for Rapid Detection of Dental Bacteria. *ACS Appl. Mater. Interfaces* **11**, 30640–30647 (2019).
17. Tian, F., Zhou, J., Jiao, B. & He, Y. Nanozyme-based cascade colorimetric aptasensor for amplified detection of ochratoxin A. *Nanoscale* **11**, 9547–9555 (2019).

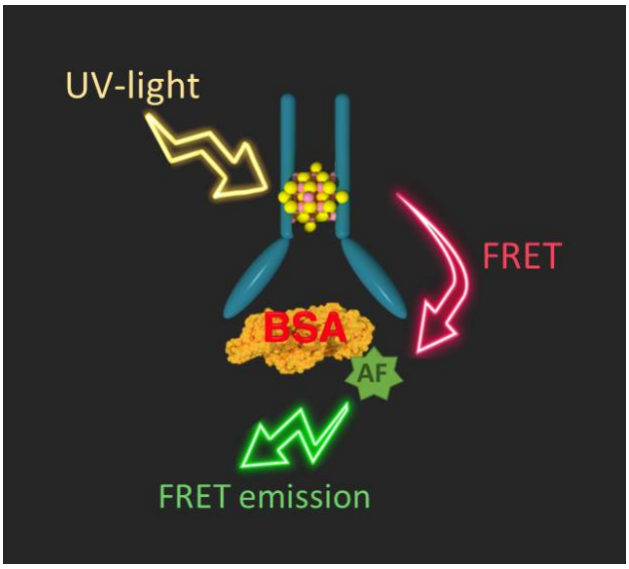


## First steps towards the development of a FRET-based homogeneous competitive immunoassay using antibody-protected CdS NCs.

In this chapter are reported the first steps towards the development of a competitive immunoassay based on FRET. The method is based on the measurement of FRET that occurs from antibody carrying fluorescent semiconductor CdS NCs to a commercial fluorophore labeled to target analyte. As a probe of concept BSA and corresponding antibody were employed. The immunoreaction between Anti-BSA IgG carrying CdS NCs and BSA labeled with Alexa Fluor 647 (acting as receptor) brings the fluorophore in close proximity to the NCs (acting as the donor) and this causes FRET to occur upon photoexcitation of the CdS NCs. During the detection event BSA labeled with AF 647 is displaced by higher affinity target analyte, creating a detectable FRET decrease due to the distancing of the fluorophore from the NCs. This homogeneous competitive detection scheme is simple and efficient, and it does not require separation steps and neither washing.

## 1. Introduction

Immunoassays are based on specific interactions between antibodies and antigens that permit the precise detection of analytes. The most used assays in biosensing and diagnostic are the heterogeneous assays ELISAs. These assays need various incubation and washing steps making them time consuming. As opposed to homogeneous assays, that are performed directly in solution without washing steps and it handle do not need expertise by the user. The development of homogenous assays based on FRET provides a single step, rapid and direct detection of analytes in a competitive and non-competitive manner[1]. FRET allows a non-radiative energy transfer from a donor to a fluorescent energy acceptor within a distance less than 10 nm. The absorption spectrum of the acceptor must overlap the fluorescence emission spectrum of the donor. Molecular binding events, such as those that take place in immunoassays between the antibody and target analyte, change the distance between the donor and the acceptor inducing FRET signals.

Organic dye molecules are traditional FRET fluorophore pairs. These dyes are characterized by closely spaced and broad absorption/emission profiles. For FRET applications these small Stokes shifts cause the direct excitation of the acceptor that difficult the analysis[2]. There is a need of new materials to overcome the deficiencies of organic fluorophores. Semiconductor QDs are one of the most promising nanomaterials for fluorescence-based biosensing and can provide significant advantages concerning multiplexing and sensitivity. Compared to classical organic fluorophores, QDs have broad excitation bands with increasing excitation coefficients from the emission wavelength down to the UV. This offers the possibility of exciting QDs at almost any wavelength with effective Stokes shift. QDs have also high photostability and high fluorescence quantum yields[3]. They have been widely employed in competitive immunoassays based on FRET from QDs labeled antibodies to organic fluorophores. For example, for the detection of the mycotoxin Ochratoxin (OTA). The energy transfer occurs from CdTe QDs covered with anti-OTA antibody to the dye Rho123[4].

Despite the advantages mentioned above and the superior optical properties in comparison with organic dyes, QDs have still not become standard labels for FRET applications. The main drawback remains a conjugation method for the QDs to

biorecognition element that allows taking advantage of the optical properties of the QDs and the functionality of the probe[5]. Also, the use of QDs is still a challenge in terms of solubility. Furthermore, the optimal FRET distance between fluorophores for the signal development is between 2 and 6 nm[6], in some cases the large dimensions of the bioconjugates can restricted the use of QDs, due to particle size and steric hindrance[5].

Antibody fragments such as Fab or $F(ab)_2$ have been employed to overcome the size limitation of full-length antibodies. This technique has been employed for the detection of morphine in saliva samples[6]. An antibody fragment specific for the immune complex composed by morphine and anti-morphine Fab fragment was selected from an antibody phage display library. Both antibody fragments were labeled with organic dyes and incubated with the saliva samples containing morphine. The detection is performed in a non-competitive mode. The presence of the analyte gets close the fluorophores and FRET emission takes place. Fab fragments exhibit a size smaller than 5 nm allowing the development of sensitive immunoassays for small analytes. The use of antibody fragments in FRET immunoassays has been employed also for the detection of tetrahydrocannabinol (THC) from saliva samples [7], mycotoxins from wheat extracts [8] and cyanobacterial microcystins and nodularins from water samples[9].

QDs are becoming popular as strong energy acceptor, instead of donor, in combination with lanthanide (europium, terbium) complexes as long-decay-time donors[10]. The use of QDs as FRET acceptors in conjunction with organic dyes has been limited due to difficulties isolating QDs fluorescence emission because of FRET interactions caused by large extinction coefficients and broad QD absorption[11]. Also, the typical QD photolomuniscence decay time is between 10-100 ns that is higher that the decay time of most of organic dye donors (less than 5 ns). Thus, QDs are rarely in their lowest energy state at the same time that organic fluorophores are in their excited state. In the case of lanthanide complexes their decay time, between 0.1-1 ms, makes possible that the QDs come to their ground state while the lanthanide complexes remains in their excited state[12]. Taking advantage of both, the use of antibody fragments and lanthanide-QDs pairs, it is possible to find in the literature a highly sensitive assay for prostate specific antigen (PSA) quantification. The analysis of the photophysical parameters of FRET components and the effect of the size of the antibody used reveal that the highest assay

sensitivity results with the Fab fragments conjugated with QDs and Terbium in comparison to the whole antibody[13].

In this work it is proposed another strategy to overcome the drawbacks above mentioned related with the use of QDs, the employment of fluorescent CdS NCs synthesized using antibodies as scaffold as energy donor in a competitive immunoassay based on FRET. With its use the conjugation step it is no longer necessary since the NCs are embedded in the antibody structure. In addition, the dimensions of the biorecognition system and the FRET distance are reduced due to the nanometric size of the atomic clusters and its position in the hinge region of the antibody.

## 2. Experimental section

### 2.1. Chemicals and materials

Cadmium nitrate ($CdNO_3$), sodium sulfide ($Na_2S$), BSA, polyclonal anti-BSA IgG (developed in rabbit), phosphate buffer saline (pH 7.4) (PBS) and other chemicals were supplied by Sigma-Aldrich. Bovine Serum Albumine conjugate with Alexa Fluor 647 (BSA-$AF_{647}$) was purchased from ThermoFisher Scientific.

### 2.2. Characterization of materials

The fluorescence spectra were performed on a Varioskan Flash microplate reader (Thermo Scientific) at room temperature. The system was controlled by SkanIt Software 2.4.3. for Varioskan Flash. The measurements were carried out using black 96-wells microtiter plates.

The 3D fluorescence emission spectra were recorded with a Perkin Elmer LS 55 fluorescence spectrometer. The emission was recorded from 300 nm to 750 nm with a scan speed of 250 nm/min and an excitation and emission slit of 5 nm. The excitation started at 300 nm and 80 scans were performed with an excitation increment of 5 nm. The measurements were carried out using a 1 mL quartz cuvette with 4 polished windows.

## 2.3. Methods

Procedure for FRET between CdS NCs-IgG and BSA-$AF_{647}$

For the evaluation of the FRET from CdS NCs-IgG to BSA-$AF_{647}$, some reaction mixtures in PBS were prepared. After incubating the reaction for 2 minutes to ensure the formation of the immuno-complex of the labeled BSA and the CdS NCs-IgG, the samples were excited at 315 nm. The emission spectra were recorded in a range from 450 to 700 nm. The experiments were performed in black 96-wells microtiter plates with a final volume of 100 µL. To evaluate the effect on FRET of increasing concentration of the BSA-$AF_{647}$, different concentrations of this reagent were added, while the CdS NCs-IgG concentration was maintained constant to 0.5 mg/mL.

Procedure for a competitive immunoassay based on FRET for BSA detection

To evaluate the ability of the system to detect BSA, a stock solution of 0.1 mg/mL was prepared and different concentrations were added to a reaction mixture containing fixed concentrations of CdS NCs-IgG and BSA-$AF_{647}$. Emission spectra of the samples were recorded after incubating the reaction mixture for 2 minutes, at the same conditions above mentioned.

# 3. Results and discussion

## 3.1. Improvement of the synthesis of CdS NCs-IgG

In Chapter 3 the synthesis of fluorescent NCs composed by CdS using Anti-BSA IgG as scaffold was described. In this chapter some parameters of the synthesis were changed to obtained NCs with higher fluorescence intensity. As described in Chapter 3, 2.5 µL of $CdNO_3$ were added to an Anti-BSA antibody solution (100 µL, 1 mg/mL). The mixture was stirred for 15 min at RT. Then, 2.5 µL $Na_2S$ were added dropwise. Different concentrations of $CdNO_3$ and $Na_2S$ were tested to obtain brighter NCs. The final concentration of $CdNO_3$ and $Na_2S$ employed for each synthesis are showed in Table 1.

Table 1. Different concentration of $CdNO_3$ and $Na_2S$ employed for each synthesis.

| Synthesis | $CdNO_3$ (M) | $Na_2S$ (M) |
|---|---|---|
| 1 | 0.01 | 0.005 |
| 2 | 0.025 | 0.005 |
| 3 | 0.05 | 0.005 |
| 4 | 0.01 | 0.01 |
| 5 | 0.025 | 0.01 |
| 6 | 0.05 | 0.01 |
| 7 | 0.01 | 0.025 |
| 8 | 0.025 | 0.025 |
| 9 | 0.05 | 0.025 |

The fluorescent properties of the CdS NCs-IgG were evaluated after the synthesis. In Figure 1. the fluorescence emission spectra at the maximum excitation wavelength (315 nm) is shown for each synthesis. The maximum emission peak and the fluorescence intensity can be tuned by changing the precursor concentrations. The ability of tuning the emission wavelength of semiconductor nanomaterials, such as QDs, has been already demonstrated. For large number of atoms, many wave functions are allowed and there is almost no difference in their energies generating a bulk band structure. When the crystal becomes smaller not all the wave functions satisfy the constraints this causes discrete quantum confined states with a band gap that increases with decreasing crystal size. This effect has been observed for CdSe QDs. The band gap can be tuned from 1.9 to 2.8 eV and the fluorescence emission from 650 to 450 nm as the QD diameter decreases from 7 nm to 2 nm[14]. A similar effect was observed by adjusting the stoichiometry of ZnSe/ZnS QDs. The emission wavelength can be tuned in the range of 390-435 nm[15]. The same effect was also observed for CdSe/CdS[16] [17] and $CuInS_2$/ZnS[18] QDs.

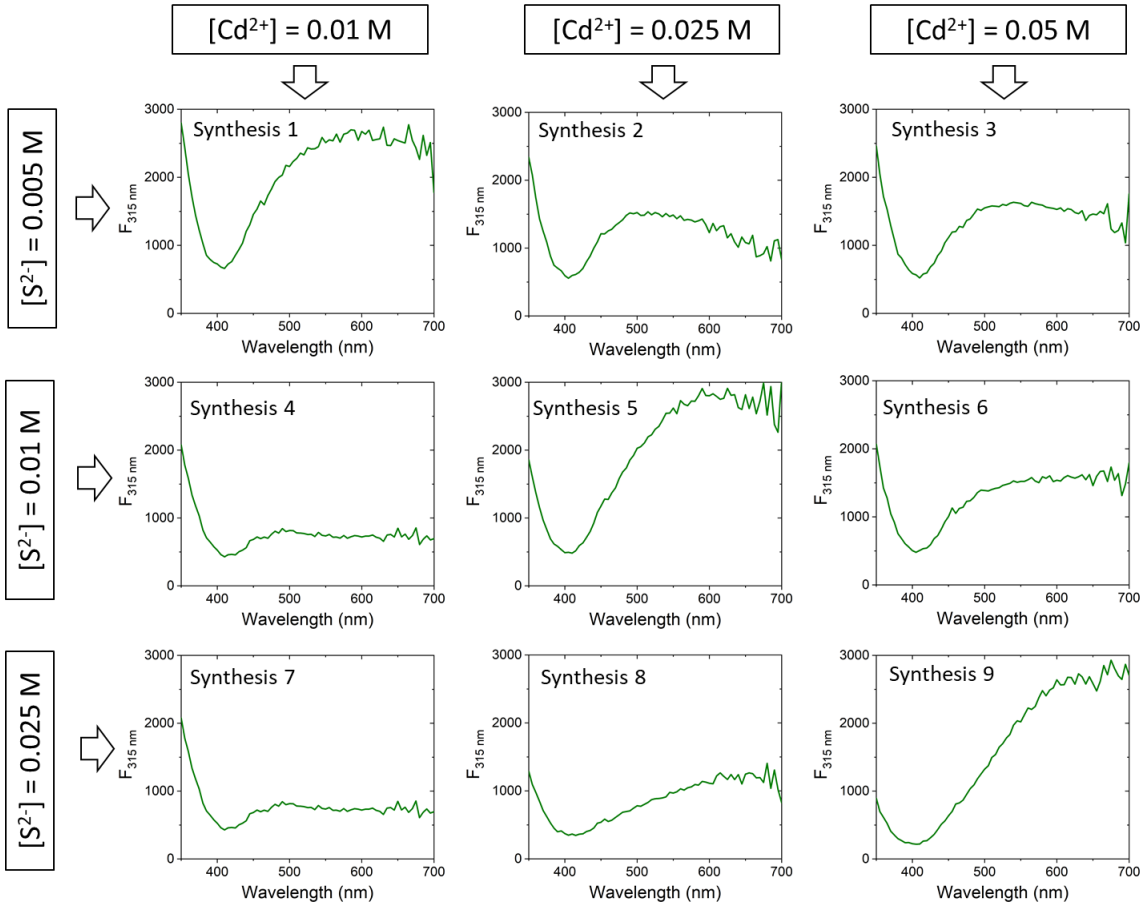


Figure 1. Fluorescence emission spectra of the different CdS NCs-IgG synthesis ($\lambda_{ex}$ = 315 nm).

Here, the conditions of synthesis 5 were chosen as the optimal ones because the NCs obtained exhibit the higher fluorescence at 650 nm (the maximum absorption wavelength of $AF_{647}$). Thus, further experiments were carried out using the CdS NCs-IgG synthesized under these conditions.

The manufacturing process has changed and to probe that the antibody presence is mandatory for the formation of the NCs, the next experiment was performed. The synthesis of CdS NCs-IgG was carried out as explained in the experiment above with and without the anti-BSA IgG. Finally, the fluorescence emission spectra of both syntheses were measured at 315 nm (Figure 2.). The CdS NCs-IgG showed the predictable fluorescent emission (orange line). However, the synthesis carried out without the IgG (green line) just exhibit a residual fluorescence emission. These results suggest that the presence of the antibody is needed to obtain fluorescent CdS NCs. It is required the presence of a capping agent that act as scaffold for the NCs formation. In this case the antibody is the scaffold. In the absence of the protein the NCs cannot growth and

therefore no fluorescence was found in the sample. This result also guarantees the NCs formation in the IgG structure and that there are not NCs outside the protein.

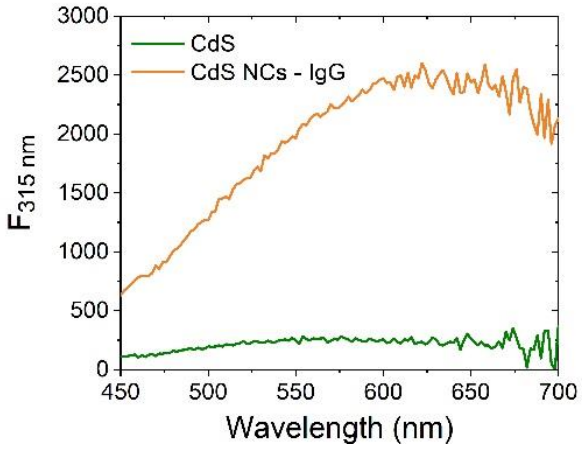


Figure 2. Fluorescence emission spectra of a CdS solution in water (orange) and CdS NCs-IgG ($\lambda_{ex}$ = 315 nm).

## 3.2. FRET between CdSNCs-IgG and BSA-$AF_{647}$

AF are highly fluorescent commercially available compounds with different excitation and emission wavelengths and they are widely used as fluorescent label in FRET assays[19, 20]. The excitation and emission spectra of BSA-$AF_{647}$ is showed in Figure 3. This compound exhibits the maximum fluorescence emission at 675 nm at an excitation wavelength of 650 nm. It was noted that the fluorescence spectrum of CdS NCs-IgG overlaps with the absorption spectrum of $AF_{647}$, which indicates that they are a good FRET donor/acceptor pair. Thus, $AF_{647}$ was selected as the acceptor to label BSA and CdS NCs-IgG were used as FRET donor.

The principle of FRET from CdS NCs-IgG to BSA-$AF_{647}$ is illustrated in Figure 4.

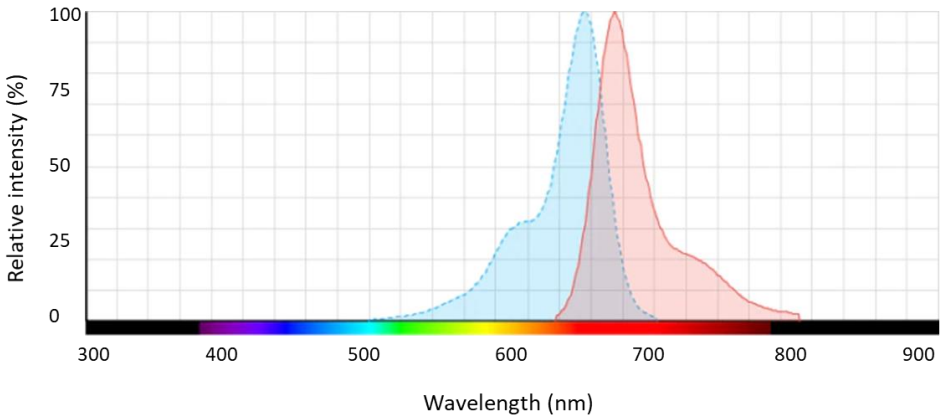


Figure 3. BSA-$AF_{647}$ excitation spectrum ($\lambda_{em}$ = 675 nm) (blue) and emission spectrum ($\lambda_{ex}$ = 650 nm)

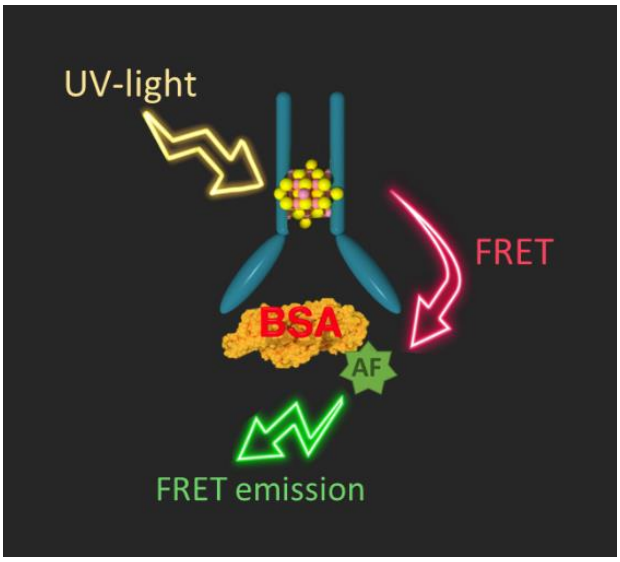


Figure 4. Scheme of FRET transmission from CdS NCs-IgG to BSA labeled with $AF_{647}$.

BSA-$AF_{647}$ was incubated with a limited amount of CdS NCs-IgG to generate the antibody-antigen immunocomplex. Due to the specific interaction between the anti-BSA antibody and corresponding antigen, CdS NCs-IgG (energy donor) was placed very close to the BSA-$AF_{647}$ (energy acceptor) in the immunocomplex, allowing FRET between them. When the system is irradiated at the excitation wavelength of the NCs (315 nm), the fluorescence intensity of the CdS NCs-IgG should decrease gradually with increasing BSA-$AF_{647}$ concentrations, because of the energy transfer from de NCs to the fluorophore. At the same time an increase on the fluorescence emission at 675 nm

should be observed with increasing BSA-$AF_{647}$ concentration, because the NCs exhibit fluorescence emission at the excitation wavelength of the fluorophore (650 nm).

In a first experiment performed to produce FRET from the CdS NCs-IgG to BSA-$AF_{647}$, both reagents were employed at equimolar concentration, with the purpose of taking up most of the available binding sites of the antibody. In Figure 5. it is showed the fluorescence emission spectra of a system containing CdS NCs-IgG and BSA-$AF_{647}$ (green line), another system that only contains CdS NCs-IgG (purple line) and a last one with only BSA-$AF_{647}$ (orange line).

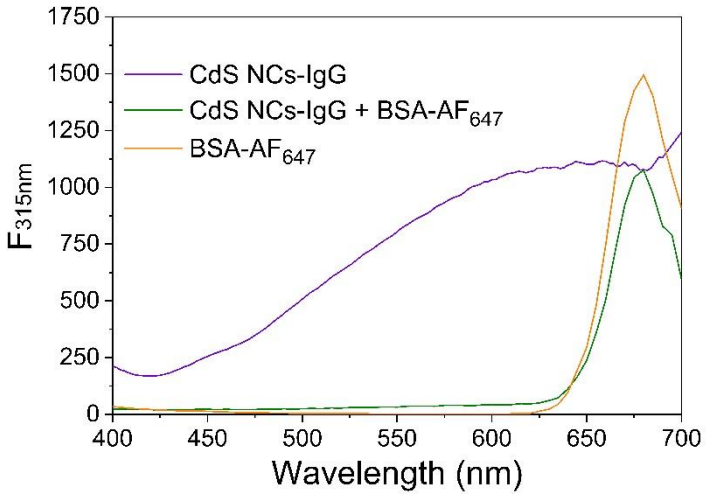


Figure 5. Fluorescence emission spectrum of a system containing only CdS NCs-IgG (purple line), CdS NCs-IgG and BSA-$AF_{647}$ (green line) and only BSA-$AF_{647}$ (orange line) ($\lambda_{ex}$=315 nm).

The three systems were excited at a wavelength of 315 nm (the excitation wavelength of the CdS NCs-IgG). The fluorescence spectrum of the CdS NCs-IgG showed the typical fluorescence emission with a broad peak with a maximum emission at 650 nm (purple line). The system containing both CdS NCs-IgG and the labelled antigen (green line), exhibit a peak at 675 nm (the emission wavelength of $AF_{647}$) and no fluorescence emission was found at 650 nm (the emission wavelength of the CdS NCs-IgG). At first it might seem that FRET is taking place between the CdS NCs-IgG and BSA-$AF_{647}$. Because the emission peak of the NCs completely disappears (650 nm) and it appears the emission peak of BSA-$AF_{647}$ (675 nm). However, when the emission spectrum of the system that only contains BSA-$AF_{647}$ is showed it was revealed that this compound exhibit intrinsic fluorescent at the excitation wavelength of the CdS NCs-IgG (315 nm).

Thus, by using BSA-$AF_{647}$ at the same molar concentration of CdS NCs-IgG it is not possible to see FRET emission of BSA-$AF_{647}$ due to its intrinsic fluorescence. The intrinsic emission at 675 nm of BSA-$AF_{647}$ when excited at 315 nm was unexpected.

To check whether this peak is part of the fluorescence spectrum or a Raman signal, several fluorescence spectrum of BSA-$AF_{647}$ were recorded at different excitation wavelengths. Fluorescence and Raman scattering are fundamentally different processes and respond in a different manner to changes in the excitation wavelength. The fluorescence emission is independent of the excitation wavelength and the spectrum will not shift if the excitation wavelength is changed. In contrast, Raman is a scattering phenomenon and the wavelength of the scattered photons are proportional to the wavelength of the excitation photons. As the wavelength of the excitation light increased the wavelength at which Raman scatter appears will also increase and this can be used to differentiate between Raman and fluorescence. Figure 6. shows the spectra of BSA-$AF_{647}$ measured at three different excitation wavelengths where it can be seen that the wavelength of the peak did not shift with excitation wavelength which reveals that the peak is not due to Raman scattering.

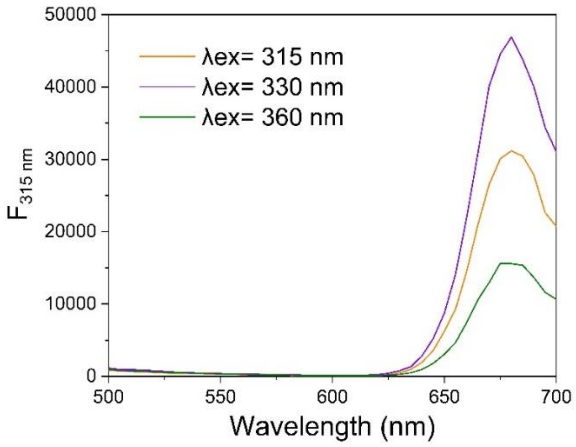


Figure 6. Fluorescence spectra of BSA-$AF_{647}$ at three different excitation wavelengths.

A 3D fluorescence spectrum was performed to obtain a spectral fingerprint of BSA-$AF_{647}$ (Figure 7.). The Signal 1 is due to elastic scattering or Rayleigh scattering. In this signal, the energy of the photon is conserved and the wavelength of the scattered light is therefore equal to the excitation light. The Signal 2 is the second harmonic and it is dependent on the excitation wavelength. The Signal 3 is due to the characteristic

fluorescence emission of $AF_{647}$ showing a maximum at 675 nm when excited at 650 nm. Finally, the Signal 4 is another fluorescence peak, that also appears at 675 nm like Signal 3 but with a weaker intensity. The signal 3 is the fluorescence signal found above in Figure 5. This signal appears when BSA-$AF_{647}$ is excited at 315 nm, the same excitation wavelength of NCs.

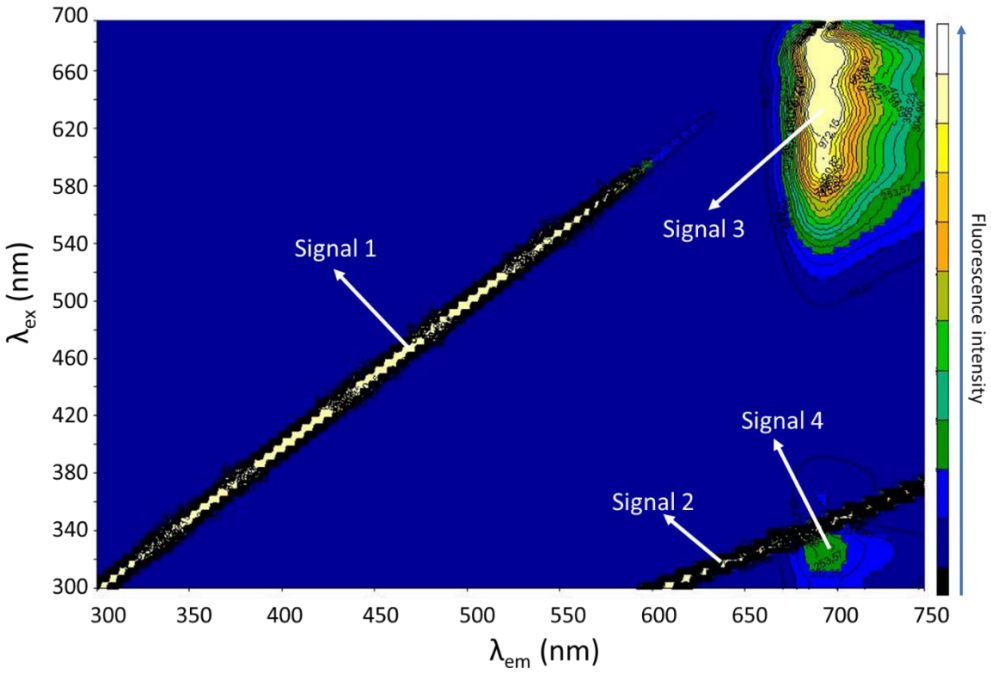


Figure 7. 3D fluorescence spectrum of BSA-$AF_{647}$.

After this result a lower BSA-$AF_{647}$ concentration was employed to reduce the emission at 675 nm due to the intrinsic fluorescence of this compound at an excitation wavelength of 315 nm and to favour the emission at 675 nm produced by FRET. Different concentrations of BSA-$AF_{647}$ ranging from 0 to 15 µg/mL were prepared and incubated with a fixed concentration of CdS NCs-IgG. In this case the BSA-$AF_{647}$ concentration was not equimolar to the CdS NCs-IgG, it was lower. As shown in Figure 8A. the fluorescence emission of CdS NCs-IgG decreased gradually with increasing BSA-$AF_{647}$ concentration at en excitation wavelength of 315 nm. On the other hand, the fluorescence emission of BSA-$AF_{647}$ (675 nm) increased due to FRET from CdS NCs-IgG. In order to assure that this fluorescence increase is due to FRET, the fluorescence emission spectra of different systems containing only BSA-$AF_{647}$ was measured (Figure 8B.).

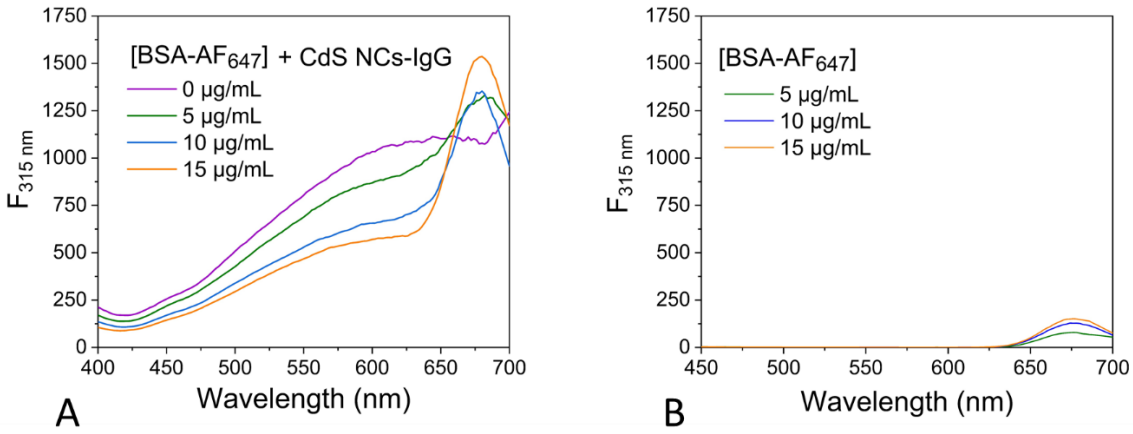


Figure 8. Fluorescence emission spectrum of a system containing a fixed concentration of CdS NCs-IgG and increasing concentrations of BSA- $AF_{647}$ (A). Fluorescence emission spectrum of increasing concentrations of BSA- $AF_{647}$ (B). ($\lambda_{ex}$=315 nm).

Just a residual fluorescence emission was obtained at 675 nm indicating that at those BSA-$AF_{647}$ concentrations there is not intrinsic fluorescence at an excitation wavelength of 315 nm. Thus, the fluorescence emission observed at 675 nm in Figure 7A. is due to FRET from the CdS NCs-IgG to BSA-$AF_{647}$.

### 3.3. FRET-based homogeneous competitive immunoassay for BSA detection

In this FRET-based homogeneous competitive immunoassay, the CdS NCs-IgG act as the donor and the acceptor is the antigen labeled with $AF_{647}$. The analyte is the unlabeled antigen. The extent of FRET decreases in the presence of the unlabeled antigen due to the higher affinity of the antibody for this one than for the labeled one. A scheme of the process is illustrated in Figure 9. On the one hand, the fluorescence intensity of the CdS NCs-IgG donor should increase with increasing concentration of the unlabeled antigen and by maintaining constant the concentration of the labeled antigen. On the other hand, the BSA-$AF_{647}$ fluorescence should decrease due to its displacement by BSA.

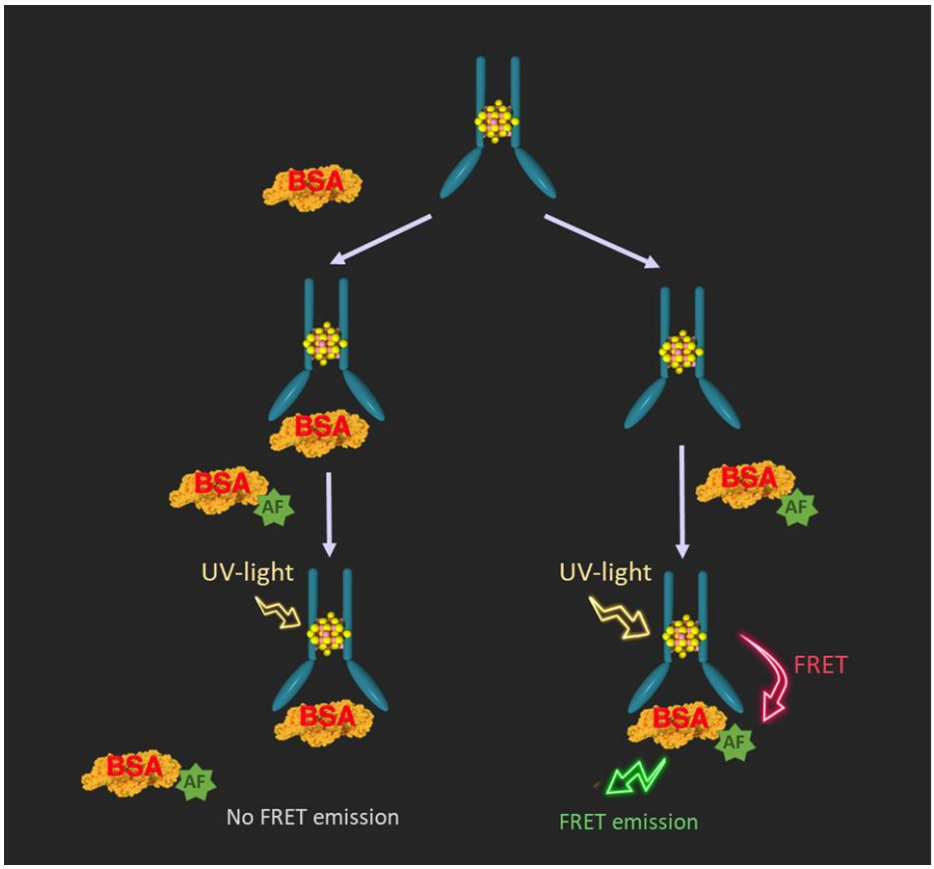


Figure 9. FRET-based homogeneous competitive immunoassay. The CdS NCs-IgG act as donor, the antigen is labeled with an acceptor molecule. The analyte is the unlabeled antigen. The extent of FRET decreases in the presence of the unlabeled antigen.

The ability of the immunoassay to detect and distinguish different target concentrations was assessed (Figure 10).

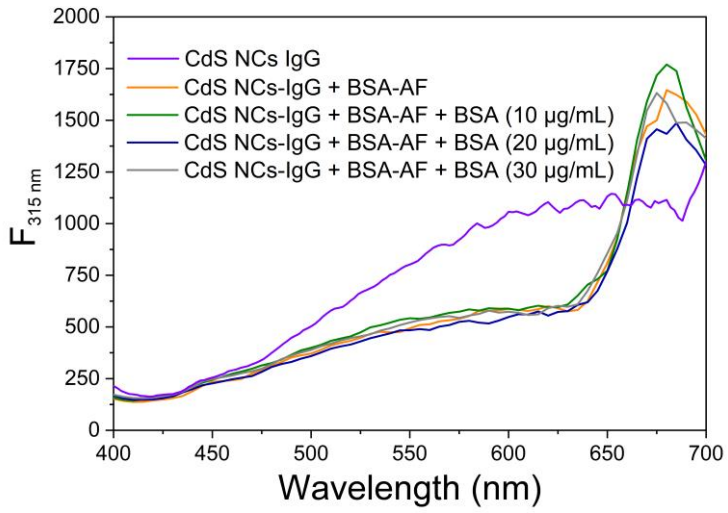


Figure 10. Fluorescence emission spectrum of a system containing a fixed concentration of CdS NCs-IgG and BSA-$AF_{647}$ with increasing concentrations of BSA ($\lambda_{ex}$=315 nm).

In the control only CdS NCs-IgG were added. Then different BSA concentrations were added to a solution containing constant concentrations of CdS NCs-IgG (0.5 mg/mL) and BSA-$AF_{647}$ (15 µg/mL). A decrease in the fluorescence at 675 nm was expected with increasing BSA concentrations, due to the displacement of the labeled antigen by the unlabeled one. However, the exposure of the system to different BSA concentrations did not produce any significant change in the fluorescence of the system. This result could be explained by the molar ratio of CdS NCs-IgG and BSA-$AF_{647}$ (referring to protein concentration in both cases). The concentration of CdS NCs-IgG in the system is 3.33 µM and the BSA-$AF_{647}$ is 0.22 µM. This means that the concentration of BSA-$AF_{647}$ is ≈ 15 times lower than the CdS NCs-IgG concentration. If it is assumed that two antigen molecules can bind to an antibody molecule, this means that every 30 available binding sites only one will be occupied with a BSA-$AF_{647}$ molecule. Thus, it is not possible to displace BSA-$AF_{647}$ by BSA because there are sufficient available binding sites and the competition did not occur. On the other hand, as it was showed, before it is not possible to increase the BSA-$AF_{647}$ concentration until the saturation of the binding sites. Thus, it is not possible to achieve a FRET-based homogeneous competitive immunoassay for BSA employing CdS NCs-IgG and BSA-$AF_{647}$.

## 4. Conclusions

The formation of the immunocomplex between the CdS NCs-IgG and BSA-$AF_{647}$ causes a change in the fluorescent properties of the NCs due to proximity effects. The fluorescence of the NCs decreases with increasing BSA-$AF_{647}$ concentrations because of the transfer of energy to the organic fluorophore. An increase in the fluorescence of BSA-$AF_{647}$ was also observed due also to FRET effects. If both compounds are employed at equimolar concentration, the unexpected intrinsic fluorescence of BSA-$AF_{647}$ at the excitation wavelength of the NCs covers up fluorescence emission due to FRET effects. Thus, the BSA-$AF_{647}$ concentration should be reduced to see a decrease in CdS NCs-IgG fluorescence and an increase in BSA-$AF_{647}$ fluorescence. At this molar ratio most of the binding sites of the antibody are free and thus when the unlabeled antigen was added, there is not a competition for the binding sites between the unlabeled and the labeled BSA and no changes in fluorescence took place. These results suggest that antibody

wearing fluorescent nanoclusters are promising materials to act as energy donor in FRET-based homogenous competitive immunoassays because it was possible to produce FRET between the NCs and BSA-$AF_{647}$. However, BSA-$AF_{647}$ is not an adequate candidate to act as fluorescence acceptor for a homogeneous competitive immunoassay for its intrinsic fluorescence emission at the excitation wavelength of the NCs (315 nm). As a future work other fluorescence acceptor would be search.

## References


1. Takkinen, K. & Žvirblienė, A. Recent advances in homogenous immunoassays based on resonance energy transfer. *Curr. Opin. Biotechnol.* **55**, 16–22 (2019).
2. Sapsford, K. E., Berti, L. & Medintz, I. L. Materials for fluorescence resonance energy transfer analysis: Beyond traditional donor-acceptor combinations. *Angew. Chem. Int. Ed.* **45**, 4562–4589 (2006).
3. Hötzer, B., Medintz, I. L. & Hildebrandt, N. Fluorescence in nanobiotechnology: Sophisticated fluorophores for novel applications. *Small* **8**, 2297–2326 (2012).
4. Mahdi, M., Mansour, B. & Afshin, M. Competitive immunoassay for Ochratoxin a based on FRET from quantum dot-labeled antibody to rhodamine-coated magnetic silica nanoparticles. *Microchim. Acta* **183**, 3093–3099 (2016).
5. Foubert, A. *et al.* Bioconjugation of quantum dots: Review & impact on future application. *TrAC -Trends Anal. Chem.* **83**, 31–48 (2016).
6. Pulli, T., Höyhtyä, M., Söderlund, H. & Takkinen, K. One-step homogeneous immunoassay for small analytes. *Anal. Chem.* **77**, 2637–2642 (2005).
7. Niemi, M. H. *et al.* A structural insight into the molecular recognition of a (-)-δ9-tetrahydrocannabinol and the development of a sensitive, one-step, homogeneous immunocomplex-based assay for its detection. *J. Mol. Biol.* **400**, 803–814 (2010).
8. Arola, H. O. *et al.* Specific Noncompetitive Immunoassay for HT-2 Mycotoxin Detection. *Anal. Chem.* **88**, 2446–2452 (2016).
9. Akter, S. *et al.* Broad-Spectrum Noncompetitive Immunocomplex Immunoassay for Cyanobacterial Peptide Hepatotoxins (Microcystins and Nodularins). *Anal. Chem.* **88**, 10080–10087 (2016).
10. Goryacheva, O. A. *et al.* Lanthanide-to-quantum dot Förster resonance energy transfer (FRET): Application for immunoassay. *Talanta* **164**, 377–385 (2017).
11. Ji, X., Wang, W. & Mattoussi, H. Controlling the spectroscopic properties of quantum dots via energy transfer and charge transfer interactions: Concepts and applications. *Nano Today* **11**, 98–121 (2016).
12. Charbonnière, L. J., Hildebrandt, N., Ziessel, R. F. & Löhmannsröben, H. G. Lanthanides to quantum dots resonance energy transfer in time-resolved fluoro-immunoassays and luminescence microscopy. *JACS* **128**, 12800–12809 (2006).
13. Wegner, K. D., Jin, Z., Lindén, S., Jennings, T. L. & Hildebrandt, N. Quantum-dot-based förster resonance energy transfer immunoassay for sensitive clinical

diagnostics of low-volume serum samples. *ACS Nano* **7**, 7411–7419 (2013).
14. Algar, W. R., Susumu, K., Delehanty, J. B. & Medintz, I. L. Semiconductor quantum dots in bioanalysis: Crossing the valley of death. *Anal. Chem.* **83**, 8826–8837 (2011).
15. Ippen, C. *et al.* ZnSe/ZnS quantum dots as emitting material in blue QD-LEDs with narrow emission peak and wavelength tunability. *Org. Electron.* **15**, 126–131 (2014).
16. Navarro-Pardo, F., Zhao, H., Wang, Z. M. & Rosei, F. Structure/Property Relations in 'giant' Semiconductor Nanocrystals: Opportunities in Photonics and Electronics. *Acc. Chem. Res.* **51**, 609–618 (2018).
17. Sowers, K. L. *et al.* Photophysical properties of CdSe/CdS core/shell quantum dots with tunable surface composition. *Chem. Phys.* **471**, 24–31 (2016).
18. Nam, D. E., Song, W. S. & Yang, H. Noninjection, one-pot synthesis of Cu-deficient CuInS2/ZnS core/shell quantum dots and their fluorescent properties. *J. Colloid Interface Sci.* **361**, 491–496 (2011).
19. Eskonen, V., Tong-ochoa, N., Mattsson, L. & Miettinen, M. Single-Peptide TR-FRET Detection Platform for Cysteine- Specific Post-Translational Modifications. *Anal. Biochem.* **92**, 13202–13210 (2020).
20. Nguyen, D. *et al.* Photostable and Proteolysis-Resistant Förster Resonance Energy Transfer-Based Calcium Biosensor. *Anal. Chem.* **92**, 7683–7689 (2020).

# CHAPTER 5: GENERAL CONCLUSIONS

## General conclusions and future work

This PhD thesis presents the advancements in biosensing based on the use of antibodies wearing nanoclusters which can be employed as a probe integrating the sensing element and the transducer in immunoassays. The use of NCs embedded in the antibody structure offer advantages in terms of sensitivity in comparison with the use of natural enzymes as antibody labels and results in the development of new efficient strategies for the detection system of immunoassays.

The main conclusions of the work conducted during this PhD thesis are summarised below:

- It was found that it is possible to synthesized NCs of different materials using a model antibody as scaffold (polyclonal Anti-BSA IgG from rabbit).
- The nondenaturing conditions used during the synthesis makes the antibody structure remains unalterable after the modification. Moreover, the antibody still has affinity for its target analyte (BSA) and protein G.
- Due to their reduced dimensions, the NCs have molecule-like properties. In particular, the CdS NCs-IgG show fluorescent and photocatalytic properties. The bimetallic NCs-IgG exhibit peroxidase-like activity.
- The synthetic route to Au/Pt NCs-IgG is robust and can be applied using different polyclonal antibodies. Nevertheless, if a monoclonal antibody is used it results in the denaturalization of the antibody and the loss of affinity for target analyte.
- The signals provide by the molecule-like properties of the NCs-IgG can be related with the BSA concentration in an immunoassay. On the one hand, the bimetallic NCs can act as detection antibody in a colorimetric sandwich-type immunosensor. The inclusion of the NCs inside the antibodies address the drawbacks related with the tethering of enzymes to antibodies and results in a decrease in the background signal and the reduction of nonspecific binding. In the Figure below the Figures 4B, 5B and 6B of Chapter 4 (Setting of sandwich-type immunosensor using antibody-protected bimetallic NCs) are merge in a single one to show the differences in background noise.

It was found that it was higher in the immunoassay which uses IgG-HRP than in the immunoassays which employ bimetallic NCs-IgG. This confirm the starting hypothesis of

the improved signal-to-noise ratio by eliminating step of a crosslink reaction between an antibody and the label. Moreover, by using antibody carrying bimetallic NCs, for the detection of BSA, the LOD was improved by 56 times in comparison with a conventional method that employs the same detection antibody but labelled with HRP.

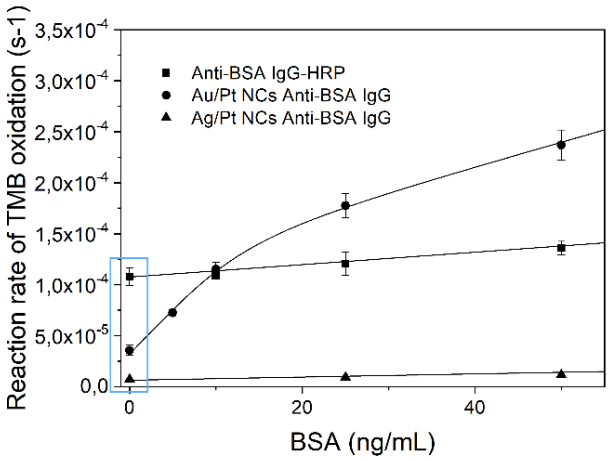


- CdS NCs-IgG were able to act as a donor energy in FRET. The formation of the immunocomplex between the CdS NCs-IgG and BSA-$AF_{647}$ causes a change in the fluorescent properties of the NCs due to proximity effects. The fluorescence of the NCs decreases with increasing concentrations of BSA-$AF_{647}$ because of the transfer of energy to the organic fluorophore. An increase in the fluorescence of BSA-$AF_{647}$ was also observed due also to FRET effects. Although it was not possible to develop a FRET-based homogeneous competitive immunoassay for BSA based on CdS NCs-IgG, they are promising materials to act as energy donor in FRET assays.

As a general conclusion the introduction of NCs embedded in the structure of an antibody results in an efficient methodology for the detection system of immunoassays. This PhD thesis open the door to the next generation of efficient labels for antibodies and further applications and advantages are still under research. Currently, the research line is focused in the study the advantages in long term storage of Au/Pt NCs-IgG over IgG-HRP. Furthermore, the use of antibody wearing NCs are being tested for the detection of IL-6, an analyte with clinical relevance, employing the patent developed during this thesis. This research is framed in the European Project DeDNAed (H2020-FETOPEN-2018-2020) in which CIC biomaGUNE and Tecnalia Research & Innovation are currently working together.

# PUBLICATIONS, CONFERENCES AND PATENTS

## Refereed full Papers

- Mora-Sanz, V., Saa, L., Briz, N. and Pavlov, V. **Antibody-Directed Synthesis of Catalytic Nanoclusters for Bioanalytical Assays.** *ACS Appl. Mater. Interfaces* 2020, 12, 26, 28993-28999

- Mora-Sanz, V., Saa, L., Briz, N. and Pavlov, V. **Synthesis and Characterization of Antibody-Protected Bimetallic Nanoclusters with Catalytic Properties**. *Chem. Mater.* 2020, 32 (19), 8286-8293.

## Patent

- Mora-Sanz, V., Saa, L., Briz, N. and Pavlov, V. **Nanocluster-antibody conjugates and uses thereof**. (2020).

## Refereed Conference Publications

- Mora-Sanz, V., Saa, L., Briz, N. and Pavlov, V. **Antibody-directed synthesis of bimetallic catalytic nanoclusters for the development of bioanalytical assays**, *JICI. V Reunión de Jóvenes Investigadores en Coloides e Interfases*, 2020, Zaragoza (Spain), oral presentation.

- Mora-Sanz, V., Saa, L., Briz, N. and Pavlov, V. **Synthesis, characterization and application in immunoassays of antibodies modified with catalytic bimetallic nanoclusters**. *3 rd Biennial Young Researchers Workshop on Biomaterials Applications (BioMAPP19),* 2019, Bilbao (Spain), oral presentation.

- Mora-Sanz, V., Saa, L., Briz, N. and Pavlov, V. **Use of antibodies modified with catalytic Au/Pt nanoclusters in immunoassays**. *International Conference on Nanomedicine and Nanobiotechnology (ICONAN)*, 2019, Munich (Germany), poster.

- Mora-Sanz, V., Saa, L., Briz, N. and Pavlov, V. **Development of bioanalytical assays based on antibodies modified with nanoclusters**. IX *International Congress on Analytical Nanoscience and Nanotechnology (IX NyNA)*, 2019, Zaragoza (Spain), poster.
- Mora-Sanz, V., Saa, L., Briz, N. and Pavlov, V. **Development of bioanalytical assays based on antibodies modified with nanoclusters**. XXXVII *Reunión Bienal de la Real Sociedad Española de Química,* 2019, Donostia-San Sebastián (Spain).

# Agradecimientos

En primer lugar, me gustaría empezar agradeciéndoles a mis dos directores, Valery Pavlov y Nerea Briz que me dieran la oportunidad de realizar esta tesis bajo su supervisión. A Valery gracias por el conocimiento que me has transmitido y apoyar mis ideas durante el tiempo que estuve en CIC biomaGUNE. A Nerea gracias también por todas las cosas que me has enseñado, por la motivación para continuar y seguir mejorando este trabajo hasta el último momento y por hacerme sentir valorada.

Agradezco a CIC biomaGUNE y Tecnalia el permitirme realizar el trabajo experimental en sus centros de excelencia internacional.

También agradecer a la Universidad del País Vasco y a mi tutora Isabel Goñi la oportunidad de realizar el doctorado y al Ministerio de Ciencia, Innovación y Universidades de España y al Gobierno Vasco la financiación.

Gracias a mis compañeras de laboratorio de CIC biomagune Laura, Bea y Silvia. En primer lugar, a Laura Saa, porque fuiste a la primera persona que conocí que me ha acompañado durante esta aventura, gracias por todo lo que me has enseñado que es muchísimo. También darte las gracias por el apoyo tanto a nivel laboral como emocional durante esta tesis. A mi compañera tanto en CIC biomagune y Tecnalia, Bea, gracias por tu compañerismo y también por tu amistad tanto dentro como fuera del laboratorio. A Silvia gracias por tu amistad, la complicidad y tu capacidad para escucharme y hacerme sentir comprendida. También agradecer a mi amiga Luchia los buenos momentos que hemos pasado juntas y las largas conversaciones apoyándonos mutuamente. Por último, agradecer al resto de compañeros de CIC biomaGUNE que me habéis acompañado durante este camino y que habéis hecho que fuera tan especial, Javi y Guille, Dina, Dani, Idoia, Anabel y Marta.

Gracias a todos mis compañeros de Tecnalia por hacerme sentir tan acogida desde el primer momento y hacerme sentir cada día como si estuviera en casa. En especial a Nerea G. por endulzarnos los días, a Xabi por su ilimitada y entretenida conversación, a Irene por su alegría, a Unai, a María, Bea O. y a J. Lou y a Marina, mis compañeros de biosensores.

A Luis muchas gracias por tu cariño, por esforzarte en hacerme feliz, por escucharme en cualquier momento que lo necesite, por hacerme sentir que puedo contar contigo y por hacerme mejor persona.

A mis amigos de Zaragoza porque cada vez que nos juntamos es como si no hubiera pasado el tiempo, gracias por todos los buenos momentos y los que vendrán, que dan fuerzas para a veces sobrellevar el día a día. En especial a mi amiga Andrea gracias por escucharme y por tus siempre buenos consejos.

Gracias a toda mi familia, a mi tía-madrina María Jesús por su apoyo incondicional, a mi tío Javi, mi tía Puri, mi tía Lili, mi prima Amaranta, mi abuela y al resto de tíos y primos. En especial, gracias a mi yayo por su amor infinito, hacerme sentir siempre tan especial y por los valores que me enseñó y que me ayudan a mejorar cada día. Pero sobre todo gracias a mis padres, porque sin su ayuda y su apoyo no habría conseguido llegar hasta aquí. Mamá, gracias por todo el amor que me has dado y me das, por estar ahí siempre cuando te necesito, ya sea escuchándome en la distancia o con un abrazo en persona y no fallarme nunca. Papá gracias por creer en mí, en muchas ocasiones más de lo que yo lo hago y haberme dado las alas que necesitaba para volar.

*No son nuestras habilidades las que demuestran quienes somos,*

*sino nuestras elecciones.*

-Albus Dumbledore-